

**PRINTED FLEXIBLE SENSORS:
FABRICATION, CHARACTERIZATION AND
IMPLEMENTATION**

By

ANINDYA NAG

A thesis submitted to Macquarie University
for the degree of
Doctor of Philosophy
School of Engineering

August 2018



MACQUARIE
University
SYDNEY · AUSTRALIA

To my parents

Ahindra Nag

Late Sikha Nag

STATEMENT OF CANDIDATE

I certify that the work in this thesis has not previously been submitted for a degree nor has it been submitted as part of the requirements for a degree to any other university or institution other than Macquarie University.

I also certify that the thesis is an original piece of research and it has been written by me.

In addition, I certify that all information sources and literature used are indicated in the thesis.

.....

Anindya Nag

Acknowledgements

I want to express my earnest gratitude towards my supervisor, **Prof. Subhas Mukhopadhyay** who took me as a doctoral student and always showed faith on me. He has helped me in every possible to go through this journey. His insightful ideas on my work have always assisted me to think and perceive the problem in a logical manner. He has devoted his invaluable time towards my work and helped me to proceed through it. With his experience and ability to handle any given problem at a point of time, he has helped me to grow as a person and a researcher. Without his assistance, it would not have been possible for me to go through this voyage successfully.

I would also like to thank my co-supervisor, **Prof. Jürgen Kosel** who has also been supportive on my work. His assistance in this entire duration was invaluable in terms of the support I have received in every phase of my degree. I also want to thank him for the six months he had invited me to work in his lab at King Abdullah University of Science and Technology, Saudi Arabia. Those six months really helped me to lay the foundation of my doctoral work. I would also like to thank Mr. Ulrich Buttner and Dr. Ahmed Alfadhel for their help with my work.

I would like to express my gratitude towards the staffs at Massey University, New Zealand where I started my doctoral degree and continued for one year. I would like to thank Niki Murray, Mario Codeniera for their assistance regarding the microscopy images and IT related work.

I would also like to thank Prof. Iain Collings to accept my candidature in this university during my transfer from Massey University in 2016. I am also very thankful to Dr. Keith Imrie for his valuable advice and useful comments during my research which helped me to improve the quality of my work and thesis.

I would also thank the administrative section of Macquarie University to provide the facilities required to perform my research during my doctoral period. I would like to thank Macquarie Engineering and Technical Services (METS) and technical assistants for their assistance whenever required.

I would also like to thank my father for being a constant support in my life. He has always given me ideas to work harder in the professional area while having an equal balance in the personal life.

I would also like to thank my friends, Nasrin Afsarimanesh, Md. Eshrat E Alahi, Van Nguyen Thi Phuoc and Shilun Feng, who has been a constant support to me and encouraged me to put more effort on my work.

I am also very grateful to Anupriya Verma for always being there for me through sickness and health.

Finally, I want to thank GOD for giving me the strength and endurance to deliver my best performance through the doctoral period.

Thank you very much!

Research Outputs

Publications related to the field of this thesis are as follows.

Journals

1. **Anindya Nag**, S. Feng, S. C. Mukhopadhyay, J. Kosel and D. Inglis, “3-D printed mould-based Graphite/PDMS sensor for low force applications”, *Sensors and Actuators A: Physical*, vol. 280, pp. 525-534, **September 2018**.
2. **Anindya Nag**, B. Menzies, and S. C. Mukhopadhyay, “Performance Analysis of Flexible Printed Sensors for Robotic Arm Applications”, *Sensors and Actuators A: Physical*, vol. 276, pp. 226-236, **May 2018**.
3. **Anindya Nag**, N. Afsarimanesh, S. Feng and S. C. Mukhopadhyay, “Strain Induced Graphite/PDMS sensors for Biomedical Applications”, *Sensors and Actuators A: Physical*, vol. 271, pp. 257–269, **March 2018**.
4. **Anindya Nag**, A. Mitra and S. C. Mukhopadhyay, “Graphene and its sensor-based applications: A review”, *Sensors and Actuators A: Physical*, vol. 270, pp. 177-194, **February 2018**.
5. Md. Eshrat E Alahi., **Anindya Nag**, S. C. Mukhopadhyay and L. Burkitt, “A temperature-compensated graphene sensor for nitrate monitoring in real-time application”, *Sensors and Actuators A: Physical*, vol. 269, pp. 79-90, **January 2018**.
6. **Anindya Nag** and S. C. Mukhopadhyay, “Fabrication and implementation of printed sensors for taste sensing applications”, *Sensors and Actuators A: Physical*, vol. 269, pp. 52-61, **January 2018**.
7. **Anindya Nag**, S. C. Mukhopadhyay and J. Kosel, “Sensing System for Salinity Testing Using Laser-induced Graphene Sensors”, *Sensors and Actuators A: Physical*, vol. 264, pp. 107-116, **August 2017**.

8. **Anindya Nag**, S. C. Mukhopadhyay and J. Kosel, “Wearable Flexible Sensors: A Review”, *IEEE Sensors Journal*, vol. 17, No. 13, pp. 3949-3960, **July 2017**.
9. **Anindya Nag** and S. C. Mukhopadhyay, “Fabrication and Implementation of Wearable Flexible Sensors”, *IEEE Standards University eMagazine*, vol. 7, no. 2, pp. 1-8, **June 2017**.
10. **Anindya Nag**, S. C. Mukhopadhyay and J. Kosel, “Tactile Sensing from Laser-ablated metallized PET films”, *IEEE Sensors Journal*, vol. 17, no. 1, pp. 7-13, **January 2017**.
11. **Anindya Nag**, S. C. Mukhopadhyay and J. Kosel, “Flexible carbon nanotube nanocomposite sensor for multiple physiological parameter monitoring”, *Sensors and Actuators A: Physical*, vol. 251, pp. 148-155, **November 2016**.
12. **Anindya Nag**, A. Zia , L. Xie, S. C. Mukhopadhyay and J. Kosel, “Novel sensing approach for LPG leakage detection: Part II: Effects of particle size, composition and coating layer thickness”, *IEEE Sensors Journal*, vol. 15, no. 8, pp. 1088-1094, **October 2015**.
13. **Anindya Nag**, A. Zia , L. Xie, S. C. Mukhopadhyay and J. Kosel, “Novel sensing approach for LPG leakage detection: Part I: Operating Mechanism and Preliminary Results”, *IEEE Sensors Journal*, vol. 16, no. 4, pp. 996-1003, **October 2015**.

Conference Proceedings

1. **Anindya Nag**, O. F. Dorsum, S. C. Mukhopadhyay and J. Kosel, “pH Sensing of Printed Flexible Sensors”, *12th International Conference on Sensing Technology (ICST)*, December 3-6, Limerick, Ireland, 2018 (accepted).
2. **Anindya Nag**, N. Afsarimanesh, S. Feng, S. C. Mukhopadhyay and J. Kosel, “Development of Novel Gold/PDMS Sensors for Medical Applications”, *12th International Symposium on Medical Information and Communication Technology (ISMICT)*, March 26-28, Sydney, Australia, pp. 1-4, **2018**.
3. **Anindya Nag**, S. Feng, S. C. Mukhopadhyay and J. Kosel, “Development of Printed Sensors for Shoe Sensing Applications”, *12th International Symposium on*

- Medical Information and Communication Technology (ISMICT)*, March 26-28, Sydney, Australia, pp. 1-4, **2018**.
4. **Anindya Nag**, S. C. Mukhopadhyay and J. Kosel, “Development of Printed Sensors for Taste Sensing”, in *1st IEEE Life Sciences Conference (LSC)*, December 13-15, Sydney, Australia, pp. 1-6, **2017**.
 5. A. Mitra, J. Bredow and **Anindya Nag**, “Mathematical Modelling of Microbolometers at Oblique Incidence”, in *11th International Conference on Sensing Technology (ICST)*, December 4-6, Sydney, Australia, pp. 1-6, **2017**.
 6. **Anindya Nag**, S. C. Mukhopadhyay and J. Kosel, “Influence of Temperature and Humidity on Carbon Based Printed Flexible Sensors”, in *11th International Conference on Sensing Technology (ICST)*, December 4-6, Sydney, Australia, pp. 1-6, **2017**.
 7. **Anindya Nag**, S. C. Mukhopadhyay and J. Kosel, “Urinary incontinence monitoring system using laser-induced graphene sensors”, in *IEEE Sensors*, October 29 – November 1, Glasgow, UK, pp. 1-3, **2017**.
 8. **Anindya Nag**, S. C. Mukhopadhyay and J. Kosel, “Transparent biocompatible sensor patches for touch sensitive prosthetic limbs”, in *10th International Conference on Sensing Technology (ICST)*, November 11-13, Nanjing, China, pp. 1-6, **2016**.
 9. **Anindya Nag**, J. Kosel, S. C. Mukhopadhyay and R. Haverkamp, “Fabrication and characterization of strain-induced electrodes for bio-medical applications”, in *8th Asia-Pacific Conference of Transducers and Micro/Nano Technologies (APCOT)*, June 26-29, Kanazawa, Japan, pp. 1-2, **2016**.
 10. **Anindya Nag**, A. Zia, S. C. Mukhopadhyay and J. Kosel, “Performance enhancement of electronic sensor through mask-less lithography”, in *9th International Conference on Sensing Technology (ICST)*, December 8-10, Auckland, New Zealand, pp. 374-379, **2015**.
 11. **Anindya Nag**, A. Zia, A. Babu and S.C. Mukhopadhyay, “Printed electronics: Present and future opportunities”, in *9th International Conference on Sensing Technology (ICST)*, December 8-10, Auckland, New Zealand, pp. 380-389, **2015**.

12. A. Zia, N. Afsarimanesh, L. Xie, **Anindya Nag**, I. H. Al-Bahadly, P. L. Yu and J. Kosel, “Improved detection limits for phthalates by selective solid-phase micro-extraction”, in *9th International Conference on Sensing Technology (ICST)*, December 8-10, Auckland, New Zealand, pp. 733-738, **2015**.

Book chapters

1. **Anindya Nag** S. C. Mukhopadhyay and H.S. Nalwa, “Carbon Nanotube-Based Flexible Sensors”, *Functional Nanomaterials and Nanodevices*, American Scientific Publishers, 2018, pp. 1-44. ISSN: 1-58883-257-0 (accepted).
2. **Anindya Nag** and S. C. Mukhopadhyay, “Wearable Flexible Sensors: Fabrication and Characterization”, *Institute of Physics (IoP)*, December **2017**, DOI: <https://doi.org/10.1088/978-0-7503-1505-0ch2>.
3. Md. Eshrat E Alahi, **Anindya Nag**, N. Afsarimanesh, S.C. Mukhopadhyay and J.K. Roy, “A simple Embedded Sensor: Excitation and Interfacing”, *Advanced Interfacing Techniques for Sensors*, Smart Sensors, Measurement and Instrumentation series of Springer-Verlag., Volume 25, pp. 111-138, **2017**.
4. **Anindya Nag**, S. C. Mukhopadhyay and J. Kosel, “Flexible Printed Sensors for ubiquitous human monitoring”, *Sensors for Everyday Life*, Smart Sensors, Measurement and Instrumentation series of Springer-Verlag., pp. 1-19, **2016**.
5. **Anindya Nag** and S. C. Mukhopadhyay, “Wearable Electronics Sensors: Current Status and Future Opportunities”, *Wearable Electronics Sensors: for safe and healthy living*, Smart Sensors, Measurement and Instrumentation series of Springer-Verlag, pp. 1-35, **2015**.

Workshops/Seminars

1. “pH dependence of fabricated printed sensors”, Engineering HDR conference, Macquarie University, Australia, June **2018**.

2. “Novel Graphite/PDMS sensors for strain sensing purposes”, IEEE Instrumentation & Measurement (IMS) Society Workshop, Macquarie University, Australia, November **2017**.
3. “Development of Novel Flexible Printed Sensors for Multi-disciplinary Applications”, 6th Annual Biofocus Research Conference, Macquarie University, Australia, December **2016**.
4. “Real-time posture recognition using shoe integrated wireless sensing system”, Dunmore Lang College, Australia, November **2016**.
5. “Fabrication and characterization of strain-induced electrodes for bio-medical applications”, 8th Asia-Pacific Conference of Transducers and Micro/Nano Technologies (APCOT), June 26-29, Kanazawa, Japan, June **2016**.

Google scholar

<https://scholar.google.com.au/citations?user=Q77uw5sAAAAJ&hl=en&oi=ao>

Awards

1. Article titled: “Wearable Flexible Sensors: A Review”, IEEE Sensors Journal, Vol. 17, No. 13, July 2017, has been one of the 25 most downloaded Sensors Journal papers between June 2017 and June 2018.
2. International Macquarie University Research Scholarship (iMQRES) for two years (August 2016 - July 2018).
3. Massey University doctoral scholarship for one year (July 2015 - July 2016).
4. Winner - Best Technical Paper-2015 for the paper titled: “MEMS Based Sensors for Detection of Contamination in Water for Home Environment” presented at the *Indian Water Works Association Conference*, Jan 30- Feb 1, 2015, Kolkata, India.



July 23, 2018

Dear Mr. Anindya Nag,

On behalf of the IEEE Sensors Council, I am pleased to congratulate you as a co-author of the paper **Wearable Flexible Sensors: A Review, IEEE Sensors Journal, Vol. 17, No. 13, July 2017**, for your paper being one of the 25 most downloaded Sensors Journal papers every month from June 2017 – June 2018.

It is exciting to note that included in this count are all Sensors Journal papers published since the Journal's foundation, about 6,450 papers in total, and that last year, 502,904 Sensors Journal papers were downloaded from IEEE Xplore. You can view the latest Top 50 papers at: <http://ieeexplore.ieee.org/xpl/topAccessedArticles.jsp?punumber=7361>

Thank you for your contribution to the IEEE Sensors Journal!

Kind regards,

Fabrice Labeau
President, IEEE Sensors Council 2018-2019

Abstract

Flexible sensors have showed immense potential to be used in the field of healthcare, environment and industrial applications. The full-blown utilisation of these types of sensors is yet to be done to have an impact on the quality of life of people. The presented work shows a great dynamicity in the utilisation of sensors in the application world. Among the different types of techniques that can be used to develop the flexible sensors differing in terms of size, cost and resolution, the use of printing technology had been done to large extent. The work on printed flexible sensors has been continuously growing due to their advantages of low-cost, enhanced electrical and mechanical properties. In this research, novel flexible printed sensors were developed using the laser cutting technique. Four different types of printed flexible sensor prototypes were fabricated, characterised and implemented for different applications. The idea behind the development of each of these sensor prototypes can be attributed to their low-cost, simple operating principle and multi-functional characteristics. The electrical behaviour of the electrodes was based on the capacitive principle due to their interdigitated structures. Electrochemical Impedance Spectroscopy was used in conjunction with the sensor prototypes to determine the output with respect to the changes in the input. The differences among these prototypes lied in their characteristics due to the different raw materials used to develop them. Multi-Walled Carbon Nanotubes, Graphene, Graphite are some of the conductive materials that were used to develop the electrodes of the sensor prototypes due to their light weight, high electrical conductivity, durability and high aspect ratio. Polydimethylsiloxane, Polyethylene Terephthalate and Polyimide are some of the polymers that were used to develop the substrates due to their low-cost, biocompatibility, low Young's modulus and ability to form flexible bilayer-structured devices. The sensor prototypes were used for different fields like monitoring of limb and other body part movements, respiration and taste sensing for healthcare, salinity and nitrate sensing for environment, and tactile and low-force sensing for industrial applications. The futuristic applications of the developed sensors could involve their real-time applications for chemical and biological sensing of proteins, different gases, temperature, humidity, etc. Due to their small size and biocompatible nature, they can also be considered as implantable sensors to determine the anatomical

changes happening inside the body. They can also be used for national purposes, for example., in military and defences, where their minuscular forms would be attached to the wings with adaptive feedback systems to determine their active flutter suppressions.

Contents

Acknowledgements	iii
Research Outputs.....	v
.....	x
Abstract.....	xi
List of Figures.....	xvii
List of Tables	xxvi
Introduction.....	1
1.1 Flexible Sensors	2
1.2 Printed Electronics	7
1.3 Conclusion	12
1.4 Research Contributions	13
1.5 Organisation of the Thesis	14
Literature Review	17
2.1 Introduction.....	18
2.2 Carbon Nanotubes and their Sensor-based Applications.....	18
2.2.1 Synthesis of Carbon Nanotubes	19
2.2.2 Characterisation and Properties	21
2.2.3 Electrochemical Sensors	22
2.2.4 Strain Sensors.....	25
2.2.5 Electrical Sensors.....	26
2.2.6 Conclusion and Future work.....	27
2.3 Graphene and its Sensor-based Applications.....	28
2.3.1 Synthesis of Graphene	31
2.3.2 Characterisation and Properties	34

2.3.3	Electrochemical Sensors	41
2.3.4	Strain Sensors.....	45
2.3.5	Electrical Sensors.....	47
2.3.6	Challenges with the Current Sensors	52
2.3.7	Conclusion and Future Work.....	57
2.4	Wearable Flexible Sensors.....	58
2.4.1	Materials for Wearable Flexible Sensors.....	60
2.4.2	Sensor Networks for Wearable Flexible Sensors.....	62
2.4.3	Types of Activity Monitoring with Wearable Flexible Sensors	65
2.4.4	Challenges and Future Opportunities.....	70
2.5	Chapter Summary	72
	Interdigitated Sensing and Electrochemical Impedance Spectroscopy	73
3.1	Introduction.....	74
3.2	Planar Interdigital Sensors	74
3.3	Electrochemical Impedance Spectroscopy (EIS).....	79
3.4	Chapter Summary	80
	Carbon Nanotubes-Polydimethylsiloxane Sensor.....	83
4.1	Introduction.....	84
4.2	Fabrication of the Sensor Patches	84
4.3	Frequency Response and Stress-Strain Measurements.....	88
4.4	Monitoring of Physiological Parameters	91
4.4.1	Experimental Setup.....	93
4.4.2	Results and Discussion	94
4.4.3	Conclusion	100
4.5	Tactile Sensing.....	100
4.5.1	Experimental Setup.....	101
4.5.2	Results and Discussion	102
4.5.3	Conclusion	105
4.6	Chapter Summary	106
	Aluminium-Polyethylene Terephthalate Sensor	107
5.1	Introduction.....	108
5.2	Fabrication of the Sensor Patches	108
5.3	Frequency Response and Stress-Strain Measurements.....	113

5.4	Tactile Sensing.....	116
5.5	Chapter Summary	122
	Graphene-Polyimide Sensor	123
6.1	Introduction.....	124
6.2	Fabrication of the Sensor Patches	124
6.3	Complex Nonlinear Least Squares Curve Fitting	127
6.4	Salinity Sensing	130
6.4.1	Experimental Setup.....	132
6.4.2	Results and Discussion	133
6.4.3	Microcontroller-based Sensing System	139
6.4.4	Conclusion	141
6.5	Taste Sensing	142
6.5.1	Experimental Setup.....	143
6.5.2	Results and Discussion	144
6.5.3	Results and Discussion	154
6.6	Nitrate Sensing.....	156
6.6.1	Experimental Setup.....	157
6.6.2	Comparative Analysis of two Different Sensors	158
6.6.3	Temperature and Nitrate-N Measurement	159
6.6.4	IoT-enabled Smart Sensing System.....	159
6.6.5	Results and Discussion	163
6.6.6	Conclusion	169
6.7	Chapter Summary	169
	Graphite-Polydimethylsiloxane Sensor.....	171
7.1	Introduction.....	172
7.2	Fabrication of the Sensor Patches	173
7.3	Frequency Response and Stress-Strain Measurements.....	177
7.4	Strain Sensing	183
7.4.1	Experimental Setup.....	185
7.4.2	Results and Discussion	186
7.4.3	Conclusion	192
7.5	Force Sensing.....	192
7.5.1	Experimental Setup.....	193

7.5.2	Results and Discussion	193
7.5.3	Conclusion	194
7.6	Chapter Summary	194
	Conclusion, Challenges and Future Work	197
8.1	Conclusion	198
8.2	Challenges of the existing work.....	199
8.3	Future work.....	200
	References.....	205

List of Figures

Figure 1.1 Schematic representation of the use of wireless sensors for physiological parameter monitoring [24].....	4
Figure 1.2 Fabrication of flexible sensors using various printing techniques. [41].....	8
Figure 2.1 (a) SEM image of vertically aligned CNTs [67]. (b) Highly magnified TEM image of CNTs grown with a catalyst. Reprinted with permission from [68]...20	20
Figure 2.2 (a) Schematic diagram of an MWCNT [79]. (b) HRTEM image of the multi-layered structure of a single MWCNT [80].....	22
Figure 2.3 (a) Transmittance spectra of SWCNT/PEDOT film in the 350 to 700 nm region. (b) The resistance change of SWCNTs@PEDOT/PDMS film as a function of bending radius. (c) LED integrated circuits under 0% and 50% tensile strains. (d) A comparison of the resistance changes of SWCNTs (red line), SWCNTs@PEDOT/PDMS (black line), and SWCNTs@PEDOT/PDMS films with 30% pre-strain (blue line) as a function of tensile strains. (e,f) The variation of resistance for the SWCNTs@PEDOT/PDMS stretchable films in the first and second stretching cycles (e), and fourth and fiftieth (f) stretching cycles. [88].....	23
Figure 2.4 Glucose/pH sensors developed from SWCNTs and PDDA. (a) The bending of standard 4-inch wafer level devices. (b) The comparison of the sensor with a coin [91].....	24
Figure 2.5 PMOS inverter developed from SWCNT/PI [128].....	27
Figure 2.6 Different forms (0D, 1D and 3D) of modified graphene [133].....	29
Figure 2.7 Schematic diagram of the structure of graphene represented in the form of a Honeycomb lattice and its Brillouin zone [206].....	35
Figure 2.8 Electronic dispersion of the honeycomb lattice in terms of (zoomed in) the energy spectrum of finite values [205, 206].....	35
Figure 2.9 Schematic diagram of the sensing mechanisms of graphene-based (a) electrochemical (b) strain (c) electrical sensors.....	40

Figure 2.10 Different protein molecules being wired by graphene on the glassy carbon electrode [247].....	42
Figure 2.11 (a) One-step approach to the formation of an H ₂ O ₂ sensor with PEDOT: PSS and AuNP and rGO. (b) Functionalisation of the formed nanocomposite with HRP for detection purposes [279].....	44
Figure 2.12 (a) PDMS-based strain sensor developed with graphene on Ni/Si/SiO ₂ film [282]. (b) Flexible graphene-PET strain sensor developed by drop-casting graphene oxide film to laser write the interdigitate circuit [283]. (c) Development of a reduced graphene oxide/polyimide nanocomposite to form strain sensors by mixing, freezing and thermal annealing with polyamic acid [284].....	45
Figure 2.13 Schematic diagram of the formation of stretchable graphene nano-papers [124].....	47
Figure 2.14 Graphene transistors on flexible substrate shown in 3-D (a), Optical (b), cross-sectional (c) and AFM (d) images [39].....	48
Figure 2.15 An overview of the potential applications and marketing areas of graphene in the upcoming years [364].....	58
Figure 2.16 Pictorial representation of the different prospects of wearable flexible devices using organic electronics [367].....	62
Figure 2.17 Schematic diagram of the transmission of data from the sensor to the monitoring unit.....	63
Figure 2.18 Schematic diagram of the hardware architecture for the sensor node for WPMS [402].....	65
Figure 2.19 Schematic diagram of electronic skins with a sensor perception on a human arm [423].....	66
Figure 2.20 (a) Schematic diagram for the materials used to develop the sensor. (b) Finished product [424].....	67
Figure 2.21 Schematic diagram of the rugged and stretchable electronic sensor for electrophysiological activities [431].....	67
Figure 2.22 (a) Schematic diagram showing the pH-sensitive chip along with the LED and photodiode. (b) Place of the sensor on a person [445].....	68
Figure 2.23 Flexible Printed Circuit Board developed for in situ perspiration analysis [466].....	70

Figure 3.1 Working principle of the sensor patch. (a) The sensor works on the idea of a parallel-plate capacitor. (b) Due to the planar structure of the electrodes, the electric field bulges from one electrode to another of opposite polarity [476].	75
Figure 3.2 Operating principle of the developed sensor patches was based on the capacitive principle [482].	76
Figure 3.3 Three-dimensional simulation done using COMSOL 3.2b to determine the change in the electric field distribution on the sensor patch for the applied stress.	78
Figure 3.4 Phase shift in the output current with respect to the input voltage.	80
Figure 4.1 Schematic diagram of the fabrication steps. PDMS: Polydimethylsiloxane. NC: Nanocomposite.	85
Figure 4.2 SEM top-view image of the nanocomposite consisting of CNTs (4% wt.) and PDMS.	85
Figure 4.3 Fabrication steps: (1) Casting of PDMS, (2) Desiccation of PDMS, (3) Curing of PDMS, (4) Casting of nanocomposite (NC), (5) Desiccation of NC, (6) Curing of NC, (7) Laser patterning of electrodes.	86
Figure 4.4 Front and rear-view images of the sensor patch.	87
Figure 4.5 Impedance behaviour of the sensor patch as a function of frequency.	88
Figure 4.6 Phase angle of the sensor patch as a function of frequency.	89
Figure 4.7 Directions of the applied stresses for the stress/strain characterisation of the sensor patch.	89
Figure 4.8 Stress-strain relationship of the sensor patch.	90
Figure 4.9 Relation between capacitance and strain of the sensor patch in the horizontal direction.	90
Figure 4.10 Sensor attachment for the biophysical parameters: (A): Monitoring of respiration with the sensor attached on the lower part of the diaphragm, (B): Sensor attached on the elbow to monitor arm movement, (C): Sensor attached on the knee to monitor leg movement.	93
Figure 4.11 Detection of left-arm movement when the subject is at rest.	94
Figure 4.12 Detection of right-arm movement when the subject is at rest.	95
Figure 4.13 Detection of left-leg movement when the subject is at rest.	95
Figure 4.14 Detection of right-leg movement when the subject is at rest.	96
Figure 4.15 Detection of right-arm movement when the subject is in motion.	96
Figure 4.16 Detection of right-leg movement when the subject is in motion.	97

Figure 4.17	Different angular measurements of the limbs of a subject.....	97
Figure 4.18	Change of capacitance as a function of the right-arm limb movement.....	98
Figure 4.19	Monitoring of respiration for two different individuals at rest.....	99
Figure 4.20	Measurement of respiration activity of an individual who was simulating respiration rates of 10/s for the first 80s, 5/s for the next 45s and 1/s for the next 20s.....	99
Figure 4.21	Measurement of respiration activity of an individual who was simulating inhalation and exhalation at different speeds.....	100
Figure 4.22	The sensor patch attached to the fingertip and connected to the LCR meter for tactile sensing.....	102
Figure 4.23	Response of the sensor patch for a pressure of 42.2 μPa	103
Figure 4.24	Response of the sensor patch for a pressure of 54.6 μPa	103
Figure 4.25	Response of the sensor patch for a pressure of 68.2 μPa	104
Figure 4.26	Response of the sensor patch for a pressure of 62.4 μPa	104
Figure 4.27	Response of the sensor patch for a pressure of 84.6 μPa	105
Figure 4.28	Variation of capacitance for different weight values.....	105
Figure 5.1	Schematic of the electrode design.....	109
Figure 5.2	Laser ablation to form electrodes.....	109
Figure 5.3	Fabrication steps of the sensor patch: (1) Raw material used for fabrication. (2) Raw material is attached to glass substrate for support. (3) Laser beam is shone on the sample. (4) Interdigitated Al electrodes are formed on PET. (5) Patch is detached from the glass substrate.....	110
Figure 5.4	Microscopic image of a single line of the electrode.....	111
Figure 5.5	Front and rear views of the sensor patch.....	112
Figure 5.6	Zoomed-in SEM image of the top view of the (a) edges (b) electrode lines of the fabricated sensor.....	112
Figure 5.7	Impedance behaviour of the sensor patch as a function of frequency.....	113
Figure 5.8	Phase angle of the sensor patch as a function of frequency.....	114
Figure 5.9	Equivalent circuit to determine the response from an interdigital sensor.....	114
Figure 5.10	Experimental set-up for characterisation of the sensor.....	115
Figure 5.11	Force-displacement relation for the sensor.....	115
Figure 5.12	Schematic for the experimental setup for tactile sensing.....	116
Figure 5.13	Response of the sensor for a pressure of 51.2 Pa of the index finger.....	117
Figure 5.14	Response of the sensor for a pressure of 66.8 Pa of the index finger.....	117

Figure 5.15	Response of the sensor for a pressure of 51.2 Pa of the thumb.....	118
Figure 5.16	Response of the sensor for a pressure of 66.8 Pa of the thumb.....	119
Figure 5.17	Response of the sensor for a pressure of 245 Pa of the palm.....	119
Figure 5.18	Response of the sensor for a pressure of 289.54 Pa of the palm.....	120
Figure 5.19	Sensitivity values for different pressures for the index finger, thumb and palm.....	121
Figure 6.1	Schematic diagram of the steps of fabrication of the graphene sensor. (a) The polyimide film, with a thickness of around 120 microns, is taken as the substrate material for the laser writing process. (b) The laser writing was done on the film. (c) The thermally induced material is shifted manually to the Kapton tape by compressing it against the generated graphene. (d) The final sensor prototype.....	125
Figure 6.2	Fabrication steps of the sensor.....	126
Figure 6.3	Front and rear views of the sensor patch.....	127
Figure 6.4	SEM image of (a) Top view of an electrode finger of the sensor patch (b) Zoomed top view showing the electrode lines.....	127
Figure 6.5	Least squares curve fitting plot in terms of Nyquist plot for the profiling of the sensor done in air. The red dots indicate the experimental data with the green line being the fitted curve.....	129
Figure 6.6	Block diagram for the proposed microcontroller-based sensing system for salinity measurement.....	132
Figure 6.7	Experimental setup showing the attachment of the sensor patch to the LCR meter via Kelvin probes. The sensing area of the patch was immersed in the solution. The LCR meter was connected to the laptop to collect the data.....	133
Figure 6.8	Response of the sensor patch for different concentrations of salt in terms of resistance and frequency.....	134
Figure 6.9	Response of the sensor patch for different concentrations of salt in terms of the reactance and frequency.....	135
Figure 6.10	Response of the sensor patch for different concentrations of salt in terms of Nyquist plot.....	135
Figure 6.11	Standard curve for different experimental concentrations.....	136
Figure 6.12	Least-square curve fitting for Nyquist plot with the experimental data.....	137
Figure 6.13	Dependence of the sensor response towards the temperature changes for different salt concentrations.....	138

Figure 6.14 Repeatability of the sensor response illustrated with six measurements with each salt concentration.....	139
Figure 6.15 Block diagram depicting the connection of the sensor to the microcontroller. The buffer and low-pass filter were added to the circuitry to improve the output from the sensor.....	140
Figure 6.16 Circuit design for the conditioning circuit used to process the sensor output before feeding it to the microcontroller.....	140
Figure 6.17 Response of the microcontroller for different salt concentrations.....	141
Figure 6.18 Experimental setup during the analysis of different chemicals.....	144
Figure 6.19 Response of the sensor for citric acid (sourness) in terms of resistance vs frequency.....	145
Figure 6.20 Response of the sensor for citric acid (sourness) in terms of reactance vs frequency.....	145
Figure 6.21 Response of the sensor for sucrose (sweetness) in terms of resistance vs frequency.....	147
Figure 6.22 Response of the sensor for sucrose (sweetness) in terms of reactance vs frequency.....	147
Figure 6.23 Response of the sensor for sodium chloride (saltiness) in terms of resistance vs frequency.....	148
Figure 6.24 Response of the sensor for sodium chloride (saltiness) in terms of reactance vs frequency.....	148
Figure 6.25 Response of the sensor for L-tryptophan (bitterness) in terms of resistance vs frequency.....	149
Figure 6.26 Response of the sensor for L-tryptophan (bitterness) in terms of reactance vs frequency.....	149
Figure 6.27 Response of the sensor for GMP (umami) in terms of resistance vs frequency.....	150
Figure 6.28 Response of the sensor for GMP (umami) in terms of reactance vs frequency.....	150
Figure 6.29 Comparison between the responses of the sensor patch to different chemicals for the concentrations of 1 ppm.....	152
Figure 6.30 Comparison between the responses of the sensor patch to different chemicals for the concentrations of 10 ppm.....	152

Figure 6.31 Comparison between the responses of the sensor patch to different chemicals for the concentrations of 100 ppm.....	153
Figure 6.32 Comparison between the responses of the sensor patch to different chemicals for the concentrations of 1000 ppm.....	153
Figure 6.33 Comparison of the conductivity detected by the sensor for different chemicals at a concentration of 100 ppm.....	154
Figure 6.34 Experimental setup for nitrate measurement.....	158
Figure 6.35 Block diagram of the smart sensing system.....	160
Figure 6.36 Software flow of the individual steps of the operating of the IoT-based system to calculate and transmission of the nitrate concentration to the cloud server.....	161
Figure 6.37 Schematic diagram of the smart sensing system.....	162
Figure 6.38 First prototype of the smart sensing system.....	162
Figure 6.39 The change of real part of the impedance with respect to frequency.....	163
Figure 6.40 Real part of the impedance as a function of temperature.....	164
Figure 6.41 Comparison of actual and measured temperatures.....	165
Figure 6.42 Calibration Standard of Nitrate-N concentration (ppm).....	166
Figure 6.43 Repeated unknown sample measurements by smart sensing system.....	168
Figure 6.44 Data transferred to the IoT based web server.....	169
Figure 7.1 The 3-D printing systems (a) were used to develop the moulds (b) using the Acrylonitrile Butadiene Styrene as the printing filament. The height of the trenches on the mould was adjusted to 500 microns.....	173
Figure 7.2 Graphite powder was cast on the 3-D printed mould (a), followed by the casting of PDMS (b) on top of it. These two layers defined the electrodes and substrate of the sensor patches.....	174
Figure 7.3 Optimization of the critical volume fraction of the graphite powder to develop the electrodes of the sensor patch.....	175
Figure 7.4 Front view of the developed sensor patch.....	176
Figure 7.5 Comparison between the sizes of the developed sensor with a 50 cent Australian coin.....	176
Figure 7.6 SEM images of the developed graphite-PDMS sensor depicting the top-view of (A) PDMS, (B) graphite-PDMS mixture and (C) cross-sectional view of the electrodes.....	177
Figure 7.7 Image of the developed sensor patch depicting its flexibility.....	178

Figure 7.8 Change in the reference spot in the sensor patch to depict their flexibility from (a) no- strain to (b) full-strain condition.....	178
Figure 7.9 Response of the sensor for the frequency sweep done to determine the operating frequency.....	179
Figure 7.10 Analysis of the stress-strain measurement. The direction of the applied stress shown is in the inset of the figure.....	179
Figure 7.11 Response of the sensor patch in the proportional limit for the stress-strain measurement.....	180
Figure 7.12 Response of the sensor patch for the change in capacitance occurring due to the applied strain.....	180
Figure 7.13 Capacitance of the sensor for a bending radius from 11 mm to 6 mm.....	181
Figure 7.14 Response of the sensor for the experiments bending the sensor patch in a cyclic manner. The bent state of the sensor patch caused a decrease in its conductivity value. The inset of the figure shows the (a) normal and (b) bent states.....	182
Figure 7.15 Response of the sensor patch in terms of relative resistance with strain....	183
Figure 7.16 Attachment of the sensor patch on the (a) middle finger of the hand with the assistance of a bandage to determine its (b) movement based on the strain induced on the sensing area of the patches. The two states, flexed and extended, refer to the bent and relaxed condition of the arm respectively.....	187
Figure 7.17 Attachment of the sensor patch on the (a) elbow of the arm with the assistance of a bandage to record its (b) movement based on the strain induced on the sensing area of the patches. The two states, flexed and extended, refer to the bent and relaxed condition of the arm respectively.....	188
Figure 7.18 Attachment of the sensor patch on the (c) neck with the assistance of a bandage to record its (b) movements based on the strain induced on the sensing area of the patches. The two states, flexed and extended, refer to the bent and relaxed condition of the arm respectively.....	190
Figure 7.19 Attachment of the sensor patch on the (a) knee to record its movements based on the strain induced on the sensing area of the patches. (b) The two states, flexed and extended, refer to the bent and relaxed condition of the arm respectively.....	191
Figure 7.20 Response of the sensor patch for a particular frequency (5 kHz) depicting the different capacitance values for the different experimental weights.....	193

Figure 8.1 Response of the graphene – PI sensor patches towards different temperatures values ranging from 30 °C to 50 °C.....201

Figure 8.2 Response of the graphene – PI sensor patches towards different humidity values ranging from 60% RH to 80% RH..... 201

List of Tables

Table 1.1 Features and challenges of some of the commonly used printing techniques to develop flexible electronic systems [41].....	9
Table 2.1 Comparison between the different characteristics of strain sensors where the electrodes are developed with graphene, CNTs and silver.....	30
Table 2.2 Comparison between the different characteristics of electrochemical sensors where the electrodes are developed with graphene, CNTs and silver.....	31
Table 2.3 Summary of some of the selected conditions of preparation of graphene using different methods.....	32
Table 2.4 Comparison between the geometrical patterns of the single-layered graphene sheets [212].....	37
Table 2.5 Summary of the graphene-based electrochemical sensors depicting the differences between the responses concerning the materials and techniques used to develop the sensors.....	44
Table 2.6 Summary of graphene-based strain sensors based on the materials and techniques used to differentiate between the gauge factor and maximum strain.....	47
Table 2.7 Summary of graphene-based electrical sensors based on the materials and technique used to compromise between the maximum strain and electron mobility [313].....	50
Table 2.8 Comparison between the different parameters for the chemical sensing done by GFETs.....	52
Table 2.9 Limitations of graphene as showcased in various research.....	56
Table 2.10 Network protocols standardised by IEEE [393].....	64
Table 4.1 Power and speed combinations of the laser cutting tool to obtain different electrode thicknesses.....	87
Table 4.2 Comparison of different force-sensing resistors available in the market.....	92
Table 5.1 Different pressure values exerted on the sensor along with the repeatability of the output.....	121
Table 6.1 Equivalent circuit parameters (as shown in the inset of Fig. 7(b)).....	130

Table 6.2 Equivalent circuit parameters along with their limits, result and error % to determining the fitted curve on the experimental data..... 138

Table 6.3 Unknown Sample measurement (in ppm) compared with Laboratory standard method..... 167

Table 7.1 Comparative study between the flexible sensors commercially available in the market..... 184

Table 7.2 Comparative study between the strain sensors developed with different fabrication techniques.....185

1

Introduction

Publications pertaining to this chapter:

- **Anindya Nag**, S. C. Mukhopadhyay and J. Kosel, “Wearable Flexible Sensors: A Review”, **IEEE Sensors Journal**, Vol. 17, No. 13, pp. 3949-3960, **July 2017**.

1.1 Flexible Sensors

The intervention of sensors for day-to-day activities has made a significant impact on everybody's life. Sensors are being utilised to monitor and analyse the changes happening in the surrounding environment, and the use of sensors in different applications is increasing every day. They are installed or connected to various objects and operated via control engineering at distant locations. Sensors are used to collect, store and analyse information from inaccessible and partially accessible areas without much human intervention and for security purposes. Sensors have been used for more than 2000 years [1]. A sensor is defined as an object to detect and respond to the changes happening in its physical environment. The first sensor to be used commercially was a thermostat. But around the early 19th century there was an increase in the use of sensors [2]. The increase in demand has always required a better quality of sensors than the existing ones [3]. The usage of sensors has almost tripled in the last two decades [4]. In today's world, nearly all the applications are somewhat connected with sensing systems [5]. The types of sensors that are developed depend mainly on the applications in which they are to be used. The differences among the kinds of sensors lie in their size, sensitivity, operating principle, etc. Some of the common types are electrical, magnetic, chemical, thermal, etc. The cost of a sensor depends on the availability of raw materials, the fabrication process and manufacturing costs. These attributes reflect the properties of the sensor which decides the applications the sensors are going to be used for, for example, sensors substrates and electrodes developed from nanomaterials and flexible substrates like polydimethylsiloxane (PDMS). In earlier days, sensors with rigid substrates were used for measurement [6-8], health monitoring purposes [9-11], etc. Until a few years ago, single-crystal silicon has been the dominant semiconductor material used as substrates for these sensors. Some of the advantages of using rigid silicon sensors include their inexpensiveness, high sensitivity, and low leakage current due to the high potential barrier in silicon. Even though these sensors are used on a large scale, there are certain associated disadvantages including the high cost of fabrication, high input power for operation, mechanical damage and stiffness. Due to the mentioned limitations of silicon sensors, flexible sensors are more and more preferred in different applications [12]. The limitations of the silicon sensors are rectified by flexible electronics. Around five decades ago, thin-film transistor circuits were developed which formed a new emerging segment for sensors. Gradually, the circuits were

enhanced in their performance, costs and efficiency. This was followed by micro-electromechanical systems (MEMS), which were developed in the late 20th century. MEMS cover a vast range of systems ranging in size from a few microns to a few millimetres. MEMS have improved significantly regarding size, efficiency, and power consumption compared to the earlier devices.

After the advent of the utilisation of sensors for ubiquitous monitoring [13], their applications in daily life have been ever increasing. They have revolutionised the quality of human life with their uses in a varied range of applications. Earlier, an event took hours to study or monitor can be addressed in minutes or seconds with the help of smart sensing systems. The dynamic use of sensors has led to an ever-growing modification of existing sensors. Nowadays, almost every industrial, domestic and environmental sector utilises sensors for improving the quality of life [7, 14-18]. They have been used for different sectors like gas sensing [6, 7], environmental monitoring [19, 20], monitoring constituents in food quality monitoring [14, 21, 22], physiological parameter monitoring [16] etc. to name a few.

Sensors can be broadly classified into two categories, flexible [12] and non-flexible [23]. The former is fabricated from materials which are malleable to a certain extent without changing their properties, whereas the latter is rigid and made of brittle materials. The non-flexible sensors were developed earlier among which the ones with silicon substrates are the most common ones. Even though these sensors find a vast field of applications, there are certain disadvantages like their brittle nature, stiffness, etc. These disadvantages are prominent, especially when the sensing system is associated with monitoring physiological parameters of a person or any application which involves some stress on the sensor, thus damaging it. This result in choosing an alternative approach where the sensor can be dynamically used, thus negates any inconvenience for the person or protecting the sensor from damage while using it on a bendable object. Apart from this, low fabrication cost, light weight, better mechanical and thermal properties are some of the advantages which make the use of flexible sensors a better approach. Figure 1.1 shows a schematic of a monitoring system to sense physiological parameters like the heart rate and respiratory rate of a person and transmit the data wirelessly to the cloud via any information gateway [24]. This is a quick and efficient system because any abnormality in the transmitted data can generate a notification to the healthcare provider or family members.

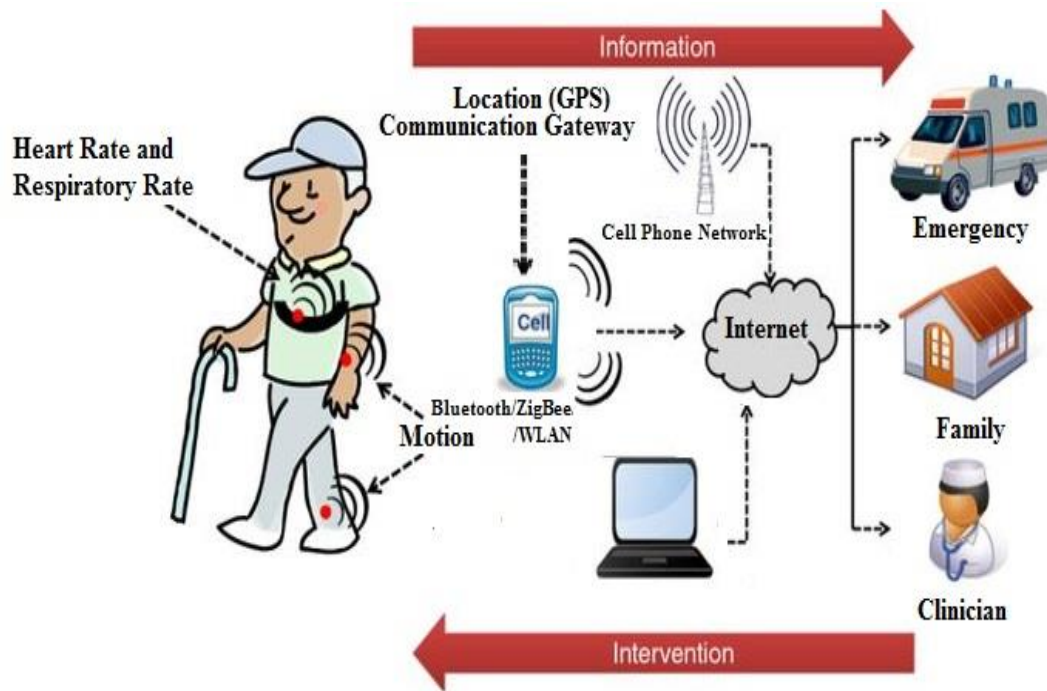


Figure 1.1 Schematic representation of the use of wireless sensors for physiological parameter monitoring [24]. Reproduced from Patel, S., Park, H., Bonato, P. et al. A review of wearable sensors and systems with application in rehabilitation. *J NeuroEngineering Rehabil* 9, 21 (2012). <https://doi.org/10.1186/1743-0003-9-21>. (CC BY 2.0)

The materials chosen for developing flexible sensors are processed with various methods depending on the dimension of the final product. For example, for sensors with tiny dimensions, as in from a few microns to a few millimetres, processes like photolithography [25], screen printing [26], 3-D printing [27], ink-jet printing [28], laser cutting [29], etc. are commonly used. Photolithography is one of the frequently used techniques in microfabrication. A photo-sensitive material called the photoresist is spin-coated on the substrate on which a geometrical pattern is formed by ultra-violet (UV) light. Two types of photolithographic processes occur, masked and maskless. The former consists of a patterned mask through which the light is passed to imprint the design on the substrate. The maskless one does not involve any photomask, rather the patterns are uploaded on the system and are directly patterned on the substrate. Exposure to light polymerises the photoresist on the substrate on the patterned locations. Following the exposure to UV light to form the patterns, the residual photoresist is removed by an etching process. Two types of etching, ionic or dry and chemical or wet etching, are performed. Screen printing is one of the oldest techniques used to develop critical devices. This process is like photolithography except that smaller dimensions can be obtained with photolithography. A pattern is produced on a stencil through which ink or a liquid is transferred to a substrate to

transfer the pattern. The design is created and attached to a mesh where the ink is poured to develop the design of the model on the substrate. The mesh is formed with polymers and fixed to a frame for support. Ink is dropped and squeezed by a squeegee to develop the pattern down on the substrate. 3-D printing is a relatively new technique which is used to generate three-dimensional objects via printing. This method began in the early 1980s. The shapes or geometries formed by this approach are designed by different computer-aided models. The models are saved in a file extension depending on the 3-D model printer. The design or model is then divided into series of thin layers which produces G-code. These codes are instrument-specific and represent the specific actions to develop the designed object. This technique has many industrial applications like metal wire processing, lamination, etc. Inkjet printing is another technique which was developed in the late 20th century to design and fabricate different types of printed devices. This technique has certain advantages like fine resolution, no warm-up time, low per-page costs, and improved picture quality compared to other printing technologies. Two types of drop-on-demand (DOD) processes are used in this method: thermal and piezoelectric. The former consists of a series of chambers with each containing one heater. When a current pulse is passed through the heating element of the chamber, the ink vaporises and forms a bubble. This increases the resultant pressure of the chamber, thus ejecting a droplet onto the substrate. The piezoelectric ones change their shape with an input voltage, thus creating an increase in pressure which forces the bubble out of the nozzle. Laser cutting is a technique developed in the early 1960s when this process was mainly used to create diamond holes. There are two different types of laser cutters, CO₂ and Nd/Nd-YAG lasers, of which the former is more popularly used than the latter. The laser material is stimulated which leads to total internal reflection to partial mirror because of which a stream of monochrome coherent light comes out of the laser nozzle. The methods used for laser cutting mainly include vaporisation, melt-and-blow and reacting cutting. This approach has certain advantages like small sample preparation time, reduced contamination of the finished sample, dimensions up to a few microns of the sample, low thermal influence, clean-cut edges and smooth finished product. Laser cutting devices are commercially available with different input powers which are decided by the sample to be sliced or ablated.

Different kinds of materials are used as substrates and electrodes in developing flexible sensors. The raw materials are selected for different products depending upon their inherent properties. For example, commercially available sticky tapes are cheaper than polymers, but they would not form a very efficient flexible substrate due to their high Young's

modulus (E). Similarly, gold has a higher conductivity than aluminium but is more brittle in nature. The threshold for the breaking point for flexible electrodes will be lower than the aluminium counterparts. Thus, a material chosen for fabrication has to offer a balance between its availability, the cost of extraction, its electrical and mechanical properties, and ultimate use as a sensing material.

Some of the substrates commonly used to develop flexible sensors are polydimethylsiloxane (PDMS) [30], polyethylene terephthalate (PET) [31], polyethylene naphthalate (PEN) [32], polyimide (PI) [33], poly(3,4-ethylenedioxythiophene):polystyrene sulfonic acid (PEDOT:PSS) [22], etc. PDMS is a polymer which is developed as repeated monomers of siloxane molecules. It is mostly preferred over other flexible substrates in applications having rheological requirements. It is also transparent, non-toxic, non-flammable and hydrophobic in nature. The biggest advantage of using PDMS is its ability to form strong interfacial bonding with any nanomaterials to form nanocomposites. PET is a carboxylate-group polymer developed mainly for synthetic fibres. It is prepared from ethylene glycol and dimethyl terephthalate. This is a semi-crystalline resin which is a more viscous polymer than PDMS. A few of the most common applications of PET are plastic bottles, packaging of foods and beverages. PEN is a polymer like PET which is also developed from carboxylate polymer and ethylene glycol. This polymer has higher dimensional and temperature stability than PET. It is mainly used as piezo-resistive tapes, for packaging, and solar-cell protection. PI is one of the oldest polymers and is mass produced for its applications. The reaction between a diamine and dianhydride is used commonly to form the polymers. It mainly exists in two types of structures, a heterocyclic structure, and a linear structure. It is mostly used as to create commercial tapes due to its high chemical resistance and good mechanical properties. PEDOT: PSS is one of the most common conductive polymers available in the market. This is developed from two isomers of the sulfonate and polystyrene groups. It is also transparent, and a flexible polymer, which makes it suitable for applications like in printing, electrolytic capacitors.

Various flexible conductive materials are used to develop flexible sensors. Some of them are Carbon Nanotubes [34], silver [35], copper [36], gold [37], iron [38], etc. The conductive material chosen to fabricate the electrodes depends on the process with which the sensor is manufactured. For example, conductive inks are used to develop the electrodes with the screen-printing technique. Nanotubes are cylindrical structures in nanoscale with extraordinary electrical, thermal and mechanical properties. These tubes are sigma-bonded

which makes them much stronger than their macro counterparts. Nanowires have a high aspect ratio, where the ratio of length to width is greater than 1000. These nanowires are grown by various techniques like the vapour-liquid-solid method, solution-phase synthesis, non-catalytic growth, etc. But the conductivity of nanotubes is greater than that of nanowires due to the lower mean free electron path of the latter. Also, the conductivity is higher in nanotubes due to the ballistic transport of electrons.

1.2 Printed Electronics

The recent advancement of printing technology has brought a leap of progress in the electrical and electronics field. Printed technology has been adapted to develop sensitive electronic systems [39, 40] due to their simplified processing steps, reduced material wastage and overall low fabrication cost. These features make it a very favourable choice to use for the development of multifunctional electronic circuitry over large areas. The use of printed electronics has taken a major role in the fabrication of microelectronics using standard printing methodologies. Contact and non-contact processes are the two categories in printing technology based on their techniques. The contact process includes the involvement of physical contact of the patterned inked surfaces with the substrate on which the design has to be imprinted. Some of the common technologies of contact printing comprises R2R, flexographic and gravure printing.

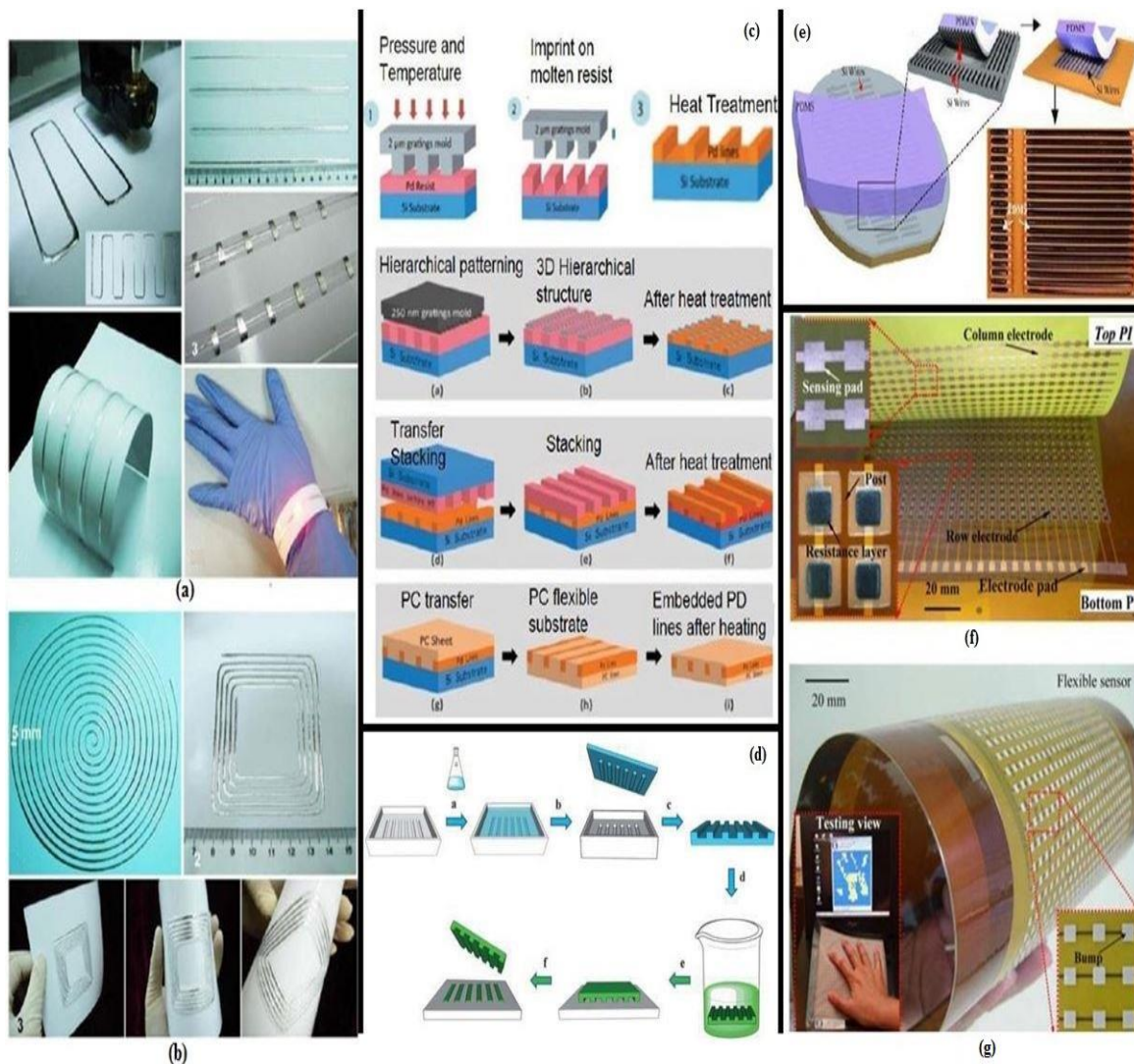


Figure 1.2 Fabrication of flexible sensors using various printing techniques. (a) Direct printing using an ink-jet printer to coat gallium indium alloy on the paper. The wires developed from printed alloys are attached to the LED. (b) Optical images of the printed sensor for various components like Inductance coil and RFID antenna. (c) Schematic diagram of nano-printing done using a silicon mould. After the flowing of the molten precursor, demoulding is done followed by heating the sample at 250 °C. Three different types of nano-printing: hierarchical patterning, transfer stacking and polymer transfer are shown to demonstrate the differences in their techniques to develop sensors. (d) Schematic diagram of micro-contact printing. The pre-polymer is poured and cured on the pre-structured master to develop the elastomer stamp. The stamp is peeled off the master, cut into small pieces and used as a printing ink to stamp the replicated shape on a surface. (e) Transfer printing is done using the conformal stamp of a polymeric stamp with silicon wires. The wires are peeled off and transferred to the final substrate. (e) Screen printing of pressure sensors done on large flexible polymer films (f) with bumped structures on the top of the film [41]. Reproduced from S. Khan, L. Lorenzelli and R. S. Dahiya, "Technologies for Printing Sensors and Electronics Over Large Flexible Substrates: A Review," in *IEEE Sensors Journal*, vol. 15, no. 6, pp. 3164-3185, June 2015, doi: 10.1109/JSEN.2014.2375203. (CC BY 4.0)

Table 1.1 Features and challenges of some of the commonly used printing techniques to develop flexible electronic systems [41]. Reproduced from S. Khan, L. Lorenzelli and R. S. Dahiya, "Technologies for Printing Sensors and Electronics Over Large Flexible Substrates: A Review," in IEEE Sensors Journal, vol. 15, no. 6, pp. 3164-3185, June 2015, doi: 10.1109/JSEN.2014.2375203. (CC BY 4.0)

Printing Type	Features	Challenges
Screen	<ul style="list-style-type: none"> • Conventional printing technique. • Fast and controlled deposition of solutions. • Open area of mesh is defined with pre-structured patterns. 	<ul style="list-style-type: none"> • Resolution greater than 30 microns cannot be obtained. • Occurrence of spreading and bleeding of printed solutions. • Deteriorated patterns due to the spreading of the inks.
Inkjet	<ul style="list-style-type: none"> • Lower viscosity of solutions compared to screen printing. • Specific deposition of droplets. • Lower material wastage compared to other techniques. 	<ul style="list-style-type: none"> • Unequal distribution of dried solute causing coffee-ring effect. • High chances of clogging because of mis-fringing. • Pixilation-related issues due to drop-on-demand.
Gravure	<ul style="list-style-type: none"> • The substrate should be smooth, have compressible porosity and wettability. • The ink should be high viscosity, solvent evaporation and drying rate. 	<ul style="list-style-type: none"> • Expensive process. • Detect and pick up related challenges due to contact printing. • Proper ratio of cell spacing to cell width.
Offset	<ul style="list-style-type: none"> • Popular technique for printing on hard surfaces. • The goal is for 100% transference. • Speed and pressure and the main process parameters. 	<ul style="list-style-type: none"> • Degree of solvent absorption effects the width of the printed line. • Spreading of line during set process. • High rolling resistance due to the fast rolling speed.

Flexographic	<ul style="list-style-type: none"> • Patterns are raised on low-cost flexible plate using photolithography. • Better pattern quality with respect to the contact printing methodologies. 	<ul style="list-style-type: none"> • Layer cracks and non-uniform films. • Tensile stress occurring due to solvent evaporation or high temperature. • Divergence from nominal specified values with speeding.
Micro-contact	<ul style="list-style-type: none"> • Stamp is inked and pressed against the substrate surface to transfer the design. • Used for biological sciences to develop micro and nano-structured surfaces. 	<ul style="list-style-type: none"> • Hydrophobic problems of some polymers like PDMS with the polar inks. • Change in the pattern sizes due to swelling to the stamp during inking process.
Nano-imprinting	<ul style="list-style-type: none"> • The master material is pressed into a polymeric material cast at specific temperature and pressure. • Creating a thickness in contrast to the polymeric material. 	<ul style="list-style-type: none"> • Damage to the fragile nanostructures while removing the cast material. • Time-consuming technique compared to other contact printing process. • Difficult to replicate structures with resolution below 50 nanometres.
Transfer	<ul style="list-style-type: none"> • Transfer and printing occurs through solution casting. • Combined techniques of photolithography and micro-contact printing. 	<ul style="list-style-type: none"> • Misalignment of neighbouring strips during undercutting. • Maintaining the surface quality of the backside of the flipped transferred structures is difficult.

The other type of printing approach, non-contact printing, allows the solution to be dispensed on the substrate through openings in a mask in a defined pattern. The substrate below the mask is moved in a pre-programmed manner to define the shape of the designed electronic device. Some of the common printing technologies adapting this technique are screen and ink-jet printing. The non-contact printing approach is more advantageous than

that of the contact approach due to the higher resolution of the patterns, speed and reduced material wastage of the former to the latter. Figure 1.2 shows various types of sensing materials developed with the contact and non-contact processes [41]. Although the non-contact processes provide certain advantages over the contact methods, there are certain challenges that needs to be addressed in both methodologies. Table 1.1 gives a summary of some of the advantages and disadvantage of the contact and non-contact processes obtained from different research work done on this area to develop flexible electronic systems.

Apart from the approach of the printing methodology, other categories such as the choice of conductive material to develop the colloidal solution are also studied to determine the rheological properties of the solutions. Various types of materials including conducting [42-44], semi-conducting [45-47] and dielectric [44, 48, 49] materials have been used to form pure and hybrid printed electronic systems from organic and inorganic polymers. The choice of the material to develop printed sensors depends on their ability to vary some of the parameters like surface tension, viscosity, electrical and thermal conductivity and compatibility of the resultant colloidal solutions. There are three main categories of conductive materials used in the printing technologies till date. In the first category of conductive materials, metals like silver [50], gold [51], and copper [52] inks are used to design the electronic part of the system. Apart from the high cost of these materials, the oxidation of some of the metallic pastes like copper and aluminium limits their applications. In order to solve this problem, some of the organic conductive polymers have been reported [53, 54] to be used in printing technologies. The conducting polymers can be of various forms, depending on the level of doping. Along with the use of the pure ones called the intrinsic conducting polymers [55], the level of doping is varied with n-type and p-type dopants to make their work function close to that of the semiconductors. Some of the common conducting polymers used for printing technology are polyacetylene [56], polyaniline [57], polythiophene [58], PEDOT:PSS [59], etc. Even though these conducting polymers are used to a large extent to develop printed electronic devices, the electrical conductivity of these materials, being much lower than for the conductive metals, curbs their applications. Another popular choice of conductive materials for the printed technology are the nanocomposites developed from using nano-fillers of different metallic nanoparticles using organic elastomers at varied ratio. The change in the amount of nanofillers in the polymer matrix is based on the percolation threshold of these materials which defines the dispersion of the former in the latter. Even though the electrical and

mechanical properties of the resultant nanocomposites vary according to the amount of nano-fillers used in the polymer matrix, the agglomeration of the nanoparticles in the polymer affects the rheological properties of the ultimate result. This is somewhat addressed using surfactants and volatile additives with the nanoparticles. In the semiconducting materials, the capability of the transduction of the free carriers of some of the elements like crystalline Si [60] and oxides of transition metals [46] makes them a popular choice for printing technology. Similar to the organic conducting polymers, the organic semiconductors [61] are also used to a certain extent due to their solubility and ability of proper dispersion to form colloidal solutions. For the use of the dielectric materials to form the colloidal solutions of the printed devices, the organic materials are preferred over the inorganic ones due to their low cost and ability to dissolve in various solvents and solutions.

The categorisation in the different types of materials used to develop the substrates of the flexible electronics is based on their physical, chemical, mechanical and optical properties including the dimensional and thermal stability, bendability, transparency and emissive properties. Thin glass, metal foils and plastics are the three types of substrates chosen to develop the flexible systems. With the disadvantages of the intrinsic brittle property of the thin glass and the surface roughness of the metal foils, the plastics lacking these two limitations certainly possess advantages over the other two. Among the different plastics used as substrates for the printing technology, amorphous and semi-crystalline polymers are the common ones. Some of the examples of amorphous and semi-crystalline plastics include Polycarbonate (PC), Polyether sulfone (PES) and polyethylene Terephthalate (PET), Polyethylene Naphthalate (PEN), and Polyether ether ketone (PEEK) respectively. Among these two types, the semi-crystalline ones are more advantageous due to their higher glass-transition (T_g) compared to the amorphous ones.

1.3 Conclusion

The chapter gives a brief introduction about flexible sensors and the printing technologies used to fabricate them. Initially, along with the introduction and background of the flexible sensors, the raw materials commonly used to develop the electrodes and substrates are explained. Some of the commonly used fabrication techniques used to fabricate the flexible sensors are also described in this section. Some of the conductive

metals and polymers mentioned in this chapter are used as the raw materials to develop the novel sensor prototypes for my PhD work. The second section explains the printing techniques used to develop flexible electronic and electrical systems. Out of the different fabrication techniques in printing technologies, laser printing and 3D printing techniques were used due to their low processing cost, easy sample preparation and ability to have smooth and flexible cuts of the finished products. The significance of printed electronics has been highlighted in terms of the different printing technology available to develop flexible sensors along with the features and challenges while operating them. This chapter marks the initiation in the development of different printed flexible sensor prototypes that are elucidated in the succeeding chapters. The sensor patches developed with the laser and 3D printing techniques were used for various purposes including monitoring of environment, industrial and health parameters. The use of the different sensor prototypes for their respective applications is because of their physiochemical suitability for that application. The development in the field of microfabrication of sensors has been highlighted in this thesis along with their potential to be used in the practical scenarios.

1.4 Research Contributions

The major contributions of this research work lie in the design, development, characterisation and implementation of four different types of novel flexible sensor prototypes. The novelty in the work lies in the conjunction of the processed materials and the techniques used for fabrication. The theory behind the working principle of the flexible sensor patches was studied and presented to depict the electromechanical changes taking place during the experimental processes. The sensor prototypes were implemented in major sectors including monitoring of health, environmental and industrial parameters. The fundamental idea behind these developed sensor prototypes was for the advancement of the micro and nano-electronic industry, which can subsequently fabricate better sensors in terms of cost, size, power consumption and efficiency.

1.5 Organisation of the Thesis

Chapter 1: Introduction

The introduction briefly describes the flexible sensors and their employment in wearable sensing systems. Here, some of the common materials along with the fabrication techniques are showcased. It also explains the definition of printed electronics and its significance in the development of flexible systems in the electronic world. Finally, it gives the research contributions along with the organisation of the thesis.

Chapter 2: Literature review

This chapter gives a detailed background study of the research work done on flexible sensors with different conductive materials like CNTs and graphene. The sensors developed using CNTs and graphene are categorised into electrochemical, strain and electrical types, based on their working phenomenon. The current challenges faced by these sensing systems along with some of the possible ways to address them are explained in this chapter. Finally, some of the significant work on wearable flexible sensors along with the sensor networks used to operate them is briefly explained.

Chapter 3: Interdigitated Sensing and Electrochemical Impedance Spectroscopy

Due to the development of the electrodes of all the novel sensor prototypes in the form of interdigitated sensors, the detailed explanation of the working principle of these sensor patches is explained in this chapter. It showcases the relation between the different electrical parameters related to the structure and working principle of the sensor patches, whose changes were monitored during the characterisation and utilisation of the sensor patches. This is followed by a brief explanation of the electrochemical impedance spectroscopy (EIS) technique and the reasons for its utilisation as the tool to determine the changes in the output of sensor patches taking place during their operation.

Chapter 4: Carbon Nanotubes- Polydimethylsiloxane Sensor

This chapter explains the design, fabrication and implementation of a novel sensor prototype developed from carboxylic acid functionalised Multi-Walled Carbon Nanotubes (MWCNTs) and Polydimethylsiloxane (PDMS) as the conductive and substrate materials respectively. The electrodes were carved out from a layer of nanocomposite developed by mixing the MWCNTs and PDMS at definite proportions. The highlight of this chapter is related to the formation of the electrodes via laser cutting of the nanocomposite layer, which was developed with the uniform mixing of minimum amounts of nano-fillers in the polymer matrix. The sensor prototypes were then characterised to determine their frequency response and characteristics for stress-strain measurements. The sensor prototypes were then used for monitoring physiological movements like limb movements and respiration. They were also used for tactile sensing of low pressures to highlight their potential uses in prosthetic limbs.

Chapter 5: Aluminium- Polyethylene Terephthalate Sensor

A novel sensor prototype was developed from aluminium and polyethylene terephthalate (PET) as the electrode and substrate materials respectively. The highlight of this chapter is related to the single step development of the sensor prototypes from a single raw material. The electrodes were carved from the aluminium side of the metallised polymer films to form the sensor prototypes. The characterisation of the sensor patches was done to determine the operating frequency and their responses towards stress-strain measurements. The sensor prototypes were used for tactile sensing using different pressures applied from thumb, finger and palm.

Chapter 6: Graphene- Polyimide Sensor

This chapter gives the fabrication of laser-induced graphene sensor prototypes from low-cost commercial polymer films. This graphene was photo-thermally generated from polymer films followed by its transfer to sticky tape to be used as electrodes to form sensor prototypes. The highlight of this chapter lies in the quick and low-cost development of the sensor prototypes with highly conductive electrodes. Due to the advantage of the biocompatibility of graphene electrodes, these sensor prototypes serve a huge potential in

their uses in industrial and environmental applications. The characterisation of the graphene sensors was done to determine the passive elements contained in the equivalent circuitry of the sensor prototypes. These sensors were then used for monitoring of different environmental parameters like the concentration of salinity and nitrate in water bodies and as taste sensors to determine the taste of various food products.

Chapter 7: Graphite- Polydimethylsiloxane Sensor

This chapter explains the design, fabrication and implementation of another sensor prototype, developed from Graphite and PDMS in 3-D moulds. The highlight of this chapter lies in the utilisation of the 3-D printed moulds to develop template for casting of graphite and PDMS on it. Due to the flexible and conductive nature of the developed sensor prototypes, they were used to determine the movement of different strain-induced body parts and for force sensing. The sensor prototypes were characterised to determine the changes in their responses for stress-strain measurements along with the repeatability of the responses for iterative bending cycles. The strain-induced application was carried out by placing the sensor prototypes on different parts whereas the sensing of very low forces was done by applying various weights to the sensing area of the prototype. These multi-functional sensor prototypes hold a key role in biomedical applications with the continuous rise in the use of the 3-D printing technique in different sectors.

Chapter 8: Conclusion, Challenges and Future Work

A conclusion and suggestions for future work are provided in the last chapter of the thesis highlighting the work done during my doctoral candidature along with future opportunities. The conclusion briefly explains the work on the use of the printing technology to develop various novel sensor patches and their utilisation for monitoring of different applications. The highlight of this chapter lies in the different techniques used to develop the flexible prototypes, each one having its important application in the sensing world. Future opportunities are given with some of the techniques that can be employed to develop the novel sensor prototypes. It also states some of the applications on which the already developed sensor prototypes can be exploited by showcasing their results.

2

Literature Review

Publication pertaining to this chapter:

- **Anindya Nag** S. C. Mukhopadhyay and H.S. Nalwa, “Carbon Nanotube-Based Flexible Sensors”, Functional Nanomaterials and Nanodevices, **American Scientific Publishers**, pp. 1-44. ISSN: 1-58883-257-0, **2018**.
- **Anindya Nag**, A. Mitra and S. C. Mukhopadhyay, “Graphene and its sensor-based applications: A review”, **Sensors and Actuators A: Physical**, Vol. 270, pp. 177-194, **February 2018**.
- **Anindya Nag**, S. C. Mukhopadhyay and J. Kosel, “Wearable Flexible Sensors: A Review”, **IEEE Sensors Journal**, Vol. 17, No. 13, pp. 3949-3960, **July 2017**.

2.1 Introduction

Since most of the research work explained in this thesis is based on CNTs, and graphene and other flexible sensors, a lot of background work has been done on these topics. The research on the preparation and properties and some of the flexible sensors based on these materials, are explained in the succeeding sections. The explanation on the different types of flexible sensors with the use of CNTs and graphene as electrodes are based on electrochemical, strain and electrical sensing. The literature review also includes the limitations and future challenges of the existing CNTs and graphene-based sensors with some of the possible ideas for addressing these issues. This is followed by the brief notes on wearable flexible sensors. This part includes the different types flexible sensors based on the processed materials, the operating principle and the techniques used to operate them. Brief explanations on the networks used to operate the wearable flexible sensors along with the different types of activities that are being monitored are also in this section. The chapter finally ends with a conclusion on wearable flexible sensors.

2.2 Carbon Nanotubes and their Sensor-based Applications

Carbon Nanotubes, in simple words, can be explained as allotropes of carbon which are cylindrically shaped and crystalline in nature. These molecules have an extremely high aspect ratio with excellent electrical, mechanical, and thermal properties. The history of CNTs goes back to the 1980s where a fullerene ball of six carbon atoms (C_{60}) was discovered. These fullerene balls were interpreted as consisting of molecules formed from pure carbon atoms. CNTs can be defined as allotropic forms of carbon shaped in a sp^2 hybridised cylindrical structure. The sp^2 hybridisation of carbon atoms in CNTs resembles that of graphite, i.e., alkynes, which is stronger than sp^3 hybridised molecules like alkanes. The strength of sp^2 hybridised carbon atoms is around 33% greater than that of sp^3 carbon atoms [62]. The CNTs are formed from a rolled graphene sheet [63]. The walls in CNTs are graphene sheets, where a single sheet is stacked on top of other graphene sheets. The nanotube sheets are stacked on top of each other at definite angles, called 'chiral angles.' Chirality is defined as the asymmetric nature of the molecule with its mirror image. The stacking of the nanotubes is called π -stacking, which happens due to the Van der Waal's forces of individual nanotubes against each other. One of the properties determining the

amount of these forces is the surface area of the atoms of the CNTs. The result is due to the exposure of the atoms on both the interior and exterior sides of the tubes, the resultant surface area of CNT is quite high, thus causing higher Van der Waal's forces [64]. These CNTs have a high strength to weight ratio compared to other contemporary materials, which makes them an attractive choice to combine with other polymers to form nanocomposites.

2.2.1 Synthesis of Carbon Nanotubes

CNTs are developed by different techniques including arc-discharge evaporation, laser vaporisation, and chemical-vapour deposition (CVD). Arc -discharge evaporation is the oldest method of all where the nanotubes are developed from an arc-discharge operation with two carbon electrodes in the presence of an inert gas [65]. One of the electrodes used to be a fixed one, and the other one was adjustable during the discharge process. Earlier, the arc current used to very high in the range of 200 - 225 A, due to the absence of a catalyst. After the process, one of the carbon electrodes used to have the deposited nanotubes which were formed from the other electrode. So, the diameter of the electrodes would change after the process, which determined the number of nanotubes formed. The catalytic synthesis of CNTs was carried out with an arc current of around 70-80 A in an argon and helium atmosphere mixed in a certain ratio [66]. The catalysts used for this method were incorporated by evaporating them with the carbon feedstock. The highly magnified (100 nm) Scanning Electron Microscopic (SEM) and Transmission Electron Microscopic (TEM) images of vertically aligned CNTs grown with a catalyst are shown in Figures 2.1(a) [67] and 2.1(b) [68]. A computer controlled stepping motor [69] was used to fabricate CNTs in the arc discharge method. This helped in maintaining a constant gap between the electrodes. Hydrogen as an alternative to helium is used as a gas in the vacuum chamber during the arc-discharge process. Another technique involved in the arc-discharge process is the filling up of the positive electrode with a mixture of metallic catalyst and graphite powder [70]. This helps in the deposition of a large amount of a homogeneous distribution of formed carbon filaments. Laser vaporisation was another technique used a lot earlier to fabricate CNTs. Here, a laser beam with a controlled laser pulse speed was focused on a metal/graphite composite object [71].

Figure 2.1 removed due to copyright

Figure 2.1 (a) SEM image of vertically aligned CNTs [67]. (b) Highly magnified TEM image of CNTs grown with a catalyst. Reprinted with permission from [68].

The beam is computer controlled and scanned through the target surface, forming carbon spots. This was swept in the presence of an inert gas to deposit carbon on a collector. The quartz tube is another option that was used to generate CNTs by the laser vaporisation method [72]. The tube was placed in the oven during the evaporation process at a fixed temperature and pressure. The developed CNTs were collected inside the tube with a filter. Near-infrared photoluminescence is one more option that was associated with the laser vaporisation method to develop CNTs [73]. Tiny structures of up to 1 nm were prepared using this approach. The photoluminescence was sensitive to the acid-treated CNTs whereas raw CNTs did not show any changes to photoluminescence. But the low yield of CNTs was one of the disadvantages of this method compared to the arc-discharge and CVD techniques. The fabrication of CNTs with catalytic CVD is the most popular and recently used method. The elements used to prepare the catalyst vary depending on the configuration of the CNTs. Work with magnesium-cobalt-molybdenum-oxygen has been done to develop double and triple-walled CNTs [74]. These elements were mixed in a fixed proportion and dissolved in deionised water with urea or critic acid as the fuel. Iron-Molybdenum, prepared from thermal decomposition, was also used to develop SWCNTs [75]. Pyrolytic decomposition of hydrocarbon gasses like methane, benzene was another process tried in CVD [76]. The lower operating temperature compared to the arc-discharge and laser-vaporisation methods are one of the advantages of using this method.

2.2.2 Characterisation and Properties

Based on their structural differences, CNTs can be classified into different categories: single-walled carbon nanotubes (SWCNTs), double-walled carbon nanotubes (DWCNTs), and multi-walled carbon nanotubes (MWCNTs). The double-walled CNTs properties have a highly resembling those of SWCNTs. This structural difference distinguishes the properties of the different types of CNTs. SWCNTs can be seen as a single strip of graphene sheet from an infinitely long rolled-up sheet [63]. These structures were the first type of Nanotubes developed after the introduction of fullerene balls in the early 1990s. These structures were fabricated by the arc-discharge process, with iron or cobalt as the catalyst in the reactor. Later, nickel and cobalt mixtures or a complex iron-carbon monoxide-acetylene were used as catalysts to manufacture SWCNTs using laser vaporisation and CVD methods respectively [77]. Hydroxyl groups are another choice used as a catalyst to generate high-purity SWCNTs [78]. The hydroxyl ion was used for its etching effect to suppress products other than the SWCNTs. MWCNTs can be defined as multiple rolled sheets of carbon atoms. The schematic diagram [79] with its HR-TEM image [80], of a single layer of an MWCNT, are shown in Figures 2.2(a) and 2.2(b). The band gap between the conducting and insulation layers in SWCNTs is higher than that of the MWCNTs because the former has a higher probability of exhibiting semi-conductive behaviour than the latter one. The assembly or accumulation of SWCNTs is weak due to their poor solubility in liquids. This was addressed by developing the SWCNTs in an aligned way [81]. This was done applying an electric field in a range of 5-10 V applied DC bias voltage. The MWCNTs can be defined as multiple sheets of graphene rolled to form concentric cylindrical tubes. These nanotubes are preferred over the SW for application purposes due to their ability to form higher interfacial bonds with the mixed matrix. MWCNTs form stronger covalent bonds with the nanocomposite material than SWCNTs. One of the disadvantages of using CNTs, especially SWCNTs, is their inability to dissolve in polar solvents due to their kinetic instability.

Figure 2.2 removed due to copyright

Figure 2.2 (a) Schematic diagram of an MWCNT [79]. (b) HRTEM image of the multi-layered structure of a single MWCNT [80].

Surfactants like sodium dodecyl sulphate (SDS) and chloroform [82] are then used to help the CNTs to dissolve in the solvents. The advantage of using MWCNTs over SWCNTs as the conductive material is that changes in their length can vary their dispersion level in the polar solvents [83, 84]. Functionalisation of CNTs is an important phenomenon to tailor the properties of CNTs. The final properties of the CNTs depend on the functionalised group attached with these nanostructures. Functionalisation groups like $-OH$, $-COOH$ can increase the conductive property of the CNTs. These groups are connected by following several steps like oxidation in a concentrated acid, ozone treatment, etc. [85]. The influence of functionalisation on pure CNTs is analysed in the succeeding sections, where some of the significant work done with and without CNTs on flexible sensors is described.

2.2.3 Electrochemical Sensors

CNT based sensors have been used as electrochemical sensors for years due to their unique chemical, electronic and thermal properties compared to other conductive materials [86, 87]. Owing to their highly hydrophobic nature, insensitivity to oxygen and light, along with high conductivity, a large surface area, as well as a high aspect ratio, CNTs have been a preferred choice for ion-selective electrodes (ISE) in potentiometric sensors. Below are

some examples of the use of CNTs as an electrochemical sensor in different applications. [88] developed flexible electrochemical sensors by coating individual single-walled carbon nanotubes (SWCNTs) with a conductive poly(3,4-ethylenedioxythiophene) (PEDOT) thin layer.

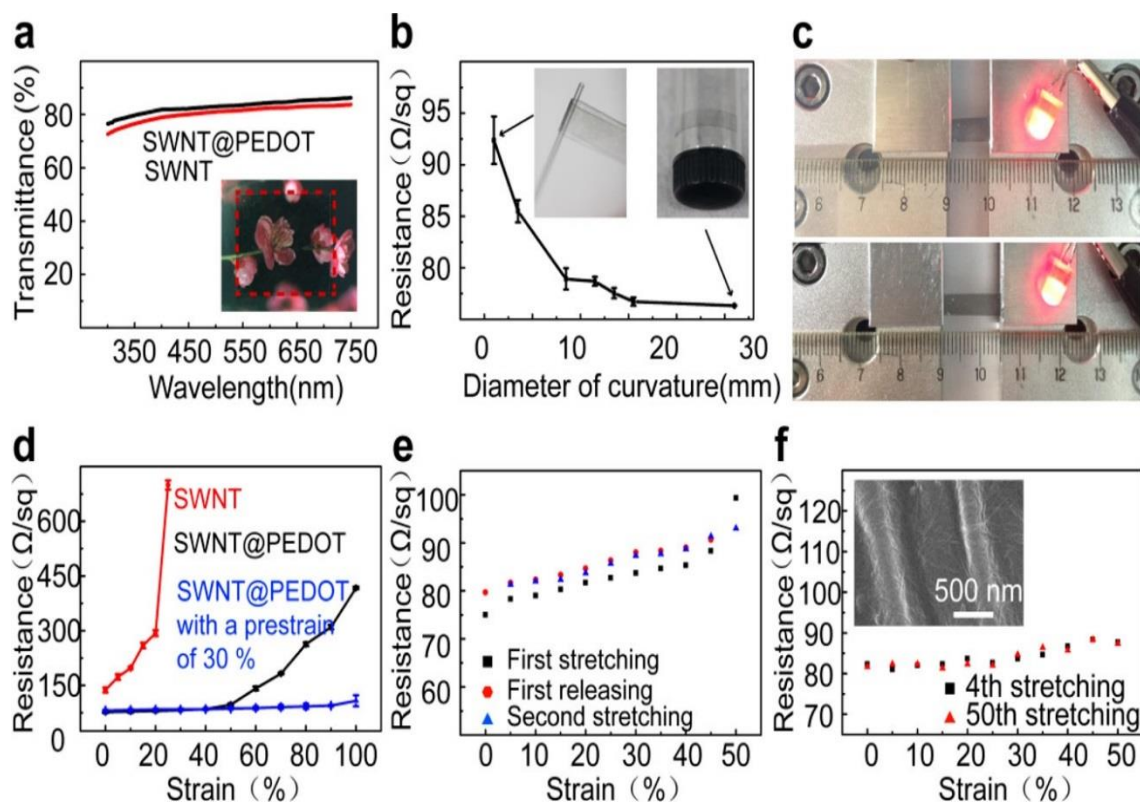


Figure 2.3 (a) Transmittance spectra of SWCNT/PEDOT film in the 350 to 700 nm region. (b) The resistance change of SWCNTs@PEDOT/PDMS film as a function of bending radius. (c) LED integrated circuits under 0% and 50% tensile strains. (d) A comparison of the resistance changes of SWCNTs (red line), SWCNTs@PEDOT/PDMS (black line), and SWCNTs@PEDOT/PDMS films with 30% pre-strain (blue line) as a function of tensile strains. (e,f) The variation of resistance for the SWCNTs@PEDOT/PDMS stretchable films in the first and second stretching cycles (e), and fourth and fiftieth (f) stretching cycles. [88]. Reprinted with permission from Zi-He Jin, Yan-Ling Liu, Jing-Jing Chen, Si-Liang Cai, Jia-Quan Xu, & Wei-Hua Huang. *Conductive Polymer-Coated Carbon Nanotubes To Construct Stretchable and Transparent Electrochemical Sensors Analytical Chemistry* 2017, 89(3), 2032-2038 DOI: 10.1021/acs.analchem.6b04616 American Chemical Society.

Both the electrical conductivity and the electrochemical properties of SWCNT/PEDOT composite films were significantly enhanced as compared to pristine SWCNTs film or PEDOT film. The PEDOT coating helps in protecting the SWCNTs junctions from separation. Figure 2.3 shows the transmittance spectra, the resistance changes of SWCNTs@PEDOT/PDMS composite films as a function of bending radius, strain and stretching cycles and LEDs under 0% and 50% strains. The sheet resistance and optical

transmittance decreased in the 350-700 nm wavelength regions as the thickness of the composite film increased. The sheet resistance of 82 Ω /square and transmittance of 81.5% were observed for 250 nm thick composite film. The SWCNTs@PEDOT/PDMS showed excellent flexibility when measured by wrapping the composite film on cylinders with 1 to 26 mm diameter curvature. No change in LED light intensity was observed when the composite film was stretched to a 50% strain. The electrochemical properties of CNTs have also been used to develop glucose [89-95] and pH [96-98] sensors. Due to the hydrophobic surface and curved sidewall of CNTs with a π -conjugative structure, they interact strongly with aromatic compounds through π -bonding and hydrophobic interactions. Due to this, the formation of a nanocomposite through the mixture of CNTs and monomers/polymers has been largely preferred to form the electrodes of the sensor.

Figure 2.4 removed due to copyright

Figure 2.4 Glucose/pH sensors developed from SWCNTs and PDDA. (a) The bending of standard 4-inch wafer level devices. (b) The comparison of the sensor with a coin [91].

One of the research work on the formation of nanocomposites involve SWCNTs mixed with poly (diallyl dimethyl ammonium chloride) (PDDA) in a layer-by-layer manner between two PET coated electrodes. The SWCNTs used to manufacture these sensors were p-type semiconductor materials functionalised with carboxylic acid (-COOH) groups. These sensors were used to monitor glucose with a sensitivity and linear range of 18-45 μ A/mN and 2-10 nM and a pH with a range of 5-9 [91]. Figure 2.4 shows the fabricated wafer and single dyes.

2.2.4 Strain Sensors

In [99], they developed strain sensors using fragmented single-walled carbon nanotube (SWCNT) papers dispersed in polydimethylsiloxane (PDMS) matrix. The SWCNT/PDMS based sensor showed a gauge factor of 2×10^6 at 5% strain which increased to 10^7 at 50% strain. The high sensitivity arises from the low electrical resistance of 5–28 Ω , of the SWCNT paper and a wide variation in resistance change (up to $10^6 \Omega$) due to the percolated SWCNT in the cracks. The 90- μm thick SWCNT paper-based sensor showed no change in electrical resistance over 10,000 cycles at 20% strain. Use of CNT based flexible sensors as pressure sensors have been done on a large scale. One of the categories of pressure sensors includes the piezo-resistive sensors [100]. The MWCNTs were homogeneously dispersed in PDMS by wrapping it using poly (3-hexylthiophene) (P3HT). The conductivity of the nanocomposite changed with the concentration of P3HT. The distance between the MWCNTs increased with an increase in the polymer, in the ratio between polymer and MWCNTs. The fabricated device showed good results in the pressure range of 0-0.12 MPa. SWCNTs have also been used to develop piezo-resistive sensors where nanotubes grown with the CVD process on a silicon substrate have been transferred into flexible substrates to use them as pressure sensors [101]. The developed sensor achieved a strain resolution of 0.004% with a gauge factor of 269. One of the applications of the pressure sensors is for tactile sensing. A tactile sensor was fabricated from a nanocomposite formed from MWCNTs and photocurable monomer [102]. The MWCNTs were mixed in the polymer with a combination of sonicated and magnetic stirring for its uniform dispersion in the polymer matrix. This nanocomposite was dispensed onto a polyurethane substrate. The resistance of the fabricated sensor changes with a force applied on it. A spatial resolution of 2 mm for the cross-section between the conductive strips was measured by the developing device. Different forces were applied to the sensor, with a threshold voltage where the difference in forces was characterised by the fast Fourier transform.

The pressure and strain sensors have been used for health monitoring purposes. One of the studies involves designing a transducer fabricated from a thin film of piezoelectric poly (vinylidene fluoride) (PVDF) coated with acid-treated SWCNTs [103]. The acid treatment aided the attachment of $-\text{COOH}$ groups to the tubes which helped them to get dispersed in water. Skin-like pressure sensors were also fabricated with CNTs which behaved as transparent strain sensors [104]. Isotropically oriented SWCNTs were deposited on a layer of PDMS after activating the layer with ultraviolet light. A maximum pressure of around

50 kPa was applied from the fingers. The developed device showed a change in conductivity as high as 2200 cm^{-1} up to the strain of 150% from its original position. Motion capturing is another application for which pressure sensors were developed, with flexible-CNT-array double helices (CNTADH) [105]. Two CNT strands were grown with lamellar-layered double hydroxides (LDHs) as the catalysts, which were sonicated with a surfactant and water for its proper dispersion. This is poured into a container to obtain a CNTADH thin film. The film was coated with thermoplastic elastomer before using it as a strain sensor. A measurable pressure of up to 410% of its original length with small hysteresis was achieved by the sensor. [105-127] are some of other significant studies done in recent years involving the fabrication of strain sensors.

2.2.5 Electrical Sensors

There have been prominent studies on the development of electrical sensors using CNTs as the conductive material. Some of the significant ones on the two types of sensors are described here. Plastic substrates like PI, PAA were used to fabricate electrical devices, like a PMOS inverter, with a sub-monolayer of random networks of SWCNTs as the conductive material forming the source, gate and drain [128]. The SWCNTs were synthesised by CVD on SiO_2 wafers and etched into strips using soft lithography. A layer of polyamic acid was used to encapsulate the source and drain electrodes and SWCNTs bundles to transfer to liquid-polyurethane-coated PI. Figure 2.5 (a-e) shows the different steps related to the fabrication and working principle of the PMOS inverter. Figure 2.5 (a) shows the architecture of the integrated circuit, with Figure 2.5(b) showing its SEM image. Figures 2.5(c) and 2.5(d) shows a magnified view of the SWCNT network with the distribution of current in it. Finally, the developed SWCNT transistor along with its circuit is shown in Figure 2.5(e). Standard deviations of around 20% and 0.05V were found for the normalised on-state current and threshold voltage. Work regarding the development of RF analogue devices, optoelectronics, photovoltaic devices, etc. based on CNTs has been substantial in recent years [129-131]. For example, fully printed transistors have been developed with SWCNTs via the inverse-gravure printing technique on flexible substrates [132]. The performance of the device is good, exhibiting a mobility and on/off current ratio of $\sim 9 \text{ cm}^2/(\text{V s})$ and 10^5 , respectively. The change in the electrical resistance of the developed transistor was measured with up to 1 mm of radius of curvature, with high bendability.

Figure 2.5 removed due to copyright

Figure 2.5 PMOS inverter developed from SWCNT/PI [128].

2.2.6 Conclusion and Future work

The research done with CNT-based flexible sensors illustrated in this chapter shows that work regarding CNTs has been significant to successfully use them as electrodes. They have been functionalised with different materials to change their properties to enhance their use for an application. Their uses have been ever-increasing due to their dynamic behaviour used regarding electrical, mechanical and thermal properties. The use of these sensors has extended to almost every sector, like gas sensors, electronic sensors, physiological sensors, etc. to name a few. Continuous work on CNTs is still going on to improve on different applications for their existing parameters and to also improve their characteristics to increase their usage for daily-life activities.

Future work could improve on the existing techniques to modify the utilisation of CNTs. The applications of CNT-based flexible sensors can be increased based on

optimising the different characteristics of CNTs. Since everything in today's world is related to improving the quality of human life, the bio-medical side of applications is another bright aspect where these nanotubes can be used on. The functionalisation of CNTs can be improved upon, where the inclusion and modification of different new and existing functional groups can help achieve better mechanical and electrical performance of the CNTs compared to the existing ones.

2.3 Graphene and its Sensor-based Applications

Graphene has always been a popular choice due to its distinct advantage of exhibiting excellent electrical, mechanical and thermal qualities. In simple words, it can be defined as a single layer of carbon atoms that are tightly packed to form a 2D honeycomb crystal-lattice structure [133]. It is the basic component for carbon allotropes which can be modified into other forms like 0D fullerenes, 1D CNTs, and 3D graphite as shown in Figure 2.6. The work on graphene has been going on for the last sixty years, but earlier it was mostly described as an allotrope of carbon to explain different carbon-based materials. It was just in recent times, around a decade back, that the free-standing 2D model of graphene was experimentally proved [134, 135]. In the applied field of research, among its wide range of applications, graphene has been mostly used in batteries and cells as anodes, and in supercapacitors due to its low charging time, high strength-to-weight ratio, and large surface area. It has also found many applications in areas like sensors, biomedical engineering, nano and flexible electronics and catalysis due to its unique properties which include a distinctive nanopore structure, high mechanical strength and high electrical and thermal conductivity. The functionalisation of graphene, to reduce the cohesive force between the graphene molecules in different forms, has made significant changes in its physicochemical properties, thus increasing their end applications [136-142]. Two different forms of functionalisation, covalent and non-covalent, are achieved for graphene molecules when the materials are chemically treated by different techniques like spin-coating, filtration, layer-by-layer assembly to cause surface modification but maintaining its intrinsic properties [143]. Even though a lot of research articles have been published based on the different techniques for the preparation of graphene and its utilisation in sensors, a thorough research work on the combination of all these aspects is yet to be done.

Figure 2.6 removed due to copyright

Figure 2.6 Different forms (0D, 1D and 3D) of modified graphene [133]. no permission

The involvement of graphene in sensors is attributed to some of its distinct advantages like the large surface-to-volume ratio, unique optical properties, excellent carrier mobility and exceptional electrical and thermal properties compared to the other allotropes of carbon. These properties are constant for the double and multi-layered graphene structures. Apart from the difference in the structure and working conditions, the use of these advantages in graphene sensors lie mainly in their capability to adjust according to the application. For example, in strain sensors, properties like the detection limit, maximum sensing range, signal response and reproducibility of the response hold a pivotal role to determine the quality of the sensor. These characteristics are attributed to the electrical and mechanical properties of graphene. In electrochemical sensors, its large surface area helps the loading of the desired biomolecules, resulting in the interaction between the analyte molecule and electrode surface due to the high ballistic transport capability and the very small band gap. Another advantage of graphene lies in its low environmental impact, making it more popular for sensing purposes than other metals [144, 145]. Tables 2.1 and 2.2 show the comparison of the performance of some of the electrochemical and strain sensors developed with graphene with that of Carbon Nanotubes (CNTs) and silver. It is seen from Table 2.1 that the Gauge Factors (G.F.) and maximum attainable strain are mostly highest for the graphene-based sensors. One disadvantage of these sensors is the

variation in the linearity in their response. For the other two types of sensors, the GFs are much less than graphene sensors, even though most of them withstand a high amount of detectable strain. It is seen from Table 2.2 that, even though the limit of detection achieved by all the three different types of sensors is the same, most of the graphene-based sensors can achieve high sensitivity with a wide linear range.

Table 2.1 Comparison between the different characteristics of strain sensors where the electrodes are developed with graphene, CNTs and silver.

Electrode material	Gauge Factor	Max. attainable strain (%)	Linearity in the response	Reference
Graphene	$\sim 10^6$	120	Linear above 1%	[146]
	10^3	106.2	Linear up to 6%	[147]
	29	70	Linear up to 77%	[148]
	300	<30 (Tunable GF)	Linear	[149]
	15-29	70	Linear	[148]
	7.1	100	Linear	[105]
Carbon Nanotubes (CNTs)	12.1	410	Linear	[150]
	0.82	280	Two linear regions	[151]
	8.7-62.3	100	Non-linear	[109]
	0.99	100	Linear	[152]
	1	150	Linear	[153]
	0.97	300	Linear	[154]
Silver	2-14	70	Linear up to 40%	[155]
	0.7	50	Linear	[35]
	1.07-12.4	100	Non-linear	[156]
	1	50	Linear up to 80%	[157]
	1	170	Linear up to 60%	[158]
	24-95	102	Linear	[159]

Table 2.2 Comparison between the different characteristics of electrochemical sensors where the electrodes are developed with graphene, CNTs and silver.

Electrode material	Limit of Detection (μM)	Sensitivity ($\mu\text{A mM}^{-1} \text{cm}^{-2}$)	Linear range (mM)	Reference
Graphene	0.2	31.2	1.0 μM - 1 mM	[160]
	6.9	266.6	0 - 3.5	[161]
	0.2	31.2	0.001 - 1.0	[162]
	1.73	0.085	0.5–3	[163]
	6.9	266.6	0 - 3.5	[164]
Carbon Nanotubes (CNTs)	21	17.76	70 – 3500	[165]
	10 ± 2	10 ± 3	0.0001–10000	[166]
	0.00129	6.8	1.29 - 12.93	[167]
	4	0.54	8.0×10^{-6} to 4.5×10^{-4} M	[168]
	0.2	2596	0-1.2	[169]
Silver	29.2	0.0266	0.0001–3.1	[170]
	10	1043	0.0005 - 7	[171]
	1200	2.55	48×10^{-5} – 31×10^{-5}	[172]
	0.2	57.5	0.2 - 70	[173]

2.3.1 Synthesis of Graphene

Optimisation of the preparation of graphene has been performed for some years, since its invention and application. Some of the significant methods that are used worldwide to generate graphene on a large scale are given below.

Chemical Vapour Deposition (CVD)

In an environment of an inert gas like N_2 a quartz-tube furnace [174] is heated, and on peaking the deposition temperature carbonaceous gases of a mixture of $\text{Ar}/\text{H}_2/\text{CH}_4$ [175-177] are passed through screens of varying dimensions such as one sq. inch of $\text{Ni}/\text{Cu}/\text{Co}/\text{Pt}/\text{Ir}/\text{Ni}$ metal that is placed in the furnace. The gases deposit carbon in the metal at elevated temperature, forming a single long atom-thick monolayer/multilayer of graphene over a prolonged period. To control and reduce the manufacturing process

temperature, plasma without a catalyst is used in the chemical vapour deposition (CVD) process [178, 179]. Graphene CVD synthesis utilising waste products is done by placing sustainable materials like butter, camphor ($C_{10}H_{16}O$) (with/without iodine), tea tree (*Melaleuca alternifolia*) extraction, waste plastic (solid form), cookies, chocolates over Ni foam, Ni/Cu metal foils, polycrystalline Ni in an atmosphere of Ar+H₂, H₂, Ar at normal /ambient pressure, elevated temperature and RF power applied for a period. A summary of some of the selected conditions for the preparation of graphene using CVD along with other methods is given in Table 2.3.

Table 2.3 Summary of some of the selected conditions of preparation of graphene using different methods.

Technique	Gas source/Reducing agent	Temperature (°C)	Substrate	Reference
SWP-CVD	CH ₄ : Ar: H ₂	300–400	Cu, Al	[180]
MWCVD	MWCVD	450–750	Ni	[181]
LPCVD	CH ₄	1000	Cu	[182]
APCVD	CH ₄ : H ₂ : Ar	960-970	Ni	[183]
LPCVD	CH ₄ : H ₂ : Ar	900	Ni, Cu on SiO ₂ /Si	[184]
ME	-	25	SiC	[185]
ME	-	25	Si	[186]
ME	-	25	HOPG crystal	[187]
ME	-	1000	NaCl crystallites	[188]
HM	KMnO ₄ , H ₂ SO ₄	20	-	[189]
HM	KMnO ₄ , H ₂ SO ₄ , H ₂ SO ₄ and H ₃ PO ₄	25	-	[190]
HM	NaNO ₃ , H ₂ SO ₄	0	-	[191]
HM	NaNO ₃ , KMnO ₄ , H ₂ SO ₄	150	-	[192]

- SWP CVD- Surface Wave Plasma Chemical Vapour Deposition
- MW CVD- Micro Wave Plasma Chemical Vapour Deposition
- LP CVD- Low Pressure Chemical Vapour Deposition

- AP CVD- Atmospheric Pressure Chemical Vapour Deposition
- ME- Mechanical Exfoliation
- HM- Hummer's Method

Mechanical Exfoliation

Scotch tape is used primarily, in this method, to stick over the graphite crystals or graphite flakes [193]. The tape leads to the entrapment of graphite layers. The tape is repeatedly peeled and observed under the microscope over a prolonged period to extract the graphene layer. The experiment can be repeated with a silicon wafer that is oxidised [194]. This method is considered analogous to rubbing of a graphite pencil in between two terminals of lead attached to the package, such that the lead develops once the graphene sheet has been extracted [195]. However, this method is not favourable for the mass-scale production required for industry [196].

Hummer's Method

Graphite powder is one of the most important constituents of the low-cost Hummer's process [189]. Over the past few years, methods have been devised to obtain graphite powder from waste products [197]. One such procedure involves utilisation of zinc-carbon batteries [198]. Electrodes from the waste batteries are ground into graphite powder after being subjected to washing for removal of impurities, before being treated with a solution of HCl: HNO₃ in the ratio of 3:1. The total solution is further subjected to extreme heating, centrifuge, water treatment followed by drying at a fairly high temperature for a prolonged period, finally obtaining purified Graphite powder. In another procedure, bagasse or waste sugar cane, when finely ground, mixed with ferrocene and passed through a furnace in a crucible for 10 minutes yields graphite powder. The modified Hummer's method eliminates the usage of NaNO₃. The method involves mixing of H₂SO₄ and H₃PO₄ at a ratio of 9:1 [190, 199]. Upon mixing the solution is stirred. During stirring graphite powder and KMnO₄ are added slowly, to reduce the temperature of the suspension. Continuously stirring is done for 6 hours such that the colour changes to dark green. The H₂O₂-containing total mixture is stirred for a brief time. The excess heat producing reaction is left for cooling in an ice bath. HCl and DI (de-ionised) water are further added to the solution for removal

of metal ions. The solution is subjected to a centrifuge at high speed for a short duration. The particles left over are washed with hydrochloric acid and de-ionised water thrice before being subjected to intense heat in the oven for a prolonged period to produce Graphene oxide (GO) in powdered form. The Graphene Oxide is further mixed with water and subjected to ultrasonication for a stipulated amount of time. Sulphur-laced reducing agent (NaHSO_3 , $\text{Na}_2\text{S}\cdot 9\text{H}_2\text{O}$, SO_2) in a very small amount is added to the mixture at an elevated temperature and low stirring speed for a long time. The mixture is further subjected to filtration and DI water washing multiple times. Upon freeze drying, powdery black graphene is obtained. The quality of graphite oxide, graphene oxide and graphene can be determined by studying the X-ray diffraction (XRD), Fourier-transform infrared spectrum (FTIR), Ultraviolet–visible (UV–vis) spectroscopy, SEM, TEM and Raman spectra. Multiple graphene layers are obtained, when, before being subjected to chemical cleaning and ultrasound treatment, in an N_2 environment at a feverish temperature, dead camphor leaves are subjected to pyrolysis. Graphene is yielded when coal-tar pitch (CTP) is subjected to spin coating on Si, followed by annealing with a Ni layer at elevated temperature, low vacuum and normal atmospheric conditions [200, 201].

2.3.2 Characterisation and Properties

Semi-metallic graphene consists of an arrangement of hexagonal covalently bonded one-atom-thick [202, 203] carbon atoms arranged together in a honeycomb lattice structure. Out of four carbon atoms, three carbon atoms exhibit sp^2 hybridisation. By the hybridisation, the trigonal system of carbon atoms exhibits a high bonding energy (~ 5.9 eV), separated with sigma bonds with a bond length of 1.42 \AA . The lone p-orbital, being half filled, forms π bonds with the adjacent carbon atoms [204, 205]. The slippery graphene sheets are normally one atom thick and are stacked one above another to form the graphite 3D structure. The sheets are held together by the weak Van der Waal's forces. The slippery nature of the sheets can be attributed to the presence of vibrational phonons, which also happen to be present in the 3D solids. Figures 2.7 and 2.8 depict the schematic diagram of the honeycomb lattice structure of graphene and its electron dispersion phenomenon in a defined energy spectrum respectively. Equations 2.1 to 2.10 shows the formulas used to determine the energy distribution spectrum for the honeycomb lattice structure of graphene.

Figure 2.7 removed due to copyright

Figure 2.7 Schematic diagram of the structure of graphene represented in the form of a Honeycomb lattice and its Brillouin zone [206].

Figure 2.8 removed due to copyright

Figure 2.8 Electronic dispersion of the honeycomb lattice in terms of (zoomed in) the energy spectrum of finite values [205, 206].

$$a_1 = \frac{a}{2}(3, \sqrt{3}), a_2 = \frac{a}{2}(3, -\sqrt{3}), \quad (2.1)$$

The reciprocal vectors are:

$$b_2 = \frac{2\pi}{3a}(1, -\sqrt{3}), b_1 = \frac{2\pi}{3a}(1, \sqrt{3}) \quad (2.2)$$

The magnitudes of the corners of the Brillouin zone of graphene are:

$$K = \left(\frac{2\pi}{3a}, \frac{2\pi}{3\sqrt{3}a} \right), K' = \left(\frac{2\pi}{3a}, -\frac{2\pi}{3\sqrt{3}a} \right) \quad (2.3)$$

Magnitudes of the vectors are:

$$\partial_1 = \frac{a}{2}(1, \sqrt{3}), \partial_2 = \frac{a}{2}(1, -\sqrt{3}), \partial_3 = -a(1, 0) \quad (2.4)$$

Nearest neighbours are located at

$$\partial_1 = \pm a_1, \partial_2 = \pm a_2, \partial_3 = \pm(a_2 - a_1) \quad (2.5)$$

The Hamiltonian has magnitude:

$$H = -t \sum_{\langle i,j \rangle, \sigma} (a_{\sigma,i}^+ b_{\sigma,j} + H.c.) - t' \sum_{\langle\langle i,j \rangle\rangle, \sigma} (a_{\sigma,i}^+ a_{\sigma,j} + b_{\sigma,i}^+ b_{\sigma,j} + H.c.) \quad (2.6)$$

Energy bands have the magnitude:

$$E_{\pm}(k) = \pm t \sqrt{3 + f(k)} - t' f(k) \quad (2.7)$$

where $f(k)$ is represented by:

$$f(k) = 2 \cos(\sqrt{3}k_y a) + 4 \cos\left(\frac{\sqrt{3}}{2}k_y a\right) \cos\left(\frac{3}{2}k_x a\right) \quad (2.8)$$

The Density of states (DOS) is given by

$$\rho(E) = \frac{4}{\pi^2} \frac{|E|}{t^2} \frac{1}{\sqrt{Z_0}} F\left(\frac{\pi}{2}, \sqrt{\frac{Z_1}{Z_0}}\right) \quad (2.9)$$

The values of Z_1 and Z_0 vary for different intervals. The DOS near the Dirac point has the magnitude:

$$\rho(E) = \frac{2A_c}{\pi} \frac{|E|}{v_F^2} \quad (2.10)$$

The massless Dirac fermions are a unique characteristic of graphene. The Dirac fermions travel at a speed ($\approx 10^6$ m/s) less than that of light. The Dirac fermions are not affected by external electrostatic potentials, exhibiting the Klein Paradox, and lead to the integer quantum hall effect, by which the chance of electrons crossing a potential barrier is always unity [206-208]. The incident Dirac electrons don't get reflected and propagate with 100% efficiency in cases where the internal scattering and symmetrical aspects of carbon atoms are neglected. The chances of reflection at angles greater than zero degrees depend on more of the barrier changing at a slower pace. The Dirac fermions are however affected by localised electrons, leading to the jittery characteristics. An inverse relationship between

electrons and holes is exhibited between velocity and momentum. The photons, like electrons, always try to search for a hole to form an image on the screen. The quasiparticles overlap with the Quasi-holes of another band on the condition that the distances between the Dirac and Fermi energies are less than the superconducting distances. Graphene's high electrical conductivity ($\sim 1.0 \times 10^8$ S/m), high melting point (4510 K), high thermal conductivity (2000-4000 W m⁻¹ K⁻¹, 5000 W/m K), highest current density ($\sim 1.6 \times 10^9$ A/cm²), including a high electron mobility (200,000 cm²V⁻¹s⁻¹ at electron density $\sim 2 \times 10^{11}$ cm⁻²) contributes to its application in electrochemical sensors, strain sensors and electrical sensors that are discussed in detail in a later section of the chapter [209-211]. The chirality of graphene is exhibited by straight, armchair and zigzag geometry. The zigzag geometry is more in control of states and resonances. The magnitudes of the tensile strength, shear modulus, and Poisson's ratio varies for each of the chiral geometries, and are summarised in Table 2.4 [212].

Table 2.4 Comparison between the geometrical patterns of the single-layered graphene sheets [212].

Geometry	a (nm)	b (nm)	Young's modulus (TPa)	Shear Modulus (TPa)	Poisson's Ratio
Zigzag	6.395	4.184	1.040	0.213	1.441
Armchair	6.153	4.263	1.042	0.228	1.285
Chiral	4.713	3.256	0.992	0.233	1.129

Steel's tensile strength is less [213] than for graphene (~ 130 GPa) [209], which may be used in structural engineering applications like that of aeroplane [214] composites. Graphene's elastic property is such that a 20% increase of its length doesn't compromise its properties [215]. It has a very high surface area (~ 2600 m²/gm) that can contribute to its application in fire-fighting appliances [216].

The characterisation of graphene is done using various techniques like XRD, FTIR, Ultraviolet-visible (UV-vis) spectroscopy, SEM, TEM, and X-ray photoelectron spectroscopy (XPS). The XRD is done to investigate the phase and structure of the fabrication samples. In [217], the diffraction peak obtained at $2\theta = 10.2^\circ$ for the graphene-CdS nanocomposites, corresponds to the (0 0 1) reflection of graphite oxide. The peaks

obtained with the samples are correlated to the structure of the compound under consideration. The alignments of graphene grown on different substrates are studied with XRD, determining the crystal directions. The diffraction peaks and *d*-spacing obtained for the nanocomposites are generally higher than those of the pure material. This is due to the random positioning of the filler inside the polymer matrix. The peak and spacing values give a very good indication of the degree of dispersion of the fillers in the matrix. The SEM and TEM images are also studied by placing a section of the material in an illuminated area at different orientations to determine the features of developed sensors in the nanometre domain. Different types of TEM like High-Resolution TEM (HRTEM) and Dark-Field TEM (DFTEM) are studied depending on the resolution of the fillers in the material. The top and cross-sectional views of the SEM images are another parameter for analysing the dispersion of the fillers [218]. The FTIR studied for the graphene-based nanocomposites determines different ranges of wave numbers with respect to transmittance to analyse the elements present in the nanocomposite. The stretching and deformation vibrations of the functional groups are mainly studied with this technique. The absorption bands related to the transmittance vary according to the functional groups present in the nanocomposite. The peaks of the different bands in the FTIR are also studied to determine the vibrations of the adsorbed molecules on the graphene domains. A comparative study between the developed nanocomposite and pure graphene is generally done to study the C-O stretching vibrations, C-O-H deformation vibrations and C=O stretching of COOH groups. The contents of the raw materials are varied based on the wave numbers to optimise the properties of the resultant sensors. UV-vis spectroscopy, like the FTIR, is studied in terms of absorption spectra with respect to wavelength to analyse the peaks corresponding to the graphene present in the compound. Different ranges of absorption spectrum are studied in UV-vis spectroscopy with a spectrophotometer to study the π -bonding between the carbon atoms. The absorption peaks may differ from each other, depending on the degree of coupling taking place between the individual elements in the compound. XPS is another technique, like UV-vis spectroscopy, which is used to study the surface compositions of the samples. The peaks obtained in XPS are studied to analyse the binding energy between the graphene and the substrate. The binding energies in XPS are also attributed to the carbon, oxygen and hydrogen bonding with other carbon atoms [219-221].

Some of the popular applications, like electrochemical, strain and electrical sensing, with graphene-based sensors pre-addressed in the preceding sections. There are distinct advantages of graphene for which it is chosen for these specific applications. It exhibits

less electrical noise and crystal defects than conventional sensing materials. Moreover, electrochemical sensors developed with graphene can be operated with simpler techniques than conventional methods like that of the mass spectrometer [222]. Other advantages would be its robustness, high flexibility, and electrical conductivity. These are the attributes for which it is used for developing electrochemical sensors for the detection of hazardous substances like hydrazine and selective detection of haemoglobin, adenine dinucleotide and biomolecules like ascorbic acid, uric acid [223-227], etc. In these applications, nanocomposites have been formed by mixing pure graphene with other materials, like Platinum (Pt) and TiO₂, to increase the sensitivity and detection capability of the sensor. When any gas is brought through channels in low concentrations, then made to flow through the graphene surface, this causes an immediate effect on its charge concentration. The difference in charge concentration brings a corresponding change in the resistance, and conductivity of graphene [228]. These help in interpreting the nature of the gas molecules. The graphene-based chemical sensors can be manufactured cheaply using acrylic plastic as a substrate. Avoiding e-beam lithography and other sophisticated techniques of lithography also brings down the manufacturing cost and time. Moreover, for a graphene-based electrochemical sensor involving a dual channel of inlet gas and analyte gas, the switching times in between the two gases are very small. The lightweight graphene chemical sensor is wearable, operates at normal atmospheric pressure and room temperature. The unique relationship between the mechanical and electronic properties of graphene has also helped it to be used for strain sensing. Due to a high mechanical stiffness of around 1 TPa and an intrinsic breaking strength of 130 GPa, it is the most robust and powerful material. This has been combined with some of the electronic properties like the high velocity of electrons (1/100 velocity of light) and a zero-band gap to form graphene-based strain sensors. Mostly for strain sensing, graphene in different forms like rGO has been mixed with polymers like PDMS to achieve highly elastic sensors. Some of them would have gauge factors as high as 630 formed by the selective coating process. The carrier mobility and electron transfer rate of graphene at ambient temperature are also very high due to its large surface-to-volume ratio [229-232]. Its unique structure has also caused certain phenomena like the Hall Effect and Klein tunnelling to take place. Due to these characteristics of graphene, a lot of research work has been going on for the last decade, especially in the areas of photonics and optoelectronics. Optical modulators with a modulating capability of frequencies over 1 GHz of guided light have been developed by tuning the Fermi levels of graphene sheets. The high carrier saturation velocity and insensitivity of its response

towards temperature variations have led it to find varied applications in infrared imaging and optical communications. Graphene has also been enlisted to develop ultrafast fibre lasers by integrating it into different configurations and without affecting its alignment [233-236]. A high output power gain has been achieved with these lasers operating at a wavelength of 2 microns. Figures 2.9(a) - 2.9(c) show the sensing mechanisms for the three different applications using graphene-based sensors. It exhibits magnificent electrochemical properties like a large potential window and a low charge-transfer resistance.

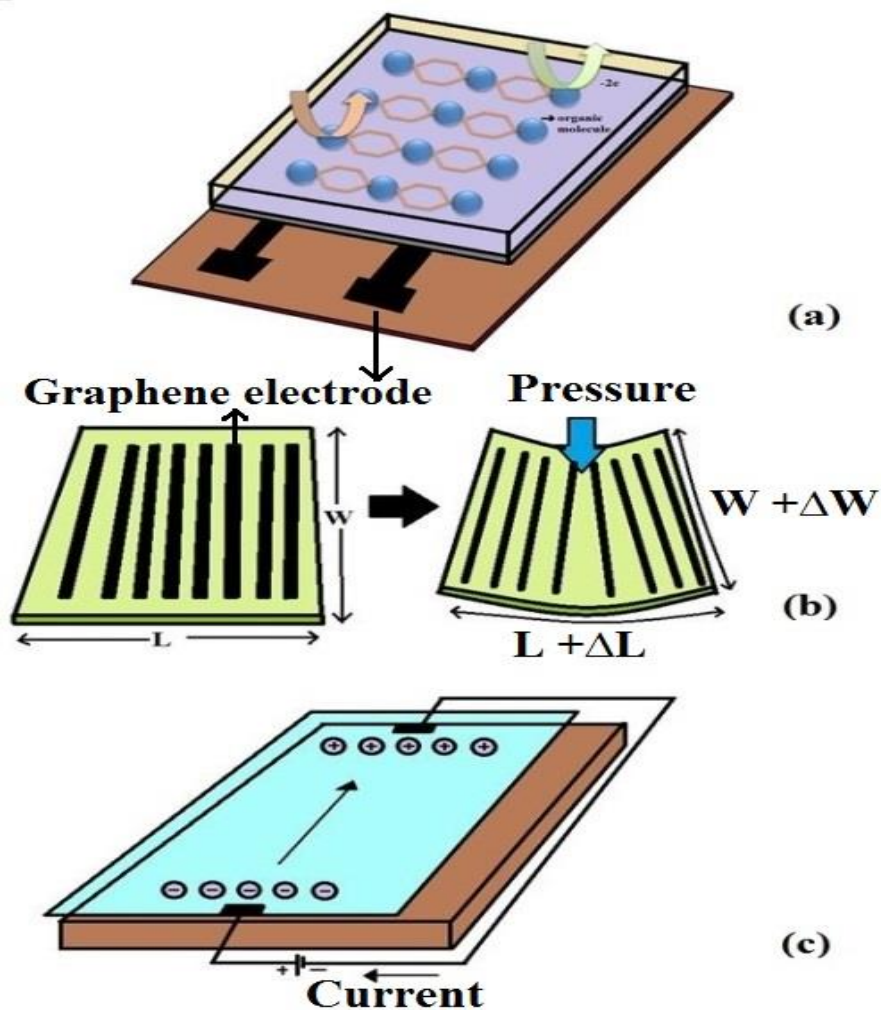


Figure 2.9 Schematic diagram of the sensing mechanisms of graphene-based (a) electrochemical (b) strain (c) electrical sensors.

The electrochemical activity of different biomolecules using graphene is assisted by its high charge-carrying capability and super electrical conductance [237]. In the case of strain sensing, the use of graphene as electrodes is highly favourable due to their highest in-plane

electrical conductivity and Young's Modulus (around 1 TPa for ideal graphene) which gives it high elastic stiffness and strength. The structural strength and load transfer capabilities of graphene allow it to be intertwined with other conductive materials like CNTs and polymers like PDMS, PMMA to improve the latter's ability to withstand large cyclic strains of over 50% without influencing the sensitivity, response, and durability. Due to its excellent conductive and elastic properties, researchers have tried to develop buckling effects of graphene with different forms like ribbons and nano-sheets [238-243]. Some of the attributes which caused the use of graphene in electrical sensors are its low resistivity, environmental stability, low signal-to-noise ratio, the effective shift of the Dirac voltage, strong absorption of surface acoustic waves over a wide frequency range, and the Hall Effect. The ability to display both metallic and semi-conductive behaviour as a single material allowed its extensive use in thin-film transistors. It can show large on device currents at very low voltages [244, 245].

2.3.3 Electrochemical Sensors

Several reasons, like a wide range of electrochemical potential, fast electron transfer rate and high redox peaks with linear cathodic and anodic currents, have made graphene and its oxidised form (GO) useful as electrochemical sensors for some time. As mentioned in the earlier sections, with the modifications done on graphene sheets with methods like electrodeposition, polymerisation, electrochemical doping, etc., different composite materials were developed for electrochemical sensing purposes. Due to its high detection capability, graphene serves as an excellent molecule for combining with redox enzymes on the electrode surface for direct-electron-transfer (DET) reactions. One of the ways of combining an enzyme on the electrode surface with graphene is via a wiring technique as shown in Figure 2.10 [246, 247]. Different kinds of enzymatic reactions have been performed where graphene has been conjugated with materials like Chitosan, gold (AuNP) and platinum nanoparticles (PtNP), Iron oxides, and PVDF to form nanocomposites on the electrode surface of glucose, cholesterol, and haemoglobin sensors [248-254]. Graphene in its pure, oxide and bio-composite forms has been modified with different nanoparticles, nano-cubes and nano-fibres to develop glucose sensors [255-260].

Figure 2.10 removed due to copyright

Figure 2.10 Different protein molecules being wired by graphene on the glassy carbon electrode [247].

Cholesterol sensors mainly involve the formation of bio-composites with different polymers. Another form of electrochemical sensing involves immuno-sensing, where graphene has been used as both a label bearer and a non-label bearer element for the detection of antigen-antibody recognition sites. When graphene was used as a label bearer, it was conjugated to antibodies and other particles to develop large electroactive molecules [261-264].

As a non-label bearer, the conductive material was used on the surface of the electrode to detect the labels. DNA sensors use another form of electrochemical sensing where the DNA sequences or the mutated genes are detected with graphene-associated sensors. Some of the sensors involved the label-free electrical detection of DNA hybridisation. But, mostly the detection of DNA would be done using biomolecular enzymes, like ssDNA, RNA and aptamers, conjugated with graphene molecules [265-268]. The differences between these sensors lie in their limit of detection (LOD) and the range between which they can perform. One study [269] involved the use of chemically reduced graphene oxide (CrGO) in a modified glassy carbon electrode (GCE) for the detection of four free bases of DNA

concurrently, which showed better results than just graphene-modified GCE. This establishment helped in the detection of the four bases for both single and double-stranded DNA without the requirement of a pre-hydrolysis step.

Another significant aspect of graphene-based electrochemical sensing, due to the fast electron transfer rate and high electrocatalytic capability of graphene, includes the detection of smaller biomolecules like uric acid, ascorbic acid and dopamine. The importance of the concentration of dopamine in the human body caused researchers to work on it in the presence of other acids. Most of the work exhibits the graphene-modified GCE [227, 270-272]. Even though some of the developed sensors had a prominent linear range and LOD, the stability of the responses degraded with time. Due to the higher electron mobility and the wide electrical window of graphene, it is largely considered for the detection of biomolecules [273]. Graphene Field-Effect Transistors (GFETs), in recent years, have been successful as a bio-sensing device, reducing the fabrication cost and response time due to their high sensitivity. There is an increase in the gate current of GFETs on the introduction of any biomolecule, causing a change in drain current. The Debye length and proper functionalisation of the receptor with a single layer of graphene for specific detection of the targeted molecules are the two parameters critically analysed for GFETs in bio-sensing applications. Detection of hydrogen peroxide (H_2O_2) with graphene-based sensors is another area where researchers have focused in recent years. Graphene in its intrinsic and N-doped (N-graphene) forms has shown excellent electrocatalytic response towards H_2O_2 [274-278]. The N-graphene form has shown a better response due to the presence of nitrogen and oxygen functional groups along with structural defects. Figure 2.11 shows a pictorial description of work done on the detection of H_2O_2 by a one-step approach [279]. A nanocomposite was formed by mixing poly (3, 4-ethylenedioxythiophene) - poly (styrene sulfonate) (PEDOT: PSS) with gold nanoparticles and reduced graphene oxide. The nanocomposite was assembled to the electrode after being functionalised with horseradish peroxidase (HRP) for the detection of H_2O_2 . The sensor showed a high sensitivity of $677 \mu\text{A mM}^{-1} \text{cm}^{-2}$ with a linear range and LOD of 5-400 μM and 0.08 μM respectively. Table 2.5 shown below addresses some of the techniques used to develop the graphene-based electrochemical sensors along with their linear range and limit of detection.

Figure 2.11 removed due to copyright

Figure 2.11 (a) One-step approach to the formation of an H₂O₂ sensor with PEDOT: PSS and AuNP and rGO. (b) Functionalisation of the formed nanocomposite with HRP for detection purposes [279].

Table 2.5 Summary of the graphene-based electrochemical sensors depicting the differences between the responses concerning the materials and techniques used to develop the sensors.

Material (with graphene)	Technique	Linear Range (μM)	Limit of Detection (μM)	Reference
Copper	Hummer's method	0- 4.5	0.5	[258]
Nickel oxide	Hummer's method	0.0005–3000	1.73	[163]
Zinc oxide	Electro-deposition	0.02 - 22.48	0.02	[276]
Carbon Nano-spheres	Screen printing	0.05 - 6	0.02	[264]
Cerium oxide	Oxidation	12 - 7200	4	[262]

2.3.4 Strain Sensors

Even though strain sensors with different materials have been formulated and developed for a sometime, the graphene-based sensors have proved to be an excellent candidate for strain-sensing applications. The advantage of using graphene over other conductive material for strain sensing lies in the generation of a pseudo-magnetic field due to the shift in the Dirac cones and reduction of the Fermi velocity. The usefulness of this magnetic field lies in its ability to determine the change in electronic structure during strain. The gauge factor (G.F.) is an important parameter which is used to determine the efficiency of fabricated strain sensors. It calculates the electric shift based on mechanical deformations. This is because, as the graphene-based sensors involve different materials amalgamated to fabricate them, the change in unit resistance to the change in unit length caused by the strain decides the amount of strain for the material. Some of the strain sensors with high G.F. use graphene composites [280, 281].

Figures 2.12 (a) & (b) removed due to copyright



Figure 2.12 (a) PDMS-based strain sensor developed with graphene on Ni/Si/SiO₂ film [282]. (b) Flexible graphene-PET strain sensor developed by drop-casting graphene oxide film to laser write the interdigitate circuit [283]. (c) Development of a reduced graphene oxide/polyimide nanocomposite to form strain sensors by mixing, freezing and thermal annealing with polyamic acid [284] Reprinted (adapted) with permission from Yuyang Qin, Qingyu Peng, Yujie Ding, et al. (2015) Lightweight, Superelastic, and Mechanically Flexible Graphene/Polyimide Nanocomposite Foam for Strain Sensor Application. ACS Nano. 9(9). pp. 8933-8941. DOI: 10.1021/acsnano.5b02781. 2015 American Chemical Society.

The amount of relative strain is more when applied parallel to the C-C bonds compared to its application perpendicular to the C-C bonds due to a higher increase in the band gap. A lot of research groups work on developing graphene films on polymer substrates like PDMS, PET, PI [282-284], getting a piezo-resistive effect by causing a non-monotonic change in the electrical resistance with the applied strain. Figures 2.12(a) – 2.12(c) show three different types of strain sensors developed with PDMS, PET, and PI done with photolithography, drop-casting, and thermal annealing processes respectively.

Strain sensors, other than being used as pressure sensors, have been employed for different applications like healthcare devices where they have been attached to the gloves, skin and organs to monitor physiological parameters. The values in the G.F., electrical conductivity, and relative strain have been reported up to 269, 2200 S/cm and 540% respectively. Another work involved the formation of a strain sensor to use it as a sound-signal acquisition and recognition device [99, 101, 104, 285-289]. The sensor was designed on fabric (GWF) by weaving graphene with PDMS. The sensor patch was placed on the muscle of a throat to analyse the change in electrical resistance with movement of the throat muscles. After the response of the sensor for every English phoneme was analysed to differentiate its output, different words were tried to validate the developed sensor further. There were other studies reported on GWF where even a G.F. factor up to $\sim 10^5$ was achieved. Graphene, in the form of nano-papers, was also used to develop strain sensors [124, 146, 290]. The sensor patch was used to detect human movements. Figure 2.13 gives the schematic diagram of the fabrication steps of the nano-cellulose based sensor patch. Crumpled graphene and nano-cellulose fibril were mixed at a weight ratio of 1:1 on a polycarbonate membrane. Following filtration of the embedded nanocomposite, the thin film was peeled off and impregnated with PDMS to develop the stretchable nano-papers. The movement of the fingers caused a 3D movement of the sensor leading to a maximum strain exceeding 50%. Table 2.6 lists some of the techniques used to develop the strain sensors with graphene electrodes along with their maximum strain percent and gauge factor.

Figure 2.13 removed due to copyright

Figure 2.13 Schematic diagram of the formation of stretchable graphene nano-papers [124].

Table 2.6 Summary of graphene-based strain sensors based on the materials and techniques used to differentiate between the gauge factor and maximum strain.

Material (with graphene)	Technique	Gauge factor	Maximum Strain (%)	Reference
PDMS	CVD	14	7.1	[282]
PET	Drop casting	9.49	7.5	[283]
PDMS	CVD	10 ⁶	7	[146]
Nano-graphene films	RPECVD	300	0.37	[289]
Graphene oxide	Hummer's method	7.1	100	[124]

2.3.5 Electrical Sensors

The use of graphene in electrical and electronic applications has been comparatively minor compared to the previously explained applications. Graphene has been largely employed as transistors for biomolecular applications. Other uses of graphene-based electrical sensors include temperature sensing, photodetectors, RF applications [291-294],

etc. Graphene has been utilised in the form of nanoribbons, nanowires and other forms of nanoparticle arrays. Among the photodetectors, the GFETs cover the terahertz, IR, visible and UV ranges [204, 295-297]. Graphene transistors are fabricated on flexible substrates (PI, flexible glass, Kapton, Polyethylene Naphthalate) that are attached to rigid substrates via or not via gelling/interface material (SiO₂, PDMS) [298-302]. The flexible substrates are introduced, through spin coating followed by a baking process, into the rigid substrates. The gate and metal contacts of varying compositions (Au (100 nm) / Ti (10 nm), Au (38 nm) / Ti (2 nm), Au, Al (40 nm) / Ni (50 nm) / Au (300 nm), Cr (1 nm) / Au (60%) – Pd (40%) alloy (20 nm)) [38-42] are made by employing one of the following processes: E-beam, photolithography, and inkjet printing followed by plasma etching in an atmosphere of O₂ at specific conditions (300 W/5 mbar/5 minutes) at room temperature.

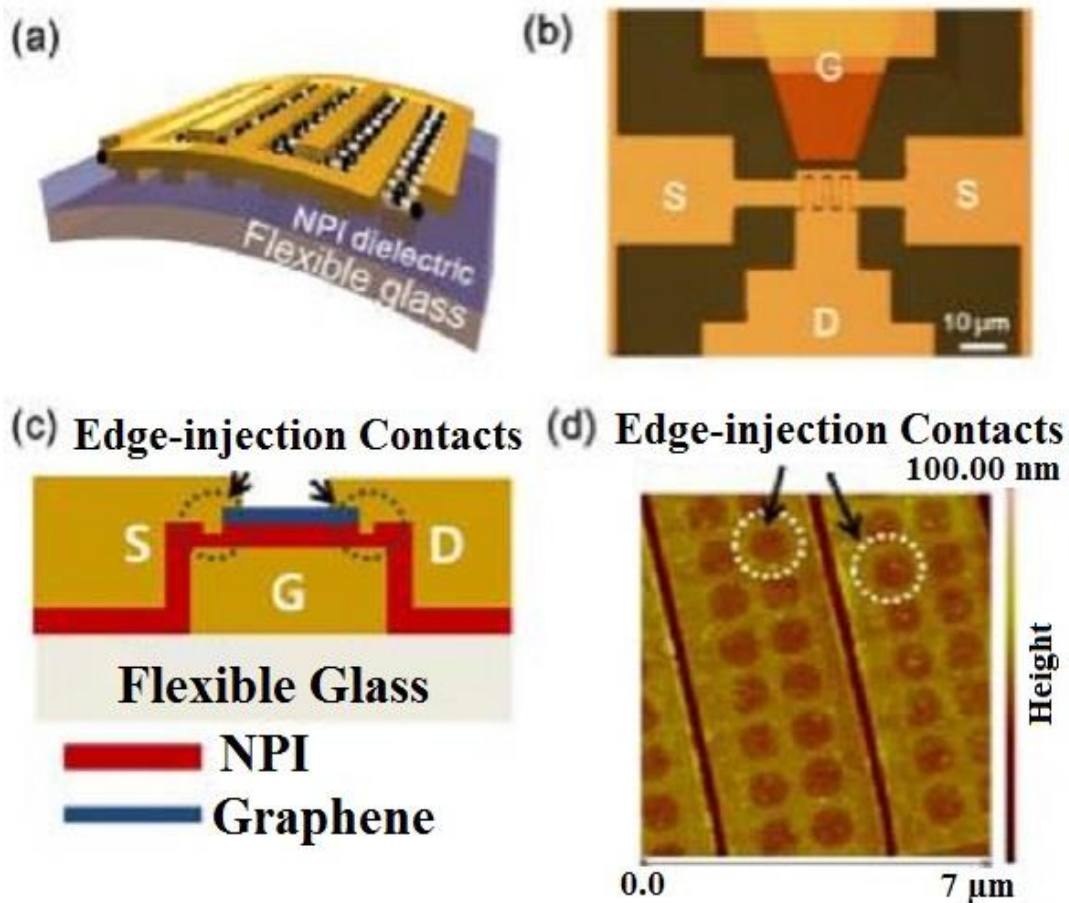


Figure 2.14 Graphene transistors on flexible substrate shown in 3-D (a), Optical (b), cross-sectional (c) and AFM (d) images [39].

The graphene is washed and transferred from CVD or other processes (inkjet printing) over the transistor's length over the gate dielectric (HfO_2 , nanoscale polyimide, Al_2O_3). The graphene forms the channel also, in the process covering the contact materials. The fabricated graphene transistor of varying gate length, channel width, and channel length is finally removed by mechanical peeling off the flexible substrate or dissolving a flexible substrate by using acetone. Figure 2.14 shows the schematic diagram of the fabrication of graphene transistors in different views [190]. The combination of nanowire field-effect transistors (NW-FETs) and GFETs interface well with electrogenic cells, resulting in a highly sensitive response towards cell membranes [291].

Other uses of graphene in electrical sensors involve its uses in lithium-ion batteries, photodetectors, inverters and optoelectronics. The inclusion of graphene in batteries is done by forming clusters with lithium or mainly by forming hybrids with other compounds. A range of compounds like Mn_3O_4 , Fe_3O_4 was mixed with modified graphene like rGO sheets and graphene nanosheets respectively in the batteries [303-305]. The hybrid materials created with different compounds help with a quicker charging and discharging capability than conventional lithium-ion batteries. Pure graphene was also used where it was doped with materials like boron and nitrogen to increase the power, energy storage and discharging capacity of the batteries. Other advantages of including graphene to develop batteries are its low cost and light weight. Graphene has also been used largely in photodetection applications like optical modulators, plasmonic devices, etc. [297, 306-309]. One of the important goals of researchers developing photodetectors is the ability to generate a material covering most of the spectrum. Two of the advantages of using graphene in photo-sensing devices is its ability to detect right across a large spectrum along with its high sensitivity towards any polarised angle. Due to the excellent transport properties of graphene, a high speed, even up to 10 GB/sec, with a very high bandwidth of >500 GHz has been achieved. It is also the only material that could be used to develop photodetectors which are CMOS compatible and able to achieve their operation over all the fibre-optic communication bands [310-312]. Table 2.7 gives a summary of some of the graphene-based transistors with their achieved maximum strain and electron mobility [313].

Table 2.7 Summary of graphene-based electrical sensors based on the materials and technique used to compromise between the maximum strain and electron mobility [313].

Material (with graphene)	Technique	Electron mobility ($\text{cm}^2\text{V}^{-1}\text{s}^{-1}$)	Maximum Strain (%)	Reference
Al₂O₃	CVD	190	0.62	[314]
Ion gel	Aerosol jet printing	422	5	[315]
Graphene oxide	Langmuir–Blodgett	4.1	3.5	[316]
PMMA	Electron beam lithography	8	1.2	[317]
Boron nitride	Mechanical exfoliation	60000	-	[318]

There has been prominent work done on the utilisation of graphene-based electrical sensors for biomolecular, physical and chemical sensing [319]. The simplicity in the design, ease of mass production and the capability to capture and amplify signals are some of the advantages of graphene-based electrical sensors which make them popular for these applications. The physical sensing includes the employment of graphene electrodes as phototransistors and thermal transistors. The unimpeded transmission of the carriers in GFETs as a result of the very small band gap makes graphene a very popular choice for phototransistors [320, 321]. Due to the high mobility of the carriers, ultrafast photodetectors have also been fabricated with graphene with a varied number of layers. Even though the highest photo-responsivity has not been very high for the graphene photodetectors, moderately high values of $\sim 1 \times 10^7 \text{ A W}^{-1}$, response rate values higher than 20 GHz and optical data links of 12 GBits/sec have been achieved. The thermal transistors developed with graphene sometimes contain an additive layer to increase its stability while protecting the sensing surface from oxidation and water. Some scientists have also tried to amalgamate the properties of graphene sensors to develop Field-Effect Transistors (FETs) having other prominent mechanical features like high strain-sensing capabilities [322-324].

The electrical sensing fields using GFETs include the employment of these sensors for studying different metallic ions in solution. Some of the heavy metallic ions like cadmium,

lead, mercury have been detected at low concentrations with the use of GFETs. The detectable concentration ranges from a few nano-molar ranges as shown in the table below. Other than the heavy ions, some of the commonly used ions like calcium, potassium, hydrogen have also been detected by these sensors. The detection of ions using these sensors takes place by non-covalent functionalisation of the sensing surface of the electrodes with the analyte ions. The other applications of GFETs in chemical sensing include the sensing of pH and different gasses like ammonia, nitrogen dioxide, and other inorganic gases. Graphene has been grown on different substrates like Silicon Carbide (SiC), poly (ethylene 2, 6-naphthalenedicarboxylate), etc. and transferred using mechanical transfer to flexible substrates. Some of the studies regarding gas sensing as shown below exhibit very low detectable concentrations as ppb at different gate voltages. Table 2.8 gives an overview of some of the selected work done on chemical sensing using GFETs. It gives the type of substrate used to grow graphene, the detected material, the range of gate voltages and the lowest detectable concentration.

Table 2.8 Comparison between the different parameters for the chemical sensing done by GFETs.

Type of substrate	Detected material	Gate voltage (V)	Detectable concentration/ Range of detection	Reference
Cu	NH ₃ , CO ₂	>1	30 ppm, 4000 ppm	[325]
N-type silicon wafer	NO ₂ , NH ₃	-5 to 5	10 ppm, 50 ppm	[326]
Cu	NH ₃	15	50 ppm	[327]
SiO ₂ /Si	H ₂	0	1 ppm	[328]
SiO ₂ layer	NO ₂ , Cl ₂	0	550 ppb	[244]
SiO ₂ , poly (ethylene 2,6-naphthalene-dicarboxylate)	pH	>0.5	Neutral to Acidic	[329]
SiC/silicon	pH	-1 to 1	4.3 - 7	[330]
SiO ₂ layer (Degenerately doped silicon wafer)	pH	-0.1 to 0.1	4 – 9.3	[331]
SiO ₂ /Si	pH	-0.8 to 0.8	6 – 9	[332]
Scotch tape, SiO ₂ layer	pH	Gate free chemiresistor	4–10	[333]
Silicone rubber/Glass	Pb ²⁺	0-1	0.02 g/L	[334]
Glass	pH	-0.2 to 0.4	3 - 10	[335]
SiO ₂ / Adhesive tape	K ⁺	-0.3 to 0.3	10 nM - 1.0 mM	[336]
SiO ₂	Hg ²⁺	-20 to 20	1 nM	[337]
PDMS	Ca ²⁺	-0.6 to 0.6	1 μM	[338]

2.3.6 Challenges with the Current Sensors

Although there has been a lot of research work done and going on with sensors based on graphene and its different forms, there are still some challenges that need to be addressed at the grass-roots level. The fabrication of graphene is a complex and expensive process. It requires a significant amount of time to generate high-quality graphene. Techniques to

generate low-cost graphene are yet to be commercialised. Some of the catalysts used during the growth of graphene increase its toxicity after its production [339]. This makes it difficult to use for biomolecular detection and other biomedical applications. This can also be addressed during its growth. The nanocomposites formed with graphene to develop or modify the electrode surfaces affect the intrinsic properties of the material. For example, the electrical conductivity of the composite decreases drastically (in terms of 10^3) compared to graphene. This could be crucial in applications demanding highly conductive electrodes. Secondly, the thermal stability also reduces in the case of nanocomposites due to a weaker interaction between the graphene and matrix compared to the pure form of graphene. These effects can be tackled by treating the formed composites with an extra step like chemical or thermal reduction [340, 341], but this would demand an extra step which could be convoluted in the case of multi-layered structures. Also, the homogeneity of graphene in oxide forms is almost impossible in the composites due to its poor dispersion. This leads to the addition of an extra step like the ball-mill mixing process to increase the rate of dispersion [342]. The vulnerability of graphene to be oxidised in oxidative environments is another major disadvantage to be dealt with. This makes it extremely difficult to utilise graphene in its pure form. Another disadvantage of obtaining pure graphene lies in the amount of raw materials required to generate it. For example, when graphene oxide (GO) is used to produce rGO, the chemical reduction causes a huge mass loss leading to very small amounts of generated samples [343].

Some of the significant research work on graphene-based sensors in different fields had been presented in this chapter. The conversion of graphene in different forms increases the dynamicity of its properties, causing an expansion in its applications. There has been some research reported by different groups on complete graphene-based sensing systems [344-346]. Their detection methodologies include mostly electrochemical sensing techniques. The data collected by the sensors are sent to the monitoring unit using different wireless protocols. Some of the electrochemical applications include bacteria detection on tooth enamel, where graphene was printed onto a water-soluble silk forming a sensing platform. This system was used for selective bio-detection of bacterial cells. The wireless conditioning circuit included a single-layer LC resonant circuit with a parallel resistive graphene monolayer. Another electrochemical application with graphene-based wireless sensors involves transparent gas sensors developed with an amalgamation of graphene and silver nanowires. Here, the wireless system contained a Bluetooth system embedded with an antenna. Electrical sensors developed with graphene include graphene varactors, which

were fabricated with a combination of a metal-insulator-graphene structure having a capacitance varying with the charge concentration as a result of the quantum capacitance effect. These devices along with an embedded LC oscillator circuit are very useful for wireless readout purposes. The quantum capacitance of graphene sensors has been put into use in other wireless sensing systems [347], even for simple detection of humidity concentrations. The results obtained from the experimental values with quantum capacitance have been cross-checked with capacitance-voltage measurements to validate the former's use in sensing systems. Other wireless protocols involved in complete graphene-based sensors involve the Wireless Integrated Sensing Platform [348]. This system used both analogue and digital wireless remote transmission principles while eliminating the use of any wire or battery operations. This system was combined with graphene-based gas sensor modules to detect NH₃ and CO gases. Another wireless protocol commonly used in complete sensing systems is the Radio-Frequency Identification Tag (RFID) combined with graphene-based sensing systems. The entire system consisted of platinum-decorated reduced graphene oxide attached to a RFID sensor tag and an RFID reader antenna connected to a network analyser. The sensing system was used to detect hydrogen gas at low concentrations [349]. The ZigBee standard is another wireless protocol involved with graphene-based sensing systems. These are used for the measurement of different pH and glucose concentrations. The sensed data were transmitted from the sensor to the XBee router via the XBee coordinator. This data was then interpreted using LABVIEW to extract significant information.

Apart from these sensing systems, in order to increase the usability of graphene-based sensors, categorisation can be done based on their strengths and limitations. Some of the advantages of graphene lie in the characteristics associated with its physicochemical structure. The sp² hybridised carbon atoms of the graphene structure make it highly conductive due to the absence of an electron in the outermost shell. The electrical conductivity of graphene is around 60 times more than that of CNTs, which makes it a favourable choice to form the nanocomposite-based electrodes of the sensors. The very low band gap between the valence and the conduction bands is another advantage which leads to the employment of these materials in supercapacitors [350-353]. There are four distinct advantages of graphene, which makes it a favourable choice for electrochemical sensors. Firstly, it exhibits a high surface area, thus having a higher and more uniform number of electrochemically active sites than other similar electrode materials. Secondly, the availability of oxygen-containing groups in its structure greatly influences the

electrochemical performances in terms of electron transfer rates. Thirdly, the presence of the oxygen groups also influences the adsorption and desorption of molecules taking place during the electrochemical reaction. Fourthly, the electrochemical modification can be done in covalent and non-covalent ways to functionalise the electrodes of the sensors with additional operations. Another big advantage of using graphene is the absence of heterogeneous materials during its production with methods like CVD, unlike CNTs which include carbon-containing gases with metallic nanoparticles as catalysts [354]. This provides two advantages to graphene over CNTs and other allotropes of carbon. Firstly, they can be used in the purest form to develop the electrodes of a sensor. Secondly, the cost of production of pure graphene is getting less than that of other materials [355]. They are also advantageous for energy-storage applications like the production of fuel cells, lithium-ion batteries and ultra-capacitors due to their ability to be charged and discharged under intercalation potentials. Different lithium-ion batteries and fuel cells have used graphene in the pure form or mixed it with other materials to increase the storage capacity. Another advantageous characteristic of graphene is its ability to display the half-integer quantum Hall effect at the speed of light, even at room temperature. The charge density of graphene can be controlled by the gate electrode, thus providing an ambipolar electric field effect having excellent electrode kinetics due to the high mobility of the carriers. It has the ability to carry super current because of the continuous charge carriers which are of high crystal quality, making light travel thousands of inter-atomic distances without any scattering [356]. The graphene-based sensors are also advantageous for bio-sensing purposes for two reasons. Firstly, they have a high-density edge plane and can act as a nano-connector between the analyte and the electrodes. Secondly, the availability of their two-dimensional electronic states on the surface makes them accessible by tunnelling techniques. This leads to the mediator-less direct transfer of electrons between the enzymes and the electrode surface. The flexibility of graphene sheets is also higher than for other allotropes of carbon like graphite, thus helping to form flexible electronic devices. Strain sensors with high GF can be developed using graphene, whose performance in terms of resistivity remains fairly constant even after a large number of bending cycles. Even though a lot of research has been done on these sensors, there are still some limitations which need to be addressed and rectified to improve the efficiency in the utilisation of these sensors on a commercial basis. Some of the limitations related to different graphene-based sensors are given in Table 2.9. It is seen from the table that there is still a lot to be done to address the fundamental characteristics of this material to make it more efficient to develop graphene-based sensors.

Table 2.9 Limitations of graphene as showcased in various research.

Sl. No.	Limitations	Reference
1.	The maximum photo-responsivity of graphene photodetectors is low. This is due to the small detection area of the graphene sheets and the very short photo-generated carrier lifetime.	[357]
2.	It is susceptible to oxidative environments. Thus, it cannot be used as a catalyst in redox reactions.	[358]
3.	Point defects are present in graphene due to its sp^2 hybridising property which results in the formation of various non-hexagonal structures. This alters the electro-mechanical properties of the resultant electrodes of the sensors.	[359]
4.	Even though a lot of graphene-based strain sensors have been developed in the laboratory environment, the stretchability is still insufficient due to the defect density in its structure.	
5.	The presence of multilayers in graphene sheets results in interlayer sliding, leading to a difference in crack densities.	
6.	Defects occur in graphene's structure during its interaction with metallic substrates.	[360]
7.	There are oxides in the surface of graphene which affect the electronic and chemical properties.	[361]
8.	There are unknown cytotoxic limitations in graphene sensors which limit their usage in bio-sensing applications.	
9.	A lot of parasitic effects are present in graphene which influences the response of the graphene-based sensors.	[362]
10.	The formation of different compounds with graphene changes its structural composition when an external load is applied, producing fracture lines, and increasing the number of dangling bonds in its structure.	[363]

2.3.7 Conclusion and Future Work

Although there have been some drawbacks of graphene and its sensor-based applications as mentioned in the previous section, graphene can still be considered one of the most promising materials in the last few decades that have been synthesised in the laboratory and employed for various applications. The number of potential applications using graphene sensors can be increased by converting more of the graphene-based sensors into sensing systems. The sensors can be embedded to form wearable sensing systems for ubiquitous monitoring of physiological parameters and chronic diseases. The sensors attached to the body should be made sturdier to sustain wear and tear for a long time. This can be attained by modifying the physical and chemical characteristics of the substrates that are used to develop the sensors. Many more day-to-day applications can be addressed by increasing the selectivity and specificity of graphene sensors. The response of graphene electrodes to target analytes and molecules should be increased while decreasing their responses to interfering molecules. Functionalisation of graphene electrodes should be utilised more, with capture agents for specific target molecules. More focus should be given to non-invasive, label-free detection of different biomolecules. The fabrication of graphene sensing systems should also be enhanced to produce low-cost, reusable sensors. One way to improve the quality of fabrication techniques is to use devices operating with less complexity and low input power. Another way to develop the fabrication procedure is to develop sensors with consistent performance in terms of efficiency. This can be achieved by not only addressing the performance of the sensors, but also the signal conditioning embedded with the sensor. Another approach to reduce the production cost is to fabricate multi-functional sensors, where different parameters can be addressed with a single sensing system. The signal-to-noise ratio of graphene sensing systems should be investigated to maximise the accumulation of useful information. When developing sensors, the structure of graphene is sometimes modified by separating the individual sheets. This changes the electrical and thermal properties of the material, thus reducing the overall efficiency. More work based on the diffusion processes and surfactants associated with graphene has to be done for its uniform dispersion in the different matrixes to form nanocomposites. The biocompatibility of graphene sensors should be exploited more by replacing the non-biocompatible commercial sensors that are currently available in the market. Graphene has always had a very bright side in its utilisation in commercial fields for various applications since its synthesis in the laboratory over the last two decades. The global market for

graphene is estimated to rise to 250 million USD by 2020 with an increase in its application. Figure 2.15 gives an overview of some of the potential applications like energy conservation, electronics industry, wearable devices, etc. where graphene is a candidate [364]. The usage of graphene in sensors, supercapacitors, and composites as explained in this chapter are predicted to be the dominant trend in different sectors like aerospace, automobiles, defence, and biomedical science in the upcoming years [365, 366]. Geographically, the Asia-Pacific market region is said to have the biggest marketing industry, while the academic and corporate sectors are predicted to have most of the usage of graphene. The consumption of graphene is increasing with time and is expected to have a huge impact on the quality of life.

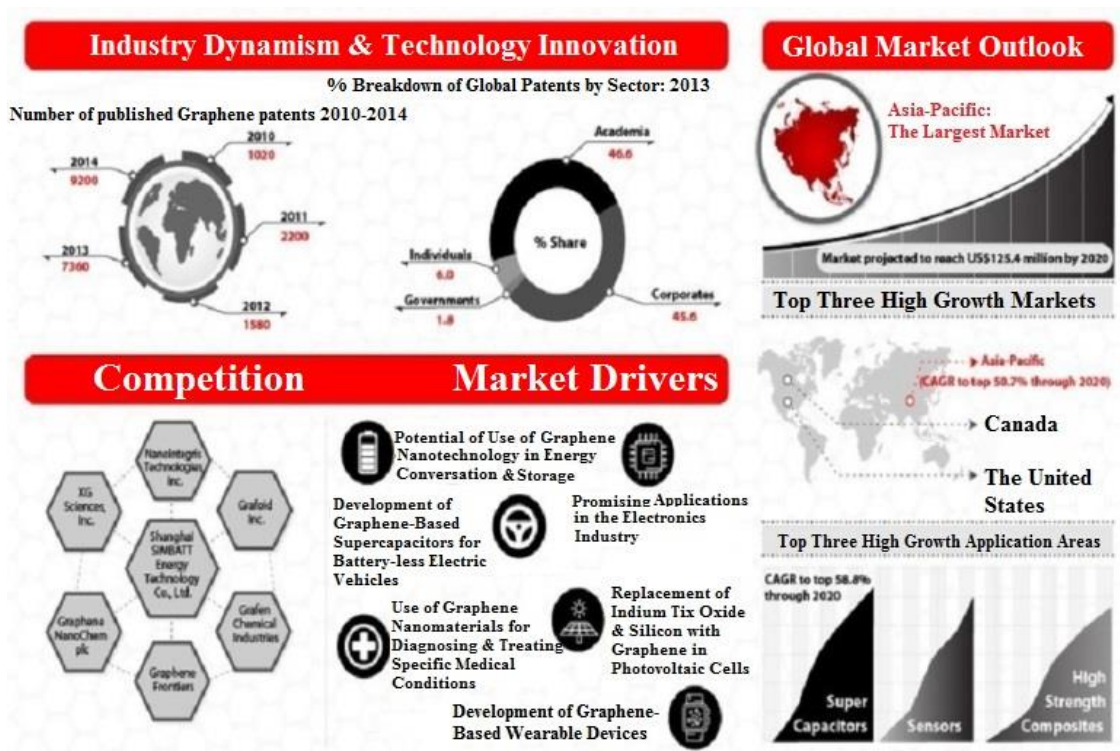


Figure 2.15 An overview of the potential applications and marketing areas of graphene in the upcoming years [364].

2.4 Wearable Flexible Sensors

In the last two decades or so, wearable flexible sensors have become a popular choice, where continuous monitoring of the patient can be performed by attaching the sensor or monitoring device on the arm, leg or organ under consideration. This has already proven

very advantageous, particularly in the case of elderly people, where the required response time is very short in the case of an emergency due to their low body strength and immunity towards diseases. These needs have led to the introduction of wearable sensing systems that can be worn for a short duration or in a continuous manner by the patient to address the problems faced by him/her and obtain a proper assessment.

Some of the advantages of using wearable sensing systems are:

1. Regular monitoring can be performed on the patient to scrutinise small changes.
2. Wearable systems exclude the use of vision sensors, which could violate the privacy of a person.
3. The response is much faster with wearable systems compared to non-wearable ones, as the patient can immediately inform the care-taker and request help in the case of an emergency.
4. The system is much more compact and easier to use compared to work-bench systems which would require the patient to visit a special place for examination purposes.

These advantages have led to the popularised use of wearable technology [7,8] in different applications. Even though the use of wearable sensors developed from inflexible sensors did serve a lot of functions in the biomedical field, there are certain disadvantages to those systems from the point of view of the structure and materials used to develop them.

Some of these disadvantages are:

1. High production costs as the cost of the raw materials used for fabrication is high.
2. The high-power usage of rigid wearable sensors (for example, silicon sensors) compared to sensors developed with flexible substrates. This causes a waste of energy in the longer run.
3. Discomfort for the patient due to the inflexible and brittle nature of the sensors, during muscular movements.
4. A greater mass compared to flexible sensors, which can cause discomfort to the person wearing the device.
5. The high risk of thermal injury caused by the inorganic nature of the electrodes and the substrates of the sensors.

The durability of the materials used to develop non-flexible sensing systems is lower because of their brittleness and rigidity. The power consumption, dynamicity, sensitivity, etc., of the sensing system are some of the other attributes where flexible sensing systems

overachieve compared to their rigid counterparts. Thus, with wearable sensors gaining popularity in commercial applications, the work on the development of wearable flexible systems was carried out on a large scale in order to integrate the advantages of flexible sensors with wearable devices. Flexible sensors have prominent advantages, which make them a significantly better choice for most applications. Some of the advantages of flexible sensors are:

1. They are thinner, and have high flexibility and bendability, which reduces the effects of their rigidity compared to their non-flexible counterparts.
2. Their impact resistance is higher than that of non-flexible sensors.
3. They are lower in cost, which is highly advantageous for production and use at large scales.
4. The substrates used to fabricate flexible sensors are organic in nature, which reduces the chances of thermal injury.

Due to the above-mentioned advantages, flexible sensors are preferable for use in wearable sensing systems for different applications [9,10].

2.4.1 Materials for Wearable Flexible Sensors

The material used for fabrication of wearable flexible sensors is decided by several factors like the application of the sensor, its availability, total cost of fabrication, etc. Organic electronics is one prime sector in the material side which has been substantially cultivated for the fabrication of flexible wearable devices [367]. Some of the prospects in the use of organic devices for flexible wearable devices are shown in Figure 2.16. These sensors have been used in the manufacturing of thin-film transistors, ionic pumps, polymer electrodes, etc.

Organic and large-area electronics (OLAE) [368] is a process to develop electronic devices printed in thin layers using functional inks. The substrates used for these processes are mainly PET and PEN due to their transparency and lower cost compared to other organic polymers. The OLAE process is currently used to develop wearable health and medical devices. The use of PDMS [369, 370], PEN [371], PI [284], P(VDF-TrFE) [372], Parylene [373] and Polypyrrole [374] have been commonly done to develop pressure sensors [375] for different applications. The electrode part of the sensor has been developed from different conducting materials like carbon-based nanomaterials and metallic nanoparticles. The carbon compounds include graphene [282, 283, 376], carbon nanotubes

(CNTs) [152, 377], carbon fibres [378], etc. Among the metallic nanoparticles, silver [155, 379], gold [37, 380] and nickel [381] are some of the most commonly used ones in flexible wearable sensors.

Biomedical signal monitoring is another sector which has been worked up with wearable flexible electronic devices [382]. Among CNTs, different sensing devices were developed with Single-Walled Carbon Nanotubes (SWCNTs) and Multi Walled Carbon Nanotubes (MWCNTs). Monitoring of metabolites on the skin was done by sensors with ion-electron potentiometric transducers developed from SWCNTs [383]. Oppositely charged multi-layered films of MWCNTs were used to develop chemo-resistive sensors [384]. The detection of sodium (Na^+) and potassium (K^+) ions was achieved using a sensor designed with a Cu/PI flexible electronic layer attached to an antenna for wireless transmission of data to an Android smartphone [385]. Monitoring of saliva for bacterial infection on tooth enamel has been done using graphene nano-sensors. These sensors were connected to an inductive coil antenna patterned with interdigital electrodes [344]. Flexible Organic electrochemical transistors (OECTs) are another type of sensor used for testing of saliva by converting biochemical signals to electrical signals. They are developed with a PANI/Nafion – graphene bilayer film [386]. These transistors were also developed by lamination of polypropylene films and amorphous silicon thin-film transistors on plasma-enhanced PI substrates. These sensors were used as pressure sensors and large area electronic sensing skins [387]. Magnetic-field sensors [388] are one category developed using inorganic functional nano-membranes with polymeric foils. A linear array of 8 sensors was formed to work on the principle of the Hall Effect to achieve high bulk sensitivity. A wearable electronic nose [389] was developed with a sensor array developed from a nanocomposite of CNTs and PEN. Hydrogel systems along with electrophysiological sensors [390] were developed with a spin-coated and thermally cured layer of PI on top of a layer of Poly (methyl methacrylate) (PMMA). The electrodes were formed with a bilayer of electron-beam-evaporated Cr and Au. These fabricated devices were applied for ECG, stress-strain measurements along with other biomedical devices [391]. Interestingly, even alloys were used in WFS to develop biometric sensors [392]. Thin-film thermocouples like Sb_2Te_3 and Bi_2Te_3 along with a Kapton substrate were used to fabricate a low-power, flexible micro-thermoelectric generator. The device is proposed to be used in Ambient Assistant Living (AAL) applications.

Figure 2.16 removed due to copyright

Figure 2.16 Pictorial representation of the different prospects of wearable flexible devices using organic electronics [367].

2.4.2 Sensor Networks for Wearable Flexible Sensors

Real-time applications of the monitoring of different physiological parameters are significantly dependent on the sensor network used to monitor and transfer the recorded data. After processing the received data in the analogue and digital divisions of the signal-conditioning circuit, the data is transferred from the sensor node to the monitoring unit via the router for further analysis. A schematic diagram for the transmission of data from the sensor to the monitoring is shown in Figure 2.17. The selection of a communication network depends on the cost of set-up, the power consumption, the number of sensor nodes, the range of trans-reception, etc. Table 2.10 shows a comparison of some network protocols standardised by IEEE [393]. Among them, Bluetooth has been the most popular one due to its cheaper installation, less hardware, and high compatibility. That is why, substantial research work has been done on developing Bluetooth integrated health-care systems [394-396]. Apart from the mentioned protocols in Table 2.10, there are some other networks with which data transmission for different biomedical flexible systems takes place. SHIMMER uses a Chipcon radio transceiver and a 2.4 GHz Rufa™ antenna [397]. Apart from this, there are other network remote technologies like Sun SPOT, IRIS, Mica2/MicaZ,

Telos [398]. Among these, Telos, developed by UC Barkley, used an IEEE 802.15.4 compliant radio claiming to use one-tenth of the power of previous mote platforms [399]. Radio-frequency (RF) is another network protocol which is used by different flexible acoustic resonators for data transmission [400]. For example, ECG monitoring systems have used the Tmote Sky platform which has an 802.15.4 radio interface at 250 kbps [401]. An wireless physiological management system (WPMS) was introduced [402] which defines carrying real-time physiological measurement data wirelessly from the medical sensors to the processing unit. The probable applications for this technique are in drug delivery systems like chemotherapy, diabetic insulin therapy, AIDS therapy [403]. The schematic diagram of the hardware architecture of the wireless sensor node for WPMS is shown in Figure 2.18 [402]. Another network protocol called Wearable Based Sensor Networks (WBSNs), based on IEEE 802.15.4, was introduced that had different probable applications like the ECG-based system, a wearable platform for light, audio, motion and temperature sensing [404]. Toumaz Technologies, UK devised a wireless system-on-chip integrated system where the transceiver operates in the 862-870 MHz and 902-928 MHz ISM bands in European and North American countries respectively [405].

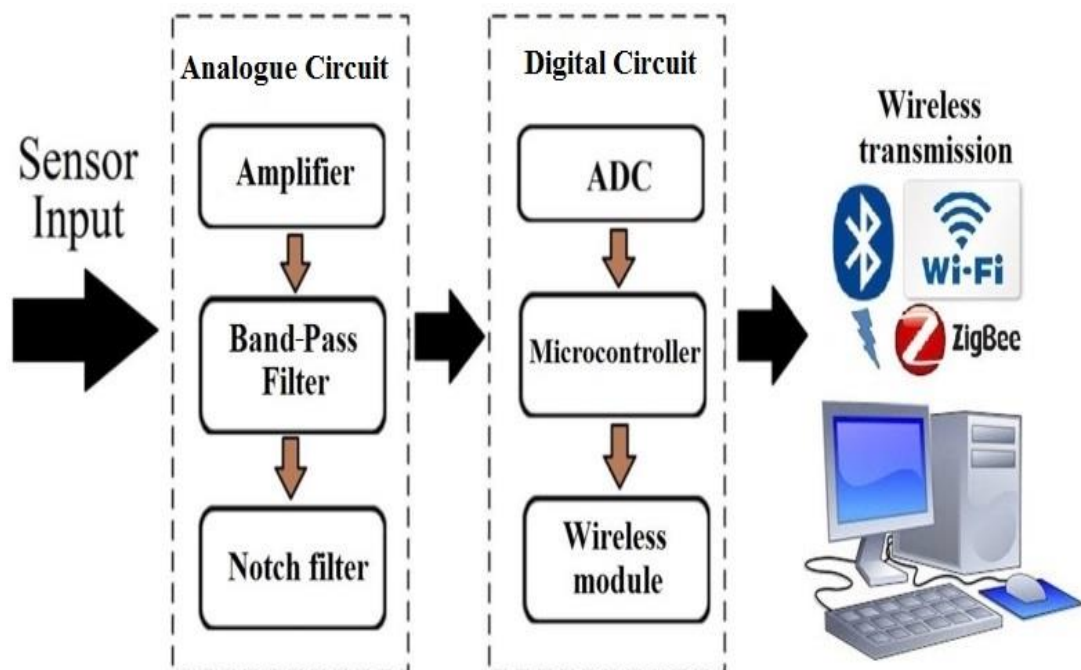


Figure 2.17 Schematic diagram of the transmission of data from the sensor to the monitoring unit.

Table 2.10 Network protocols standardised by IEEE [393].

Standard	ZigBee (IEEE 802.15.4)	Bluetooth (IEEE 802.15.1 WPAN)	Wi-Fi (IEEE 802.11 WLAN)	Wi-Max (IEEE 802.11 WWAN)
Range (m)	100	10	5000	15000
Data rate (kbps)	250-500	1000-3000	1000-45000	75000
Bandwidth (GHz)	2.4	2.4	2.4, 3.7 and 5	2.3, 3.5 and 3.5
Network Topology	Star, Mesh and Cluster trees	Star	Star, Tree, P2P	Star, Tree, and P2P
Applications	Wireless Sensors (Monitoring and Control)	Wireless Sensors (Monitoring and Control)	PC-based Data acquisition, Mobile Internet	Mobile Internet

Research projects with antennas and RF systems integrated into clothing have also progressed, working on Body Area Networks (BAN) where low-powered devices would be surface mounted on the clothing in a fixed position [406]. BAN is categorised into three categories: off-body, on-body, and in-body [402, 407]. Battery-operated systems was another option that was considered, where the developed system would be powered by a battery integrated into the system [408, 409]. The advantage of using self-powered systems [410-412] is that the battery or the power unit of the wireless system does not have to be replaced every time the charging-discharging cycle completes.

Figure 2.18 removed due to copyright

Figure 2.18 Schematic diagram of the hardware architecture for the sensor node for WPMS [402].

2.4.3 Types of Activity Monitoring with Wearable Flexible Sensors

Different types of flexible wearable sensors are used in the application world based on the parameter being monitored. These parameters, as a result, would decide the fabrication technique of the sensor prototypes. For example, monitoring of physiological parameters [413] of a person like limb movements [16], motions like walking, running, etc. [35], gait analysis [414] would require the sensor patches to be bigger and more flexible. But parameters like respiration [415], heart rate [416], cardiorespiratory signals [417] would require the sensors to be very small and sensitive. Another application of WFS is as glucose sensors via different media like tear [418], immobilisation of glucose oxidase [419, 420], etc. Electronic skins or e-skins [421, 422] are another category which was developed to mimic the functions of a natural skin and determine the changes in temperature, pressure or even health conditions. These sensors [423] are integrated with thermal actuators and organic displays. Figure 2.19 shows the schematic of one type of electronic skin developed with elastomeric substrates. One of the examples is the development of a wearable-on-the-skin [424] sensing systems that could be used as physiological sensors, non-volatile

memory and for drug release [425-427] and therapeutic actuators [428, 429]. Figure 2.20 shows schematic for the fabrication of the device and the finished product. Flexible sensors with high mechanical sensitivity, flexibility and durability were designed for speech recognition and physiological signals [430] in the geometry of a spider's sensory system. Biomedical signal monitoring was done involving monitoring of hydration state and electrophysiological activity monitoring using Optical, electrical and radio-frequency sensors [431]. Spin-coated thin layers of PDMS and PI were used as substrates and bi-layers of sputtered Chromium (Cr) and Gold (Au) as electrodes. Monitoring of skin hydration through thermal conductivity, blood oxygenation, electrocardiogram (ECG), electromyogram (EMG), electrooculogram (EOG) are some of the suggested parameters that could be covered with these sensors. Figure 2.21 shows a schematic diagram of a rugged and stretchable electronic sensor. Strain sensors [242, 432, 433] are the most important category of flexible sensors, and have been used for multiple disciplinary applications. Human-motion detection [151, 434], forces and acoustic vibrations [37], artificial skins [435] are some of the other applications for those sensors. Flexible sensors have been widely used as pressure sensors [37, 375, 436] due to their high flexibility and bendability, depending on the raw material used for their fabrication. They also have great potential in the field of robotics, aviation, etc.

Figure 2.19 removed due to copyright

Figure 2.19 Schematic diagram of electronic skins with a sensor perception on a human arm [423].

Figure 2.20 removed due to copyright

Figure 2.20 (a) Schematic diagram for the materials used to develop the sensor. (b) Finished product [424].

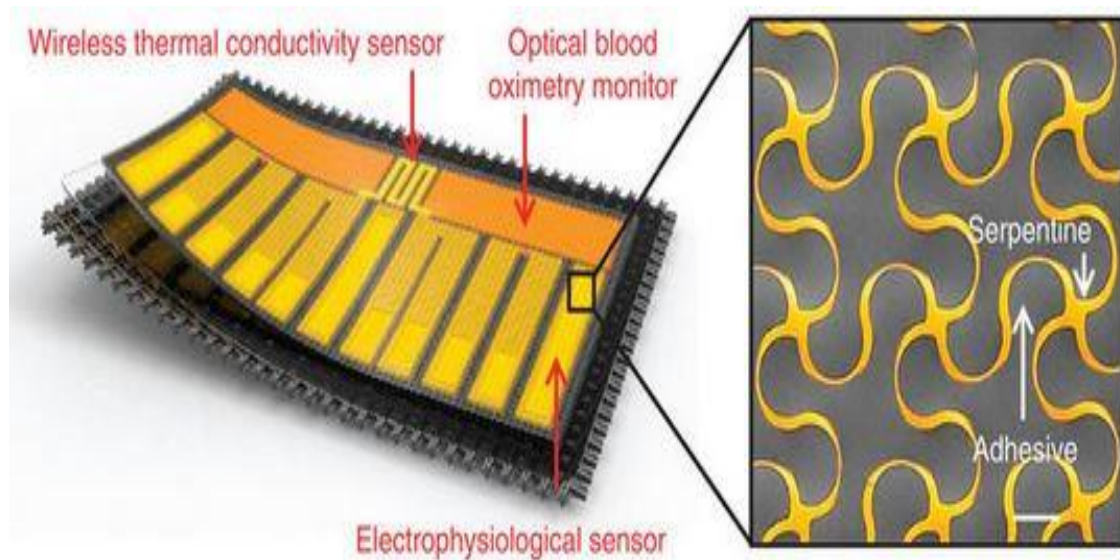


Figure 2.21 Schematic diagram of the rugged and stretchable electronic sensor for electrophysiological activities [431].

Another prominent aspect of the application of WFSs is the monitoring of biological fluids like sweat and saliva [437] via skin-tattooed nano-sensors connected on the wrist and within the mouth respectively. These sensors were also used to monitor glucose electrochemically from tears of a person by embedding the wireless sensor with a contact lens. Tattoo-based sensors have been widely developed [438] and used for different applications like potentiometric [439] and amperometric [440] sensor based systems. These devices have significant applications for skin-worn silver (Ag) – zinc (Zn) alkaline batteries [441] and monitoring of change in pH [442] and ions like sodium and ammonium [443, 444]. Chemical and biological sensing also involve pH measurements [445] by strapping the embedded system around the waist contained with the sensor connected with microcontrollers and LED. The schematic diagram of the system and its attachment to a subject is shown in Figure 2.22. WFSs have also been designed and experimented with for detecting different kinds of gasses. Carbon monoxide (CO) and carbon dioxide (CO₂) [445] gas sensors were fitted in the garments or boots of people like firefighters for safety measures.

Figure 2.22 removed due to copyright

Figure 2.22 (a) Schematic diagram showing the pH-sensitive chip along with the LED and photodiode. (b) Place of the sensor on a person [445].

Oxygen (O₂) sensing systems [446, 447] were designed and fitted on the wrist of a person to determine the continuous change in oxygen level happening in haemoglobin during respiration. Microelectromechanical systems (MEMS) fabrication techniques have been largely involved in fabrication of WFSs for biological applications, for example, a blood-cell-counting sensor developed with micro silicon chips [448]. The technique was also used to aid patients with hearing problems by developing micro-acoustic sensors for sound-source localisation [449] and hearing purposes [450]. It was also used to develop a wearable flexible biomedical sensor to monitor the change in temperature inside the brain during mental activities and for study of circadian rhythms [451]. Textile-based systems were also designed and developed for monitoring purposes. One of the advantages of these systems is the comfort of the patient being monitored without the trouble of wearing a separate wearable system. The contact of the textile with most of the skin makes it a popular choice to attach sensors for monitoring purposes [380, 452]. Many projects, like VTAMN (France), Life Shirt (USA) and Wearable Health Care Systems (WEALTHY) (Europe), are going on with different research groups with fibre-based sensor systems for medicine, home healthcare and disease prevention [453]. Fibre-based sensors were also developed largely from piezo-resistive fibres, elastic and regular polyester fibres. These sensors were used for conducting experiments for different applications like respiration [454] and cardiovascular diseases [455]. Another category, called plastic optical fibres was used for pressure sensors [456]. Followed by treatment with acetone to remove its stickiness, raw flexible silicone fibres were weaved to form pressure sensors with a thickness of around 0.51 mm. The fibre-based generator [457] is one of the applications where the electrostatic charge generated on the fibre during biomechanical vibrations can be converted into electricity. These Nano-generators work in a non-contact mode relying on air pressure [458], and thus can be used as ultrasensitive sensors for performing medical diagnostics and as measurement tools. The fibre was also integrated with a computer [459], and named Planar Fashionable Circuit boards (P-FCB), for sweat monitoring using RFIP tag antennas. P-FCBs were also associated with ECG monitoring [460], physiological-signal monitoring [461] and as a health-monitoring system [462, 463]. Another application for fibre-based systems is a motion sensor [464], temperature sensor [465], etc. Flexible printed-circuit boards (FPCBs) were also developed for in situ perspiration analysis [466]. The design of one of the FPCBs is shown in Figure 2.23. A drug delivery pump (DDP) [467] is another idea that the researchers have worked upon, developed with PDMS and a negative photoresist by standard photolithographic technique. This sensor was used as a pressure sensor, where the

drug can be ejected based on the applied pressure. The concept of DDP can be employed as a smart bandage along with a temperature sensor which can detect the minute changes in body temperature while doing physical activities.

Figure 2.23 removed due to copyright

Figure 2.23 Flexible Printed Circuit Board developed for in situ perspiration analysis [466].

2.4.4 Challenges and Future Opportunities

Even though a lot of work has been done with WFSs, there are still some issues that need to be dealt with. Researchers are trying 24/7 to develop sensors with better performance, regarding sensitivity and sustainability, than the existing ones and easier fabrication and implementation, for ubiquitous monitoring. The massive amount of data generated by the sensors wearable system causes a difficulty to handle and store them. Also, it becomes a tedious job for the system to filter out the significant data from the massive database for future analysis. Due to the enormous amount of monitored data, there needs to be a proper security system to curb any mishandling and misuse of the received data. Time-varying traffic is another issue raised during data transmission from different sensor nodes in a real-time topological system. This causes a delay in data reception in the monitoring unit, thus decreasing the efficiency of the system. Also, some of the significant

data might get lost due to the high traffic generated by AAL applications. The data transmission for a central coordinator system in Wireless Sensor Networks (WSNs) should be handled properly to minimise traffic and the loss of data. The connectivity and interoperability of the embedded system should be significant, to minimise the power and data loss. From a patient's point of view, the person should not face any kind of discomfort to wear the WFS. There should not be any breach of privacy for the patient from the monitoring. The embedded system attached to the sensor should not loosely attach to the body or clothes worn by the person, who could alter the data depending on movements and the surrounding environment. There is also a risk of thermal effects of the attached sensors from the tissues of the patient. A lot of factors decide these thermal effects [468]. The number of sensors used in the embedded system should be kept as small as possible. The location of the sensor is also important. The positioning of the sensor on the arm will have more thermal effects than its positioning on the chest. The operating frequency of the sensor and network protocol should be as low as possible. Power consumption by WFSs is another significant issue that needs to be addressed. Sensors like SHIMMER, Telos with low power consumption should be considered for monitoring purposes to reduce the overall power consumed by the WFS. The continuous supply of power to the system is another challenge that needs to be addressed for future systems. The system should be designed for on-node processing and reduce the effects of motion artefact and distributed interference.

There is a prominent future for flexible electronics in wearable systems based on its market values [469]. The market value of printed and flexible electronics is estimated to be over 75 billion USD by 2025 [470]. There is a substantial opportunity to use these flexible systems for monitoring health parameters. The estimated cost of WFSs by 2020 is more than 3 billion USD [471], and over 40 billion USD with more than 240 million annual unit shipments by 2025 [472]. The challenge for the companies is to design the systems to decrease in the overall fabrication cost. One way to achieve this is to use cheap, safe and biocompatible materials for the designs. FlexEnable, one of the UK-based companies, has predicted a rise in organic electronics among a WFSs [473]. With growing interest of consumers, the companies should design systems which would serve the people, not only to meet the application purposes, but also their economic condition. The systems should be made cost-effective so that it can address the wider community in the society.

2.5 Chapter Summary

A brief review on some of the prominent research works done on WFS had been depicted in the chapter. The sensor types based on different materials along with the communication networks used for monitoring purposes are described in this section. The scope of research work on this topic is increasing every day with the growth in its market value. The estimated figures for the use for WFS for the next 10-15 years have been mentioned along with the challenges that the WFS is producing companies needs to address. The growth in MEMS along with Nanoelectromechanical (NEMS) technology is expected to reduce the cost of fabrication of the flexible sensing systems leading to a wider range of applications in recent future. The utilisation of the existing manufacturing techniques along with upcoming ones will assist in developing new sensing systems should avail the people to have a better quality of life in near future.

3

Interdigitated Sensing and Electrochemical Impedance Spectroscopy

Publications pertaining to this chapter:

- **Anindya Nag**, N. Afsarimanesh, S. Feng and S. C. Mukhopadhyay, “Strain Induced Graphite/PDMS sensors for Biomedical Applications”, **Sensors and Actuators A: Physical**, Vol. 271, pp. 257–269, **March 2018**.
- **Anindya Nag** and S. C. Mukhopadhyay, “Fabrication and implementation of printed sensors for taste sensing applications”, **Sensors and Actuators A: Physical**, Vol. 269, pp. 52-61, **January 2018**.

3.1 Introduction

This chapter describes the structure of the sensor prototypes that are developed in the succeeding chapters. It explains the operating principle of the sensors in terms of their electrical and mechanical behaviour. The sensors were developed to serve the dual purpose in terms of the change in dimensions because of the applied force, as well as the change in their electrical behaviour while using them in an electrochemical cell. It also showcases the phenomenon of impedance spectroscopy used to characterise the sensor patches and subsequently analyse the changes occurring in them during different operations. All the sensor prototypes were flexible in nature with interdigitated electrodes. The electrical conductivity of the sensors depended on the type of material used as electrodes of substrates, while their flexibility was decided by the fabrication technique used to develop them. A singular type of electrode design was used to develop all the sensor prototypes due to the distinct advantages mentioned in the subsequent sections in this chapter. Electrochemical impedance spectroscopy (EIS) was used as the measurement tool for the developed prototypes to determine the changes for each application. The response of the systems was determined as a function of frequency to calculate the changes occurring in linear and non-linear systems. EIS served as an excellent tool for measurement, as the sensors were operated at dynamic interfaces where specific system parameters were monitored.

3.2 Planar Interdigital Sensors

Flexible sensor patches with an interdigitated electrode pattern were chosen for structural designing. The electrodes were shaped in an interdigitated manner due to three distinct advantages. Firstly, they operate in a non-destructive and non-invasive manner, generating a rapid response [474]. Secondly, the resultant sensitivity of the sensor is high due to the increased change in the net electric field as a result of the applied stress [475]. Thirdly, the self-resonant frequency of the sensors is minimised due to the planar shape of the electrodes.

The sensor patches work on capacitive sensing, where one electrode is considered as the excitation one where a voltage is provided, and the other one is considered as a reference electrode. The planar structure of the electrodes was employed for single-sided, non-

invasive measurements. Figure 3.1 shows the electrical phenomenon of the designed electrodes [476]. When a time-dependent voltage signal is provided to the excitation electrode, an electric field is generated between the oppositely charged electrodes. This field bulges between them due to their planar structure. A one-directional measurement condition was chosen with an insulating substrate to the electrodes. When any material is considered for testing purposes, it is kept in contact with or in proximity to the sensing area of the sensors. The field bulges through the Material Under Test (MUT) while travelling from one electrode to another of opposite polarity. This changes the properties of the electric field, which is studied using any of the response analysers to determine the dynamics of the system [21]. With a change in the stimulus to the system or device, the change in the characteristics of the electric field is studied to determine the change in the MUT. The penetration depth of the electric field is varied by varying the spatial wavelength (distance between the electrode fingers of the same polarity), which makes it a popular choice for domestic [7], industrial [8, 14, 477] and scientific [478-480] applications.

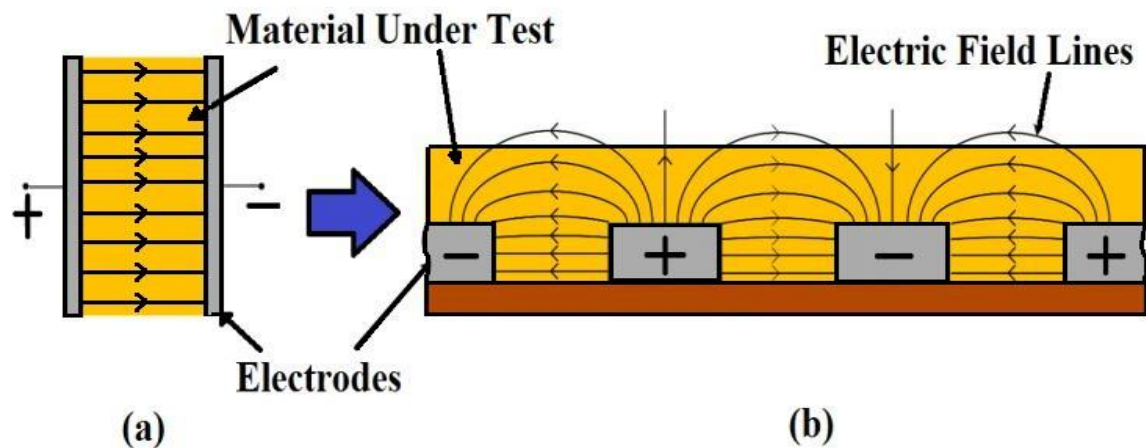


Figure 3.1 Working principle of the sensor patch. (a) The sensor works on the idea of a parallel-plate capacitor. (b) Due to the planar structure of the electrodes, the electric field bulges from one electrode to another of opposite polarity [476]. Reproduced from Khan, M.R.R.; Kang, S.-W. Highly Sensitive Multi-Channel IDC Sensor Array for Low Concentration Taste Detection. *Sensors* 2015, 15, 13201-13221. <https://doi.org/10.3390/s150613201>. (CC BY 4.0).

Due to the flexible nature of the sensor patches, there is a change in the response because of the stress induced on them. The operating principle for the fabricated sensor patches is shown in Figure 3.2. Based on a parallel-plate capacitor, the capacitance of any interdigitated sensor can be assumed as a parallel-plate capacitive device can be generally expressed by equation 3.1,

$$C \propto (\epsilon_0 * \epsilon_r * A) / d \quad (3.1)$$

where C is the capacitance, $\epsilon_0 = 8.85 \times 10^{-12} \text{ F} \cdot \text{m}^{-1}$ is the permittivity of vacuum, ϵ_r is the relative permittivity, A is the effective area ($A \gg d$), and d is the effective spacing between electrodes of different polarity.

A change of d or A causes a change of the capacitance. This can be exploited to monitor a physiological event through the change in capacitance based on the deformation-reformation of the sensor patch. The exertion of a tensile stress on the patch via a physiological event changes the capacitance from its normal value [475, 481]. Figure 3.2 depicts the notion. L and W stand for the length and width of the sensor patch, respectively. ΔL , ΔW , and Δd are the changes in length, width and interdigital distance of the sensor patch, respectively, caused when deformed.

Figure 3.2 removed due to copyright

Figure 3.2 Operating principle of the developed sensor patches was based on the capacitive principle [482].

Using equation 3.1, the change in capacitance can be calculated as a function of the change in length (ΔL), width (ΔW) and interdigital distance (Δd) as shown in equation 3.2.

$$\Delta C = C * \left(\frac{\Delta L}{L} + \frac{\Delta W}{W} - \frac{\Delta d}{d} \right) \quad (3.2)$$

where ΔC is the change in capacitance; ΔL , ΔW and Δd are the changes in length, width and interdigital distance of the sensor patches respectively.

The effective reactance and impedance changes as a function of the change in the resultant capacitance of the sensor patches:

$$\Delta X = f(\Delta C) \quad (3.3)$$

The stress exerted on the sensor patches leads to the re-orientation of the graphite powder in the PDMS-contained electrodes. This changes the complex resistance and, as a result, the complex conductivity of the electrodes,

$$\Delta R = R * \left(\frac{\Delta l}{l} - \frac{\Delta A}{A} - \frac{\Delta \sigma}{\sigma} \right) \quad (3.4)$$

So, the overall change in impedance can be expressed as

$$\Delta Z = f(\Delta R, \Delta X) \quad (3.5)$$

where l is the effective length of the electrodes, σ is the effective conductivity, $\Delta \sigma$ is the change in conductivity, ΔR , ΔX and ΔZ are the changes in the effective resistance, reactance and impedance respectively.

The change in the response of the sensors can also be related to the change in the complex conductivity. The biggest advantage of measuring the output in terms of conductivity is due to two reasons. Firstly, due to the high electrical conductivity of the electrodes, even a small change in dimension of the sensor prototype because of the applied stress can be monitored in terms of conductivity. Secondly, employment of the sensor prototypes for different applications would exert different ranges of forces on them, as a result of which, the change in conductivity of the electrodes can be studied easily. As the sensors do not behave as ideal capacitors, the variation in the conductivity values with respect to frequency can be analysed from the complex conductivity as shown from equation 3.6.

$$\sigma_{complex} = \sigma + j2\pi f\varepsilon \quad (3.6)$$

where $\sigma_{complex}$ is the complex conductivity, σ is the effective conductivity, ε is the permittivity, f is the operating frequency.

The electric-field density distribution for an applied stress between two electrode fingers of opposite polarity for one of the developed sensor prototypes is shown in Figure 3.3. The analysis was done using COMSOL 3.2b. Vacuum was considered for the simulation environment while assigning graphite and PDMS as the electrode fingers and substrate of the sensor, respectively.

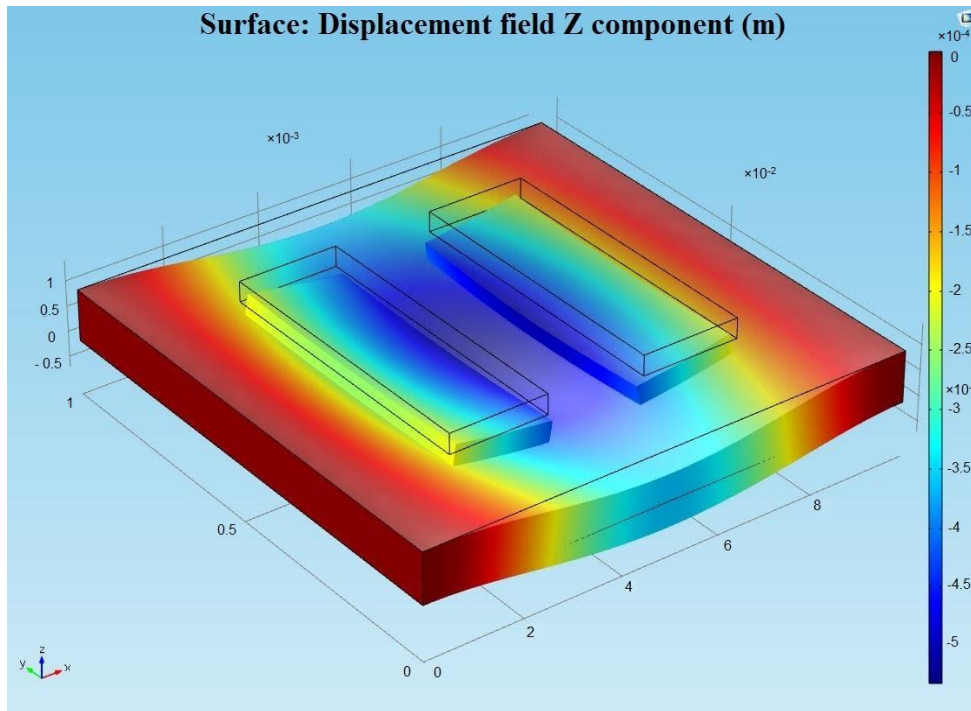


Figure 3.3 Three-dimensional simulation done using COMSOL 3.2b to determine the change in the electric field distribution on the sensor patch for the applied stress.

The electric field density was calculated in terms of the displacement field in the same direction (z-direction) of the applied stress. It is seen from the figure that the maximum electric field is concentrated at the centre of the fingers, thus causing a maximum change around that region. Due to the capacitive structure of the sensor patch, the charge density on the electrode fingers varies with the resultant electric displacement field. So, the net

charge density on the electrode fingers changes with the applied stress, thus causing a variation in the response.

3.3 Electrochemical Impedance Spectroscopy (EIS)

Electrochemical Impedance Spectroscopy (EIS) is one of the most powerful tools for sensor investigations due to its robust and non-invasive nature [483]. Even though it is mostly used to characterise the electrical double layer at the electrode/electrolyte interfaces [484], the response of the sensors as a function of frequency is also very useful in non-linear processes. EIS is a powerful technique with a high sensitivity towards interfacial phenomenon that is used to determine the change in impedance of a system in the presence of an external medium. In this process, frequency response analysis is done in the presence of a small amplitude of AC signal on top of a controlled DC polarisation potential. The internal dynamics of the system are determined from its response towards the change in frequency. The real and imaginary parts of the impedance are usually considered to represent the changes occurring in the system. When a small-amplitude excitation voltage is applied to a system, there is a change in the phase angle (Φ) between the input voltage and the output current. This response is said to be pseudo-linear considering its change to a low potential. In a linear system, there will be a sinusoidal output current with respect to the input sinusoidal voltage with a shifted phase angle (Φ) as shown in Figure 3.4.

The excitation signal to any cell can be represented as:

$$E_t = E_0 \sin \omega t \quad (3.7)$$

where E_t is the output voltage at time t , E_0 is the amplitude of the input signal, ω is the angular frequency ($\omega = 2\pi f$) expressed in terms of radians/second, f is the frequency in Hertz.

The output current of a linear circuit with a phase shift of Φ can be expressed as,

$$I_t = I_0 \sin(\omega t + \Phi) \quad (3.8)$$

Therefore, the total impedance can be expressed as,

$$Z = \frac{E_t}{I_t} = \frac{E_0 \sin \omega t}{I_0 \sin(\omega t + \theta)} \quad (3.9)$$

$$Z = Z_0 \frac{\sin(\omega t)}{\sin(\omega t + \theta)} \quad (3.10)$$

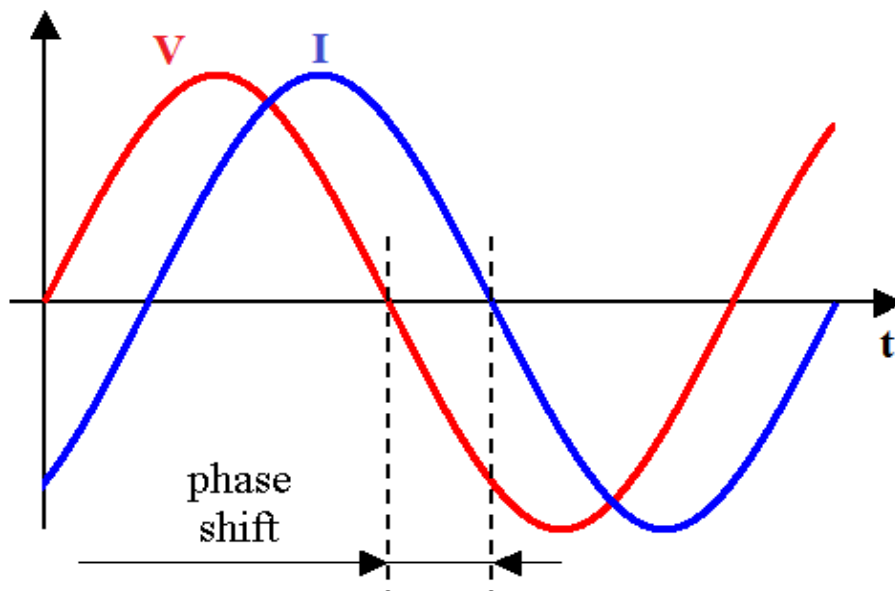


Figure 3.4 Phase shift in the output current with respect to the input voltage.

The responses of the sensor prototypes fabricated and employed for different applications were monitored using different impedance analysers. Physiological movements, tactile sensing, salinity sensing, force and strain measurements and taste sensing are some of the applications they were chosen for. The analysers were tuned in accordance with the application, operating over a specific frequency range. The connection of the analysers to the system has been explained in the experimental section of each application.

3.4 Chapter Summary

This chapter gives a summary of the working principle of all the developed sensor prototypes. Flexible sensor patches with interdigitated electrodes were developed which served a dual purpose in terms of electrical and mechanical attributes. The electrical

changes in the sensors occurred due to the capacitive nature of the interdigital electrodes, while the mechanical changes occurred due to the flexible nature of the sensors. EIS was used as the technique to monitor the responses of the sensor prototypes for each application. The impedance analysers were chosen to do the measurements for the linear and non-linear systems in the succeeding chapters.

4

Carbon Nanotubes- Polydimethylsiloxane Sensor

Publication pertaining to this chapter:

- **Anindya Nag**, S. C. Mukhopadhyay and J. Kosel, “Flexible carbon nanotube nanocomposite sensor for multiple physiological parameter monitoring”, **Sensors and Actuators A: Physical**, Vol. 251, pp. 148-155, **November 2016**.
- **Anindya Nag**, S. C. Mukhopadhyay and J. Kosel, “Transparent biocompatible sensor patches for touch sensitive prosthetic limbs”, 10th International Conference on Sensing Technology (ICST), 11-13, Nanjing, China, pp. 1-6, **November 2016**.

4.1 Introduction

The development of the novel flexible sensor patches using PDMS and MWCNTs is described in this chapter. The sensor patch utilises polydimethylsiloxane (PDMS) as the substrate and a nanocomposite of PDMS and carbon nanotubes (CNT) as electrodes. PDMS had been substantially used [485-487] for the development of flexible sensors due to its low cost, non-toxicity, inertness and hydrophobic nature. CNTs were preferred as the conducting material over other metallic nanowires because of their biocompatibility, high flexibility, resistance towards temperature change, low stiffness, and high tensile strength. Multi-walled carbon nanotubes (MWCNTs) were used for the experiments, functionalised with carboxylic groups (-COOH). The functionalised MWCNTs have a better dispersing capability inside a polymer compared to un-functionalised or single-walled carbon nanotubes (SWCNT). This leads to a better interfacial bonding between the nanotubes and the polymer, resulting in a higher conductivity. Interdigitated electrodes were patterned on the nanocomposite layer, allowing for a non-invasive and single-sided strain measurement. The patterns were produced using CO₂ laser ablation [488, 489]. Compared to other fabrication techniques like 3-D printing [490], photolithography [491], inkjet printing [492], etc., it excels in the ease of sample preparation without the need for any templates or additional material. This method fabricates very thin and flexible materials and can cut smooth edges which are approximately perpendicular to the surface. By attaching the sensor to the skin, respiration and limb movements were tested on different people as shown in the experimental results section, to verify its functionality. They were also used for tactile sensing of low pressures by attaching the sensor patches on the finger of the arm and placing different weighted objects on it.

4.2 Fabrication of the Sensor Patches

A schematic diagram of the fabrication steps is given in Figure 4.1. PDMS (SYLGARD[®] 184, Silicon Elastomer Base) was cast at a ratio of 10:1 of base elastomer (pre-polymer) and curing agent (cross-linker) on a Poly (methyl methacrylate) (PMMA) template. The template was patterned using a laser cutter (Universal Laser Systems). PMMA was chosen because of its impassiveness towards PDMS, and the cured material can be easily peeled off from the base without any additional steps.

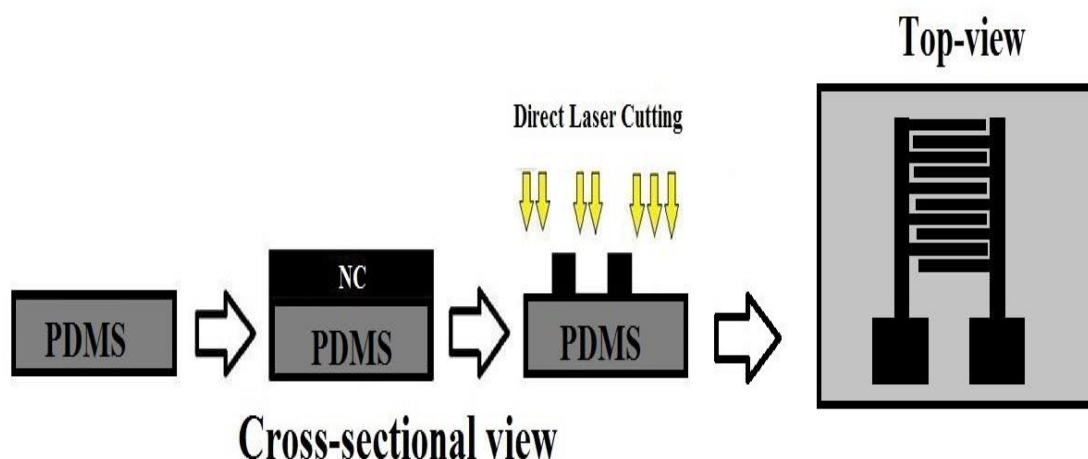


Figure 4.1 Schematic diagram of the fabrication steps. PDMS: Polydimethylsiloxane. NC: Nanocomposite.

The thickness of the cast PDMS was adjusted to 1 mm by a casting knife (SHEEN, 1117/1000 mm). The sample was then desiccated for 2 hours to remove any trapped air bubbles. The sample was cured at 80 °C for 8 hours to form the substrate for the sensor patch. A mixture consisting of functionalised MWCNTs (Aldrich, 773840-100G) and PDMS was then cast onto the cured PDMS.

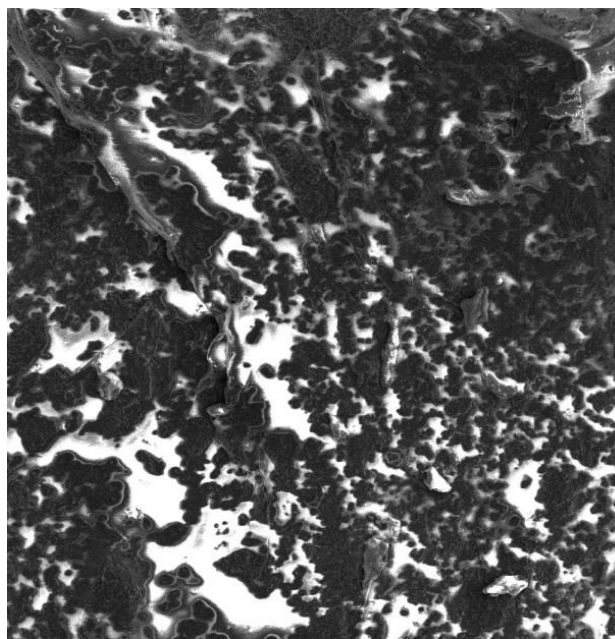


Figure 4.2 SEM top-view image of the nanocomposite consisting of CNTs (4% wt.) and PDMS.

4 % wt. of CNT was used after an optimisation between the conductivity and dispersion of CNT into PDMS. After the adjustment of the thickness of the nanocomposite layer by the casting knife to around 600 microns, the sample was again desiccated for 2 hours to remove any trapped air bubbles. Then the nanocomposite layer was cured at 80 °C for 8 hours. Laser induction (Universal Laser Systems) was then employed to form the electrode pattern on the cured nanocomposite. A SEM image of the nanocomposite is shown in Figure 4.2. The white regions in the image are the PDMS, and their counterpart black regions are the CNTs. Images of the individual steps are shown in Figure 4.3. After a series of short-circuit and transparency tests on the different electrodes, the one fabricated with a combination of the power of 24 W and speed of 70 m/min turned out to be the most viable one and was used for further characterisation and experimentation. The front and rear views of the sensor patch are shown in Figure 4.4. The black spots in the PDMS shown in the rear view of the sensor patch are some agglomerations of CNTs that lie within the PDMS layer. Table 4.1 shows the combination of power and speed settings tried for an optimal cut of the sensor patch.

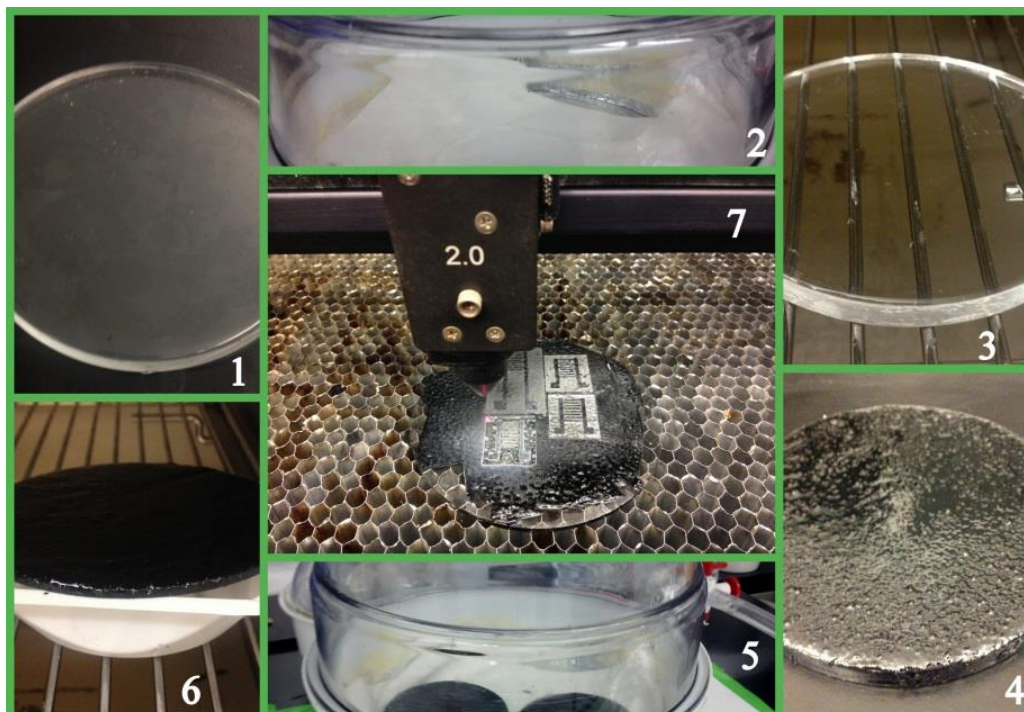


Figure 4.3 Fabrication steps: (1) Casting of PDMS, (2) Desiccation of PDMS, (3) Curing of PDMS, (4) Casting of nanocomposite (NC), (5) Desiccation of NC, (6) Curing of NC, (7) Laser patterning of electrodes.

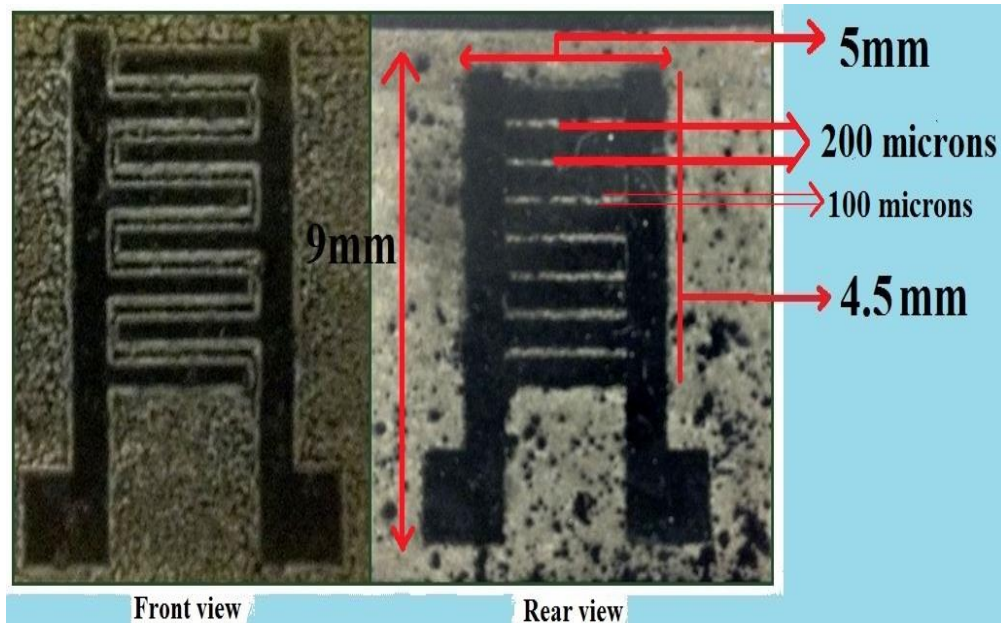


Figure 4.4 Front and rear-view images of the sensor patch.

Power (W) refers to how energetically the laser fires on the sample. Speed (m/min) refers to the rate of movement of the laser nozzle in the X and Y directions. The Z-axis was used to adjust the focal point of the laser beam on the ablated material. This is done by moving the laser head in the z-direction. The thicknesses of the electrodes were measured by a profilometer (XP-200). When fabricating sensors with very low power and speed settings, a hardening effect on the patch was observed, this led the nanocomposite to come off upon application of stress to the patch.

Table 4.1 Power and speed combinations of the laser cutting tool to obtain different electrode thicknesses.

Power (W)	Speed (m/min)	z-axis (mm)	Thickness of the electrodes (microns)
1.2	4.2	2	137
2.4	7	2	140
12	42	2	150
24	70	2	175
42	126	2	180

4.3 Frequency Response and Stress-Strain Measurements

Impedance measurements of the sensor patch were performed by a Precision Impedance Analyser (Agilent 4294A). Open and short calibrations were done before measurements to remove the effect of stray capacitances. The frequency was swept from 10 kHz to 10 MHz, and the impedances (Z) and phase angles (Θ) recorded are shown in Figures 4.5 and 4.6. The sensor patch is capacitive in its nature with the largest phase angle observed at 150 kHz. Hence, further characterisation was conducted at the operating frequency of 150 kHz. The stress-strain relationship of the sensor patch was determined using an INSTRON extensometer tensile/compressive force testing system (VS02477052 R: F). Stresses applied in the horizontal and vertical directions to the sensor patch are shown in Figure 4.7. As can be seen from Figure 4.8, an expected stress-strain relationship [493] is followed in the horizontal direction but not in the vertical direction. This could be due to the anisotropic geometry of the electrodes. The fracture points for the tensile stress were (1420 μm , 2060 mN) and (-1680 μm , -840 mN). The lower limit of negative strain was caused due to the excessive bending of the patch. The capacitance-strain relationship of the patch is shown in Figure 4.9.

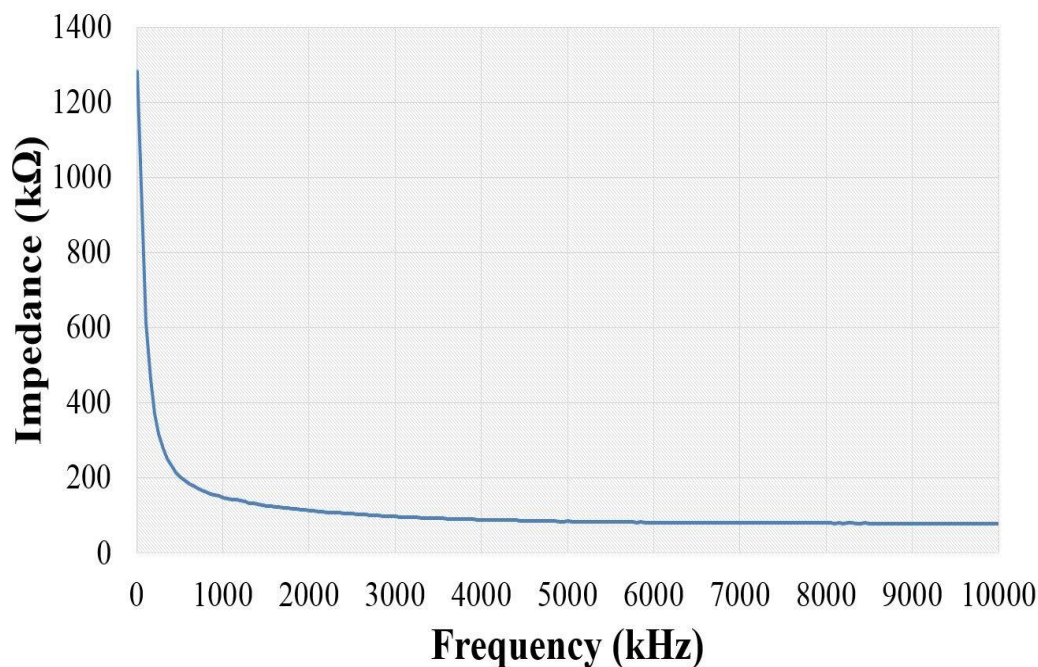


Figure 4.5 Impedance behaviour of the sensor patch as a function of frequency.

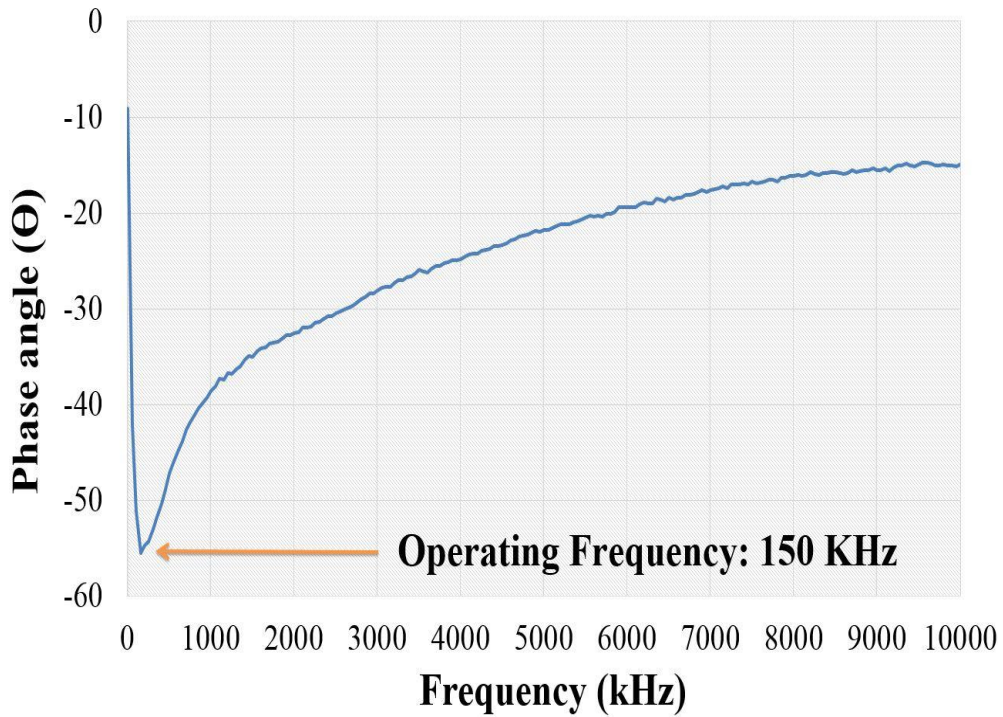


Figure 4.6 Phase angle of the sensor patch as a function of frequency.

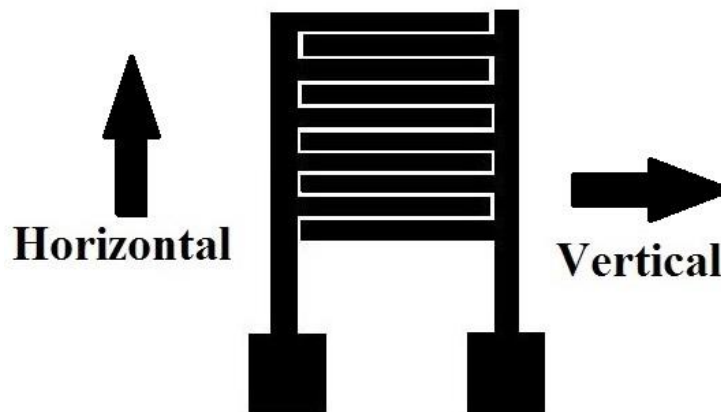


Figure 4.7 Directions of the applied stresses for the stress/strain characterisation of the sensor patch.

The sensor showed a prominent change in capacitance at the operating frequency (150 kHz). The sensitivity is calculated from the curve with the optimum frequency of 150 kHz.

$$\text{Sensitivity} = \frac{\Delta C}{\Delta \text{Strain}} = \frac{179.2 - 122.3}{1187.5 - 728} = 0.124 \text{ pF}/\mu\text{m}.$$

The linear region of the frequency line is from 610 μm to 1120 μm . The saturation strain at the operating frequency curve (150 kHz) is 2160 μm .

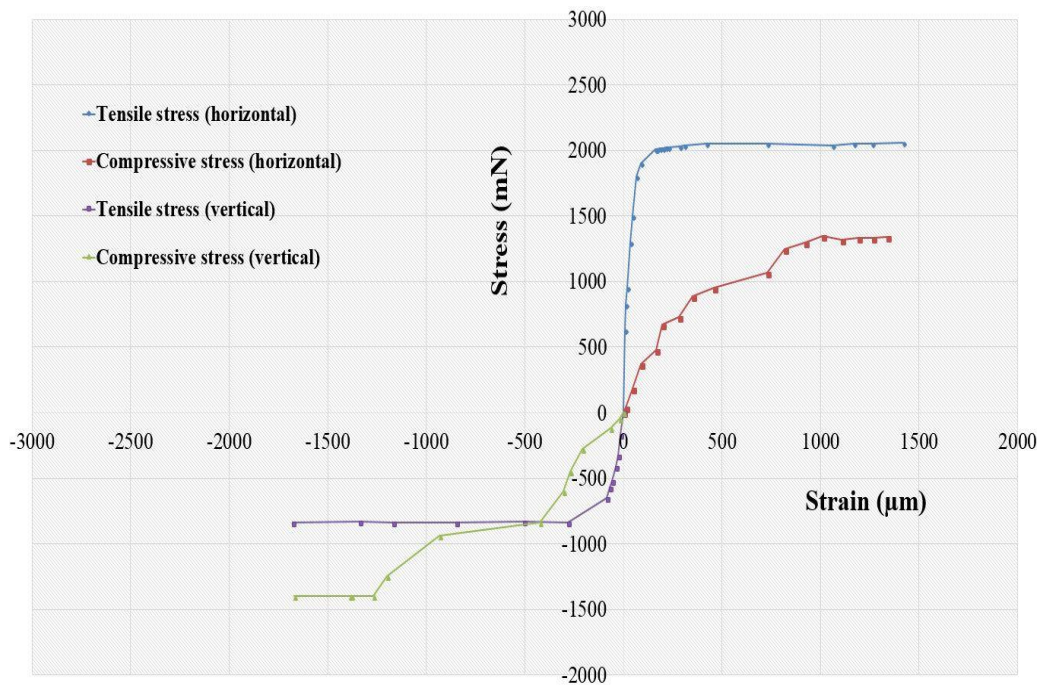


Figure 4.8 Stress-strain relationship of the sensor patch.

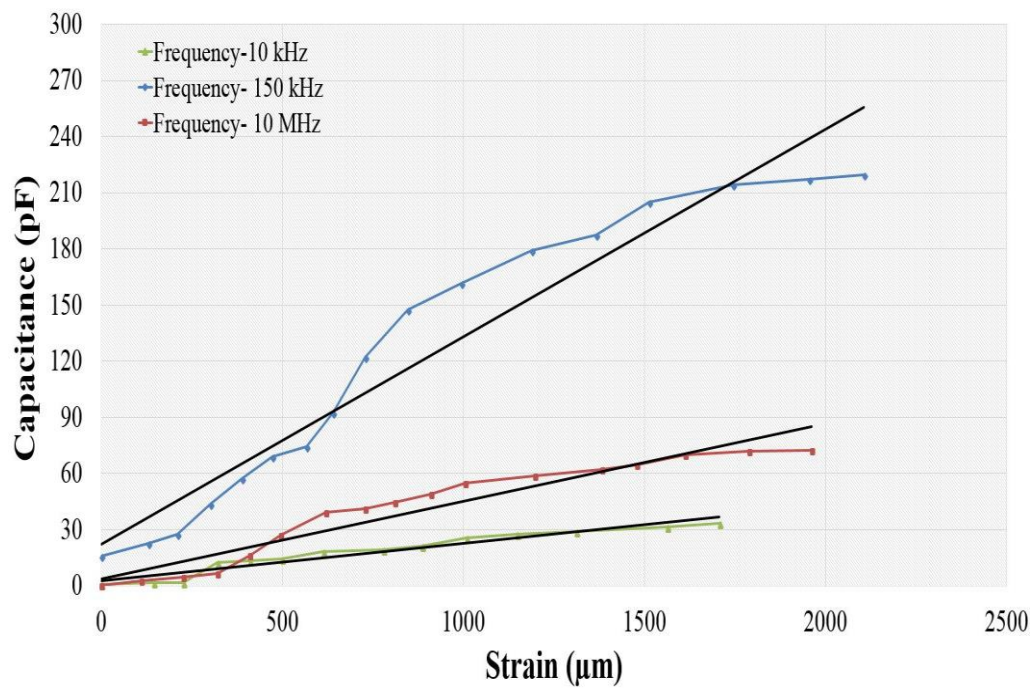


Figure 4.9 Relation between capacitance and strain of the sensor patch in the horizontal direction.

4.4 Monitoring of Physiological Parameters

The CNT-PDMS sensor patches were tested to monitor the physiological parameters of human beings. The sensor patches were attached to different parts of the body to monitor the movement of the limbs and respiration. The idea behind the choice of these two parameters is related to the use of the CNT-PDMS sensor patches for biomedical applications. Due to their strain-sensitive nature, these patches would be advantageous to detect voluntary physical changes happening on a person's body. Some of the prospective applications lie in their employment to analyse the post-rehabilitative movements of patients who suffered from stroke or muscle spasms. The concept of sensors to monitor people's health and lifestyle has been capitalised over the past two decades [494, 495]. Different types of sensors have been used to monitor the activities and physiological parameters of individuals to understand and generate a pattern for human behaviour [496-498]. Sensors with flexible substrates are one sector where prominent research work [499-502] has been done in recent times. Light weight, low cost of fabrication and long lifetime are some of the reasons for their increased usage over rigid substrates. The sensors developed for smart home usage are mainly dedicated for single-parameter monitoring purposes like PIR sensors [503], pressure sensors, etc.

Multi-parameter monitoring is of great interest due to the disadvantage caused by separate sensors for individual applications. For example, the cost is largely reduced in using a multi-functional sensor. The sensor-patch development shown in here is much simpler and easier to fabricate than previously developed sensors, which had been fabricated for multiple functions containing a coil [504-506] operating on a magnetic principle.

Significant research work has also been done on the detection of joint and limb movements. The majority of them involve fixed sensors [507] or the study of an artificial robot [508] to analyse the human behaviour. Wearable sensors [509] and accelerometers [510] are other techniques used to monitor human movement. Shoe sensors [511] and braces [512] are some types of wearable sensors used for monitoring of physical activities involving limb movements. The existing concepts have distinct disadvantages. Some would be wearable sensing devices required to be worn by the person at times; others would involve complicated gadgets working on specific computational algorithms involving some expertise to operate them. Thus, there is a need for a simple, non-invasive, sensing device which upon its attachment to the monitored region would precisely detect the movements,

even on a smaller scale. Research work to monitor the rate of respiration has been done previously using devices with and without flexible substrates. The photoplethysmographic technique [513, 514] is widely used for the detection of respiratory rate. But this technique is complex and requires technicians at the time of monitoring. Piezo-resistive [515], fabric attached sensing [516, 517] and optical sensors [518] are other ways used to monitor respiratory rate. Technical complexity, cost and specific positioning of the subject during monitoring are some of the demerits of these techniques. Monitoring of respiration and other physiological parameters has also been done using PVDF-based piezoelectric sensors [519, 520]. But the disadvantages of using PDVF are the strongly temperature-dependent performance along with high hysteresis of the sensors. There are different force sensors available in the market. Table 4.2 classifies them based on price, size and some applications related to physiological parameter monitoring. Typically, either the price of the sensors is very high, or the sensor size is large. In the following experiments, we show the change in capacitance of an interdigitated electrode on a flexible sensor patch by simply attaching it to the lower part of the diaphragm of an individual. The inhalation and exhalation rates were monitored based on the strain induced on the sensor patch. This could be used for applications like the abnormality in the rate of respiration caused due to hypoxemia and hyperaemia which can be analysed by monitoring the change in sensor capacitance between a healthy person and a patient.

Table 4.2 Comparison of different force-sensing resistors available in the market.

Sensor	Size (mm)	Force sensing capacity (lbs)	Price (USD)	Application
RB-Phi-121	25*11	11.24	45.00	Pressure-sensitive touch user interface.
Flexiforce A101 Sensor	15.6 * 7.6	10	34.00	Bed monitoring systems, force-sensitive video games.
SKU: SEN 09376	3.5*3.5	4.49	14.28	Tactile sensor for robotic appendages.
SEN-09375	2.375* 0.75*0.5	2.24	6.75	Bicycle handlebar glove, human symbiotic robot.

4.4.1 Experimental Setup

To test the sensor for biophysical parameter monitoring, the patch was attached to the skin using biocompatible tapes (VHB 3M RP) as shown in Figure 4.10. The sensor was attached only after the skin was completely dried to minimise the effect of sweat or water on the attachment of the tapes. The presence of sweat would lead to an additional capacitive layer between the sensor and skin, leading to erroneous results. The measurements of the change in capacitance of the sensor were done by a Precision LCR meter (E4980A) at 150 kHz. BNC-to-alligator clips were used to connect the instrument to the sensor patch which was attached to the body.

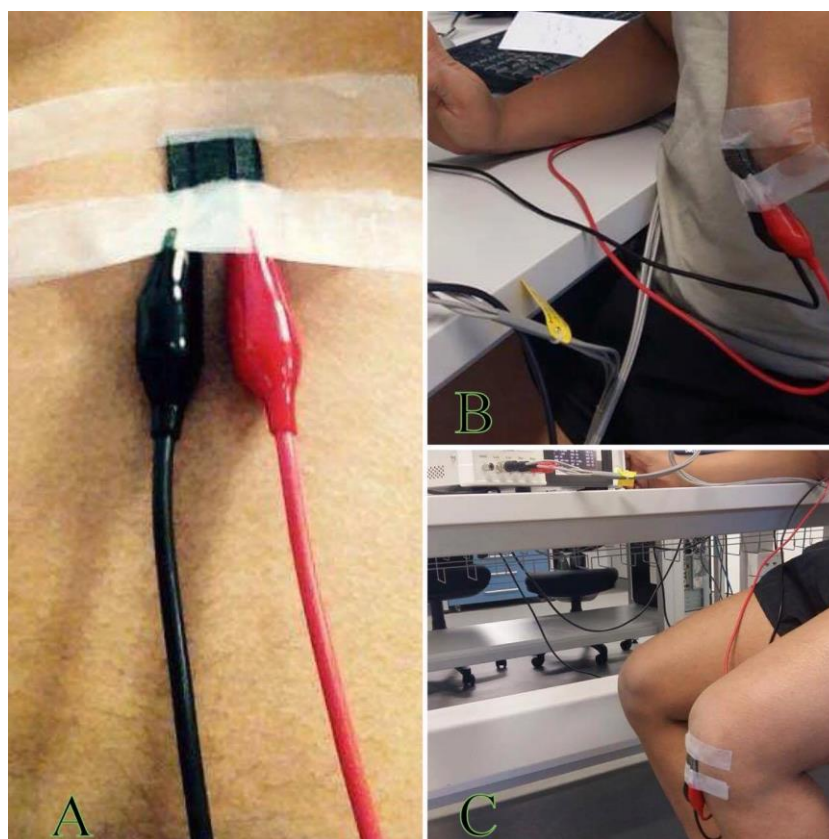


Figure 4.10 Sensor attachment for the biophysical parameters: (A): Monitoring of respiration with the sensor attached on the lower part of the diaphragm, (B): Sensor attached on the elbow to monitor arm movement, (C): Sensor attached on the knee to monitor leg movement.

Respiratory measurements were done by attaching the sensor at the lower end of the diaphragm. The readings were taken for two different conditions. The sensor was attached to the trochlea of the elbow and the patella of the knee to detect the movement of limbs.

The terms ‘flexed’ and ‘extended’ shown in the figures refer to states of the limb position. The arms were moved from a fully extended position, i.e., resting on the table to a fully flexed position via bending the elbow. The leg movement was done in a similar fashion by bending the knee from an extended to a flexed position. The sensor position on the body is crucial regarding the life span and reproducibility of the results. For example, if the sensor is placed in a tilted position, the stress exerted on the patch would not be distributed equally. This would stretch the patch non-uniformly, generating an unequal interdigital distance (d) between the electrodes, producing erroneous results.

4.4.2 Results and Discussion

People of different age groups were tested for monitoring limb movements and respiration to validate the functionality of the sensor patch. Figures 4.11 - 4.14 show the sensor output when the subject was at rest and the limbs were moved in an oscillatory fashion. The results show that limb movements can be clearly detected with the sensor patch. The limbs were flexed up to an angle of 130° , considering the extended limb to be zero degrees. There are a few issues that can be addressed to optimise the performance. For example, in Figures 4.11 and 4.12, fluctuations are observed, during the flexed state.

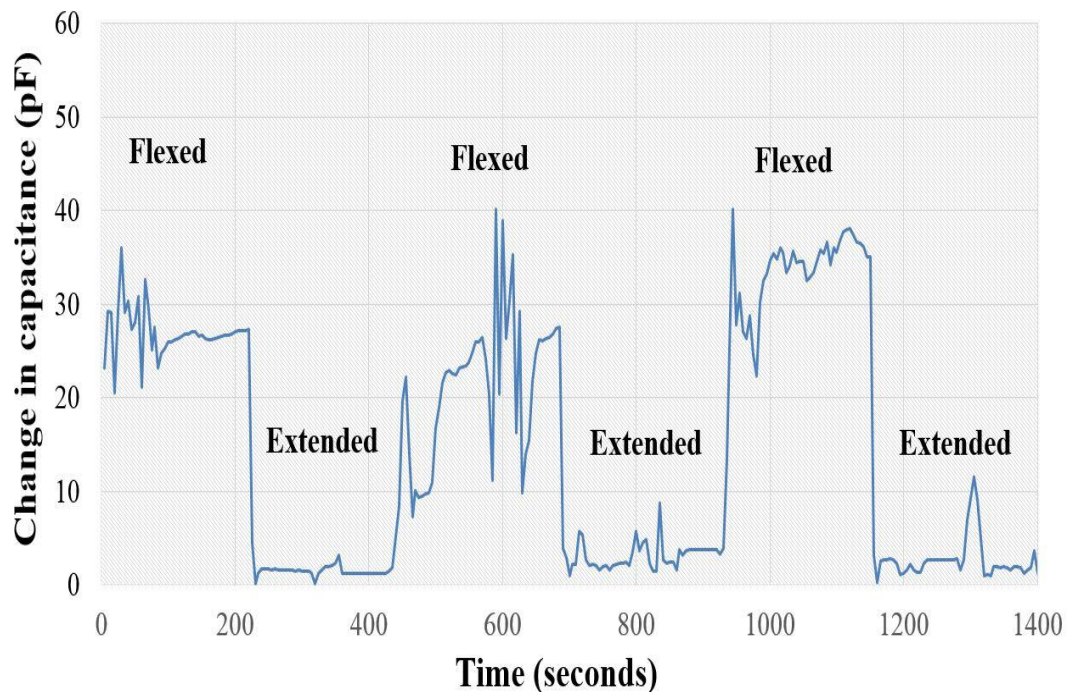


Figure 4.11 Detection of left-arm movement when the subject is at rest.

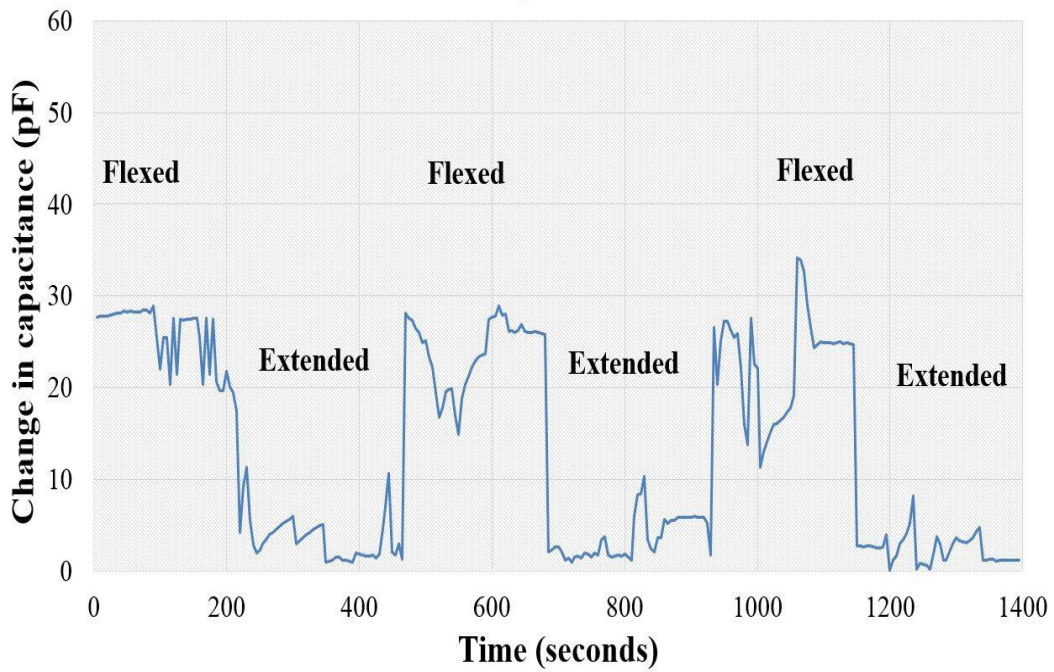


Figure 4.12 Detection of right-arm movement when the subject is at rest.

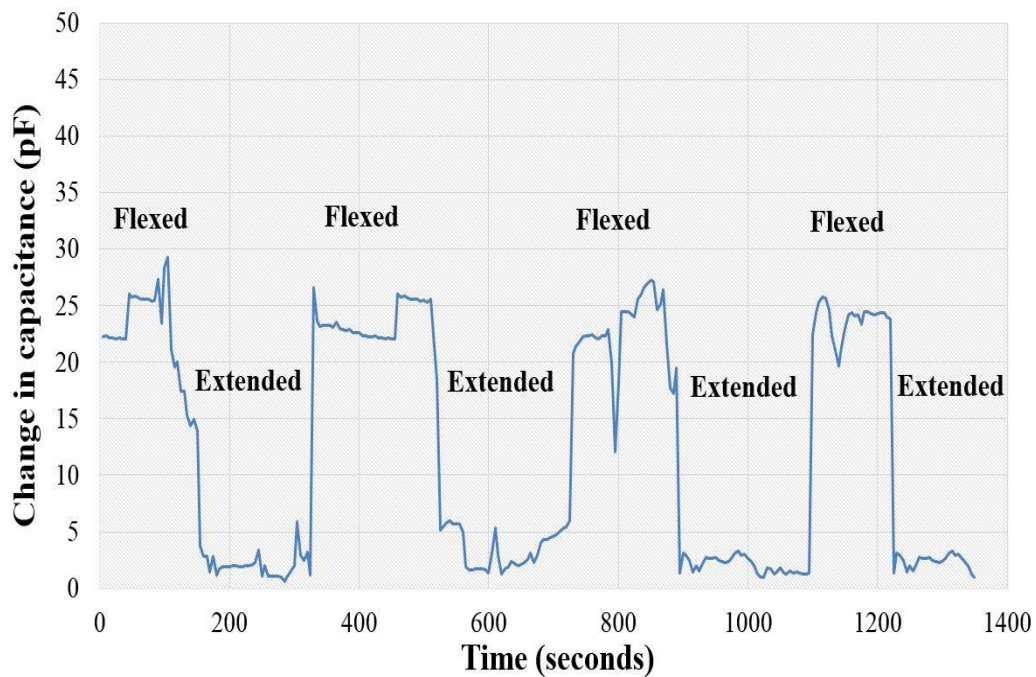


Figure 4.13 Detection of left-leg movement when the subject is at rest.

This can lead to contradictory assumptions of the state of the limb. The reason could be movement of the cables. This issue would be addressed by the wireless operation. Movements of the limbs loosened the sensor patch from the skin, leading to the observed artefacts. The signals in the flexed position showed to some extent different values. The

reason for this is that the movement of the limbs was not completely identical for two different situations. Figures 4.15 and 4.16 show the sensor output when the person is at motion. The change in capacitance was monitored when the person moved his limbs while walking. Not much difference is found in this case compared to the output when the subject is at rest.

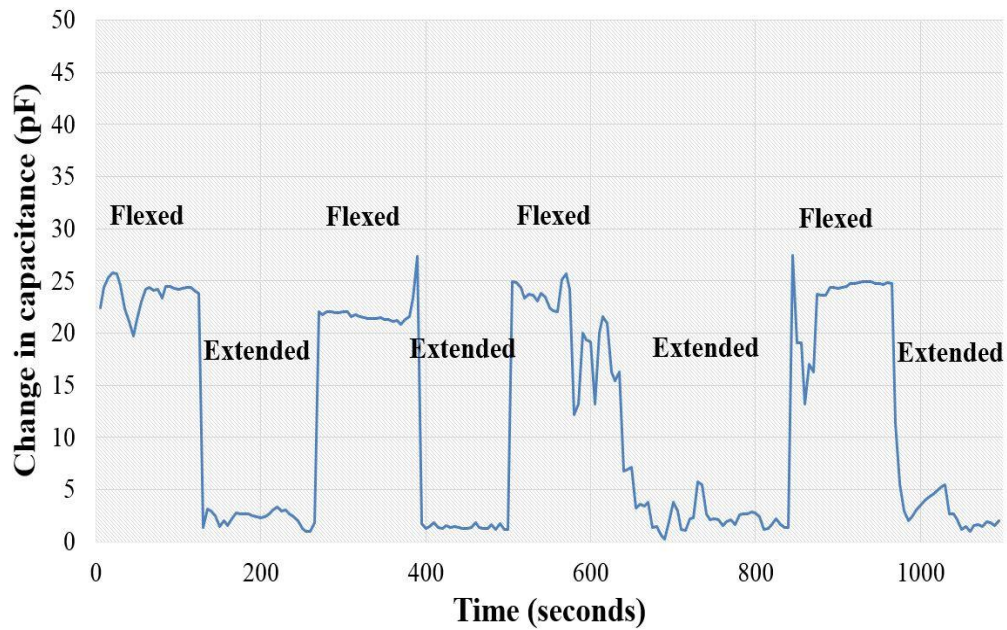


Figure 4.14 Detection of right-leg movement when the subject is at rest.

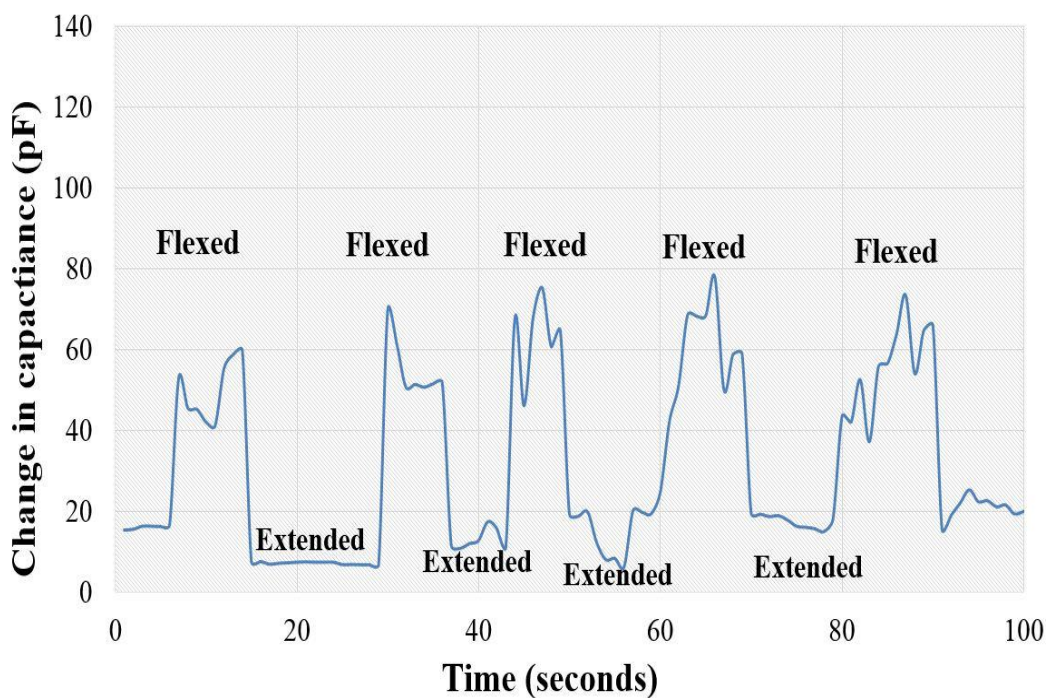


Figure 4.15 Detection of right-arm movement when the subject is in motion.

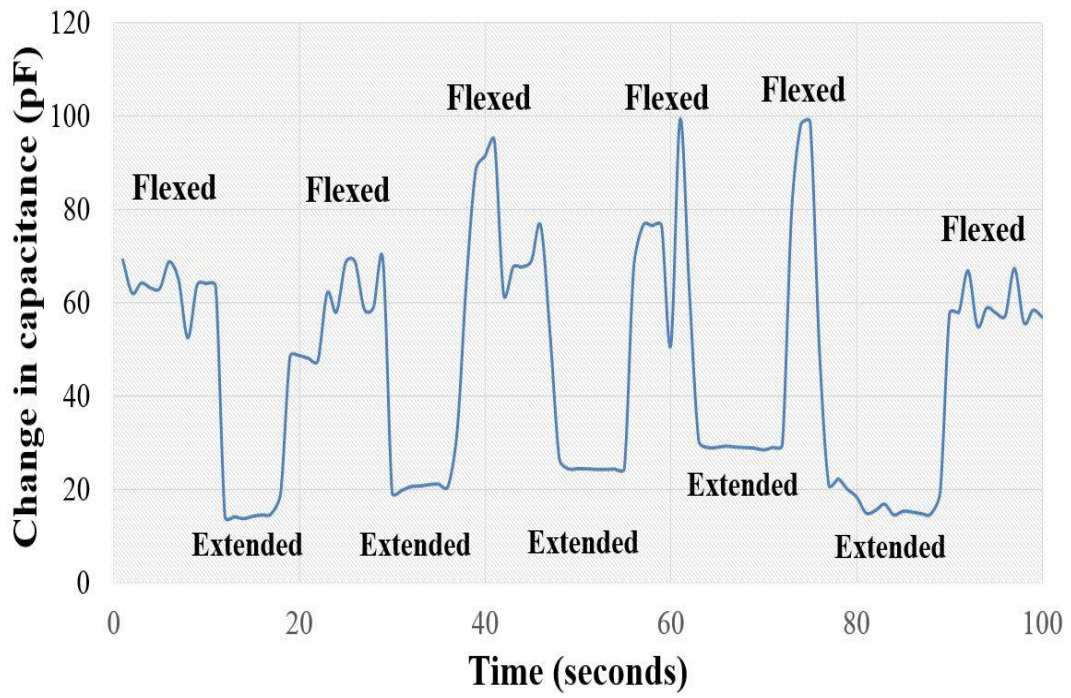


Figure 4.16 Detection of right-leg movement when the subject is in motion.

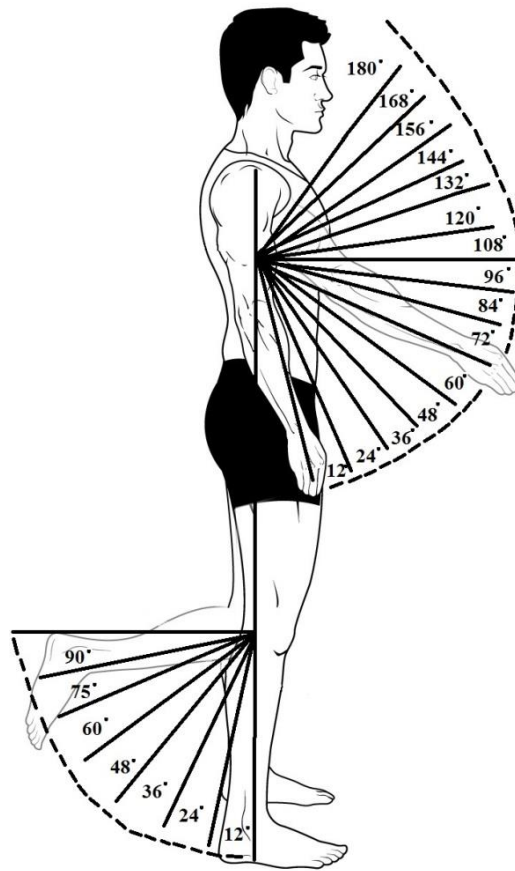


Figure 4.17 Different angular measurements of the limbs of a subject.

The difference between the two situations, flexed and extended, can still easily be distinguished. The different angular changes from a reference state of a limb of a subject are shown in Figure 4.17. The measurements were taken using a Winkeltronic angle finder (450 mm). This experiment was performed to determine a relation between the changes in capacitance on each degree movement of the limb. It is seen from Figure 4.18 that the sensor patch's change of capacitance is linear with the degree of movement of the limbs. The angular variation of the limbs was considered up to 130° because the limbs do not bend further with respect to the reference.

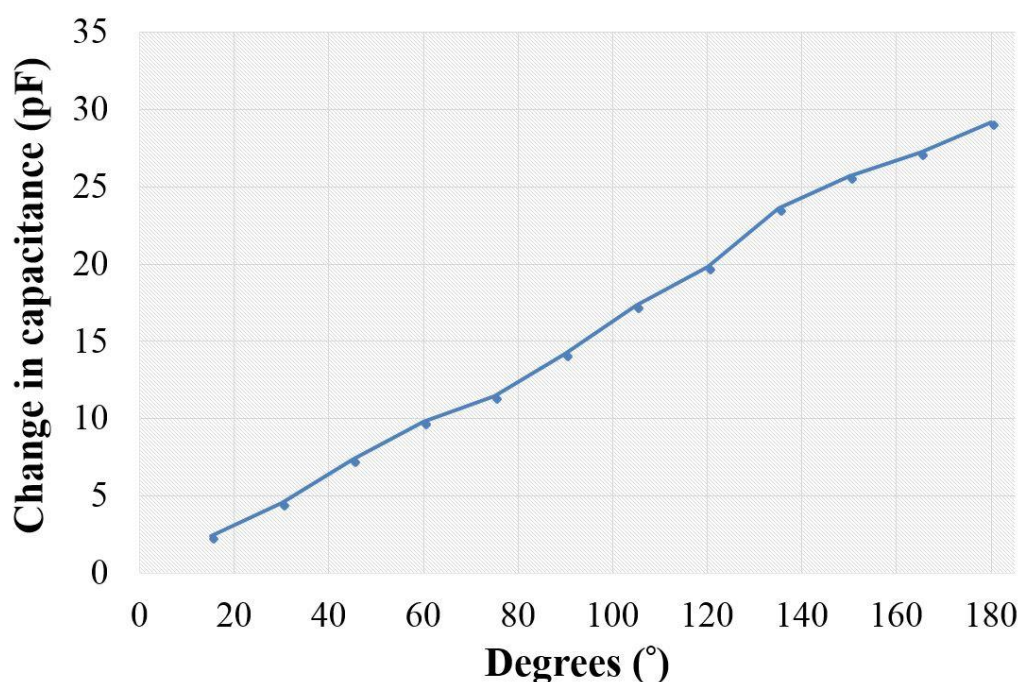


Figure 4.18 Change of capacitance as a function of the right-arm limb movement.

Figure 4.19 shows the output of the sensor when used for the detection of respiratory activity. The readings shown in two colours define two different individuals. Figure 4.20 depicts the different rate of respiration signals. The contraction and expansion happening to the sensor patch simultaneously with the movement of the diaphragm caused a change in inter-electrode distance (d) and area (A) of the sensing surface of the sensor. Hence, the sensor patch can precisely differentiate the different rates of inhalation and exhalation by a prominent change in capacitance. The inhale and exhale rates were also varied in a controlled fashion to further analyse the sensitivity of the sensor patch as shown in Figure 4.21.

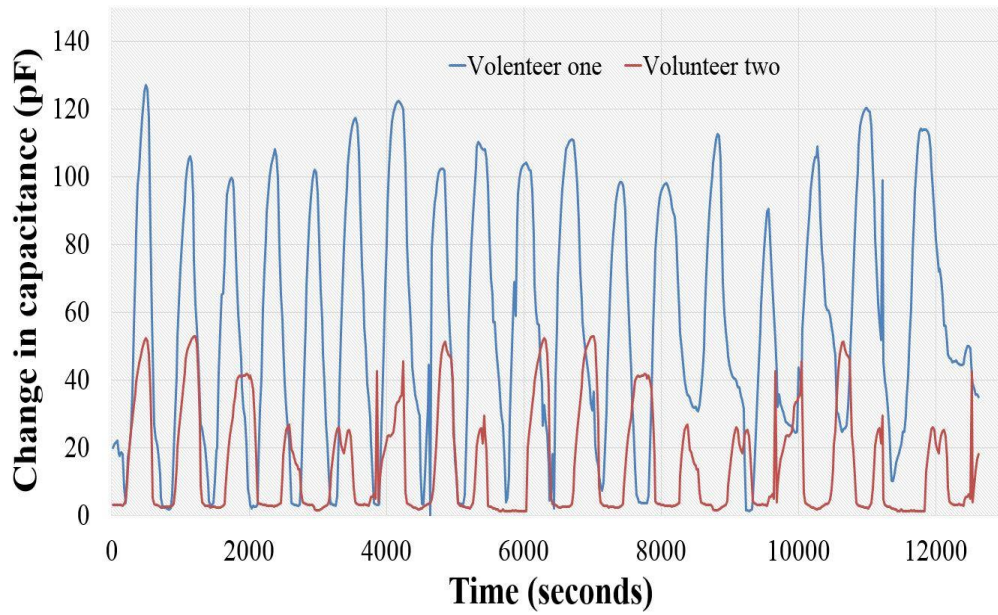


Figure 4.19 Monitoring of respiration for two different individuals at rest.

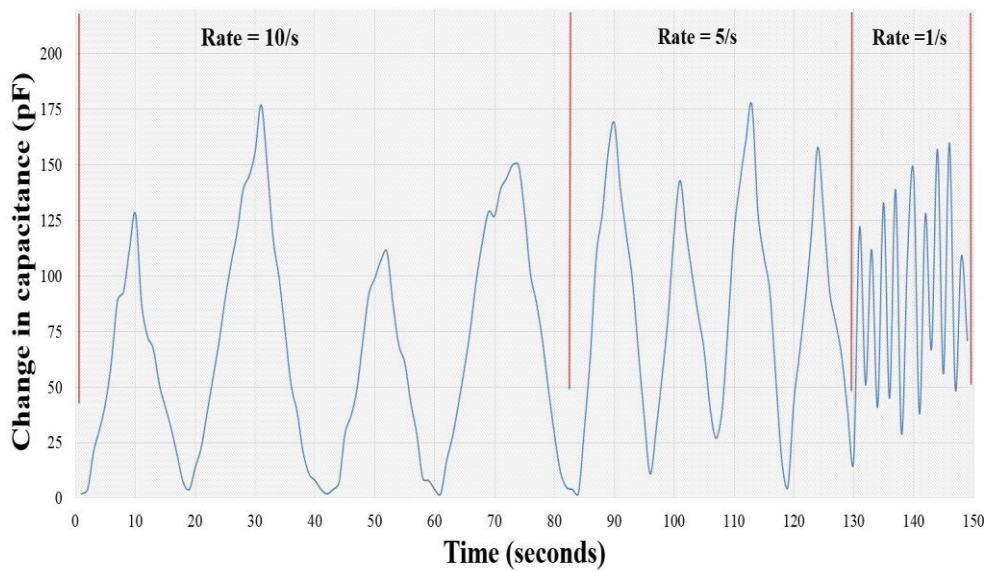


Figure 4.20 Measurement of respiration activity of an individual who was simulating respiration rates of 10/s for the first 80s, 5/s for the next 45s and 1/s for the next 20s.

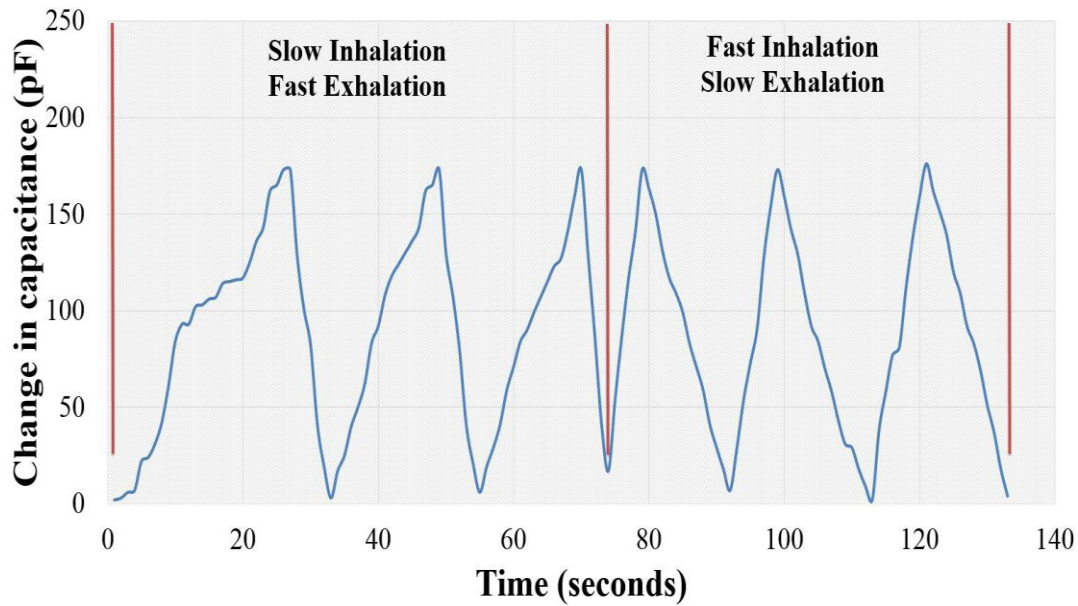


Figure 4.21 Measurement of respiration activity of an individual who was simulating inhalation and exhalation at different speeds.

4.4.3 Conclusion

Using functionalised MWCNTs as a conductive material embedded in a PDMS substrate, flexible sensors has been designed and fabricated. The MWCNTs were chosen as filler for the nanocomposite due to their high electrical conductivity and flexibility along with their aspect ratio. The functionalisation groups like -COOH, -C=O and other oxygen carboxyl groups helped in increasing electrical conductivity and allowed better dispersion of the nanotubes in the polymer [521]. PDMS has a low Young's modulus, required for a high-performance patch in terms of strain range and durability. It is also cheap compared to other polymers (Polyethylene naphthalate, Polyethylene terephthalate) used commonly to develop flexible sensors. Due to its hydrophobicity, PDMS as a sensor substrate minimises the effects of sweat on the sensor output and attachment. The size of the sensor is small, around 50 mm², making it convenient to use for monitoring physiological parameters of elderly people or infants while minimising discomfort.

4.5 Tactile Sensing

Prosthesis has been used for a long time to replace a missing part of an amputee's body with an artificial one. The most common type of prosthesis done in the medical field is limb

prostheses [522-524], where different amputee organs of the upper or lower part of the body are replaced to help in restoring a normal life to the person. The common materials used for fabricating prosthetic organs are fibreglass, nylon, Dacron, carbon, and Kevlar [525]. Control of stiffness and strength are some of the advantages of using these materials. But their brittle nature and the inability to remould the device once created are some of the common disadvantages associated with them. A material like Dacron in prosthetic devices can lead to the inability of the region to repair and grow due to the stiffness of the replaced part. This effect on the growth of tissue of the affected portion can lead to multiple replacements. In the case of Kevlar, it is difficult to shape the material into the form of the amputated organ unless operated with special tools and equipment. This increases the cost of the overall treatment [526]. The material also corrodes in contact with chlorine. Thus, it is a state of the art to develop sensors as a replacement for the commercially used devices.

Touch-sensitive prosthetic limbs are an intriguing development in the sector of prosthesis where substantial work [527, 528] has been done over the past decade. Researchers have been trying to develop touch-sensitive somatosensory organs which would send sensory feedback to the amputee's brain. The devices have been tested so far on robots [529, 530] and artificially fabricated organs [531, 532]. An attempt was made [533] to develop a brain-machine interfaced prosthetic limb. Higher-cost, complex testing systems and weak response are some of the disadvantages of such systems. In the succeeding sections, the use of the CNT-PDMS sensor patches for tactile sensing has been described.

4.5.1 Experimental Setup

The sensing performance of the sensor patch was evaluated by using it as a tactile sensor at the tip of the forefinger. The patch was connected to the LCR meter via Kelvin probes as shown in Figure 4.22. An alternating voltage of 1 V peak-to-peak was given as an input to the connected sensor patch. A tactile signal was obtained by analysing the change in capacitance in pF with respect to time.

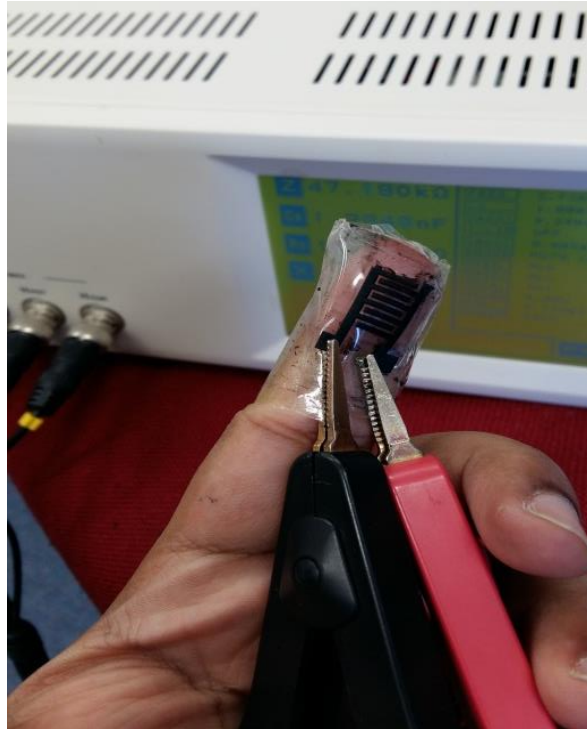


Figure 4.22 The sensor patch attached to the fingertip and connected to the LCR meter for tactile sensing.

4.5.2 Results and Discussion

Figures 4.23 - 4.27 show the sensor responses for two conditions; touch and no touch. The results are represented in the change of absolute capacitance against time. Touch refers to the situation when the sensor attached to the finger is pressed against a plane surface. No touch refers to the situation when the finger is free from any contact. The results differ in the range of capacitance in the touched condition due to the application of different pressures with the finger on the object. As seen from the results, the sensor patch responds well to the two defined conditions, and the touched condition reaches higher values, distinguishing it from the no-touch condition. The change in capacitance with different weights is shown in Figure 4.28. Different weights were kept on the sensing area of the patch to analyse the change in capacitance with weight. It is seen from the graph that the readings change linearly with the weight. Some glitches can be observed during the touched condition, which might be related to the experimental setup, where it is not possible to apply a constant pressure with the finger to the object. Also, since the sensor patch was connected with tapes at the tip of the finger, the tapes might come loose on bending the patch which could be a reason for the sudden change in capacitance. The capacitance in the

no-touch condition has some non-zero values. This is due to the minimum strain on the sensor patch caused due to its bending around the finger.

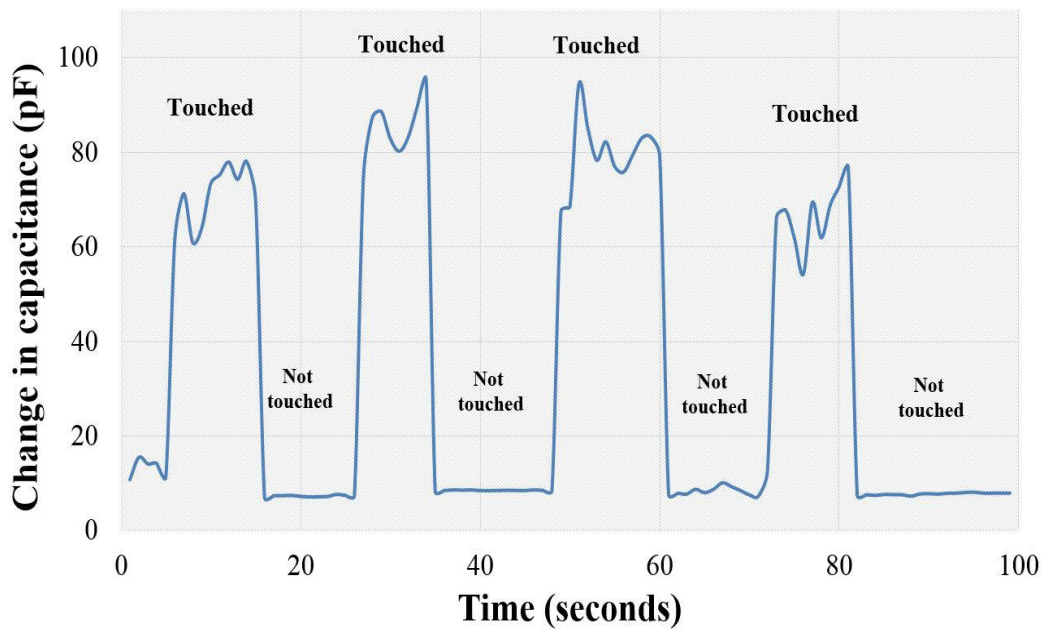


Figure 4.23 Response of the sensor patch for a pressure of 42.2 μPa .

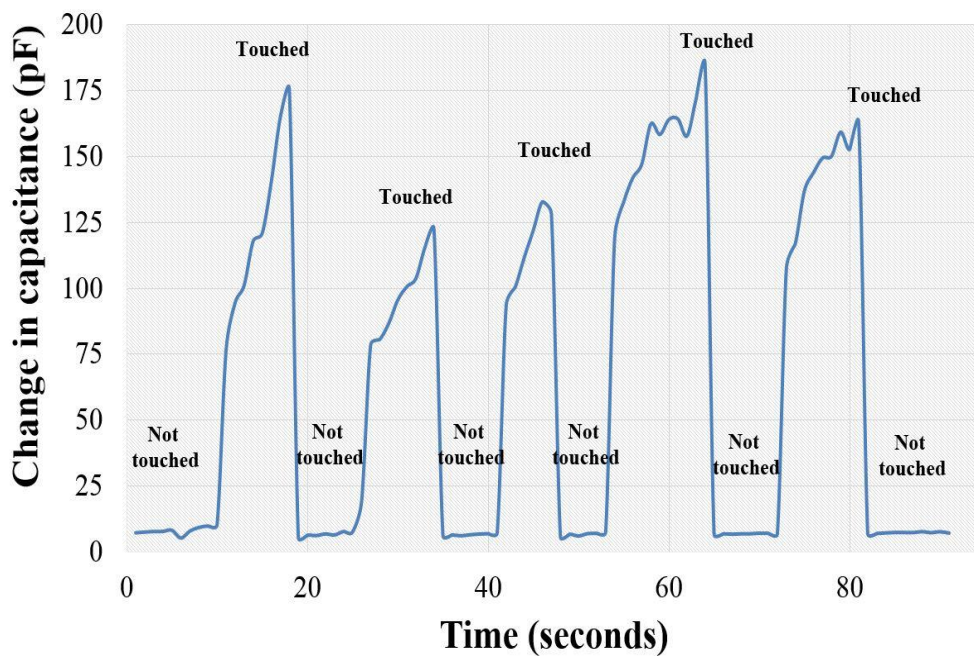


Figure 4.24 Response of the sensor patch for a pressure of 54.6 μPa .

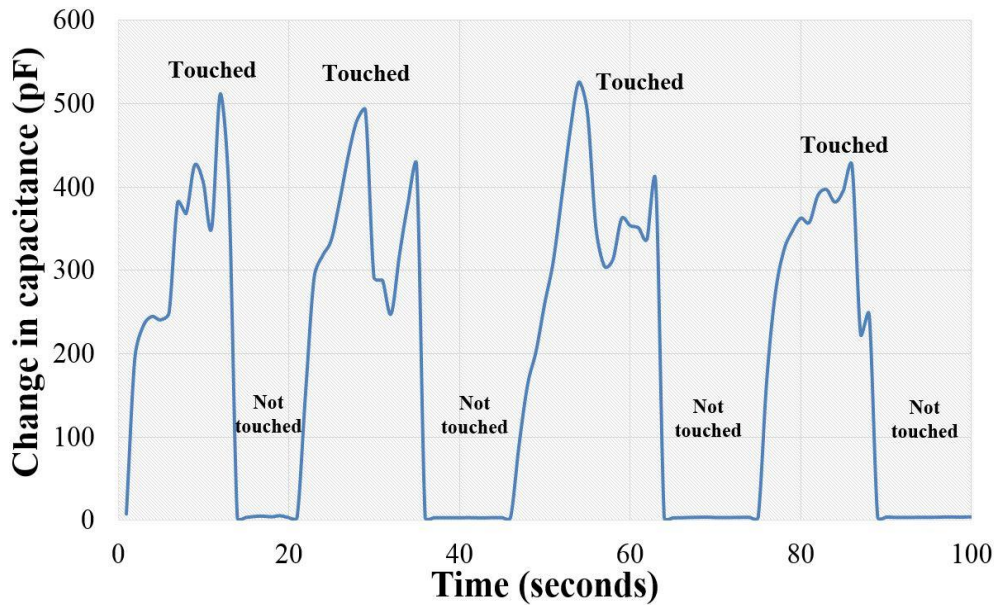


Figure 4.25 Response of the sensor patch for a pressure of 68.2 μPa .

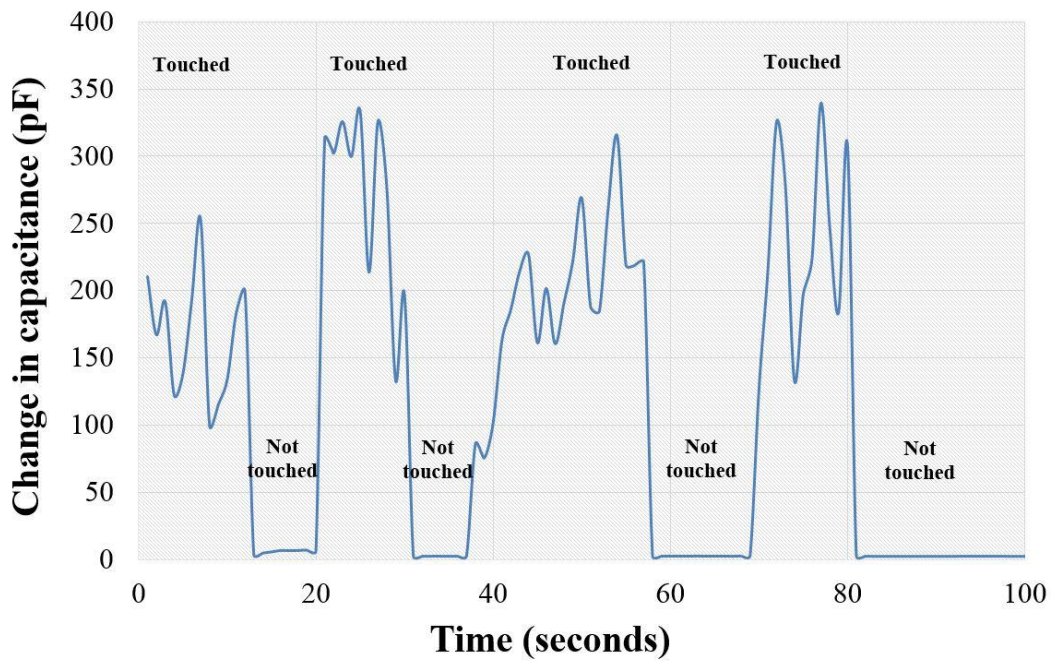


Figure 4.26 Response of the sensor patch for a pressure of 62.4 μPa .

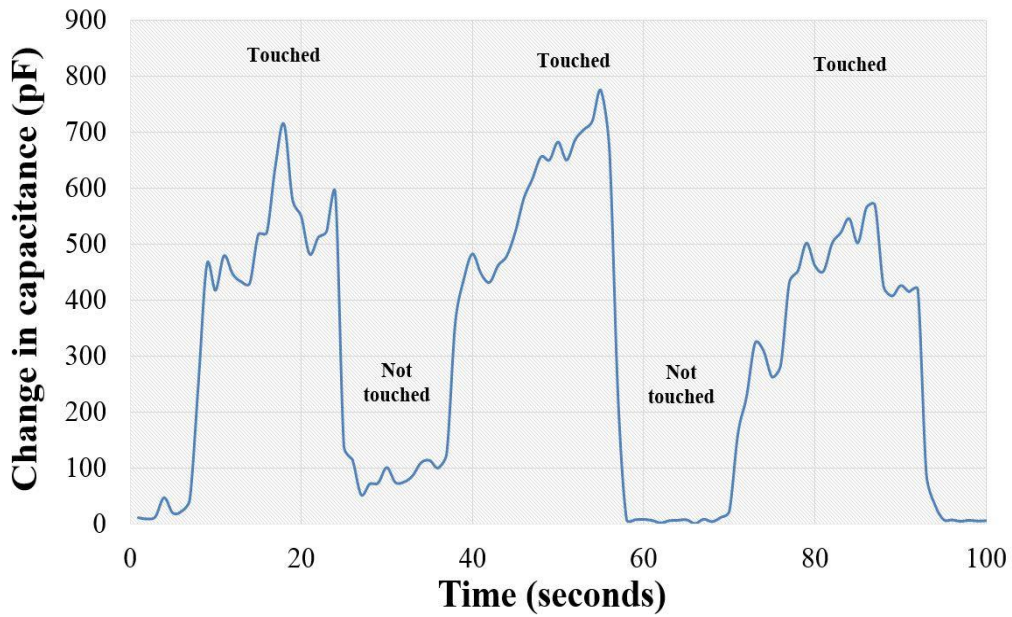


Figure 4.27 Response of the sensor patch for a pressure of 84.6 μ Pa.

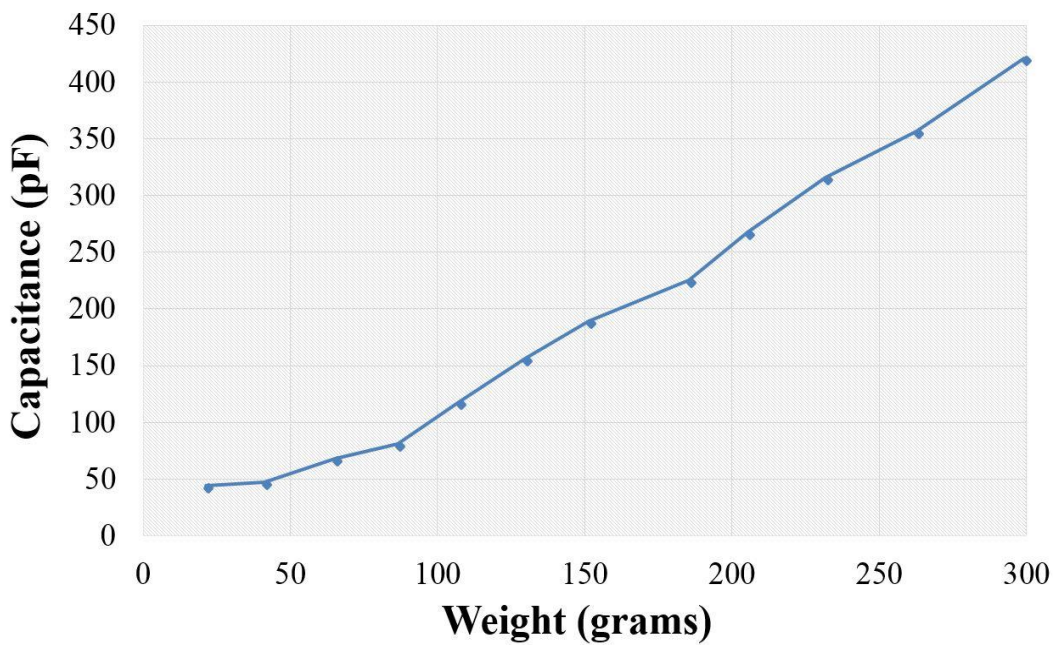


Figure 4.28 Variation of capacitance for different weight values.

4.5.3 Conclusion

The use of the CNT-PDMS sensor patches for tactile sensing has been described. Manual force was exerted on the sensing area of the patches to determine their responses towards low pressure. The obtained results are very satisfactory and could be used to extend the work behind this idea. This could help to reduce the fabrication cost and equip prosthetic

organs with efficient tactile sensors. The next step would be to use the sensor prototypes to validate their functionality, and to include them in an embedded system would also be an option to develop a complete prosthetic system for human sensing.

4.6 Chapter Summary

The design, fabrication and implementation of the CNT-PDMS sensor patches were described in this chapter. Due to the flexible nature of the sensor patches, they were being employed for different applications like physiological-parameter monitoring and tactile sensing. The major advantages of these sensor patches lie in their low cost, simple operating principle and multiple applications. The potential of these sensor patches in terms of the applications can be extended for monitoring the quality of human health by using them for elderly-care purposes. Other than limb movements and respiration, detection of other physiological parameters like heart monitoring, fall detection, etc. can also be done using these sensor patches. These patches can be embedded with a signal-conditioning circuit to make them portable and point-of-care devices, which would be useful for the ubiquitous monitoring of the daily activities of a person. The above-mentioned description of these sensor patches along with their future opportunities does make them a viable option to be used in multifunctional sensing systems.

5

Aluminium-Polyethylene Terephthalate Sensor

Publication pertaining to this chapter:

- **Anindya Nag**, S. C. Mukhopadhyay and J. Kosel, “Tactile Sensing from Laser-ablated metallized PET films”, **IEEE Sensors Journal**, Vol. 17, No. 1, pp. 7-13, **January 2017**.

5.1 Introduction

This chapter describes the fabrication and implementation of the second type of sensor patches developed from Aluminium (Al) and Polyethylene Terephthalate (PET). One distinct difference of the structure of these sensor patches are their formation from a single raw material. Due to this attribute, these sensor patches are different in terms of performance from other sensors. This also helped in curbing the complexity in the construction process of the sensor prototypes and so decreasing the overall cost of fabrication. PET is one of the common polymers used as a substrate to develop flexible sensors for different strain [534, 535] and pressure [536, 537] sensing applications. The absence of any post-processing steps, high flexibility and smooth cut edges are some of the advantages of this polymer [538, 539]. Aluminium particles also have certain advantages which makes Aluminium a viable option for the electrode material [540]. Some of them are high corrosion resistance, high electrical and thermal conductivity, and flexibility [541]. Similarly, to the CNT-PDMS sensors, laser cutting was used to develop the electrodes of these sensor patches. After fabrication and characterisation of the sensor patches, they were implemented for tactile sensing for low pressure.

5.2 Fabrication of the Sensor Patches

The reasons for choosing PET as a substrate material are high clarity, recyclability, good chemical resistance, and high impact resistance, and it is a good moisture barrier. This gives an edge over other substrate materials PET for developing devices that are used for sensing physiological parameters. The advantages of using aluminium as electrodes are its low-cost, high electrical conductivity, light weight, recyclability and high corrosion resistance. CO₂ laser cutting [542] is a popular technique for developing flexible sensors on a large scale. Easy sample preparation and formation of very thin and flexible materials are some of its advantages. It also does not require any mask or template for designing the structure, unlike photolithography [543], screen printing [544] etc. Laser cutting of polymers [545] [546] has been done previously because of its reduced cost and complexity compared to other techniques. CorelDraw X7 software was used to design the schematic of the interdigital electrodes as shown in Figure 5.1. The inter-electrode distance obtained for this sensor patch was 150 microns. The laser ablation process on the PET film attached to

the glass substrate is shown in Figure 5.2. The glass substrate was attached to the platform of the laser system with tapes (3M™VHB™) on the sides to stop it moving during the ablation process. A schematic of the fabrication steps of the sensor patch is shown in Figure 5.3.

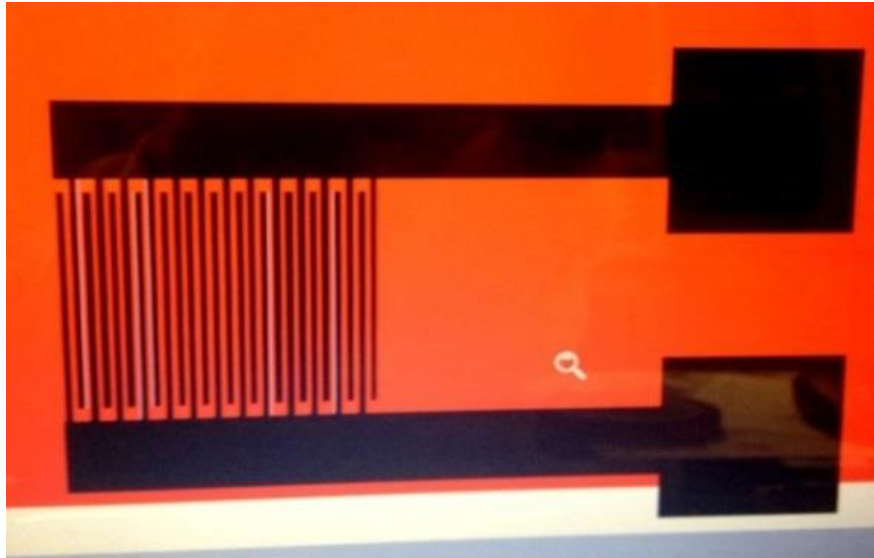


Figure 5.1 Schematic of the electrode design.

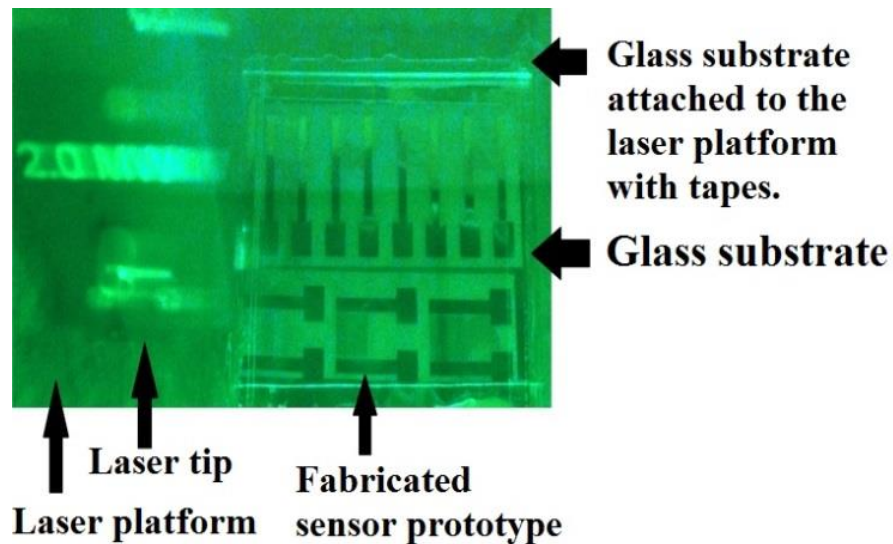


Figure 5.2 Laser ablation to form electrodes.

The substrate/electrode material was attached to a glass substrate for its support before laser ablation. Metallized PET films (HO-107) were used for fabrication, with Al present on one side. The difference between the Al and the PET side was based on the higher

conductivity and smoothness of the former than the latter. The sample was then loaded onto the laser system (Universal Laser Systems) to form interdigital electrodes on the Al side. After the exposure, the sensor patch was taken off the glass substrate. 24 fingers were present in each patch with each one having a length and width of 1.2 mm and 41 microns respectively and a pitch of 300 microns between two electrodes of the same polarity. The thickness of the PET substrate and Al electrodes were around 500 microns and 300 microns, respectively.

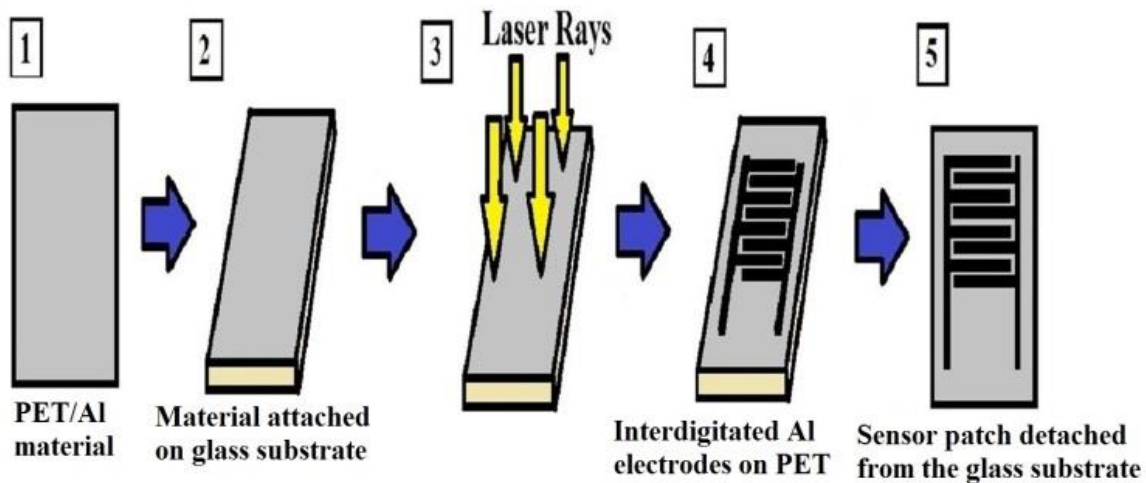


Figure 5.3 Fabrication steps of the sensor patch: (1) Raw material used for fabrication. (2) Raw material is attached to glass substrate for support. (3) Laser beam is shone on the sample. (4) Interdigitated Al electrodes are formed on PET. (5) Patch is detached from the glass substrate.

The sensing area of the patch was 44 mm². Different properties of the laser device like power, speed, frequency and z-axis were optimised on the way to develop the sensor patches. A series of experiments were performed with different values of the laser properties as shown in equation (5.1). Each parameter was changed as a function of other three parameters until each of them was optimised. The values for the parameters are given below.

$$f(p) \rightarrow f(s) \rightarrow f(z - axis) \tag{5.1}$$

$p = 18, 21, 24, 27, 30$; $s = 20, 30, 40, 50, 60$; $z-axis = 1, 1.1, 1.2, 1.3, 1.4$.

where, p represents the power in watts, s represents the speed in mm/min, z -axis represents the distance of the laser nozzle above the sample material in mm.

Power- 21%, speed- 30%, and z -axis- 1.20 mm were the optimised values for which the best electrode line was obtained. These values were kept constant during the entire process to fabricate the sensor patches. The thickness of each electrode line cut by the laser beam was optimised to 41 microns as shown in Figure 5.4. The image was taken with a Zeiss confocal microscope. The front and rear views of the final sensor patch are shown in Figure 5.5.

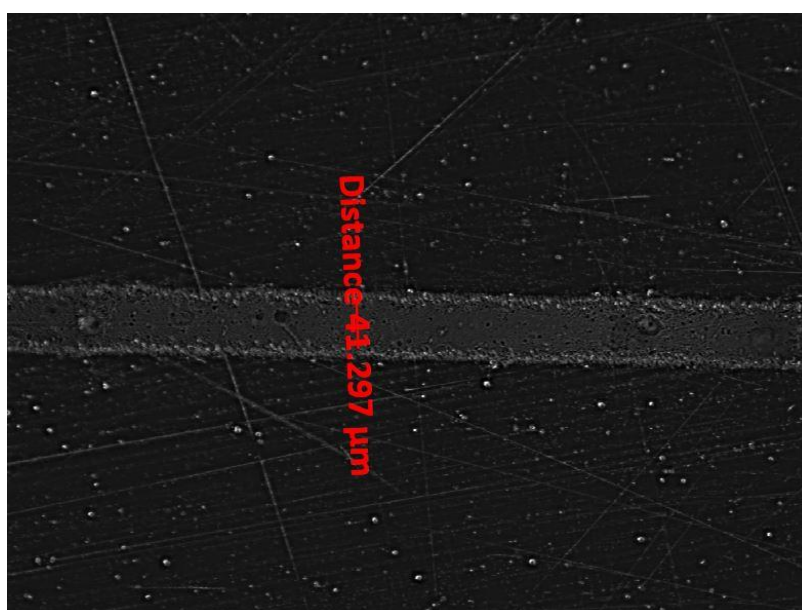


Figure 5.4 Microscopic image of a single line of the electrode.

The top-view SEM images of the edges and electrode lines of the fabricated sensor patches are shown in Figure 5.6. The smooth surfaces are the substrate PET film, and the complementary rough surfaces are the Al electrodes. The uneven cavities in the electrodes are due to the simultaneous moulding and demoulding process of the aluminium due to the heat generated by the laser. It is seen from the images that the horizontal lines of the electrodes are symmetrical and mostly perpendicular to the substrate and the edges at the cross-section are quite smooth. Therefore, no additional steps are required to remove any sharp edges for using the patches for bio-sensing purposes.

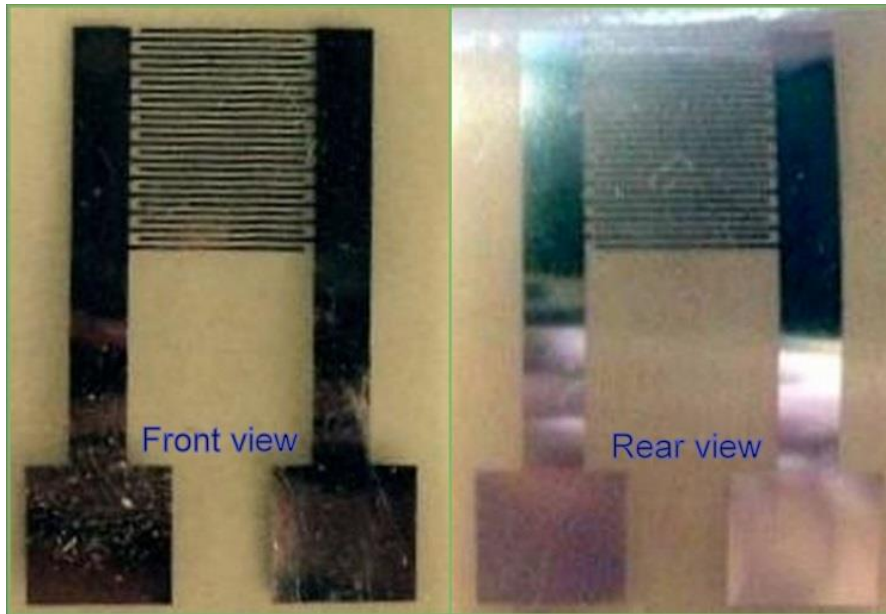


Figure 5.5 Front and rear views of the sensor patch.

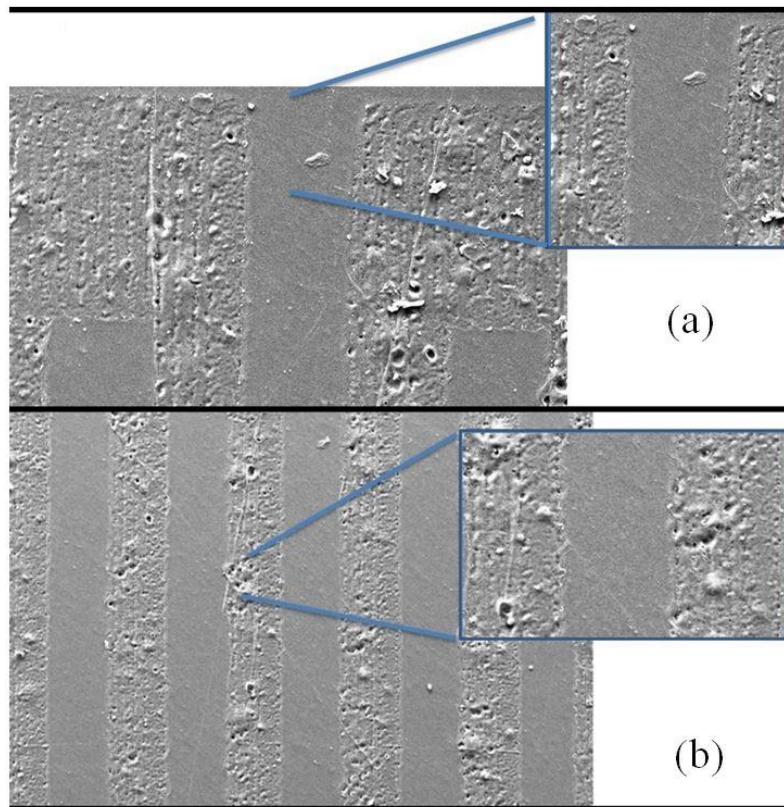


Figure 5.6 Zoomed-in SEM image of the top view of the (a) edges (b) electrode lines of the fabricated sensor.

5.3 Frequency Response and Stress-Strain Measurements

The fabricated sensor patches were then characterised to determine the optimal frequency for operation. An HIOKI IM 3536 LCR High TESTER was used to test the sensor patches. A time-dependent peak-to-peak voltage (V_{in}) of 1 V was applied to the sensor. A frequency sweep was done between 1 kHz and 100 kHz to determine the optimum operating frequency. Figures 5.7 and 5.8 depict the response of the sensor patches in terms of impedance and phase angle. The operating frequency for the test sensor patch was chosen as 305 kHz. Figure 5.9 shows the equivalent circuit for the sensor operation. V_{sense} is the voltage across the series resistor to determine the current passing through the sensor. R_{sense} and C_{sense} are the real and imaginary parts of the sensor patches. Figure 5.10 shows the experimental set-up for analysing the relation between the forces applied to the sensor along with the displacement caused on the patch from its normal position. Elongative and compressive stresses were applied in the horizontal direction of the sensor patch which is perpendicular to the electrode fingers whose responses are shown in Figure 5.11.

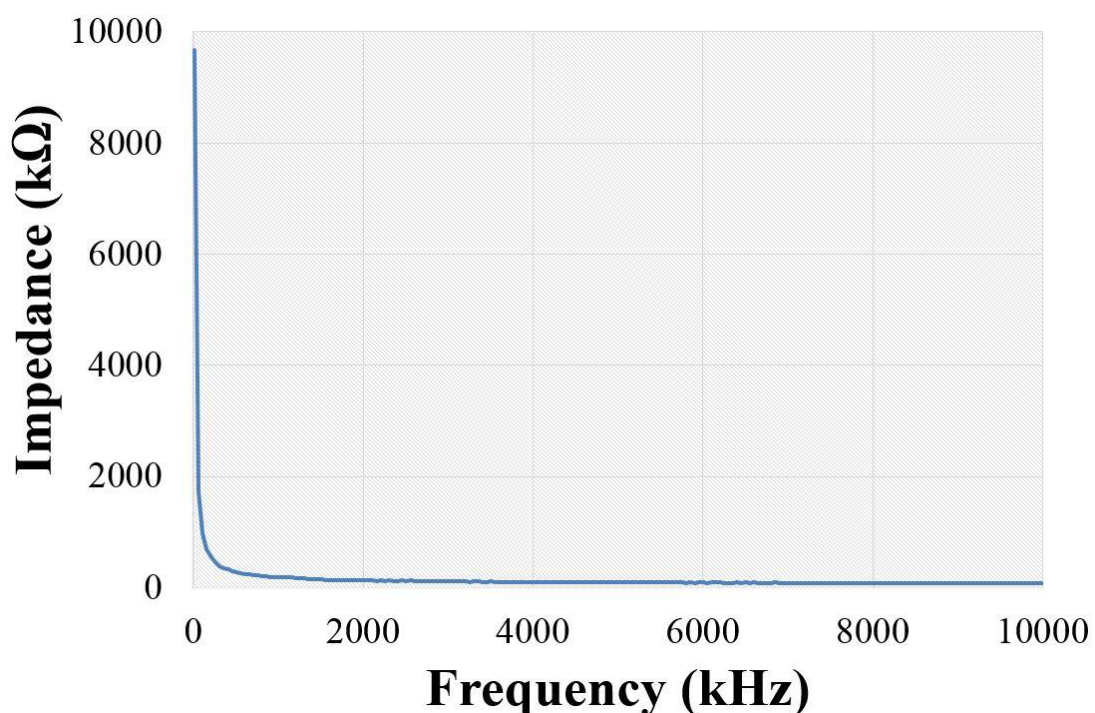


Figure 5.7 Impedance behaviour of the sensor patch as a function of frequency.

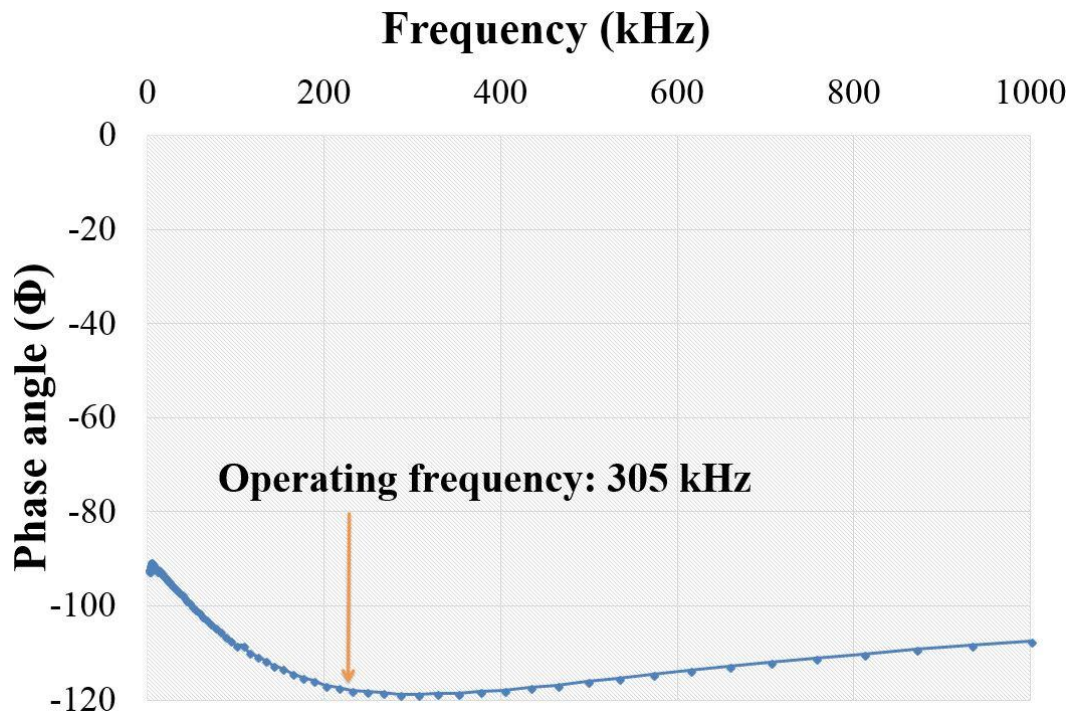


Figure 5.8 Phase angle of the sensor patch as a function of frequency.

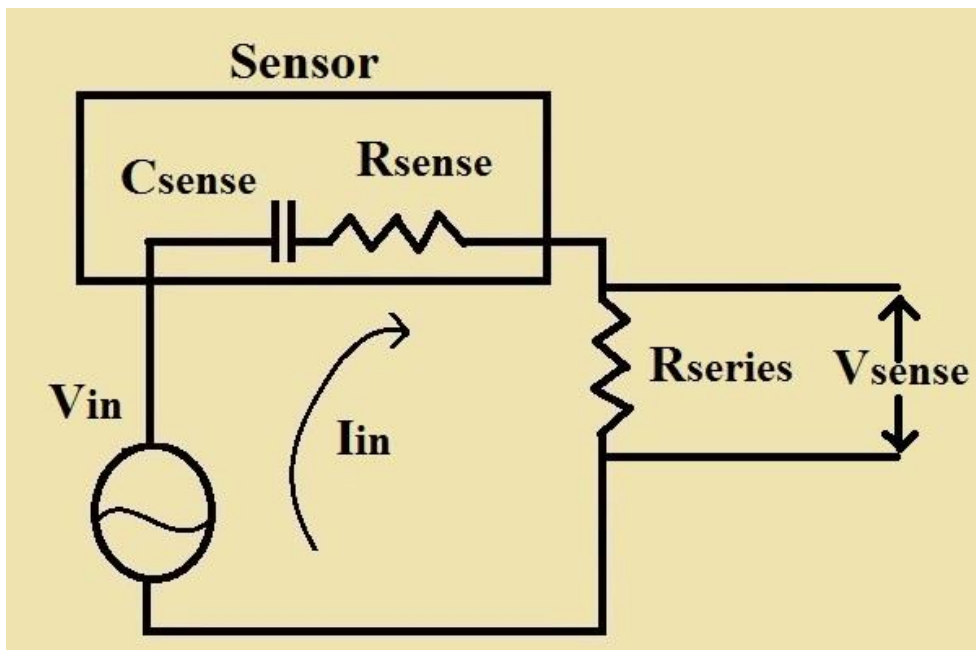


Figure 5.9 Equivalent circuit to determine the response from an interdigital sensor.

The sensor patch was clamped and moved vertically upwards or downwards depending on the force. The elongative stress was applied by moving the sensor upwards from its normal position to the highest point (breaking point). The compressive stress was applied

by starting the experiment from the highest point (breaking point) and moving downwards till the patch reached its normal position (starting point for the elongative force). The breaking point for the tensile and compressive stresses are (388.7 μm , 420 mN) and (-510 μm , -250 mN) respectively.



Figure 5.10 Experimental set-up for characterisation of the sensor.

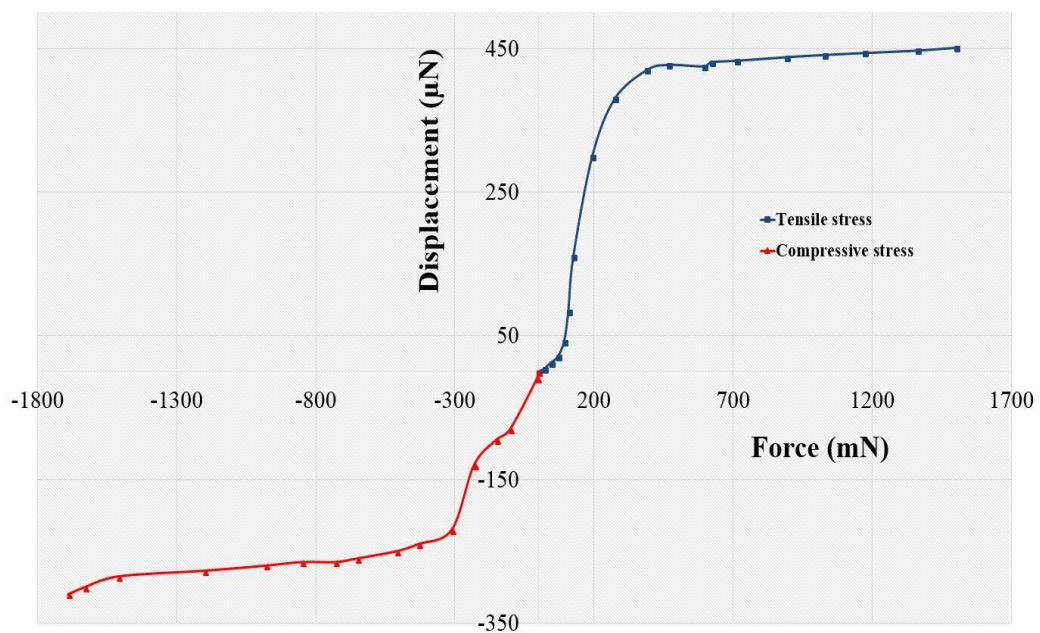


Figure 5.11 Force-displacement relation for the sensor.

5.4 Tactile Sensing

Tactile sensing [547] is one of the recently growing sensing fields [548-550], spanning different applications in everyday life like elevators, automobiles, strain gauges, etc. The current technologies available for tactile sensing are either high in cost [551-554], complex in operation [436, 555, 556] or have been tested only in artificial intelligence [557, 558]. The threshold pressure is also comparatively high (kPa) [549, 559] for the available sensors. Thus, there is a need to develop novel tactile sensors which are lower in cost and have a simple operating principle with high sensitivity. The testing was done manually to determine the sensor response for low pressure applications. High sensitivity and repeatability were obtained with the tested patches. These patches could be used as cheap sensing devices on a large scale, thus replacing the currently used commercial devices for tactile sensing. In order to test the sensor patch for tactile sensing different forces were applied manually over the sensing area of the patch to determine the sensitivity. The sensor signal was studied with the HIOKI 3532-50 LCR High TESTER that was already used for its characterisation. The LCR device was interfaced with the desktop computer using an RS-232C interface device. The schematic for the experimental setup is shown in Figure 5.12. The frequency of operation was fixed at 305 kHz.

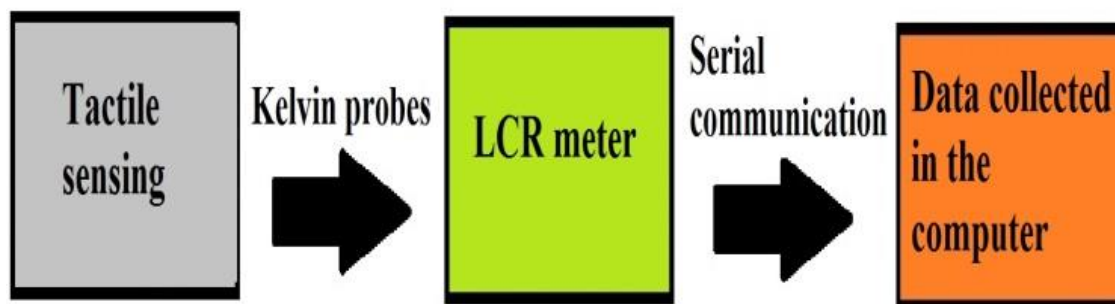


Figure 5.12 Schematic for the experimental setup for tactile sensing.

Figures 5.13-5.18 show the sensor response to the different forces applied to the patch. An oscillatory motion was executed to determine the repeatability of the results upon exertion of pressure.

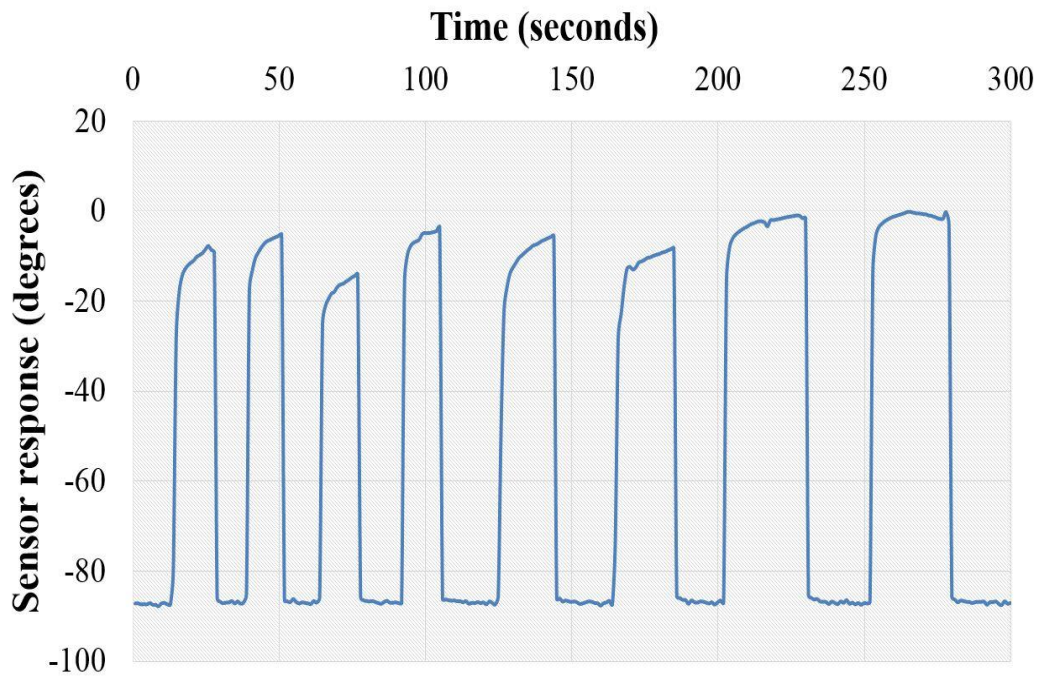


Figure 5.13 Response of the sensor for a pressure of 51.2 Pa of the index finger.

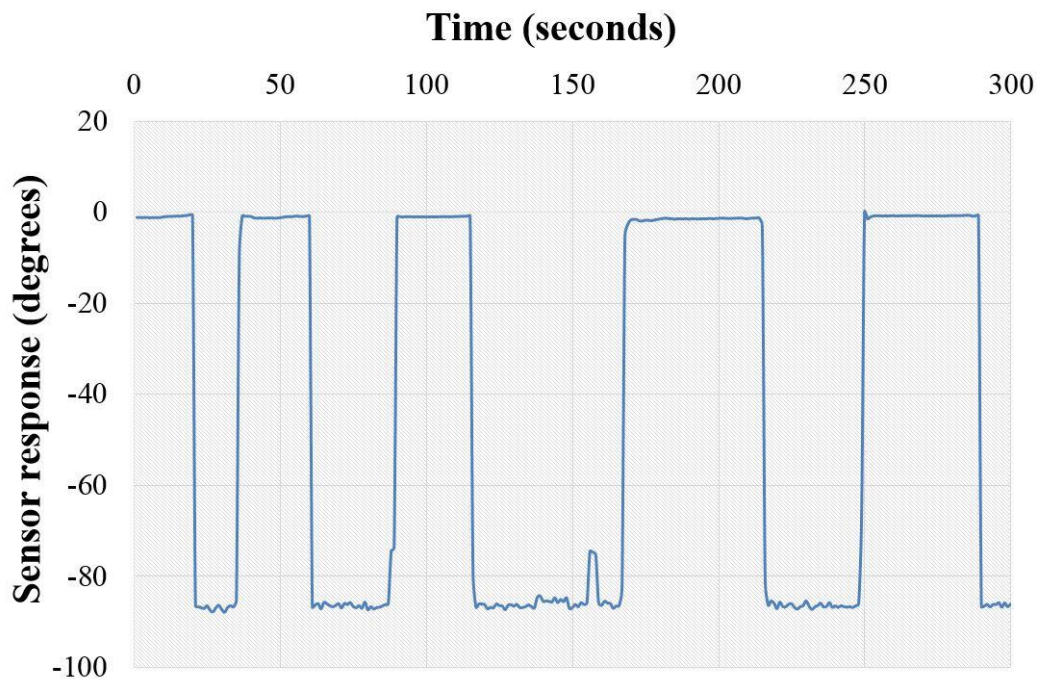


Figure 5.14 Response of the sensor for a pressure of 66.8 Pa of the index finger.

The index finger, thumb, and palm were used to exert pressure on the sensing area. The two fingers and the palm were used for experimentation because the tactile sensors used commercially [560, 561] for sensing purposes rely mainly on these portions of the hand.

The sensor responses were analysed for the change in phase angle over time. Initially, the value of the phase angle of the patch at undisturbed condition was around -90° .

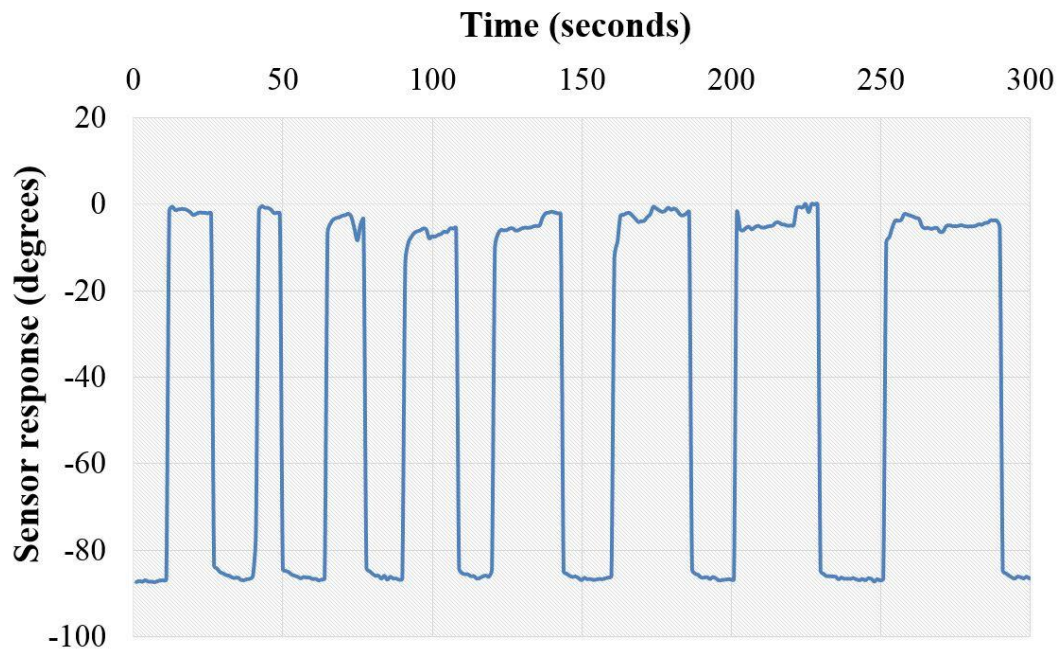


Figure 5.15 Response of the sensor for a pressure of 51.2 Pa of the thumb.

When the sensing area was touched at a definite pressure, the sensor responded with an increase in phase angle. Two different forces of 2.25 mN and 2.94 mN were applied by the index finger (Figures 5.13, 5.14) and thumb (Figures 5.15, 5.16). These forces were determined by connecting digital force gauges (DFX-II) to the patch. The pressure on the patch was calculated by dividing the force applied by the sensing area of the patch (0.36 cm^2). Different pressures were exerted on the sensor patch to determine its response. The pressures applied to the sensor as shown in the figures (Figure 5.13 – 5.18) was considerably lesser compared to a normal finger pressure ranging between 540 Pa to 400 kPa [562, 563].

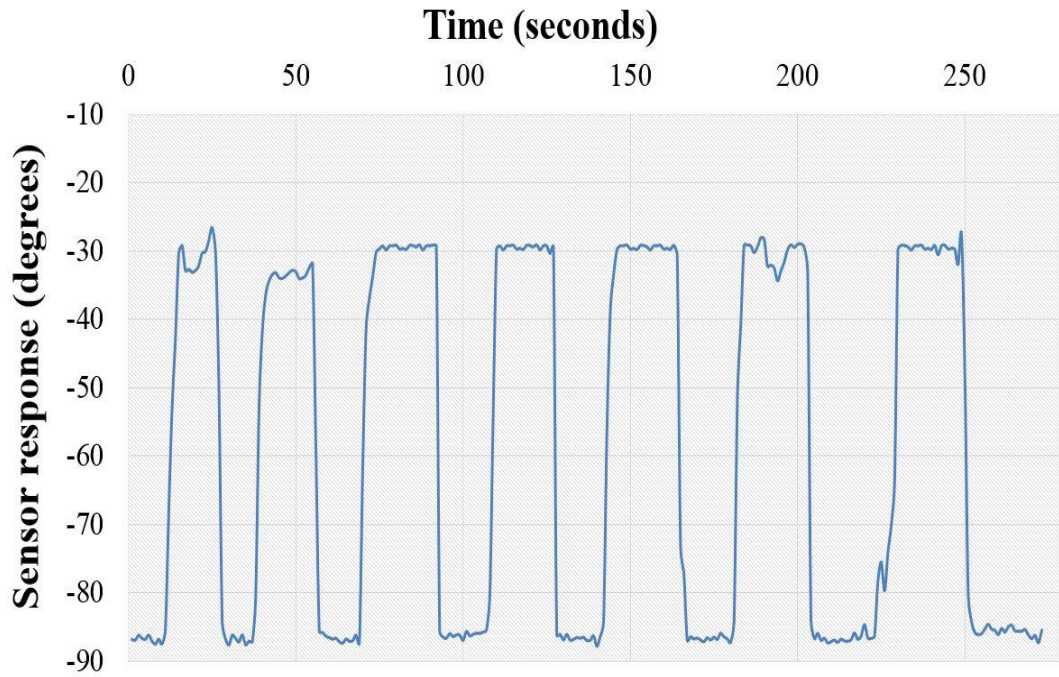


Figure 5.16 Response of the sensor for a pressure of 66.8 Pa of the thumb.

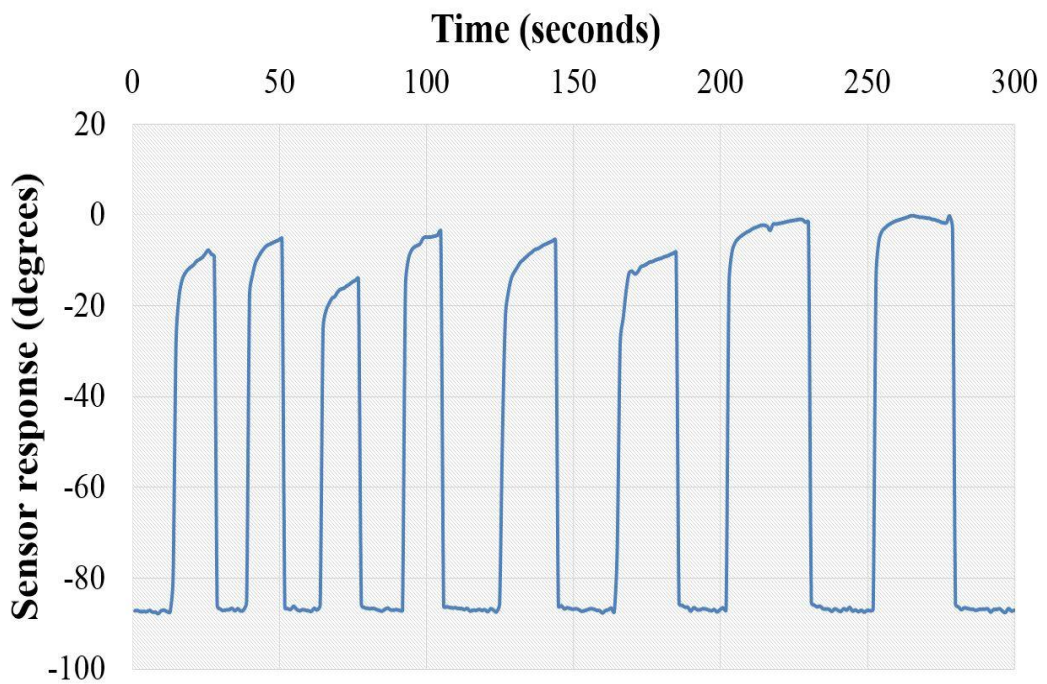


Figure 5.17 Response of the sensor for a pressure of 245 Pa of the palm.

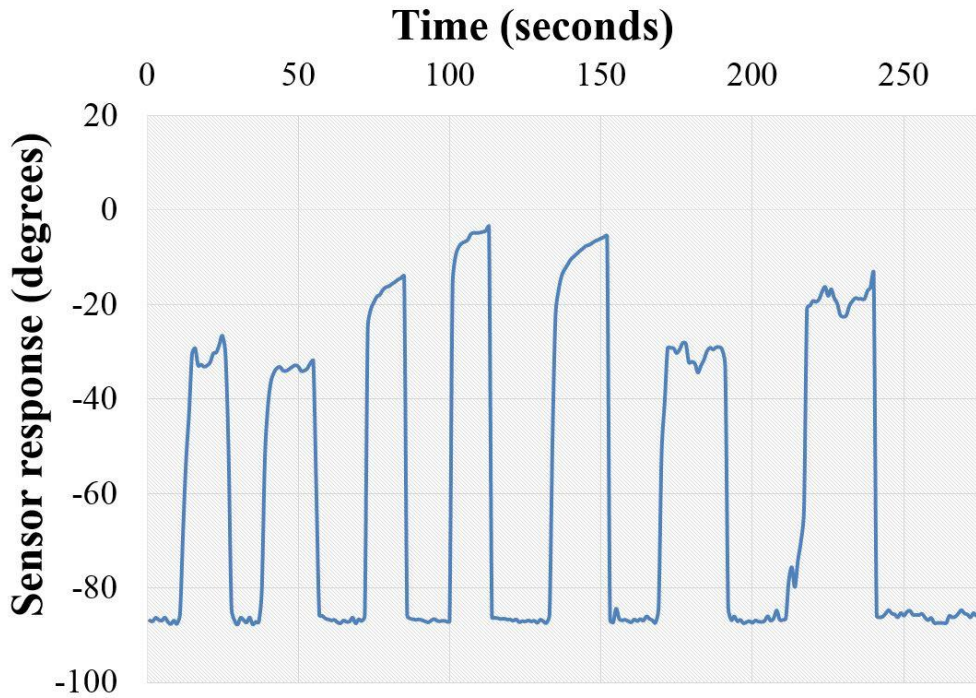


Figure 5.18 Response of the sensor for a pressure of 289.54 Pa of the palm.

This can be considered as a faint touch on the patch by the finger. Figures 5.17 and 5.18 show the responses of the sensor patch upon exertion of pressure with the palm. Table 7.1 shows the different pressure values applied on the sensor patch along with the repeatability of the sensor output. It is seen that the repeatability of the sensor output ceases when the pressure applied is beyond a limit. The reason behind this could be attributed to the breaking point of the sensor. The sensitivity can be calculated from equation (5.2).

$$\begin{aligned} \text{Sensitivity} & \quad (5.2) \\ & = \frac{\text{Change of phase angle}}{\text{Change in pressure}} \end{aligned}$$

$$S_p = \frac{\Delta\Phi}{\Delta p} \quad (5.3)$$

where, S_p is the pressure sensitivity, $\Delta\Phi$ is the change in phase angle, Δp is the change in pressure applied on the sensor.

The sensitivity curves for the two fingers and the palm are shown in Figure 5.19. There is not much difference in the sensor readings for the pressure applied by the palm from that

with the fingers. This shows the consistency in the response of the sensor patch irrespective of the force is exerted on it.

Table 5.1 Different pressure values exerted on the sensor along with the repeatability of the output.

Pressure (Pa)	Finger used for pressure	Repeatability
51.2	Index	Yes
66.8	Index	Yes
51.2	Thumb	Yes
66.8	Thumb	Yes
245	Palm	No
289.54	Palm	No

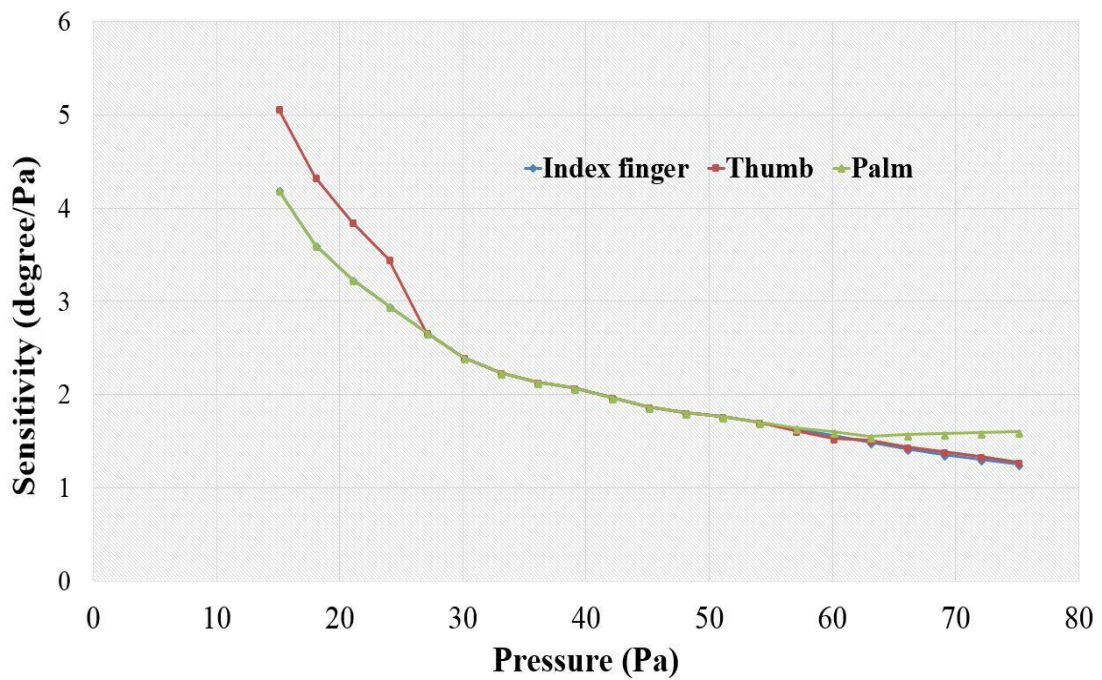


Figure 5.19 Sensitivity values for different pressures for the index finger, thumb and palm.

5.5 Chapter Summary

This chapter described the fabrication and application of a novel sensor prototype developed from metallised polymers. Commercial PET films, coated with aluminium on one side, were laser ablated to form interdigitated electrodes. Experimental results for tactile sensing were shown and were done manually to determine the response of the sensor patch to human touch. The pressures from two different fingers and the palm were tested to analyse the response in terms of phase angle with time. It is seen from the results that the patches respond well to very faint pressures (in Pa). The development of these low cost, easily fabricated patches would help to replace the existing tactile sensors like those used in prosthetic limbs, robotic grippers, pressure sensors etc. The repeatability of the sensor response was observed for different pressures. The next step will be to use the sensors in specific applications to validate the functionality via using them in real-time applications.

6

Graphene-Polyimide Sensor

Publication pertaining to this chapter:

- Md. Eshrat E Alahi., **Anindya Nag**, S. C. Mukhopadhyay and Lucy Burkitt, “A temperature-compensated graphene sensor for nitrate monitoring in real-time application”, *Sensors and Actuators A: Physical*, Vol. 269, pp. 79-90, **January 2018**.
- **Anindya Nag** and S. C. Mukhopadhyay, “Fabrication and implementation of printed sensors for taste sensing applications”, *Sensors and Actuators A: Physical*, Vol. 269, pp. 52-61, **January 2018**.
- **Anindya Nag**, S. C. Mukhopadhyay and J. Kosel, “Sensing System for Salinity Testing Using Laser-induced Graphene Sensors”, *Sensors and Actuators A: Physical*, Vol. 264, pp. 107-116, **August 2017**.

6.1 Introduction

The third type of novel sensor prototype was fabricated from laser induction of commercial polymer films. This type of sensor patch is very different from the other two types described in Chapters 4 and 5 as this fabrication technique can generate conductive material from low cost material. The manufacturing cost per sensor is one of the issues faced during the fabrication of any flexible sensor. This is due to the high value of the equipment or the raw materials used in the process. For example, photolithography [491], which is one of the standard methods employed for developing flexible sensors, has a high equipment cost and requires several steps for the preparation of the sample before the electrodes can be designed on the substrate. It also requires specialised people to handle the raw materials for processing them. Thus, there is interest in the implementation of a technique that is easy to use and enables the development of cheap sensors. Recently, the idea of generating conductive materials from polymers [564] has been approached by researchers. This is intriguing as it helps to develop sensors at a low cost on a large scale. Graphene, a conductive material for fabricated sensors, has certain advantages over other elements. Apart from being highly conductive, it is extremely corrosion resistant [565], which would minimise the effect of oxidation on the electrodes. This chapter presents the design and fabrication of laser-induced sensor patches that use the generated graphene as electrodes on commercial tapes. The developed sensor patches were then utilised with solutions of different saline concentrations to validate their ability to be used a salinity sensor in different large and small water bodies. Experiments and analysis with these sensor patches were also done for solutions of different concentrations developed from five chemicals which categorises fundamental types of taste. The potential applications of these sensor patches are many, due to their easy fabrication process, and excellent electrical and mechanical properties.

6.2 Fabrication of the Sensor Patches

A schematic diagram of the fabrication process of the sensor patches is given in Figure 6.1. Commercial PI films (Zibo Zhongnan Plastics Co., Ltd.) were used as raw materials to develop the sensors. A CO₂ laser system (Model: OLS 6.75 CO₂ laser system, laser spot diameter: 150 microns) was used for the thermal induction of graphene on the PI films.

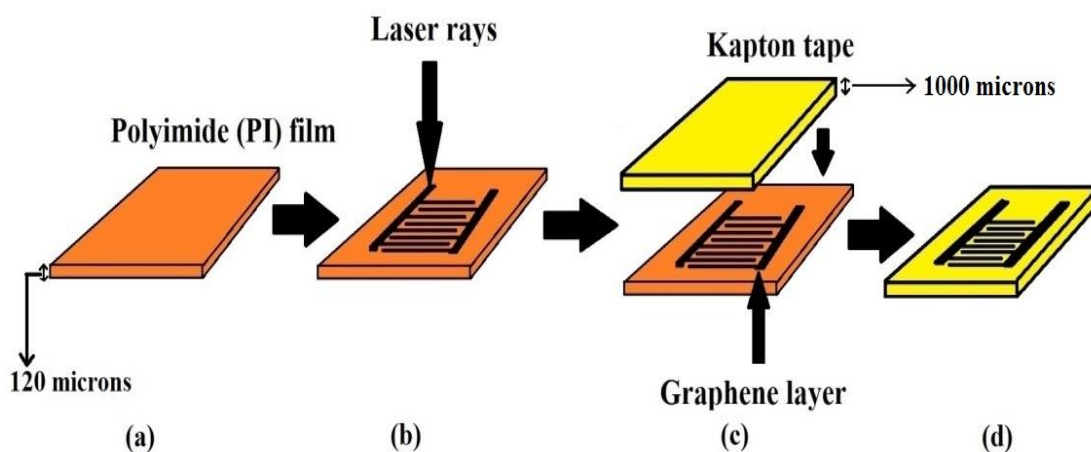


Figure 6.1 Schematic diagram of the steps of fabrication of the graphene sensor. (a) The polyimide film, with a thickness of around 120 microns, is taken as the substrate material for the laser writing process. (b) The laser writing was done on the film. (c) The thermally induced material is shifted manually to the Kapton tape by compressing it against the generated graphene. (d) The final sensor prototype.

The individual fabrication steps are illustrated in Figure 6.2. The polymer film was attached to a glass substrate for support as shown in Figure 6.2 (a). CorelDraw software was used to design the electrodes in an interdigitated pattern. Six pairs of electrodes were designed with the length and width of 500 microns and 100 microns, respectively. Figure 6.2 (b) shows the laser induction process of the attached polymer film. The sp^3 hybridised carbon atoms of the polymer film were photo-thermally converted to sp^2 hybridised atoms forming graphene. Power, speed and z-axis were the parameters of the laser system that were optimised for the laser-induced electrode-fabrication process. Power (W) determines the amount of energy the laser nozzle operates on. Speed (m/min) refers to how quickly the nozzle moves over the sample in the X-Y directions. Z-axis (mm) determines the focal point of the laser over the sample. This was done by changing the height of the laser platform in the z-direction. The final values used for developing the sensor patches were: Power: 9 watts, speed: 70 m/min, z-axis: 1 mm. The photo-thermally formed graphene was transferred to a Kapton tape with a thickness of 1000 microns. Even though both the ablated film and Kapton tape are made of PI, the reason commercial polymer films were considered as the raw material for laser writing for two reasons. Firstly, due to the greater thickness of Kapton tapes, it is not possible to photo-thermally disintegrate the sp^3 hybridised carbon atoms of the PI into sp^2 hybridisation. This was only possible using thinner films.

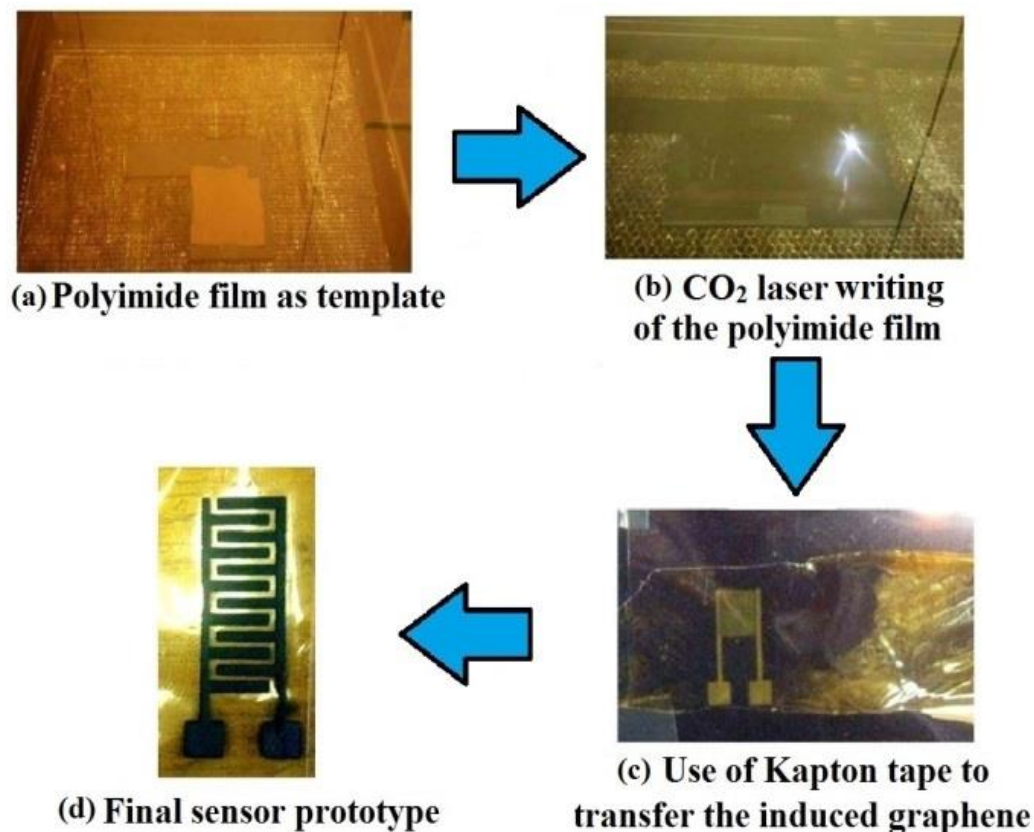


Figure 6.2 Fabrication steps of the sensor.

Secondly, the stickiness of the Kapton tape would have led to the immediate coagulation of the thermally-induced graphene, affecting the design of the electrodes. The placement of the Kapton tape over the induced graphene is shown in Figure 6.2 (c). This transfer was done via manual pressure in the vertical direction, all over the tape. The pressure was applied first to the electrode pads and then moving over to the sensing area of the sensor design to make sure of proper adherence of the induced graphene to the Kapton tape. The tape was then pulled off carefully from the PI film to avoid any damage to the transferred graphene. Figure 6.2 (d) shows the sensor patch consisting of transferred conductive material on the Kapton tape. A difference in conductivities of <20 mS/m was observed between the induced and transferred graphene. The front and rear views of the sensor patch are shown in Figure 6.3. The SEM images of the top and cross-sectional views are shown in Figures 6.4 (a) and 6.4 (b). It is seen from the images that the edges and electrode lines of the transferred graphene came off cleanly onto the Kapton tape.

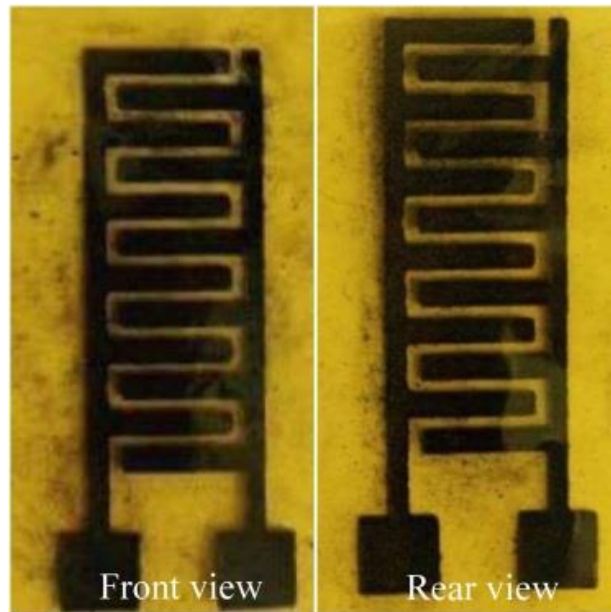


Figure 6.3 Front and rear views of the sensor patch.

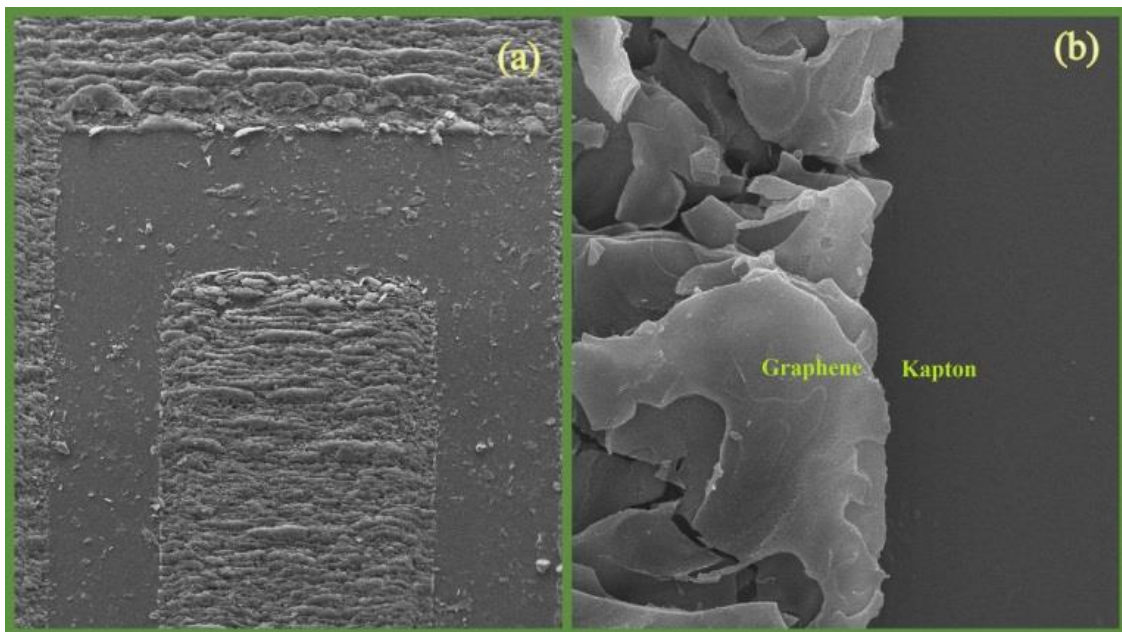


Figure 6.4 SEM image of (a) Top view of an electrode finger of the sensor patch (b) Zoomed top view showing the electrode lines.

6.3 Complex Nonlinear Least Squares Curve Fitting

Characterisation of these sensor patches was done to determine their responses towards different dielectric materials having different permittivity. Initially, the equivalent circuit for the electrical parameters was determined using the complex nonlinear least square curve

fitting (CNLS) technique. It uses the electrochemical spectrum analyser algorithm by making a comparison between the experimental values with the theoretical response. This was done to determine the system kinetics explaining the diffusion process taking place at the electrode-electrolyte interface. The Nyquist (Cole-Cole) plot for each chemical was analysed by plotting a curve with the real part (resistance) as the x-axis corresponding to the imaginary part (reactance) of the impedance as the y-axis. Statistical analysis was performed by a specific algorithm to calculate the amplitude of the residual mean-square value using equation 6.1 [477]:

$$r_{amplitude}^2 = \sum_{i=1}^N \frac{(Z'_{iobs} - Z'_{icalc})^2 + (Z''_{iobs} - Z''_{icalc})^2}{Z'_{iobs}^2 + Z''_{iobs}^2} \quad (6.1)$$

where

$r_{amplitude}^2$ defines the quantitative values of the difference between the simulated and experimentally obtained values.

Z'_{iobs} and Z'_{icalc} defines the observed and calculated values of the real part of the impedance.

Z''_{iobs} and Z''_{icalc} defines the observed and calculated values of the imaginary part of the impedance.

The profiling of the sensor was done in air to determine its equivalent circuit is shown in Figure 6.5. The change in the response of the sensor patch was studied in terms of the real (R) and imaginary (X) parts of the impedance (Z). An average of three values was taken from the instrument in order ensure repeatability of its response. These impedance values were fitted into the electrochemical spectrum analyser to determine the equivalent circuit with respect to the response of the sensor patch in air. The least square curve fitted Nyquist plot is obtained where the circuit shown in the inset gives the equivalent circuit with a similar response as seen from the overlapping theoretical and experimental graphs. The total impedance in the circuit consisted of different components (C_{int} , C_{sol} , and R_{sol}). These individual parameters affect the overall kinetic response of the sensor. C_{sol} and R_{sol} are the solution capacitance and resistance respectively which depend on the properties of the medium. When the solution medium is changed, the conductive properties of the sensor and the relative permittivity (ϵ_r) also change. This changes the solution resistance and

capacitance. C_{int} is the internal capacitance which arises due to the structure of the electrodes.

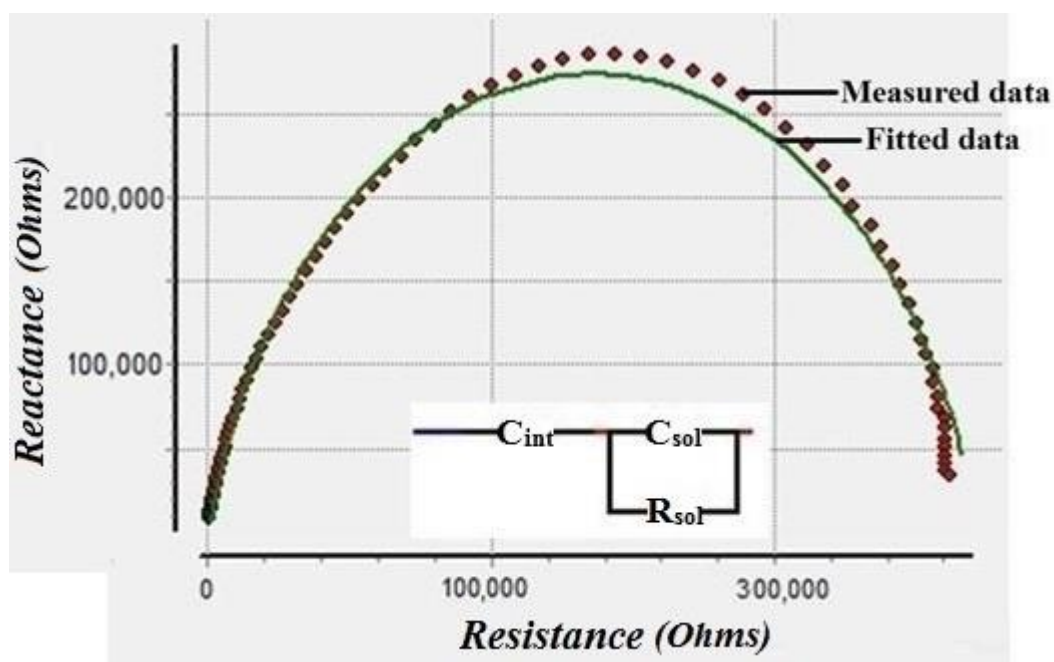


Figure 6.5 Least squares curve fitting plot in terms of Nyquist plot for the profiling of the sensor done in air. The red dots indicate the experimental data with the green line being the fitted curve.

The internal capacitance also changes when the solution medium is changed, but this change is negligible compared to the changes in the solution capacitance and resistance. The internal capacitance mainly changes by changing the surface area (A) and interdigital distance (d) of the electrodes. The electrode resistance can be considered negligible in this case; as the electrodes of the sensor patches are conductive, the change in current due to the resistance (R) will be low. The simulation was carried out with the electrochemical spectrum analyser with the same range of frequency sweep (1 Hz – 10 kHz) to compare the experimental results with the theoretical ones. Table 6.1 shows the different values, including the error obtained as the difference between the experimental and curve fitted values for the electrical parameters in the equivalent circuit. It is seen that the mean square value is in the range of 10^{-2} which suggests an error of less than 5% [566].

Table 6.1 Equivalent circuit parameters (as shown in the inset of Fig. 7(b)).

Equivalent circuit electrical parameters	Curve fitted value	Error%
C_{int} (pF)	71.22	1.95
C_{sol} (pF)	8.99	0.82
R_{sol} (k Ω)	343	4.05

6.4 Salinity Sensing

Sea water consists of different elements sustaining plant and animal life. Each constituent has a certain effect on its life-sustaining ability. One of them is the effect of salinity on marine life [567, 568]. Salinity can be defined as the amount of salt present in water bodies like sea and rivers. It is expressed by the electrical conductivity per unit distance ($\mu\text{S}/\text{cm}$) at a particular temperature. There are ongoing studies to determine the effects of changes in the salinity level in water bodies. Rise in temperature, oil spills in water bodies, discharging of waste materials and climate changes are some of the common reasons for the change of its levels. A rise of salinity in sea water is detrimental to plants. The growth of plants and seed germination is affected by even slight changes in the salt concentration. Higher levels of salinity can cause difficulty for plants in extracting water from the soil and can be toxic. A small increase in salinity increases the density of water bodies like rivers, thus sinking it to the bottom and floating it across river basins. Currently, a lot of research work [569-572] is going on to determine the optimum concentration of salt in sea water. It is expensive to remove excess salt from sea water due to the high-quality equipment needed to extract the salt. The Murray-Darling Basin report 2015-16 [573] showed that around 524,728 tons of salt water were removed from the River Murray, Australia in one year. This is alarming considering that this is the amount of salt present in just one water body.

There has been some research done [574-582] on the monitoring and evaluation of salinity. Certain disadvantages attached to each developed technique make them inefficient to use on an industrial scale. Optical sensors used for salinity testing [574] measure a concentration of 200 mM to 2M. Apart from the higher initial cost of fabrication of the sensor developed with the chloride-quenchable fluorescent probe, the sensor does not measure small changes, i.e., it has a small sensitivity. Other techniques involve the use of

SMOS satellites developed by NASA [575] for soil moisture and ocean salinity testing. Even though this technique would be much more accurate than the previous one, the infrastructure cost is high and would be difficult to support if applied to smaller water bodies. Grating sensors for salinity and temperature measurements made of acrylate and polyimide-coated fibres for testing the sensor at Bragg's wavelength have also been developed [576]. The biggest disadvantage of using a coating on the fibres is that it is difficult to be re-used. Thus, it is a state of the art to develop a low-cost, efficient sensing system which would help to determine any change in the salinity level to permit immediate remedial measures. Some impedance measurement systems have been proposed earlier [581], but there are disadvantages like low sensitivity, and a complicated associated sensor framework. The sensors, being developed with MEMS technology, have a high its cost of production. Also, these sensors were operated in the MHz range which is undesirable in real-time applications. The laser induced sensors prototypes developed in this system were initially tested with different salt concentrations with the idea of developing a fully functionalised sensing system. After validation of the functionality of the sensor with a data acquisition system, a microcontroller-based sensing system was developed. Figure 6.6 gives the block diagram of the proposed microcontroller-based sensing system. The sensor was controlled by the attached conditioning circuit which processes its output to generate an amplified signal. The development of this system is explained step by step in subsequent sections.

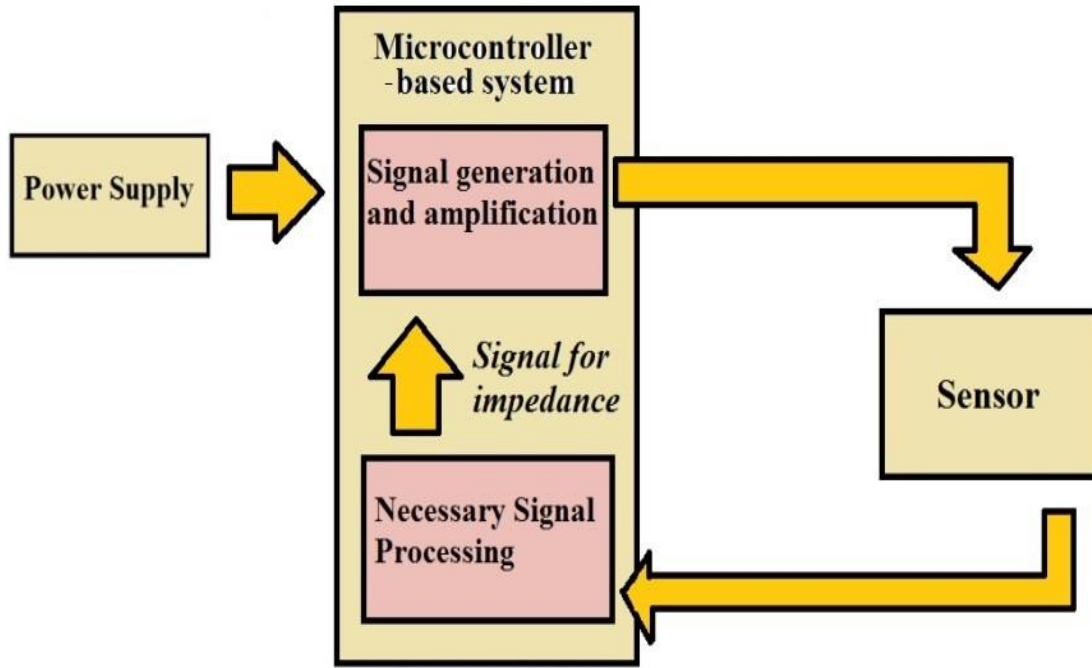


Figure 6.6 Block diagram for the proposed microcontroller-based sensing system for salinity measurement.

6.4.1 Experimental Setup

Sodium Chloride (SA046- 500G) was used as the solute to develop the salt solutions. De-ionised MilliQ[®] water (Resistance: 18.2 MΩ cm and pH: 6.71) was used as the solvent for the experiments. Serial dilution was performed to develop a series of solutions from 40000 ppm to 4 ppm. Initially, a principal solution of 40000 ppm was prepared by mixing 4 g of solute to 100 ml of solvent. After performing the experiment with this solution, the second solution was prepared by pipetting 10 ml of the principal solution to 90 ml of de-ionised MilliQ[®] water. This formed 4000 ppm of salt solution. After this second reading, the third solution was formed by pipetting 10 ml of stock solution into 90 ml of deionised MilliQ[®] water to form 400 ppm of salt solution. This process was continued till a 4-ppm salt solution was prepared. The experimental setup is shown in Figure 6.7. The experiments were performed with a HIOKI IM 3536 LCR Hi precision tester. The sensor patch was connected to the LCR meter via Kelvin probes for data analysis.

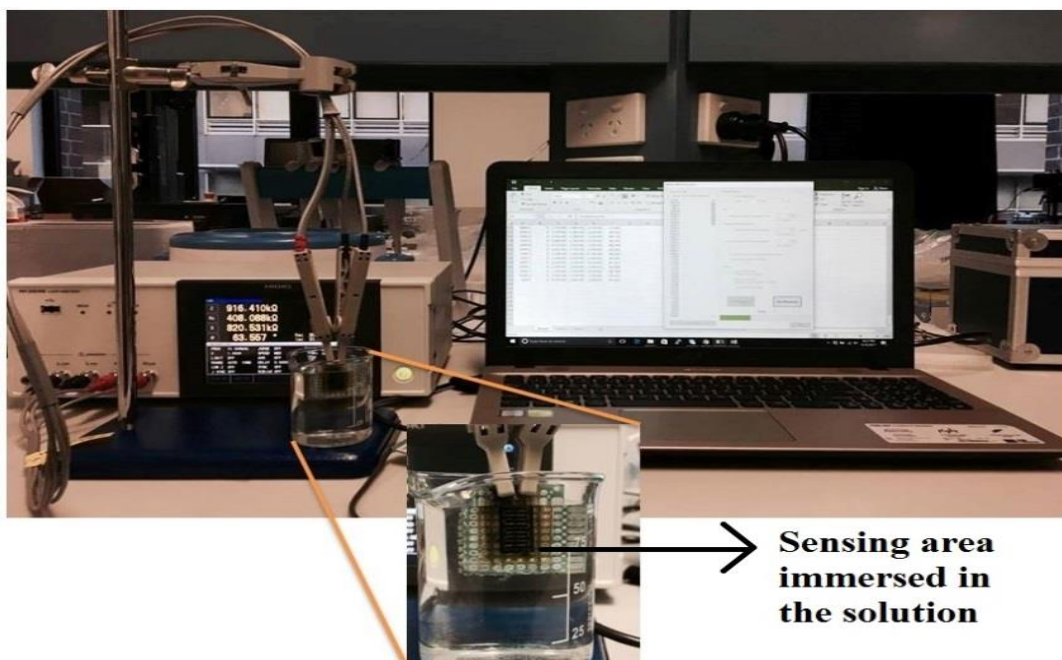


Figure 6.7 Experimental setup showing the attachment of the sensor patch to the LCR meter via Kelvin probes. The sensing area of the patch was immersed in the solution. The LCR meter was connected to the laptop to collect the data.

The LCR meter was connected to the computer by a USB - USB cable to collect the data in an Excel file via an automatic data-acquisition algorithm. The sensor patch was fixed to a board with biocompatible tapes (3M Ruban Magique^{MC}) for its stability in water during the testing it. The sensing area of the patch was carefully immersed into the solution to make sure that the bonding pads of the sensor and the connected probes do not come in contact with the solution. After each experiment, the sensor patch was thoroughly washed with MilliQ[®] water and dried in the oven for 10 minutes before re-using it for the next experiment. A sinusoidal signal with a fixed voltage of 1 V peak-to-peak was applied from the LCR meter, and the frequency was swept from 1 Hz to 10 kHz. The resistance (R) and reactance (X) were taken from the LCR meter.

6.4.2 Results and Discussion

The response of the sensor patch to the tested samples is shown in Figures 6.8 and 6.9 in terms of resistance (R) and reactance (X) respectively. It is seen that the sensor patch is distinctively sensitive towards the different tested salt concentrations. Even though it is seen from Figure 6.8 that the resistance changes symmetrically for all the tested solutions, the change in reactance as seen from Figure 6.9 is prominent only within a certain range.

The resistance decreases with increase in the salt concentration due to the increase in ionic current passing through the circuit.

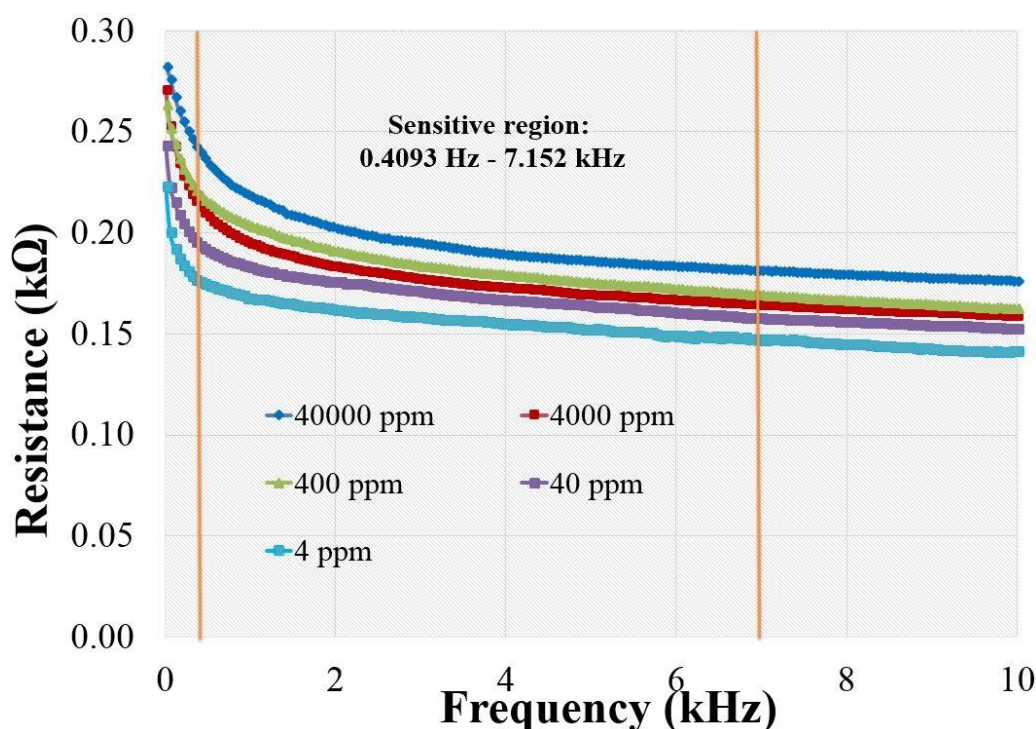


Figure 6.8 Response of the sensor patch for different concentrations of salt in terms of resistance and frequency.

The frequency of operation had a major role to play for the change in reactance compared to the change in resistance. For the change in reactance, the frequency range between 0.4093 kHz – 7.152 kHz displays a strong change for different concentrations. The reactance changes as a result of the capacitive part of the sensor which depends on both the frequency and the concentration of the sample. The changes in the response for the reactance occur due to the faradic currents going through the tested sample. Figure 6.10 shows the Nyquist plot between the real and imaginary parts of the impedance. The readings shown in the Nyquist plot also show a clear distinction between the different test concentrations. This plot is different from Figure 6.5 that was obtained during the profiling of the sensor in air. These changes occur because of changes in the elements constituting the equivalent circuit. A particular frequency (4.205 kHz) was chosen from the sensitive region to develop the characteristic curve as shown in Figure 6.11. The chosen frequency gave the highest difference in the experimental values of the salt concentrations. The sensitivity of the sensor patch is 0.005 Ω/ppm, as can be seen from the slope of Figure 6.11.

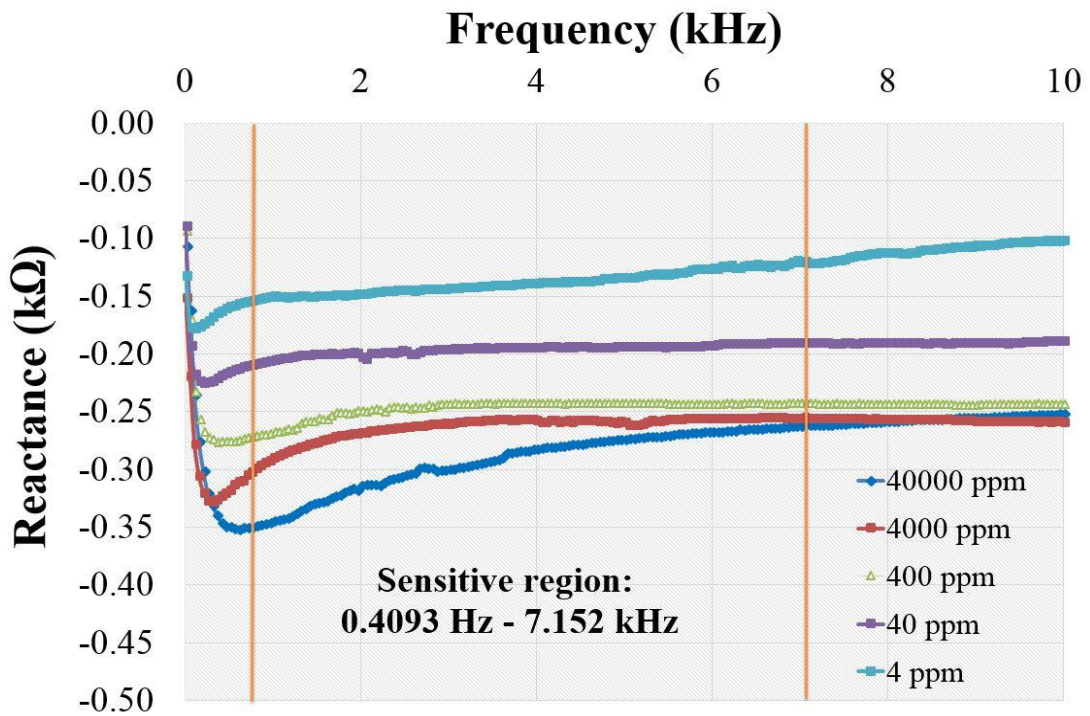


Figure 6.9 Response of the sensor patch for different concentrations of salt in terms of the reactance and frequency.

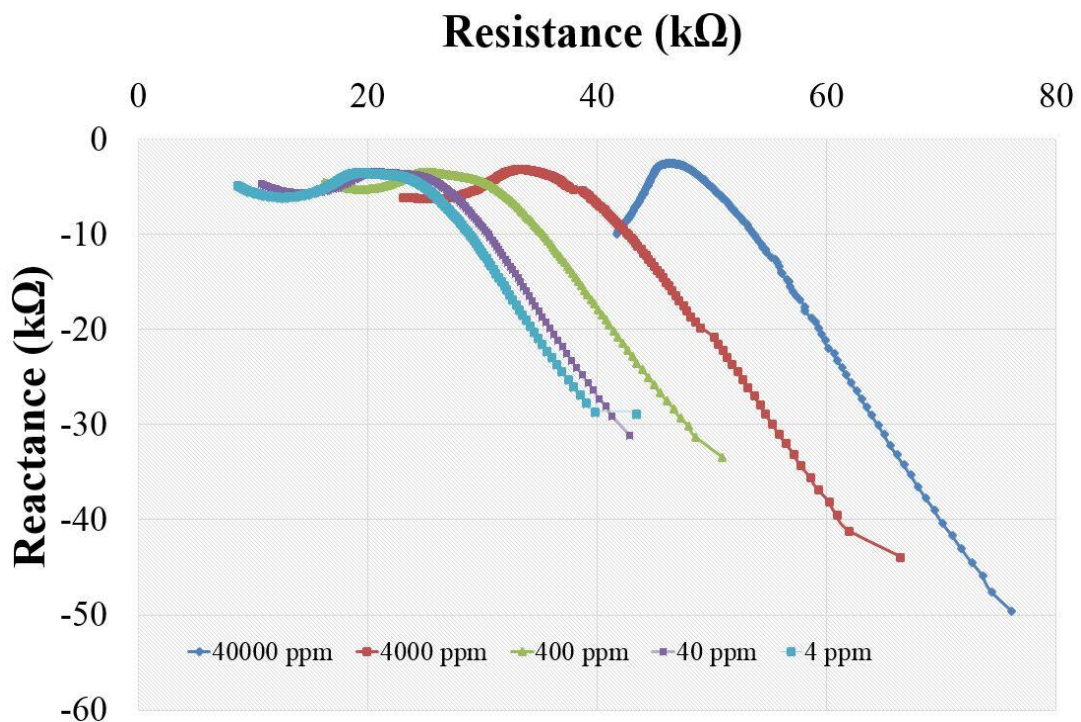


Figure 6.10 Response of the sensor patch for different concentrations of salt in terms of Nyquist plot.

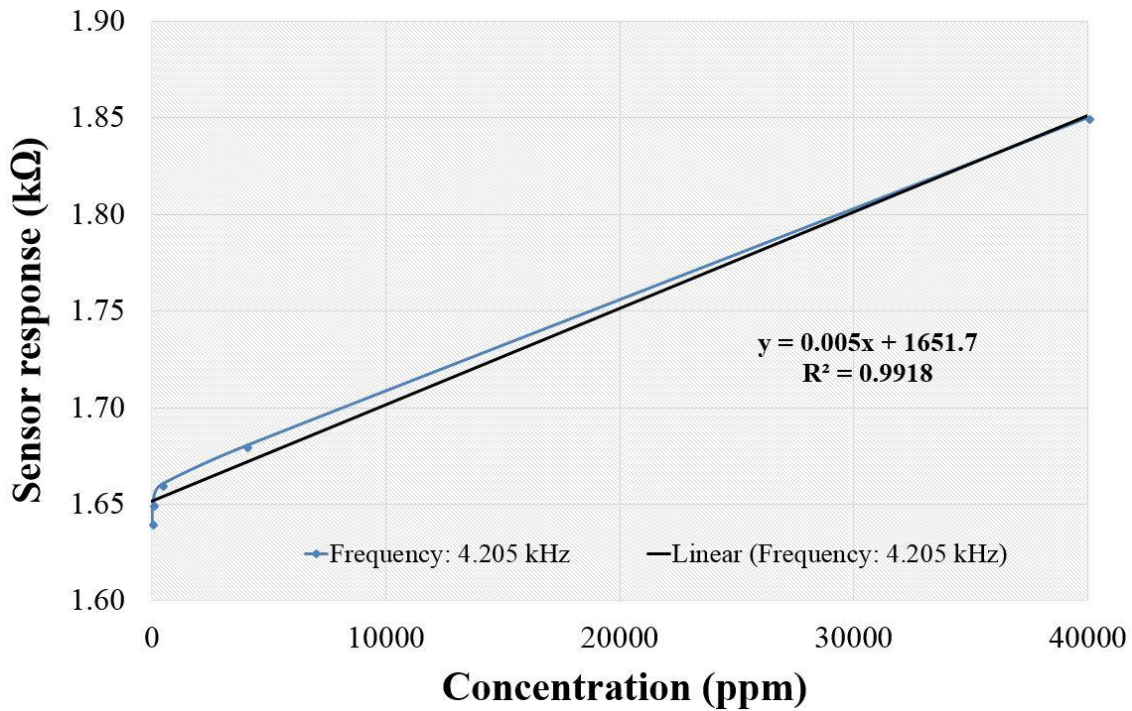


Figure 6.11 Standard curve for different experimental concentrations.

A real-time sample of unknown concentration was considered for testing to validate the developed system. After performing a frequency sweep between 1 Hz and 10 kHz, the response of the sensor towards the chosen frequency value was considered to develop the standard and sensitivity curve. The measured values of the tested sample at that frequency (4.205 kHz) were: Resistance (R): 1828.35 Ω , reactance (X): 1651.7 Ω . Substituting the resistance value to the equation obtained from the standard curve,

$$y = 0.005 * (x) + 1651.7 \quad (2)$$

$$1828.35 = 0.005 * (x) + 1651.7 \quad (3)$$

$$x = \frac{1828.35 - 1651.7}{0.005} \quad (4)$$

$$x = 35330 \quad (5)$$

The experimental value of the real sample was 35330 ppm. This was cross-checked with a refractometer; a standard device used to determine the salinity level of real samples in the marine and biological industries [583, 584]. The actual concentration of this sample was 35000 ppm. This proved our experimental value to be very close to the actual value. The error calculated from this sample measurement was 0.9%. Figure 6.12 shows the

equivalent circuit for the Nyquist plot developed from the experimental values. It is seen from Figures 6.5 and 6.12 that there is a change in the components of the equivalent circuit.

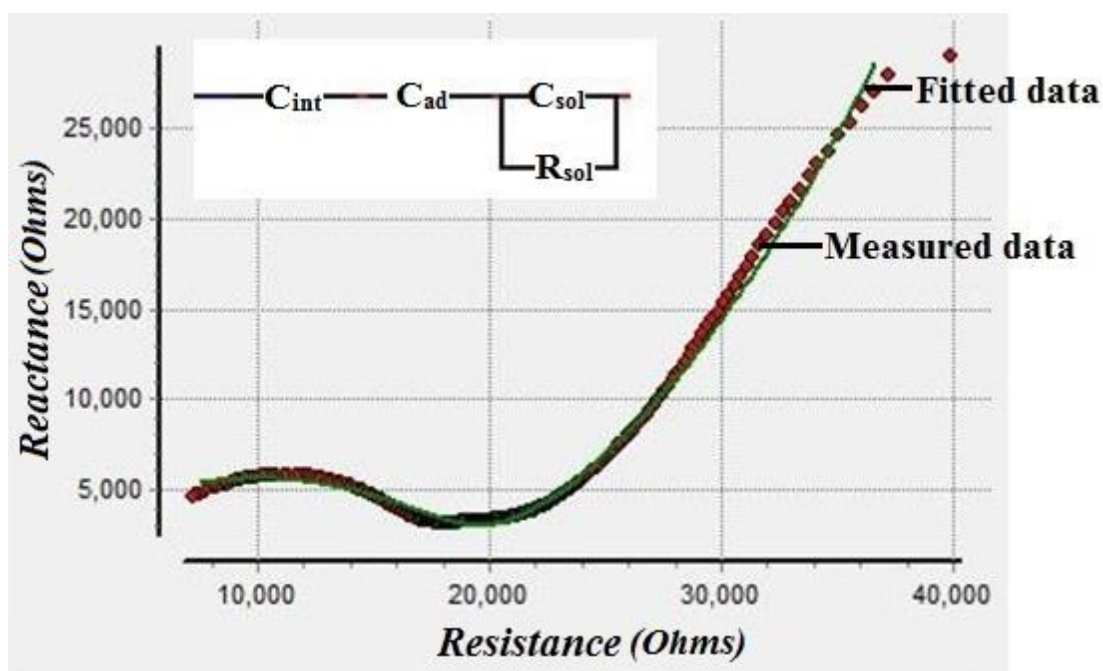


Figure 6.12 Least-square curve fitting for Nyquist plot with the experimental data.

A constant-phase element (CPE) has been added in series with the internal capacitor of the sensor. The presence of the CPE in the circuit is represented as the adsorption capacitance (C_{ad}). This C_{ad} arises due to the ion diffusion process between the sensing surface of the electrodes and the bulk solution [585]. The solution capacitance (C_{sol}) and resistance (R_{sol}) are two important parameters to determine the change in response. Table 6.2 presents the different parameters along with their values and error rate. It is seen that the error for each of the elements in the generated equivalent circuit is less than 5% [586]. Figure 6.13 shows the response of the sensor to changes in temperature in terms of resistance values. The measurement of the five concentrations was taken at five temperature values (10 °C – 50 °C) at the chosen frequency (4.205 kHz). It is seen that the changes in resistance is negligible despite changes in temperature for each concentration. Figure 6.14 shows the repeatability of the sensor responses, where experiments with each concentration were carried out six times with duration of two hours between each experiment. It is seen from the response that the difference between the sensor responses to each concentration for the six cases is very negligible and the deviation from the mean value lies below 2%.

In order to develop a sensing system, the same frequency value (4.205 kHz) was fixed in the microcontroller to determine if the change in the concentration of the solution can be determined by the embedded system. A conditioning circuit was developed with the microcontroller before testing the sensor with solutions of the same concentrations as before.

Table 6.2 Equivalent circuit parameters along with their limits, result and error % to determining the fitted curve on the experimental data.

Equivalent circuit electrical parameters	Curve fitted value	Error%
C_{sol} (μF)	1.171	2.46
R_{sol} ($k\Omega$)	18.6	0.49
C_{int} (μF)	6.8	0.95
C_{ad} (μF)	113	2.53

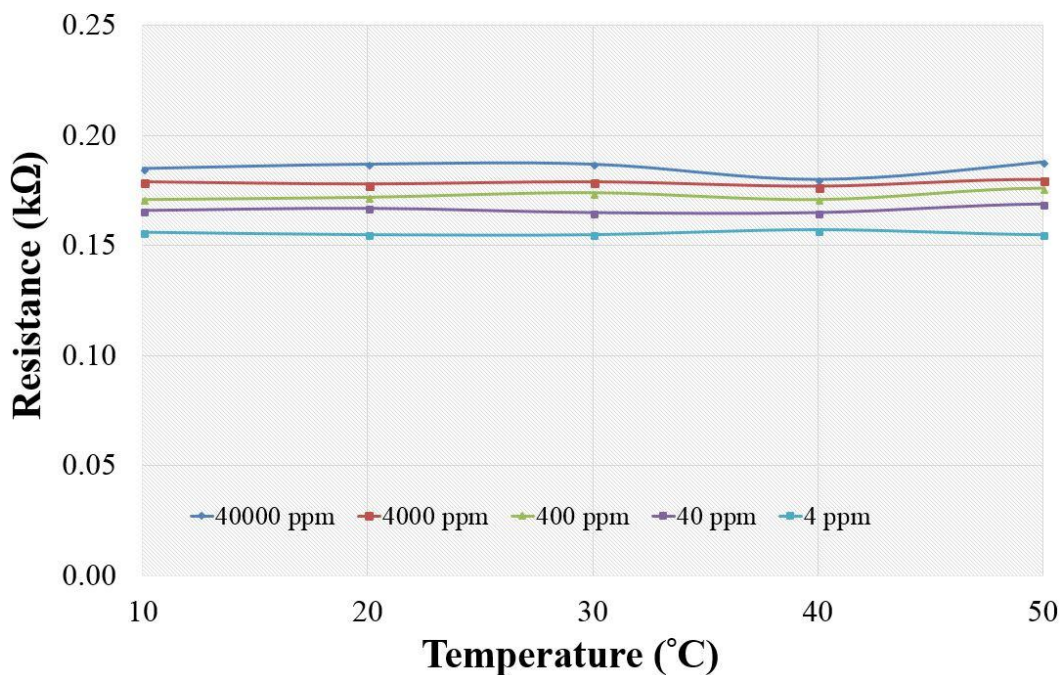


Figure 6.13 Dependence of the sensor response towards the temperature changes for different salt concentrations.

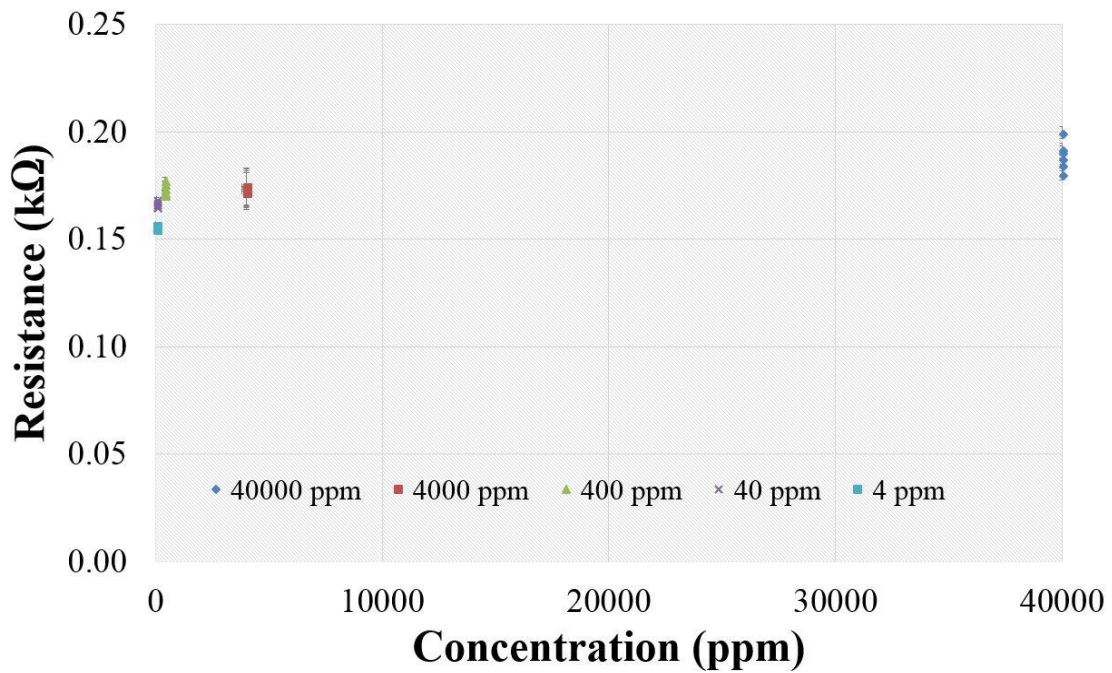


Figure 6.14 Repeatability of the sensor response illustrated with six measurements with each salt concentration.

6.4.3 Microcontroller-based Sensing System

Arduino Uno and the Arduino Integrated Development Environment (IDE) were used as the microcontroller (μC) device and the associated software, respectively, to test the sensor patch for different salt concentrations. Figure 6.15 shows a block diagram for the connection of the sensor to the microcontroller. The sensor output was passed through a buffer and a low-pass filter to the microcontroller. The power supply voltage fed to the microcontroller was fixed at 3.3 V with a sinusoidal voltage signal applied to the sensor, the output was passed through an amplifier circuit. This consisted of a buffer and an active low-pass filter. This was done to obtain the maximum response of the sensor by reducing the noise and amplifying the signal. The schematic diagram of the sensor with the amplifying circuit is shown in Figure 6.16. The non-inverting gain provided to the output signal from the sensor was 23. This was done to have an amplified response of the output voltage from the sensor occurring due to the difference in salt concentrations. The output of the low-pass filter was used as the analogue input to the microcontroller's analogue-to-digital converter. Figure 6.17 shows the voltage readings for the measured concentrations. It is seen from the figure that the response of the sensor changes almost linearly with the change in concentration. This suggests that the microcontroller embedded sensing system

can detect the small changes happening in the solution. The ultimate motive is to develop a system to give a full-scale voltage during the real-time testing of sea water samples. The microcontroller-based system would be useful in real-life situations where the system, apart from the sensing surface of the sensor patch, can be capsuled inside a waterproof case to examine the changes in salinity in the water.

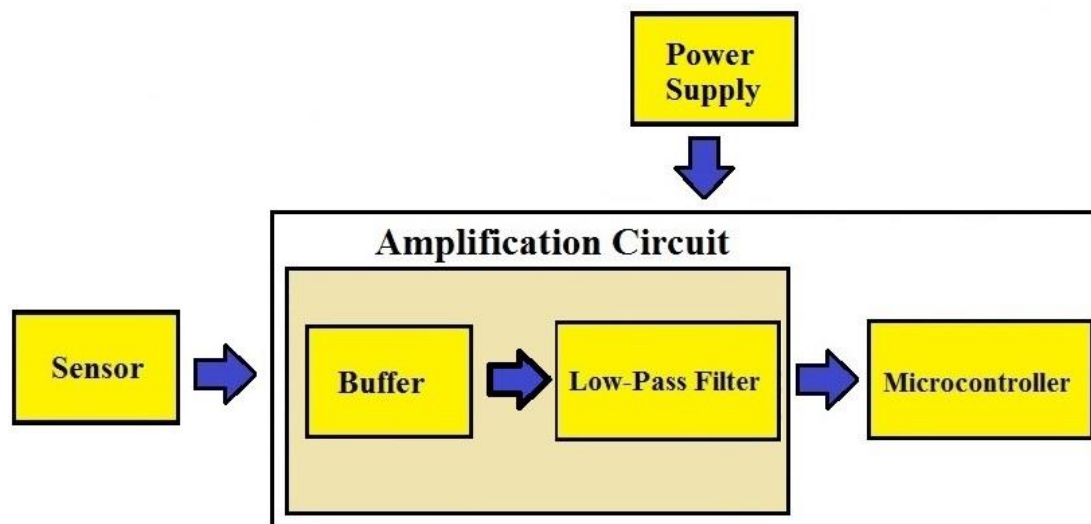


Figure 6.15 Block diagram depicting the connection of the sensor to the microcontroller. The buffer and low-pass filter were added to the circuitry to improve the output from the sensor.

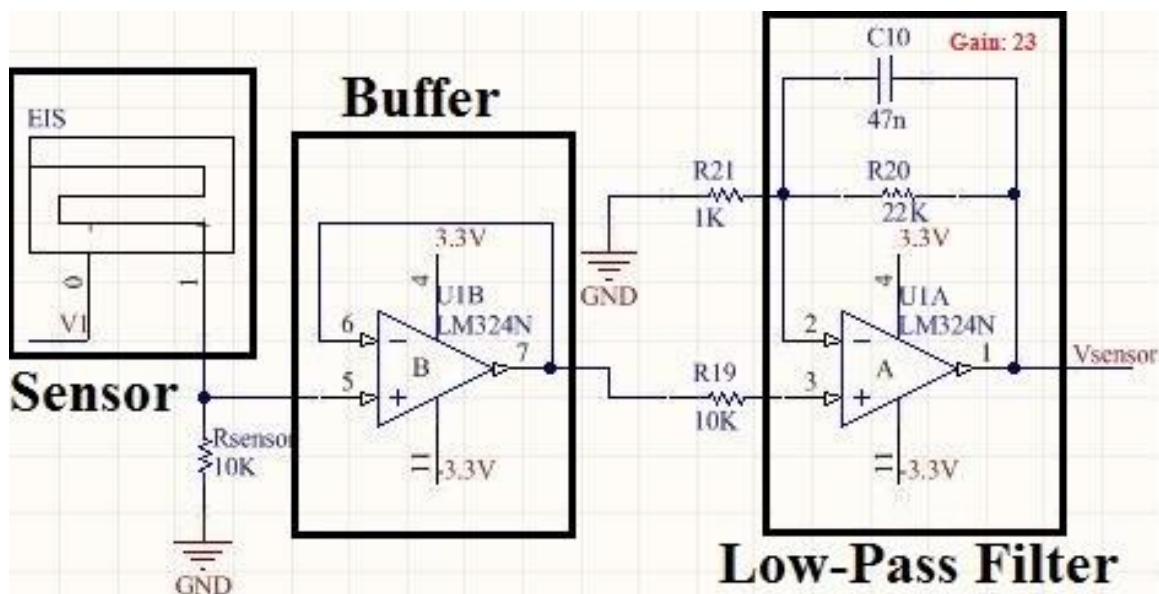


Figure 6.16 Circuit design for the conditioning circuit used to process the sensor output before feeding it to the microcontroller.

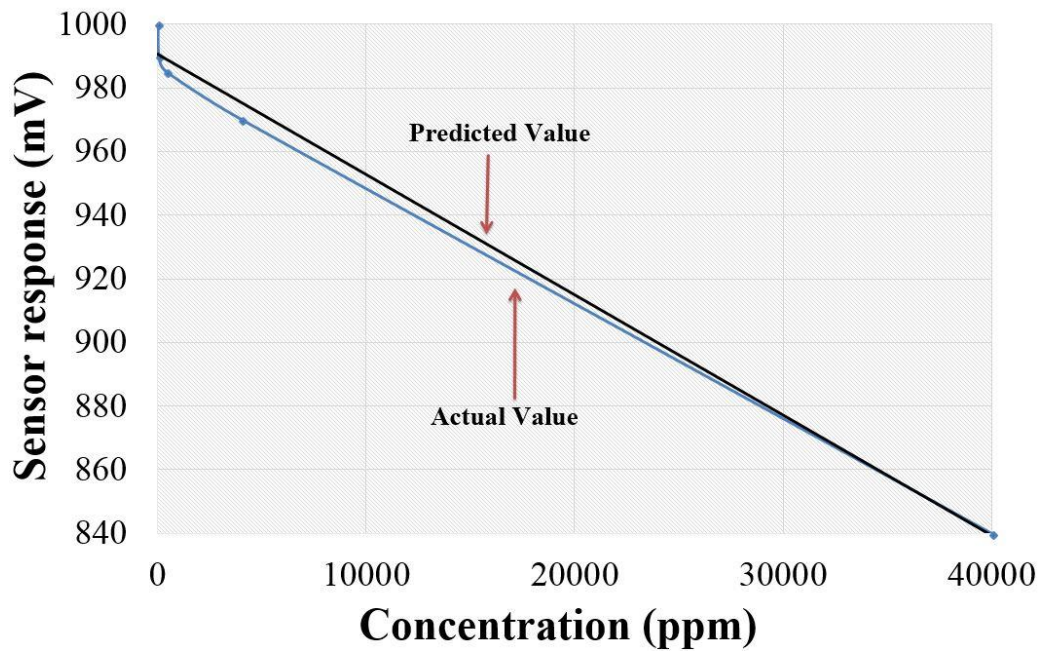


Figure 6.17 Response of the microcontroller for different salt concentrations.

6.4.4 Conclusion

This section showcases the development of a sensing system for the detection of different salt concentrations in water bodies. The main motive to develop this system was to measure the problems faced by flora and fauna existing inside water bodies. But, there are some issues that need to be resolved before implementing the proposed system for real-time applications. Firstly, apart from sodium chloride, there are other molecular constituents present in sea water. This can affect the sensor response in real-time applications. This can be resolved by attaining selectivity towards the chosen molecule. Secondly, the response of the sensor can also be influenced by elements having ionic properties similar to sodium and chloride ions. The similarity in properties arises mainly from the similarity in structure, density, and electron affinity. The problem of similarity occurs especially with salts with sodium as the cation. This would mislead the monitoring unit, thus generating erroneous results. These problems are to be addressed and reported soon after developing a low cost, fully-functionalised salinity measurement system.

6.5 Taste Sensing

Among the five different senses of sight, touch, smell, hearing, and taste, least work is done on the taste sense. Taste sensing does impart very significant information about the condition of a person. A human tongue has thousands of taste buds, each of which consists of hundreds of taste cells [587]. People having taste disorders [588] present one of the more significant problems of recent years. Each year, more than 200,000 people suffer from taste disorders, with one out of every ten children affected [589] in Australia. This is a very alarming statistic, as a taste disorder can lead to other disorders like obesity and high blood pressure. Even though a normal person starts losing his taste buds after the age of 50, there are other causes like respiratory infections, radiation therapy and surgeries near the head or neck region, which lead to the loss of taste buds. Even though otolaryngologists have been a common choice of medical assistance for people suffering from taste disorders, researchers have been working to comprehend it scientifically [590, 591].

An electronic tongue (e-tongue) has been a popular innovation for taste sensing during the last decade [592, 593], where a complex system had been developing which replicates the functions of a human tongue. Even though the e-tongue does offer comparable functioning to a regular tongue, there are certain disadvantages which are compelling researchers to give alternative options. Starting from the high cost to develop the structure [594], the overall structure is complex [595], causing it to be difficult to afford for financially constrained patients [596]. Another major disadvantage related to the e-tongue is the dependence of its functionality on temperature and humidity [597]. Also, the adsorption of the analyte on the selective sensing surface limits the re-usability of the sensor [598]. Thus, it is desirable to develop alternative options that could be used as taste sensors. Even though some research groups have developed systems for taste assessment [599], there are certain limitations associated with their work. The systems were based on the identification of just one [600] or two [601] taste types. The idea behind our work is to have a sensor which can clearly classify the five fundamental taste types. This could help us to develop a system that can be used to identify and monitor the concentration of a taste in a food material. This section reports a brief description of the fabrication with the focus on the implementation of these sensors as taste sensors.

The taste buds of a normal human being can be divided into five categories: sour, salty, bitter, sweet, and umami. Even though there are millions of food materials that can be

categorised in one of these sectors, researchers have established [602] the following chemicals for experimental purposes that can be exactly replicated to these five tastes:

- Sour: Citric acid
- Salty: Sodium chloride
- Bitter: L- tryptophan
- Sweet: Sucrose
- Umami: Guanosine monophosphate (GMP)

After the sensor was fabricated, the above-mentioned chemicals were tested at four fixed concentrations. The concentrations were based on the minimum amount [600, 603] of that chemical present in food. Then a comparison was done on each of the four concentrations of the five taste types to verify the differences in their responses.

6.5.1 Experimental Setup

The experiments with the sensor patch and different chemicals were performed in the laboratory environment at a fixed temperature (25 °C) and humidity (RH 50%). Figure 6.18 shows the setup for the experiments and data collection. The sensor patch was attached to a wiring board with biocompatible tape (3M 810D Ruban Magique^{MC}) to keep it fixed inside the solution during experiments. The sensing area of the patch was immersed carefully such that the bonding pads did not touch the solution. A HIOKI IM 3536 LCR High Precision Tester was connected to one end of the sensor with Kelvin probes while testing during experimentation to determine the changes analysed by the sensor. An alternating voltage of 1V_{rms} was provided as the input to the tester. The tester was in turn connected to a computer via a USB-USB cable for collection of the sensor data in Microsoft Office Suite using an automatic-data-acquisition algorithm. An average of three readings per solution with an interval of 5 seconds between each cycle of reading was taken to ensure the repeatability of the response of the sensor patch. The sensor after each experiment was thoroughly washed with de-ionised water and dried in an oven for 10 minutes before using it for the next measurement. Five different chemicals, namely Citric acid (Sigma- Aldrich, 791725-500G), Sucrose (Sigma- Aldrich, S7903-250G), Sodium Chloride (Chem-Supply, SA046-500G), L-Tryptophan (Sigma- Aldrich, T0254-25G) and GMP (Sigma- Aldrich, G8377-5G) were tested to determine the response of the sensor to the tastes of sweet, sour,

salty, bitter and umami respectively. The solutions were prepared by mixing the chemicals with deionised MilliQ water[®] (Resistance: 18.2 M Ω cm and pH: 6.71) as a solvent. Experiments with four different concentrations (1000 ppm, 100 ppm, 10 ppm and 1 ppm) for each chemical were performed using a serial dilution mechanism. The first solution of 1000 ppm for a particular chemical was formed by mixing 0.1 gm of the solute with 100 mL of deionised water. After performing measurements with this solution, 10 mL from this solution was pipetted to 90 mL of de-ionised water to form a solution of 100 ppm. Similar steps were followed to develop solutions of 10 ppm and 1 ppm for experimental purposes.

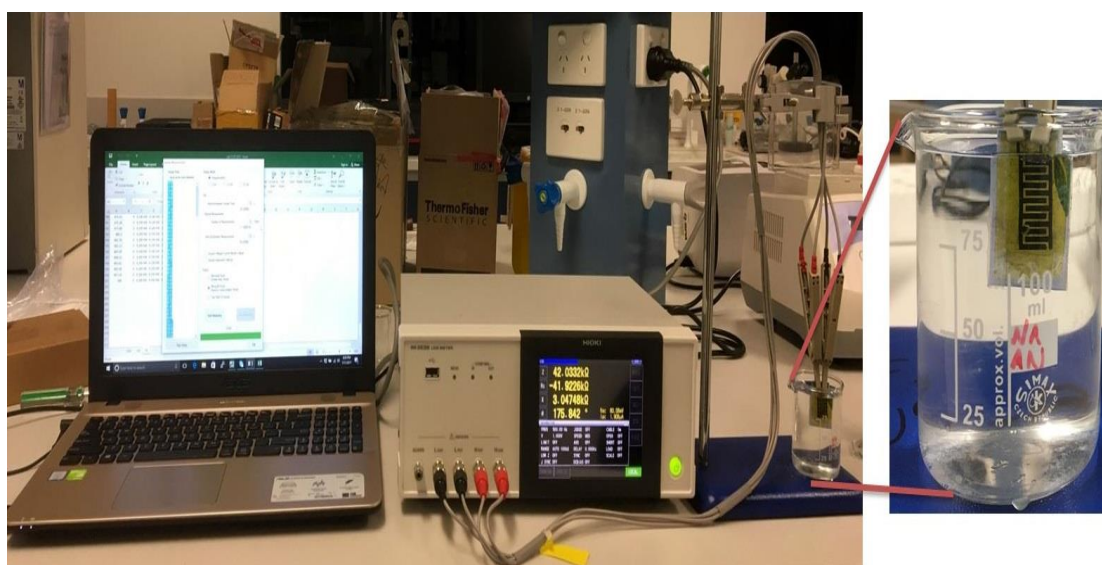


Figure 6.18 Experimental setup during the analysis of different chemicals.

6.5.2 Results and Discussion

Figures 6.19–6.28 show the responses of the sensor patches towards different chemicals expressed in terms of resistance and reactance with respect to frequency. In Figures 6.19 and 6.20, there is a significant change for citric acid in the resistance and reactance with respect to frequency. The presence of two distinct sensitive frequency ranges for the resistance values of citric acid can be attributed to the four single-bond hydroxyl ions (OH) in its structure [604]. The increase in the resistance values at higher frequencies can be attributed due to the presence of solution resistance (R_s) [605]. The behaviour of the reactance values for citric acid is attributed to the adsorption capacitance (C_{ad}) of the solution and the presence of the double-layer capacitance (C_{dl}) at the electrode-electrolyte

interface. This causes an initial increase in reactance values with frequency which gradually decreases after a certain point due to the shorting of the double-layer capacitance.

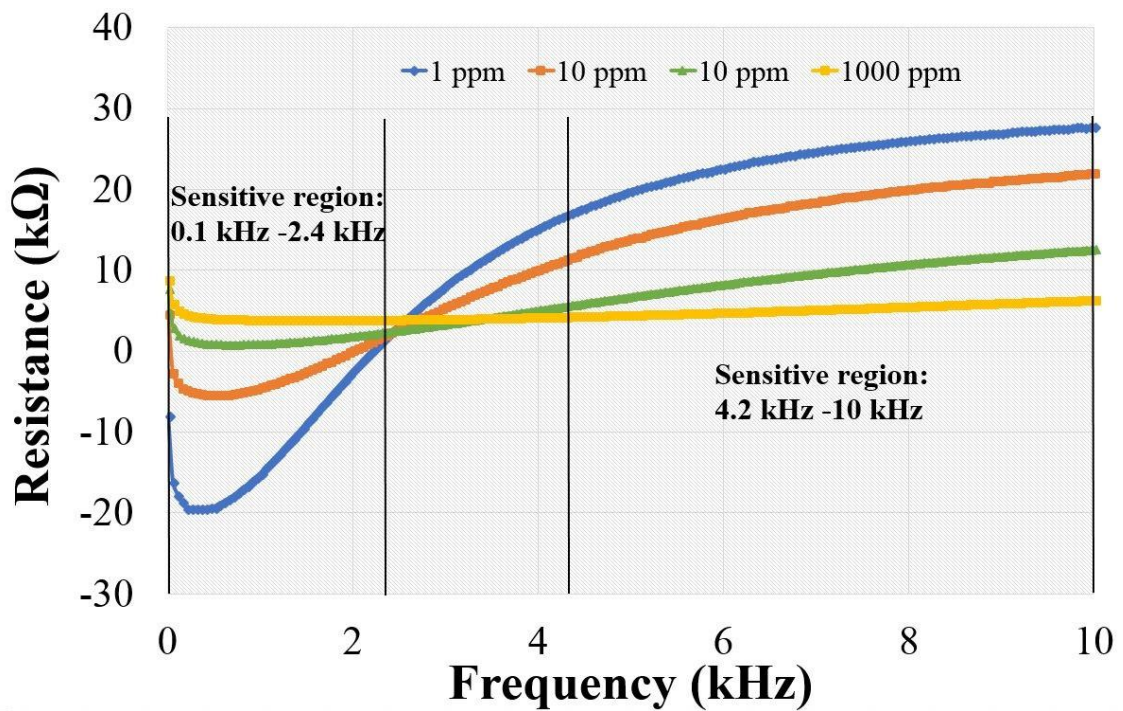


Figure 6.19 Response of the sensor for citric acid (sourness) in terms of resistance vs frequency.

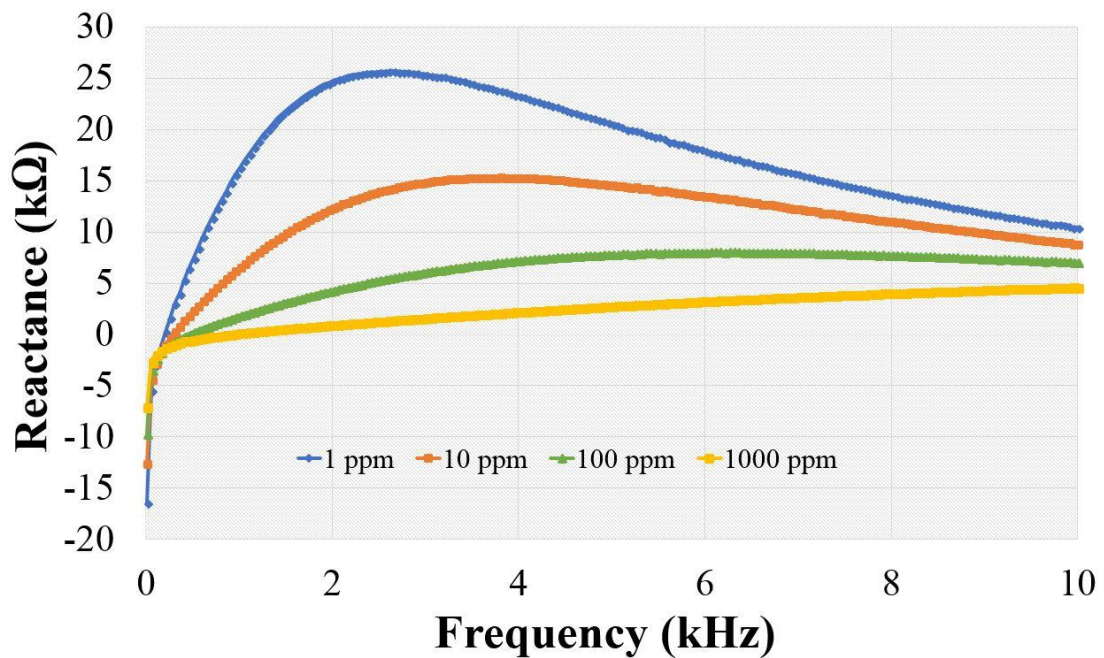


Figure 6.20 Response of the sensor for citric acid (sourness) in terms of reactance vs frequency.

The electrochemical behaviour of sucrose as seen from Figures 6.21 and 6.22 can be analysed by noting the presence of two isomeric forms of this material. The presence of the glycosidic linkage between carbon atoms of the glucosyl and fructosyl subunits is largely responsible for the change in the impedance behaviour of sucrose. The resistance values increase with an increase in frequency due to the increased ion-solvent interactions at higher frequencies [606]. The behaviour of the reactance values for sucrose can be attributed to the same mechanism as for citric acid. The double-layer capacitance (C_{dl}) plays a pivotal role in the change in the nature of the reactance values at lower and higher frequencies. The behaviour of the sodium chloride as seen in Figures 6.23 and 6.24 shows that the conductivity of sodium chloride is the highest of the tested chemicals. This is due to the ionic properties of its structure. The change in resistance and reactance values at lower concentrations can be attributed to polarisation of the ions. After a certain concentration, the behaviour of the resistive and reactive values is constant for all frequencies, as the sensor provides an output caused only by the solution resistance (R_s) and adsorption capacitance (C_{ad}) respectively. The electrochemical behaviour of L-tryptophan and GMP, as seen in Figures 6.25-6.28, are very similar in nature. This is due to the similarity between their structures. The change in resistance for both these chemicals can be solely ascribed to the solution resistance (R_s). The behaviour of the reactance for L-tryptophan can be ascribed to the presence of a carboxylic functional group and a secondary amino group in its structure.

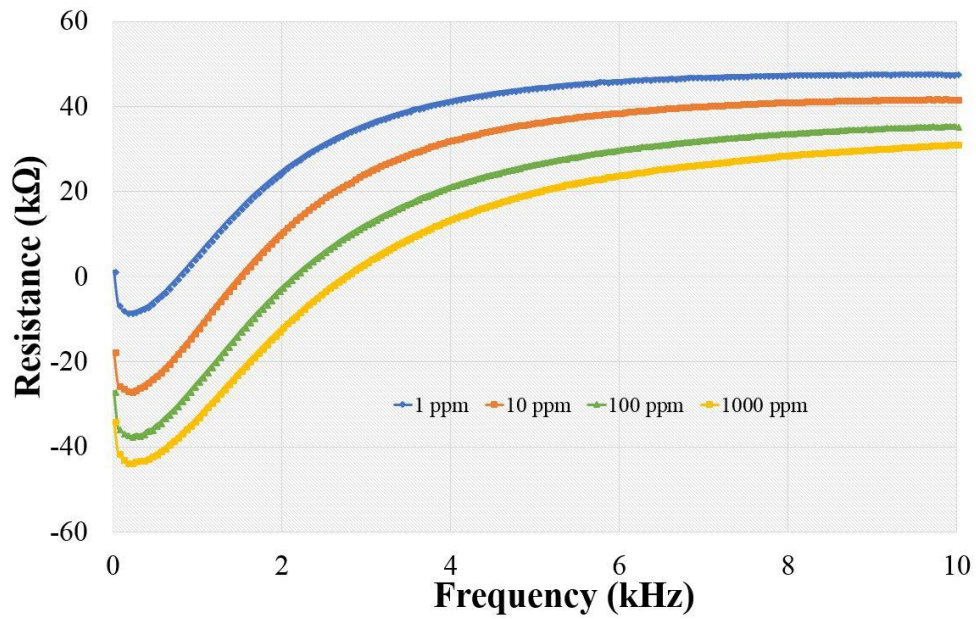


Figure 6.21 Response of the sensor for sucrose (sweetness) in terms of resistance vs frequency.

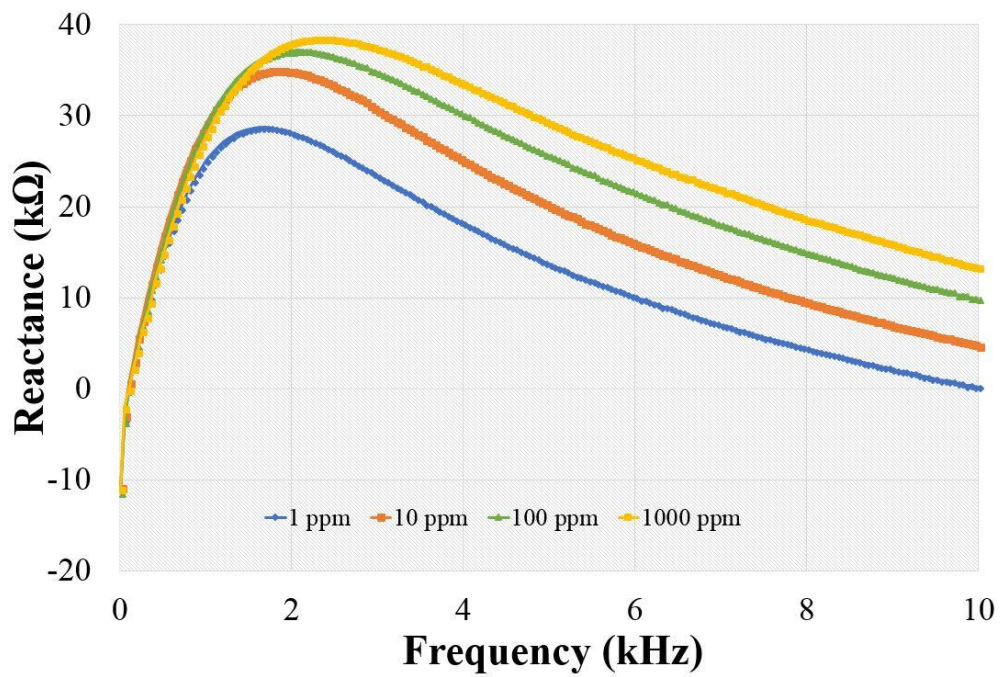


Figure 6.22 Response of the sensor for sucrose (sweetness) in terms of reactance vs frequency.

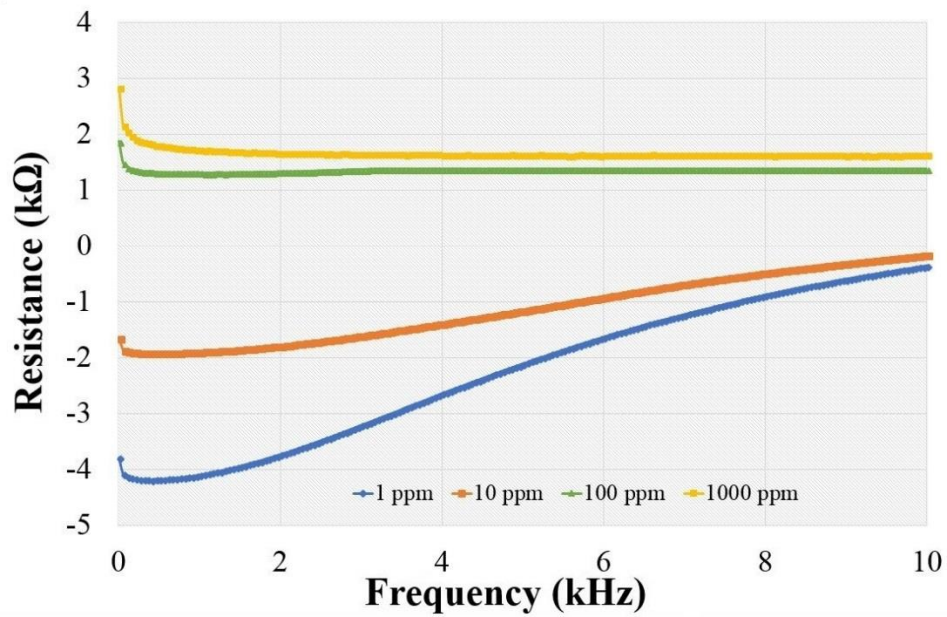


Figure 6.23 Response of the sensor for sodium chloride (saltiness) in terms of resistance vs frequency.

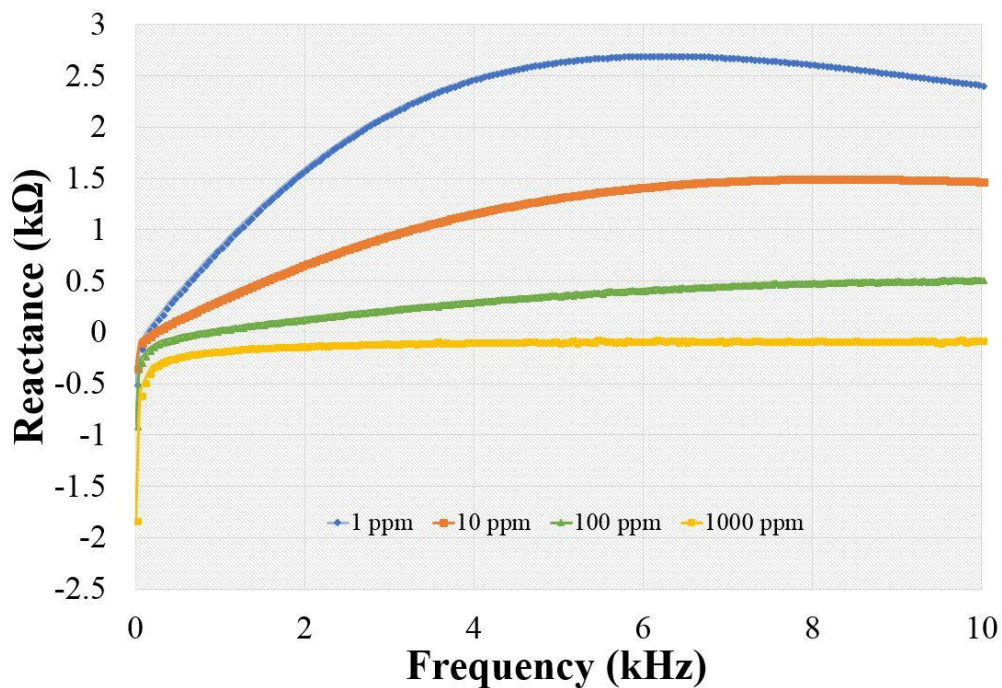


Figure 6.24 Response of the sensor for sodium chloride (saltiness) in terms of reactance vs frequency.

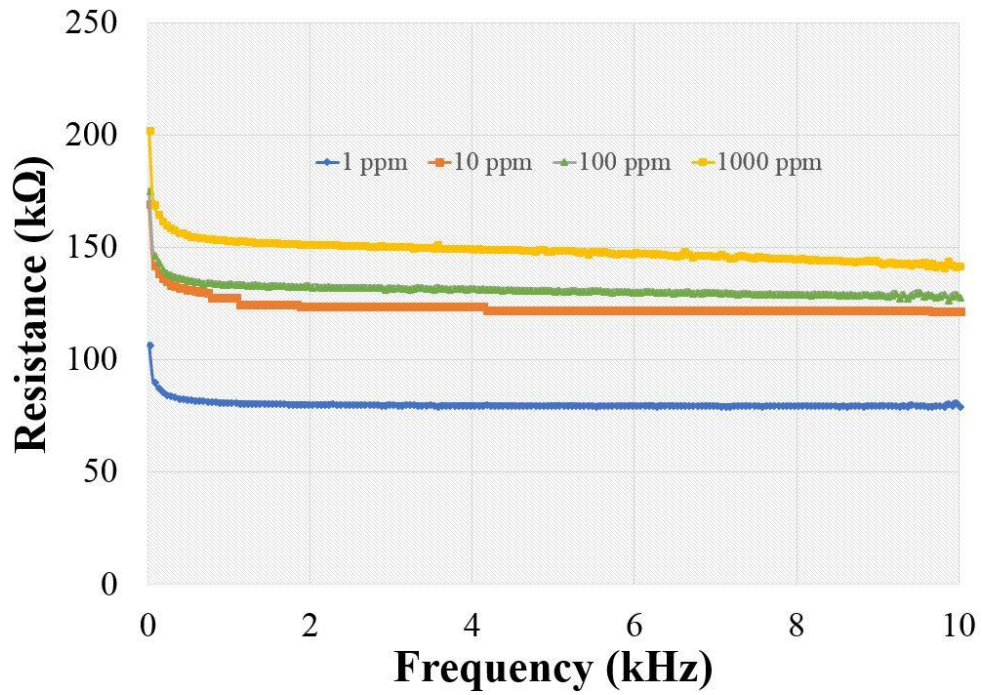


Figure 6.25 Response of the sensor for L-tryptophan (bitterness) in terms of resistance vs frequency.

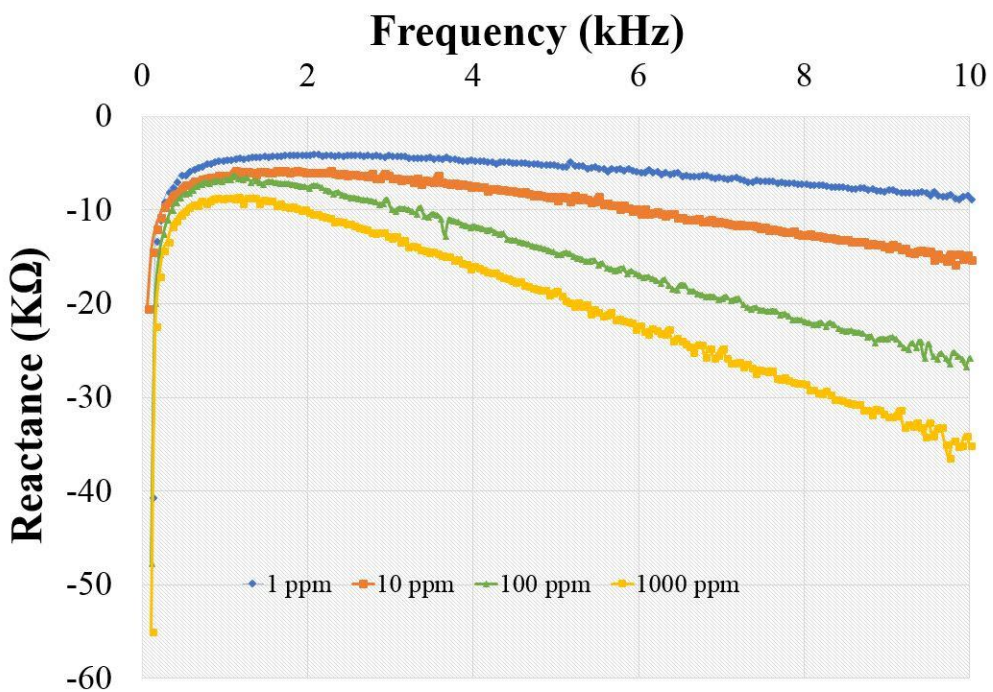


Figure 6.26 Response of the sensor for L-tryptophan (bitterness) in terms of reactance vs frequency.

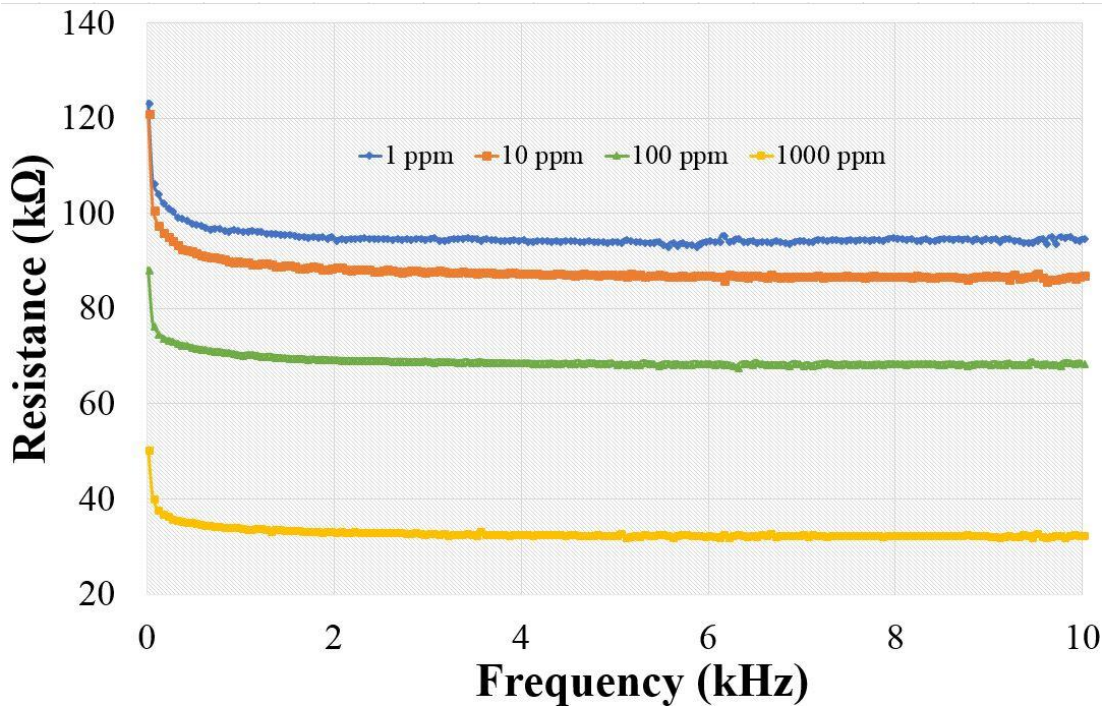


Figure 6.27 Response of the sensor for GMP (umami) in terms of resistance vs frequency.

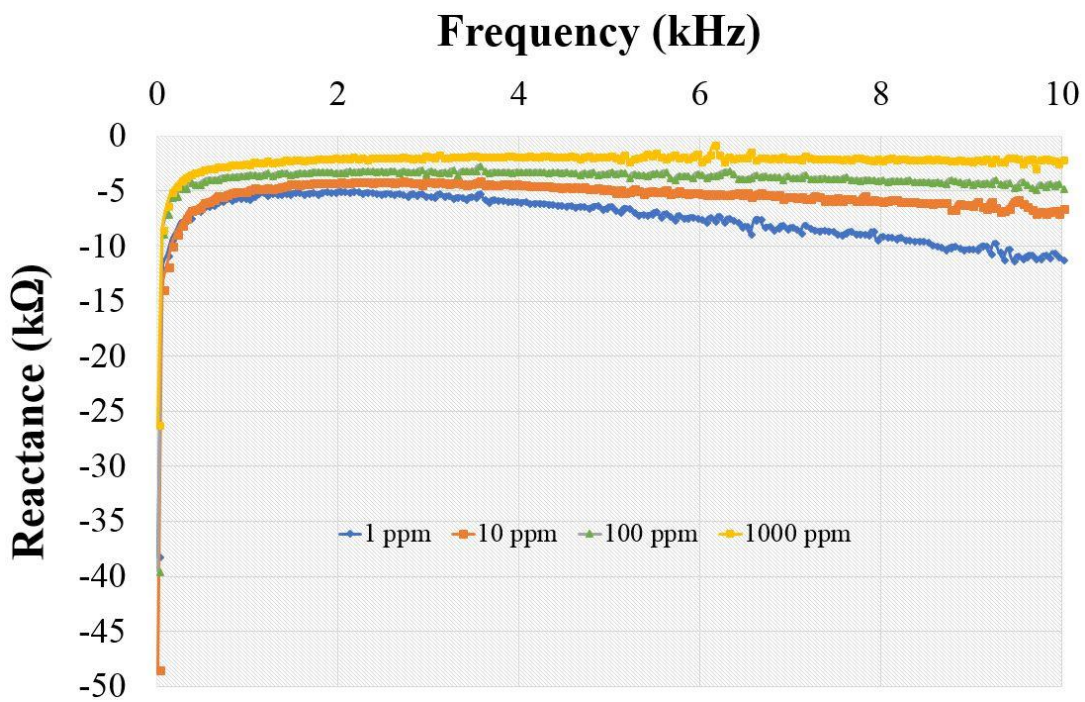


Figure 6.28 Response of the sensor for GMP (umami) in terms of reactance vs frequency.

The double bond in the oxygen of the carboxylic group causes an increase in the current at higher frequencies [607], eventually reducing the reactance values. The electrochemical behaviour of GMP can only be ascribed to the phosphate group present in its structure. At lower frequencies, the sp^3 hybridised bonds between the phosphorus and oxygen atoms do not allow GMP to respond to the applied electric field. At higher frequencies, polarisation of the oxygen atoms takes place which increases the electronegativity [608]. This leads to a slight change in the reactive values.

A comparative study of the reactive responses of the sensor to the five chemicals was done to determine the differences between their responses. The reactance was given preference over the resistive values as the response of the former indicated change in the relative permittivity (ϵ_r) between the electrode-electrolyte interfaces. Figures 6.29 – 6.32 depict the reactive values of the five chemicals for the four tested concentrations. It is seen from the figures that there are prominent differences between all the values of the chemicals for each concentration. Even though for two chemicals, L-tryptophan and GMP, the responses are close to each other, the nature of their change in the reactance values with an increase in concentration is different. The comparative responses of the reactive values can certify that the sensor patch can differentiate each chemical. One of the concentrations (100 ppm) was chosen to study the change in conductivity with respect to frequency for these chemicals. The change in electrical conductivity of the five solutions can be related to the relative permittivity of the samples. Even though the relative permittivity and electrical conductance are defined as the static and dynamic properties of the sample, an increase in conductivity will cause a gradual increase in the relative permittivity of the sample [609, 610].

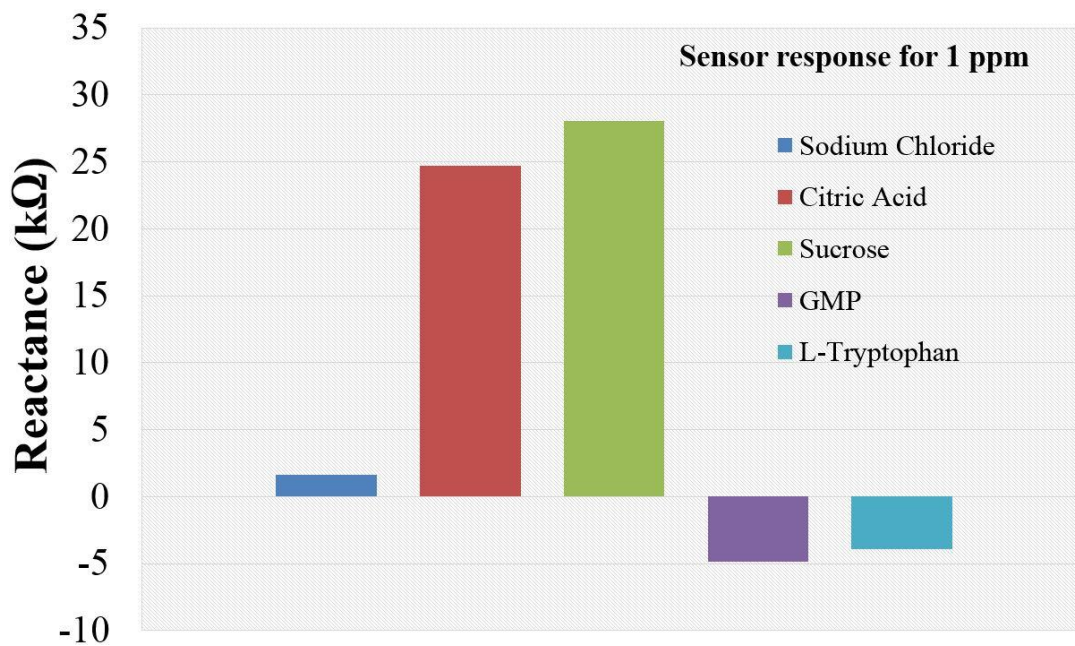


Figure 6.29 Comparison between the responses of the sensor patch to different chemicals for the concentrations of 1 ppm.

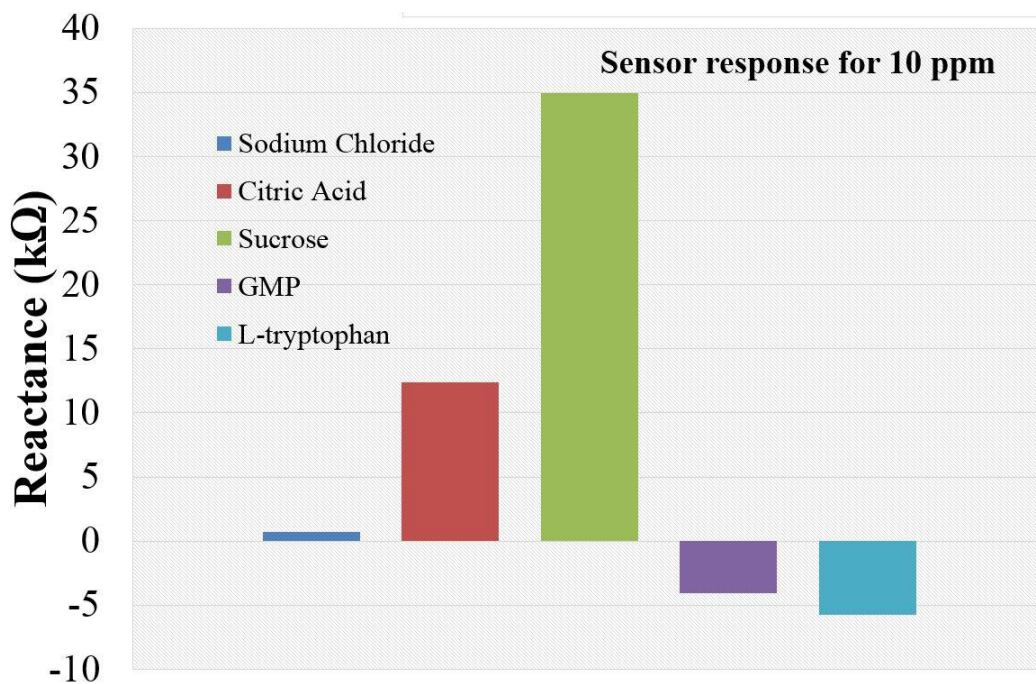


Figure 6.30 Comparison between the responses of the sensor patch to different chemicals for the concentrations of 10 ppm.

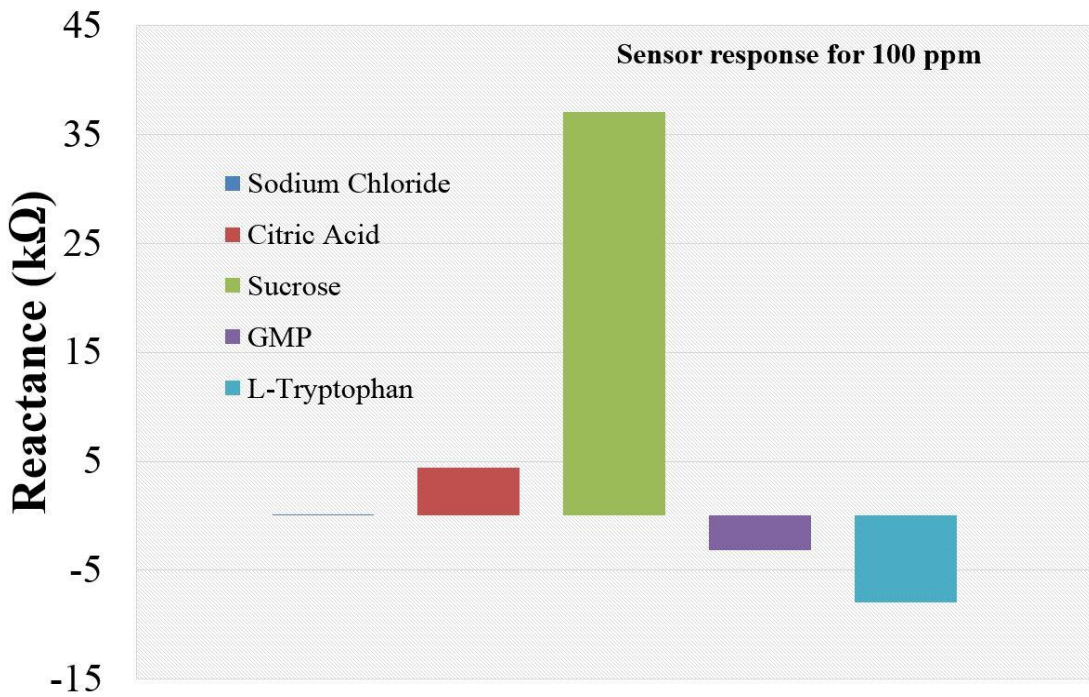


Figure 6.31 Comparison between the responses of the sensor patch to different chemicals for the concentrations of 100 ppm.

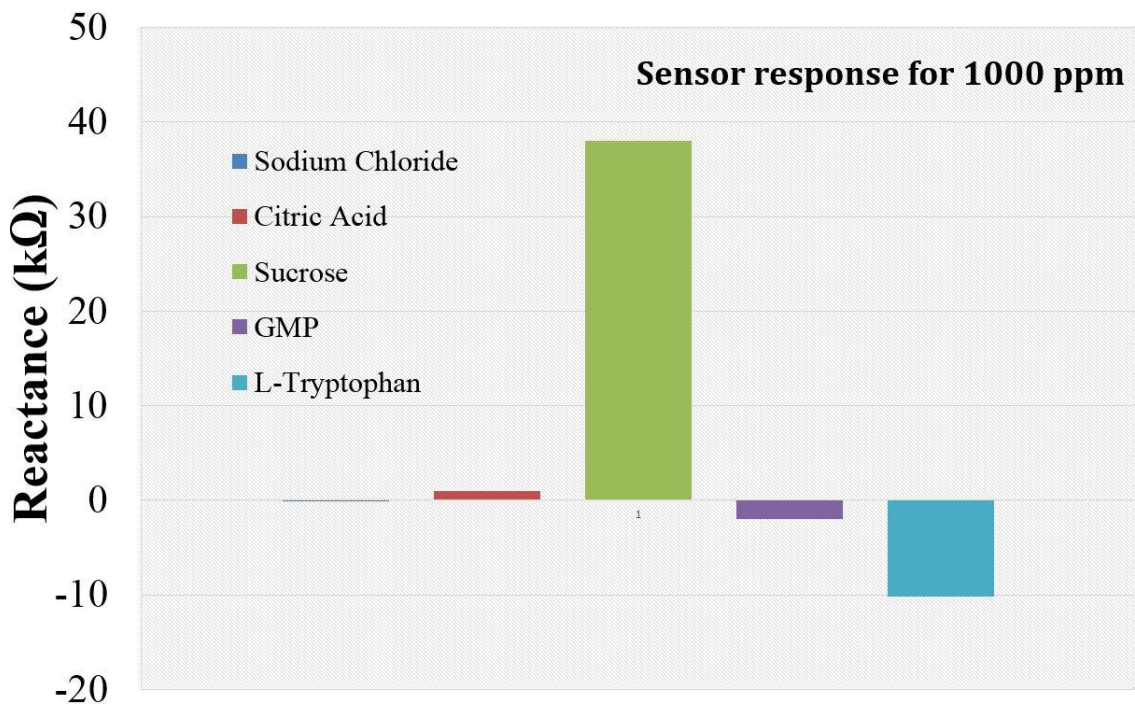


Figure 6.32 Comparison between the responses of the sensor patch to different chemicals for the concentrations of 1000 ppm.

Figure 6.33 shows the differences in conductivity expressed in $\mu\text{S}/\text{m}$ among the five tested chemicals. It is seen that sucrose has the least conductivity of the five chemicals, as

is evident from the comparative reactance values in Figure 6.22. Similarly, sodium chloride has the highest conductivity, which can be related to the least impedance as evident from Figure 6.24. L-tryptophan and GMP are the second and third least conductive chemicals because of the stability of their structures compared to sodium chloride and citric acid.

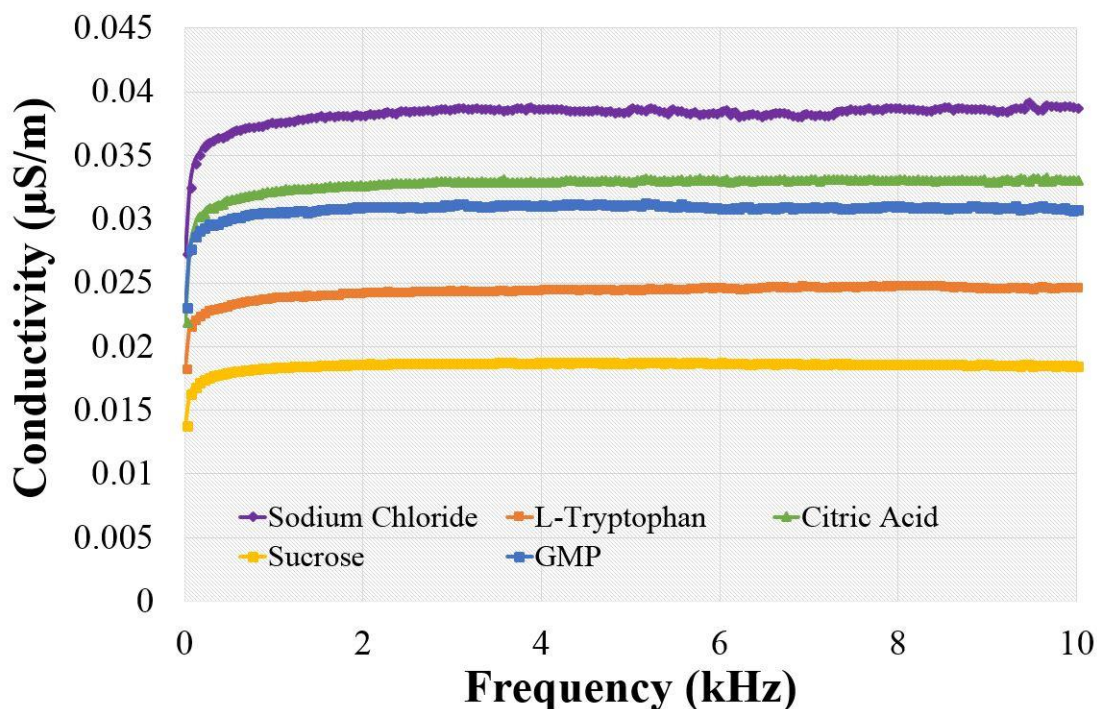


Figure 6.33 Comparison of the conductivity detected by the sensor for different chemicals at a concentration of 100 ppm.

6.5.3 Results and Discussion

This section presents the use of the graphene-polyimide sensors as a taste sensor. These patches were used to test different chemicals that comprise the constituents of differently tasting food products. It is seen that the sensor patches can individualise the chemicals by having different sensor responses to different chemicals. The sensor patches showed significant repeatability of their responses towards the tested chemicals. There was no hysteresis present in the response to any of the concentrations of the five chemicals. The response time of these sensor patches was around two seconds, indicating their capability to respond to dynamic conditions. The recovery time during the experimental process was around 10 mins, including the thorough washing of the used sensor patch with deionised water followed by drying it.

The experimental results look promising for utilising the sensor patches. The use of these sensor patches can be thought to be a replacement for the commercially used e-tongue. These patches can be used for any person suffering from a taste-disorder disability or can be installed in any food-producing industry to determine the concentration of a particular taste. The sensor patches can also be used by the pharmaceutical industries prior to the injection of drugs in a patient to determine their effects [611]. Other than consumable products, the patches can also be employed for testing chemicals like dyes [592], where the degree of concentration of any particular synthesised material holds the utmost importance. Another big advantage related to these sensor patches is that their output to the tested chemicals has no dependence on temperature or humidity, which makes them suitable to be used at any operating condition. The simple operation and low fabrication cost of the sensor, and the response of the sensor patches being independent from variations of temperature and humidity, are some of the attributes of these patches over the sensors used in previous research work done on taste sensing.

However, there are some issues that need to be addressed prior to its real-time application. The reactive values of the sensor at low frequencies for L-tryptophan and GMP for the four tested concentrations are very close to each other. This might create confusion for the monitoring unit regarding the exact value of a specific concentration, which makes it mandatory to operate these sensors at higher frequencies. Secondly, when using them in real-time applications, the cleaning of the sensing area of the patches during experimentation holds a pivotal role in an appropriate response to the tested solutions. One of the ways to achieve this could be the installation of an automated robotic arm fitted with the sensor patch and a water-hose nozzle. The arm could be programmed in such a way that the hose nozzle would wash the sensor patch after each experimental round followed by allowing it to dry for 10 minutes prior to the next round. Thirdly, the results shown here provide us with a platform for a novel sensing system that can be used as a taste sensor, by experimenting with different chemicals individually. The analysis of amalgamation of the chemicals should be done before using it as a real-time system. The sensor patches would be tested with a composite of chemicals to identify the presence of a particular chemical or a chemical with a specific concentration. One of the ways this could be achieved is by introducing selectivity on the sensing surface of the sensors. The electrodes could be coated with a layer containing cavities of the chosen template molecule. This would make it particularly selective into that chemical, thus indicating its concentration. These problems would be resolved with wireless operation of the sensors by including RFID tags with the

patches to upgrade their performance for taste-sensing purposes. RFID tags can be implanted on the sensor patches during their fabrication to indicate a chosen frequency of operation. Based on the application shown above for the graphene sensors, low-frequency passive RFID tags are suitable for installation in the chips. This would be advantageous for industrial applications, as a reader could be placed at the monitoring unit to avoid any kind of manual intervention during the testing and data-collection stages. The rectification of the above-mentioned issues with their possible solutions would certainly assist to develop a fully-functionalised taste sensing system.

6.6 Nitrate Sensing

Nitrogen is one of the important nutrients for the nitrogen cycle for the living beings of the Earth and comes from one of the nitrate nutrient sources. Excessive nitrate leaching losses from soil into water cause a threat to aquatic environments and human health [612-614]. It can be found widely in the environment due to their solubility in water. It is well known that surface water is contaminated in New Zealand by nitrate ions due to excessive agricultural land use and cattle farming which can pose a serious threat to surface water quality [615, 616]. An excessive amount of nitrate-N in rivers helps to grow periphyton and macrophytes to nuisance levels [617]. They reduce the oxygen level in the water, which can hamper the aquatic life of fish. Contaminated nitrate-N water may cause serious illnesses such as birth defects, spontaneous abortions intrauterine growth restriction and potential cancer risk [618-621]. Further, long-term accumulation of nitrate-N is a potential risk to animal and human health. The blue-baby syndrome can be caused by drinking water with elevated nitrate concentrations [622].

There has been a significant amount of work to determine the amount of nitration in water. The spectrophotometric method is used to determine nitrate-N in water using chemical reagents [623]. The Griess reaction is used for the reduction of nitrate ions [624]. Ion chromatography [625], optical fibre sensors [626, 627], planar electrode sensors [628], ion-selective electrodes [629], palladium nanostructures [630] are used to measure nitrate ions in water. Even though the above-mentioned techniques have been successfully operated, most of them are laboratory based and generate a lot of chemical waste which is harmful to the environment.

Some of the regional councils or local governments of countries like New Zealand monitor water samples from different sampling locations, such as rivers, lakes, and

groundwater. The water manager collects those samples at regular intervals, usually once or twice in a month. The laboratory-based methods such as spectrophotometry or ion chromatography were used to measure nitrate-N concentrations. However, it is difficult to measure accurately the effect of leaching nitrate-N into rivers or lakes due to the fluctuating dynamic water system all through New Zealand. Therefore, the monthly sampling measurements would be unable to provide the actual nitrate-N profile. Missing information could influence the understanding of the seasonal effects, and in the process, the total nitrate-N estimation would be wrong. This missing information hampers policy makers wanting to take proper decisions. The work described below uses an Internet of Things (IoT) enabled smart sensing system to measure the nitrate-N concentration in real time. The purpose of using the IoT is to create an environment in which the basic information of the developed network is shared in real time. The proposed system can also measure the nitrate-N concentration in real time and transfer the data to the cloud server to allow the system to be used as part of a distributed network. A compensation for temperature is also included in the system, which will increase the efficiency of measurement. The fabrication process, nitrate-N and temperature measurement and validation of the smart sensing systems are explained in the subsequent sections.

6.6.1 Experimental Setup

Electrochemical Impedance Spectroscopy (EIS) is a highly sensitive method for an unsteady and variable system in equilibrium, and its instant impedance measurement is required for non-stationary systems. Different methods are available for impedance measurement, but the Frequency Response Analyser (FRA) is considered the de facto standard for EIS measurement. FRA requires a single input sinusoidal signal with amplitude of 5-15 mV. The frequency of the signal sweeps in a certain range on a direct current bias voltage. The signal is applied to on the working electrode and a resulting voltage is taken from the sensing electrode. The measurement process is done in a certain frequency range to get a complete impedance profile. The following can be used to specify the impedance of a system:

$$Z = R + jX \quad (7.2)$$

where Z is the impedance (Ω); R is the resistance (Ω), which is also the real part of the impedance; X is the reactance (Ω), which is the imaginary part of the impedance.

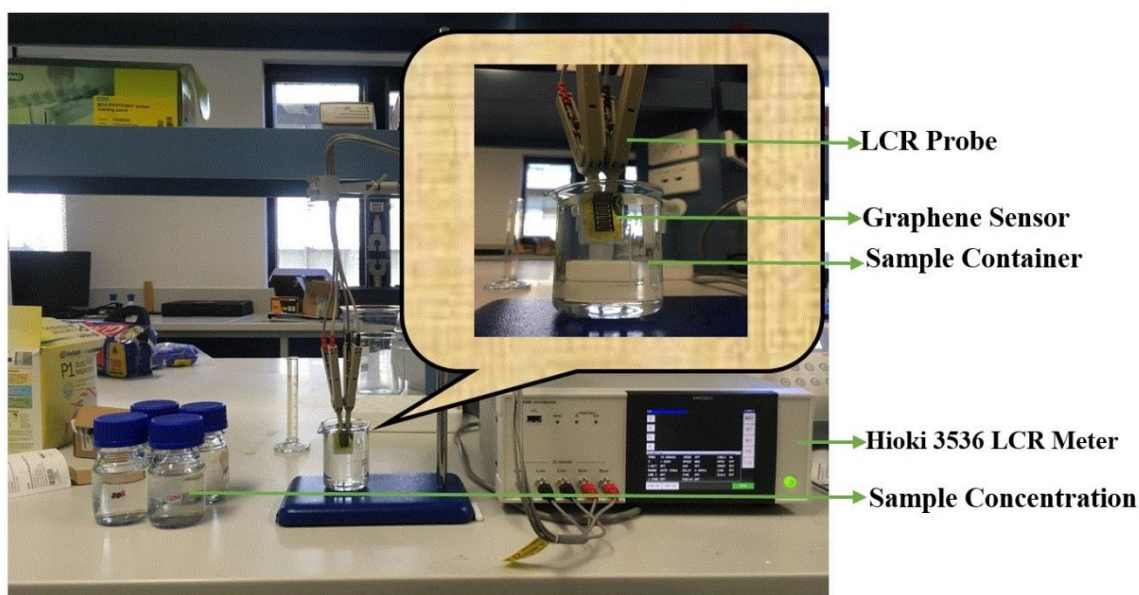


Figure 6.34 Experimental setup for nitrate measurement.

The impedance profile data can be represented graphically as a Bode plot and a Nyquist plot, also called a Cole-Cole plot. The plot also reflects the electrochemical procedures taking place at the electrode-electrolyte edge. A clamp connects the sensor with the HIOKI IM 3536 LCR meter. 10 Hz to 100 kHz frequency sweeping was used to profile the sensor for EIS measurement. A standard temperature and humidity were maintained during measurement. Deionised water was used as a control solution. A standard nitrate-N solution was used to prepare the working solution for different concentrations. The average pH of the samples was 6.60. Initially, the sensors were characterised in air to extract the experimental reference curve. Then the deionised water and sample water were used to continue the experiments. Figure 6.34 shows the data-acquisition laboratory setup used for EIS measurements.

6.6.2 Comparative Analysis of two Different Sensors

10-ppm Nitrate-N sample water was taken, and the real part of the impedance was measured for different sensors. The real part of the impedance of the deionised water was also measured. The temperature and humidity of the waters were identical due to the same

laboratory environment. The pH of the water was also the same during the measurement. The sensor's response was calculated by using equation 7.3.

$$\text{Sensor's response (\%)} = \frac{R(\text{milliq}) - R(\text{sample})}{R(\text{milliq})} \times 100 \quad (7.3)$$

where, R indicates the real part of the impedance of the sensors.

6.6.3 Temperature and Nitrate-N Measurement

The graphene sensor was first used to measure temperature changes in water. Temperature changes the mobility of ions in water; therefore, it is important to measure the changing behaviour of the graphene sensor at different temperatures. An experimental setup similar to Figure 6.34 was used to measure the temperature. The GEX MS 7-H550 Digital Hotplate, mercury thermometer, LCR meter and the computer was used for data acquisition. The thermometer was immersed inside the deionised water to measure the temperature instantly. The sensing surface of the graphene sensor was immersed inside the water and the frequency was swapped from 10 Hz to 100 kHz to characterise the sensor under different temperatures. 1, 10, 30, 50 and 70-ppm standard nitrate-N solutions were taken for another experiment 100 ml in five beakers. 100 ml of deionised water was also taken as a control solution. The sensor was immersed in the sample waters until the completion of the measurements. The real and imaginary impedance were taken by the LCR meter. The measurement was taken five times and an average was presented in the final graph.

6.6.4 IoT-enabled Smart Sensing System

Internet of Things (IoT) enabled smart sensing system is proposed to collect the sensor data for nitrate-N measurement. An AD5933 [631] was used as an impedance analyser to measure the real part of the impedance of the graphene sensor. Arduino Uno Wi-Fi [632] is used as a master microcontroller to collect the impedance data from the impedance analyser. It has an integrated Wi-Fi module, which would help to send data wirelessly to a cloud server. Thingspeak [633] is the IoT-based free web server to store the measured data and show it in real-time. The Arduino Ciao [634] library was used to transfer the data to the designated private channel in Thingspeak. Ciao is a library which is capable of

interfacing with system resources and communicating with the most common protocols such as (MQTT, XMPP, HTTP, SMTP, etc.). HTTP POST was used to send the measured concentration to the *ThingSpeak* cloud server. Security is an important issue in IoT research due to the large scale of the objects and the heterogeneity. It will be discussed in a future research article when the actual distributed network will be installed to monitor in real time. The AD5933 is the impedance analyser where it measures the impedance and the phase shift of the sensor. Before starting the measurement, the AD5933 had to be calibrated to get the gain of the impedance analyser. An ADG849 is used as a switch from a calibration resistor to the sensor, and the impedance is calculated by using that calibrated gain. The phase shift is also calculated from the impedance analyser. Frequency sweeping is not required as the final measurement depends on the single frequency. The I²C protocol is used to communicate to the impedance analyser to extract the real part of the impedance from the impedance analyser and store that in the main microcontroller. A data processing algorithm is used to convert that real part of the impedance into meaningful temperature and nitrate-N concentration values.

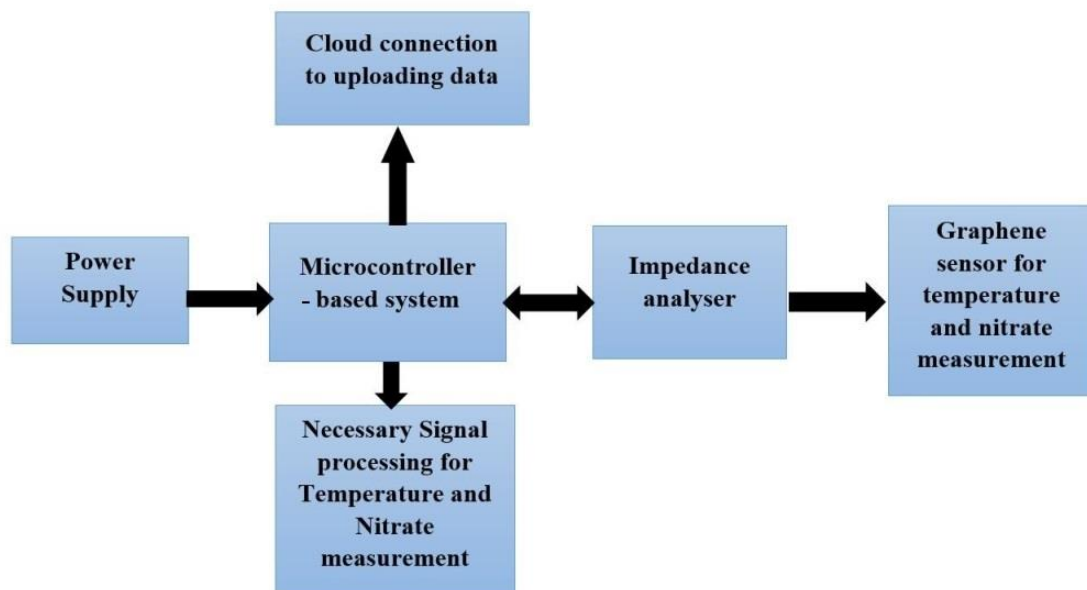


Figure 6.35 Block diagram of the smart sensing system.

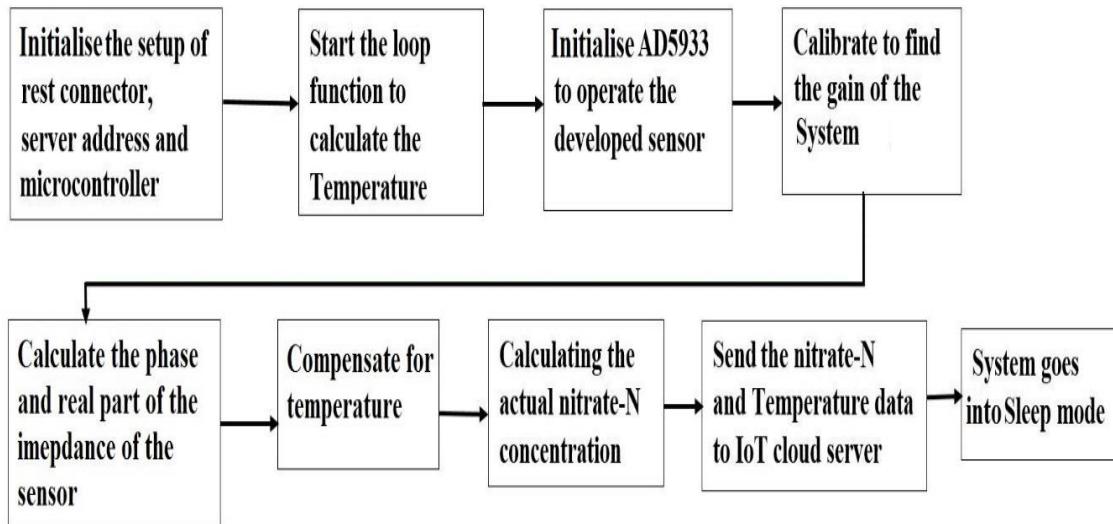


Figure 6.36 Software flow of the individual steps of the operating of the IoT-based system to calculate and transmission of the nitrate concentration to the cloud server.

Finally, the temperature and nitrate-N data are send to the IoT-based cloud server to store for further processing. Some of the sample water, which was collected from different locations, is measured by the developed sensing system. Figures 6.35 and 6.36 show the block diagram and software flow of the developed sensing system. Arduino Sketch was used to by write the programming code. Initially the system starts, and the microcontroller is initialised the setup function to establish the rest connector, provided with the cloud-server API (Application Programming Interface) number which will be necessary to send the measured data to the designated IoT server. The impedance analyser is used to measure the phase and real part of the impedance of the sensor. The developed calibration standard for temperature measurement was used to measure the temperature of the deionised water. After that, the nitrate-N concentration was calculated, with the temperature compensation. The system communicates with the IoT cloud server to send the measured data. Finally, the microcontroller goes into sleep mode to save power.

Figures 6.37 and 6.38 show a schematic diagram of the conditioning circuit and the first prototype of the sensing system respectively. Circuit maker [635] was used to draw the circuit diagram of the sensing system.

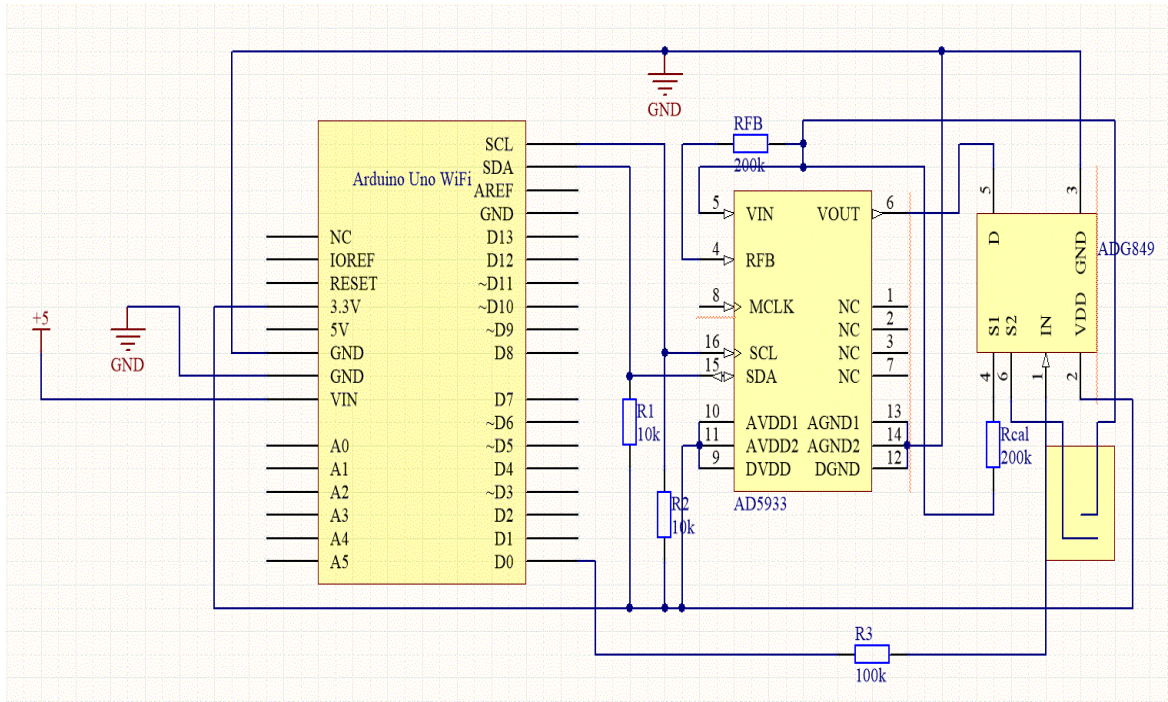


Figure 6.37 Schematic diagram of the smart sensing system.

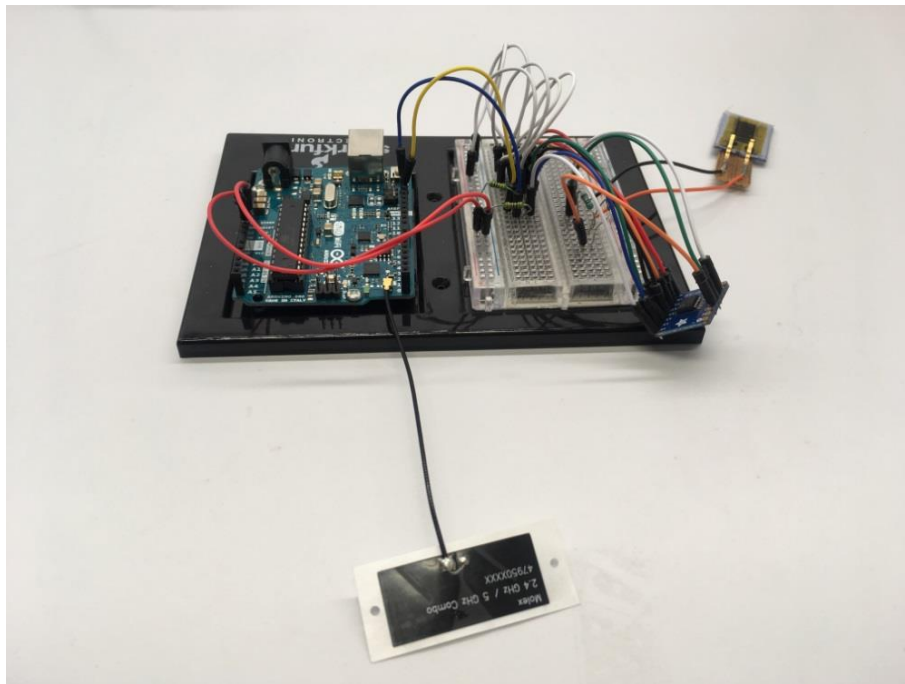


Figure 6.38 First prototype of the smart sensing system.

6.6.5 Results and Discussion

Nitrate Measurement

Figure 6.35 presents the real impedance for different concentrations with a frequency range from 1 Hz to 100 kHz. It is seen that the real part of the impedance is changing due to the different concentrations of nitrate-N in the sample water. Due to the presence of nitrate-N ions in the water, the impedance profile is changed for different concentrations due to the properties of the interdigital graphene sensor. It is observed that 1200-1700 Hz is the sensitive region for different concentrations. Of the real and imaginary parts of the impedance of the graphene sensor, the real part of the impedance shows the most change between the sample nitrate-N concentrations.

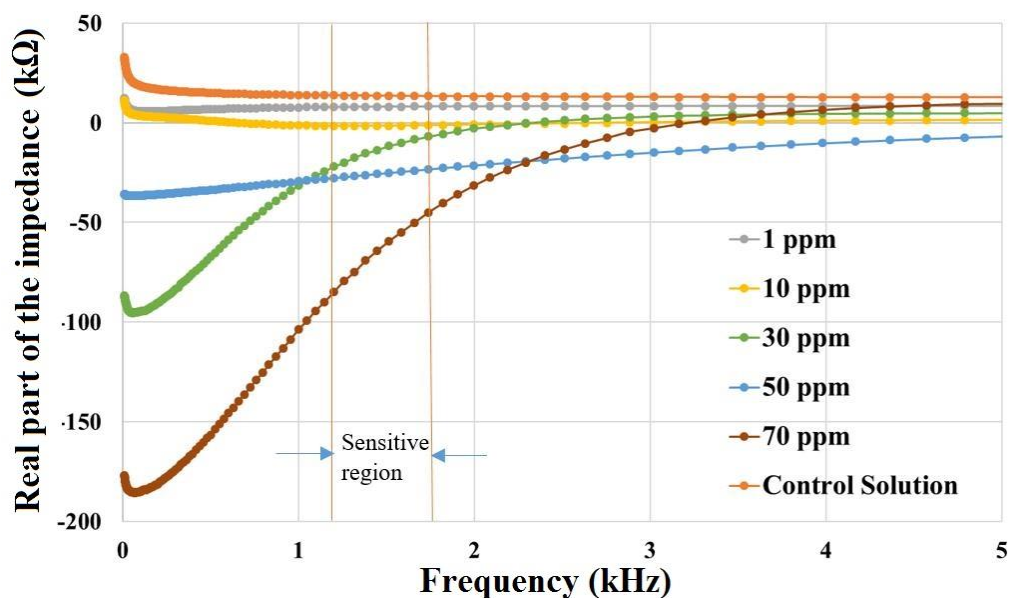


Figure 6.39 The change of real part of the impedance with respect to frequency.

Temperature Measurement

The dielectric properties of the deionised water were measured by this described method. The EIS measurement technique was used to measure the real and imaginary parts of the impedance of the sensor. The real part gives a more significant change compared to imaginary impedance. The temperature was varied from 7 °C to 50 °C and the corresponding real part of the impedance was plotted on Figure 6.36.

From the linear regression analysis, it is seen that the temperature is well correlated with the real impedance ($R^2=0.99$). Therefore, the temperature can be calculated from equation 6.4:

$$T (^{\circ}\text{C}) = \frac{(R_T + 29153)}{404.87} \quad (6.4)$$

where, R_T is the measured real part of the impedance for a certain temperature and T is the calculated temperature.

The slope of the straight line indicates the change of real part of the impedance per unit change of temperature, which is $\alpha=404.87 \text{ } \Omega/^{\circ}\text{C}$. It is to be noted that, the operating frequency of the graphene sensor of the temperature measurement was 1650 Hz. Figure 6.37 shows the temperature measured by the sensor and compares it with the actual temperature. It is seen that they are well correlated with each other and $R^2=0.99$ which indicates that the sensor can quite accurately measure the temperature of sample water.

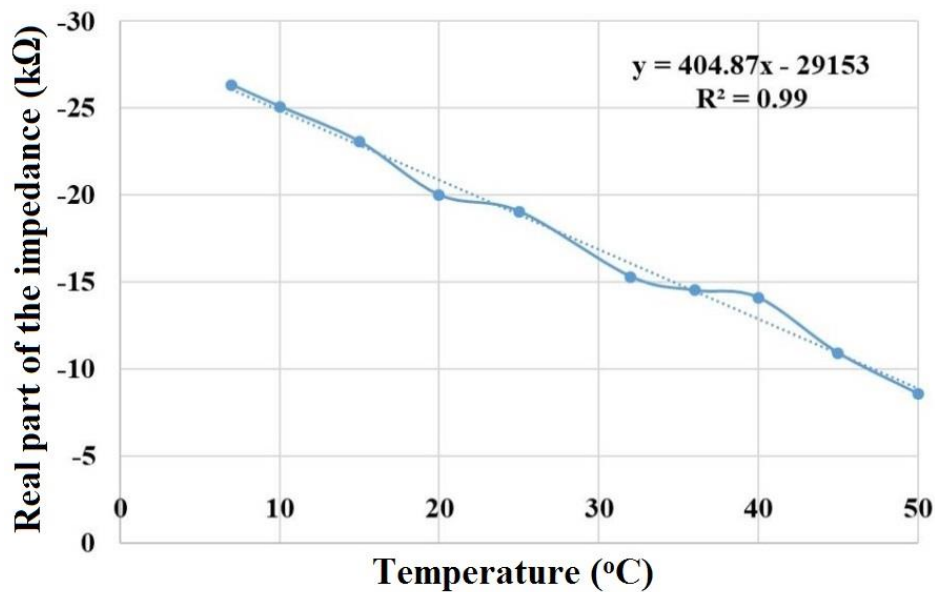


Figure 6.40 Real part of the impedance as a function of temperature.

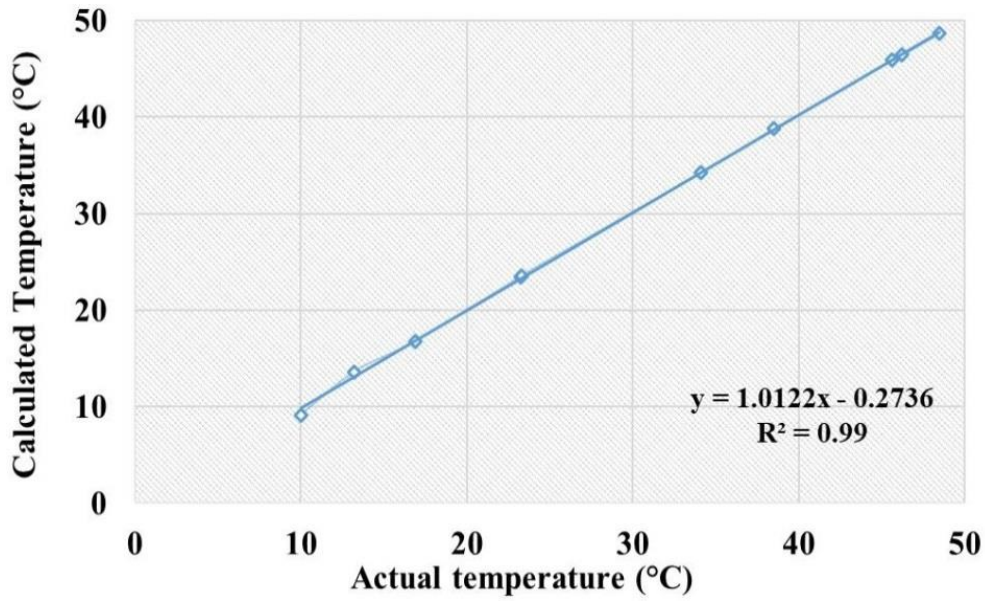


Figure 6.41 Comparison of actual and measured temperatures.

1650 Hz was taken as the operating frequency to develop the calibration standard from a standard nitrate-N sample measurement. All the measured concentrations were considered as the x-axis and the corresponding real part of the impedance was considered as the y-axis. Figure 6.38 shows the final calibration standard for nitrate-N measurement. Linear regression analysis can be calculated by from equation 6.5:

$$C = \frac{R_{cal} - 9196.9}{-667.97} \quad (6.5)$$

where, C (ppm) is the actual concentration and R_{cal} (Ω) is real impedance measured by the graphene sensor.

Equation 6.6 was used to calculate any unknown nitrate-N concentration in water. Since the sensor was sensitive to temperature and the ions mobility changes with temperature, the measured real part of the impedance was adjusted by a correction factor α . The R_{actual} is the modified real part of the impedance due to temperature and was calculated by.

$$R_{actual} = R_{cal} + \alpha \times (T - 25) \quad (6.6)$$

Therefore, the standard formula to calculate the actual concentration after applying a correction factor for the graphene sensor is represented from equation 6.7.

$$C_{actual} = \frac{R_{actual} - 9196.9}{-667.97} \quad (6.7)$$

where C_{actual} is the final corrected concentration due to the temperature change.

The final equation was used to measure any unknown nitrate-N concentration, including temperature compensation. It is also seen that the sensitivity of the sensor is 667.97 Ω /ppm, which will help to measure nitrate-N concentrations accurately.

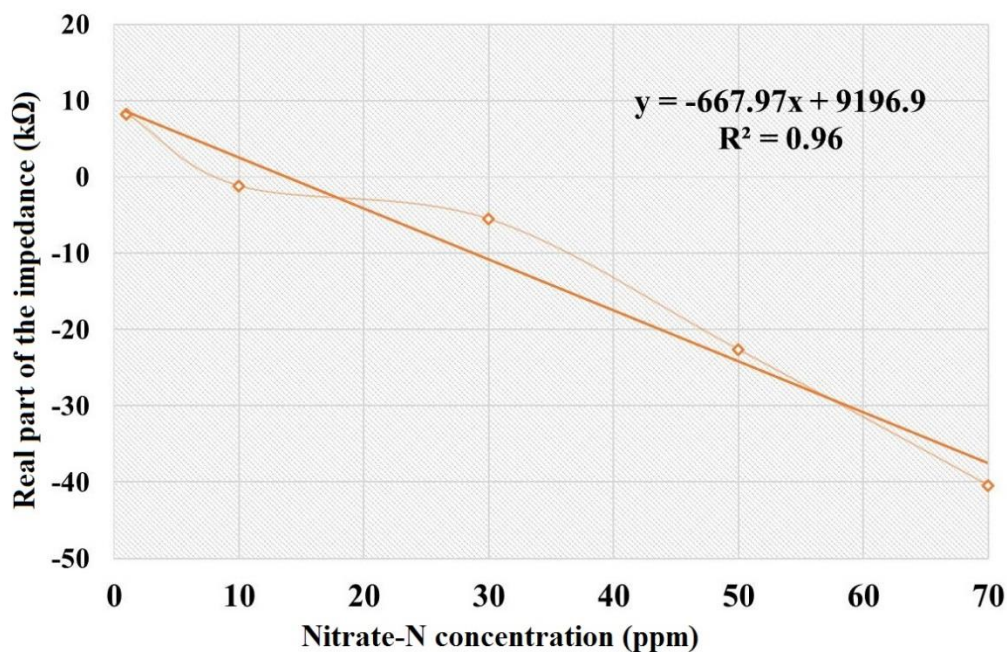


Figure 6.42 Calibration Standard of Nitrate-N concentration (ppm).

To measure the unknown sample, different samples of water were collected from different sampling locations, such as river, lake, stream, tap water. Naturally, the concentration of nitrate-N level was not high. So, some nitrate-N samples were added with those water samples to elevate the level of nitrate-N concentration. The fabricated graphene sensor was used to measure the temperature, followed by a final measurement of nitrate-N. Among all the other samples, River water was taken as an example to show the calculation process and measure the nitrate-N concentration. The real part of the impedance was measured for deionised water and gave that $R_T = -19750 \Omega$. Therefore, from equation 7.4,

the calculated temperature is $T (^{\circ}C) = 23.2$ °C. The sensor was used to measure the sample concentration and the real part of the impedance was found, $R_{cal} = -4568 \Omega$. Using equation 7.6, R_{actual} becomes -5288.67Ω . Therefore, the final concentration is 21.69 ppm, which comes from that sample water measurement. This result was verified by the laboratory standard method of UV-spectrometry. Other sample waters are measured and compared with the laboratory standard method in Table 7.3. It is seen that the graphene sensor shows very good performance compared to the laboratory method. The error rate was less than 5%, which is an acceptable performance of the sensing system and the developed sensor. The error was considered as a measurement error due to the presence of other ions in water. However, the accuracy of the sensor and sensing system was more than 95% and consistent.

Table 6.3 Unknown Sample measurement (in ppm) compared with Laboratory standard method.

Sl. No.	Sampling Number	1st Run	2nd Run	3rd Run	4th Run	5th Run	Laboratory Method
1.	River Water	21.69	21.56	21.54	21.63	21.35	21.5
2.	Tap Water	5.25	5.1	5.35	5.15	5.75	5.5
3.	Canal Water	56.75	56.7	56.6	56.65	56.55	56.5
4.	Stream Water	65	65.2	65.1	65.3	65.15	65
5.	River Water	32.35	32.65	32.55	32.45	32.62	32.5

The developed sensor is robust and maintains good repeatability. Figure 6.39 shows the reusability performance of the sensor and the sensing system. The sensor can provide an almost identical result in each run of the measurement. Graphene is corrosion free [636] and protects the sensing electrodes from oxidation during the sample measurement, which helps when using the sensor in a repetitive manner. Mechanically it is also robust [637] and shows good performance during measurements.

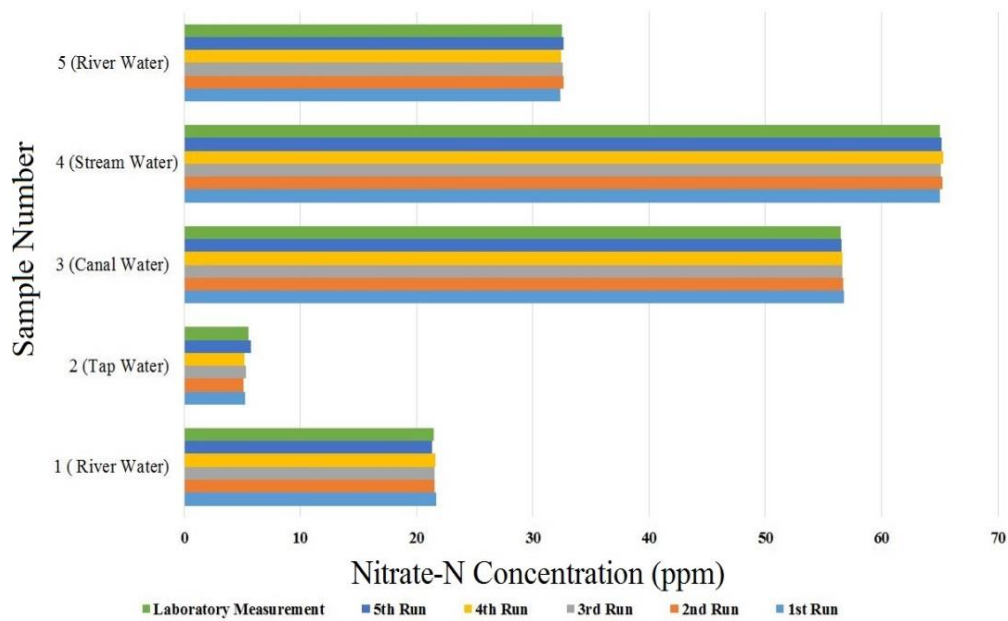


Figure 6.43 Repeated unknown sample measurements by smart sensing system.

Figure 6.40 shows the transfer of the data to the IoT-based cloud server. The concentration of nitrate-N was 25.5 ppm and the temperature were around 22 °C. The system was used for nearly three hours to monitor the actual data in real time. It was observed that the developed system was consistent in terms of monitoring continuous data at fixed intervals. They have transferred the data simultaneously, which would help to monitor the measured data in real time. There is a certain delay (30 seconds) from *ThingSpeak* cloud server. The sensing system will also be useful to develop a distributed monitoring system to monitor the temperature and nitrate-N concentration in real time.

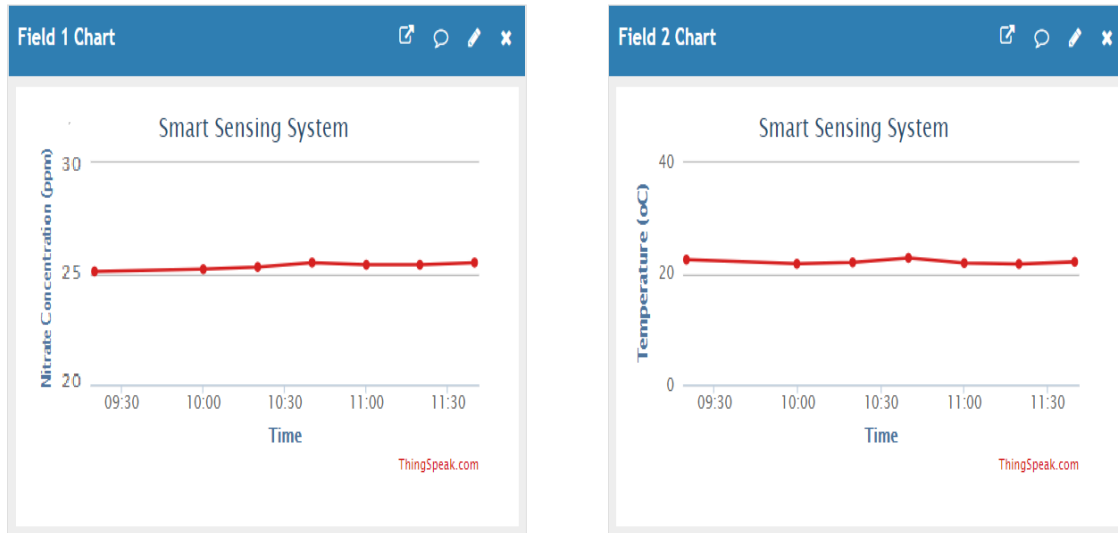


Figure 6.44 Data transferred to the IoT based web server.

6.6.6 Conclusion

This section explains the IoT-enabled sensing system for the detection of nitrate-N concentrations in water. Temperature compensation was included to improve the performance of the sensing system. The sensor performance was measured in terms of its ability to monitor different concentrations of the nitrate-N in the water samples. Due to the low fabrication cost of the sensor, it was easier to develop a low-cost sensing system to monitor the water in real time. The sensor was also robust, which helps to repeat the measurements with good repeatability. The developed sensor and the smart sensing system can be used to monitor the real-time nitrate-N concentrations and develop a low-cost distributed network with effective performance.

6.7 Chapter Summary

This chapter describes the design, fabrication and implementation of laser-induced graphene sensors from commercial polyimide films. The conductive material was transferred to Kapton tape for using them as electrodes on a sensor patch. Some of the major advantages of these sensor patches were their low cost, simple operating principle, high conductivity and the corrosion-resistant nature of the electrodes. The advantages of these sensor patches lie in their excellent mechanical and electrical properties. The sensor patches were used for environmental monitoring purposes where laboratory-made solutions

were tested to determine the capability of the sensor patches to distinguish nitrate and saline solutions of different concentrations. They were also employed for industrial uses by experimenting with different solutions developed from five fundamental chemicals which are categorised for taste-sensing purposes. The capability of these patches to distinguish the five chemicals was based on the differences in their outputs. Apart from utilising these patches for industrial and environmental purposes, they can also be exploited for health monitoring via embedding them with a signal conditioning circuit in wearable sensors. The corrosion resistant nature of the electrodes also makes the use of these sensor patches possible for ubiquitous monitoring of sweat, urine [638], etc. The addition of selectivity to the electrodes of these sensor patches would further increase their potential applications in different sectors of society.

7

Graphite-Polydimethylsiloxane Sensor

Publication pertaining to this chapter:

- **Anindya Nag**, N. Afsarimanesh, S. Feng and S. C. Mukhopadhyay, “Strain Induced Graphite/PDMS sensors for Biomedical Applications”, *Sensors and Actuators A*, Vol. 271, pp. 257–269, **March 2018**.

7.1 Introduction

This chapter presents the design, fabrication and implementation of novel graphite/PDMS sensors for different strain-sensing applications. The fabrication involves 3-D printed moulds which were developed using acrylonitrile thermoplastic polymer as the filament. One of the better ways to fabricate sensors with flexible substrates has been the use of 3-D printing where the initial mould can be printed with specified dimensions at very low cost, followed by their use to develop the patches. Another big advantage of using 3-D printing for fabrication purposes is the use of thermoplastic polymers to develop the templates. The high tensile strength, easy bendability, recyclability and high performance in terms of fatigue properties compared to metals [639] makes the thermoplastic polymers [122] cheaper and a favourable choice for 3-D printing purposes. Graphite and PDMS were used to develop the electrodes and substrate of the sensor patches respectively. The advantages of using PDMS over the other mentioned polymers are its low cost, high tensile strength, hydrophobicity and ability to form excellent interfacial bonding with added fillers [640]. The advantages of graphite lie in its high compressive strength, high electrical and thermal conductivity and corrosion resistance. But the biggest advantage of graphite is its biocompatibility [641], which makes it a popular choice to develop devices for biomedical applications. The electrodes were patterned in an interdigitated manner with the casting of graphite powder on the 3-D printed moulds. The operating principle of the sensor patches is described along with the COMSOL simulation result which depicts the electric field density distribution between the two groups of electrode fingers of opposite polarity under an applied stress. The characterisation of the sensor patches was done to determine their responses towards the change in frequency and applied stress. The experimentation of sensor patches was done by analysing the changes in their conductivities and capacitances at different operating conditions. The sensor patches were then employed for two different applications. One was regarding strain-sensing application by attaching them on different parts of the body like finger, elbow, neck and knee. Strain sensing was successfully done based on the bending of the different joints on which the sensor patches were attached. The other application was regarding low-force sensing measurements. The promising results shown by the sensor patches increase the chances of utilizing them in future in different sectors like biomedical field, microfluidic and tactile applications. The advantages of the proposed sensor patches over the existing methods lie in its low-cost of fabrication, low

cost of processing materials, easy operating principle and a wide range of applications. The proposed sensor patches are also light and small, which makes them easier to be replaced if damaged. The electrodes of the sensor patches being capacitive in nature make them easy to be adjusted and fabricated, achieve a high sensitivity with little stress, require low input power and have a good resolution and response to frequency. Apart from exploiting the flexible nature of these sensor patches, they can also be used for monitoring non-metallic targets and dielectric materials.

7.2 Fabrication of the Sensor Patches

The fabrication of the sensor patches was performed in laboratory conditions. Figure 7.1(a) shows the 3-D printing system used to develop the moulds. Acrylonitrile Butadiene Styrene [642] was used as the printed filament to develop the moulds. This material was chosen, as it has high flexural strength and ductility compared to other thermoplastics used for 3-D printing purposes. After attaching the filament with the printing device (3-D PRINTING SYSTEM), the printer was then pre-heated for fifteen minutes before starting the process.

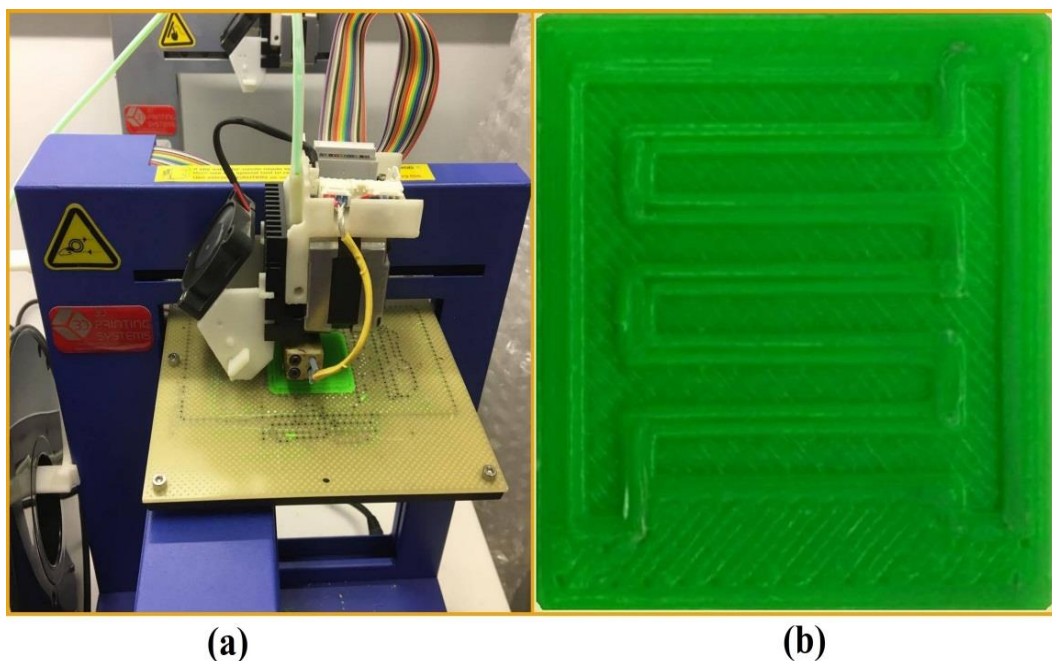


Figure 7.1 The 3-D printing systems (a) were used to develop the moulds (b) using the Acrylonitrile Butadiene Styrene as the printing filament. The height of the trenches on the mould was adjusted to 500 microns.

This was done to allow the device to attain the fixed temperature required for the operation. Then design of the electrodes to be fabricated on the sensor patch was done on the designing software CREO Parametric 2.0 that was associated with the printing system. The height of the trenches formed on the mould was adjusted to 500 microns. The mould formed by the printing system is shown in Figure 7.1(b). After the moulds were formed, they were thoroughly washed with 2-isopropanol to remove any kind of snippets of the printing filament attached on it. Graphite powder (Sigma-Aldrich 282863-25G, $<20\ \mu\text{m}$) was then cast on the trenches of the mould as shown in Figure 7.2(a), to develop the electrodes of the proposed sensor patch. An optimisation on the volume fraction of the graphite powder used to develop the electrodes was done based on its critical volume fraction for changing the electrical conductivity and flexibility of the sensor patch.

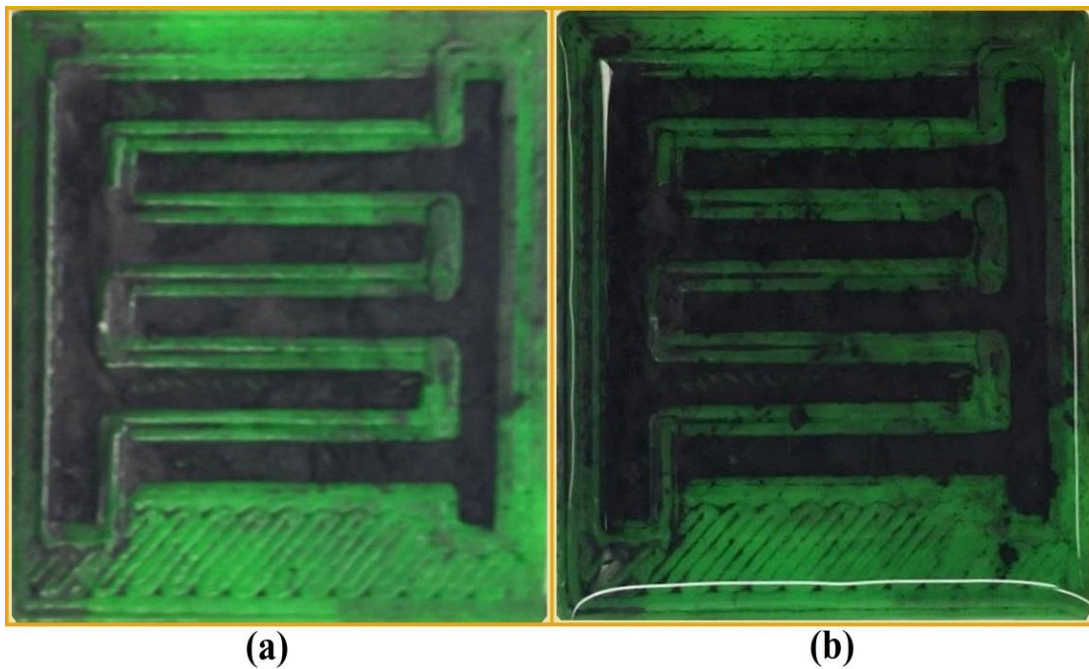


Figure 7.2 Graphite powder was cast on the 3-D printed mould (a), followed by the casting of PDMS (b) on top of it. These two layers defined the electrodes and substrate of the sensor patches.

As the homogenous weight fractions and volume fractions can be approximated to be equal for an uniform and homogenous system [643], the optimised critical volume fraction of the graphite powder to PDMS was 4.38% as shown in Figure 7.3. The residual graphite powder was taken off the mould to avoid short-circuits between the electrodes. This was followed by casting a layer of PDMS (SYLGARD® 184 SILICONE ELASTOMER KIT) on the top of the graphite powder as shown in Figure 7.2(b), formed by mixing the

pre-polymer and curing agent at a ratio of 10:1. The height of the cast PDMS layer was adjusted to around 1000 microns to define the substrate of the sensor patches by the printed 3D mould margin with a casting knife (SHEEN, 1117/1000mm). Then, the sample was desiccated for an hour to remove the air bubbles trapped in it, followed by curing done it in the oven at 70 °C for 2 hours. This cured the PDMS, solidifying it to form the substrate of the sensor patches. Figure 7.4 shows the dimensions of the developed sensor patch.

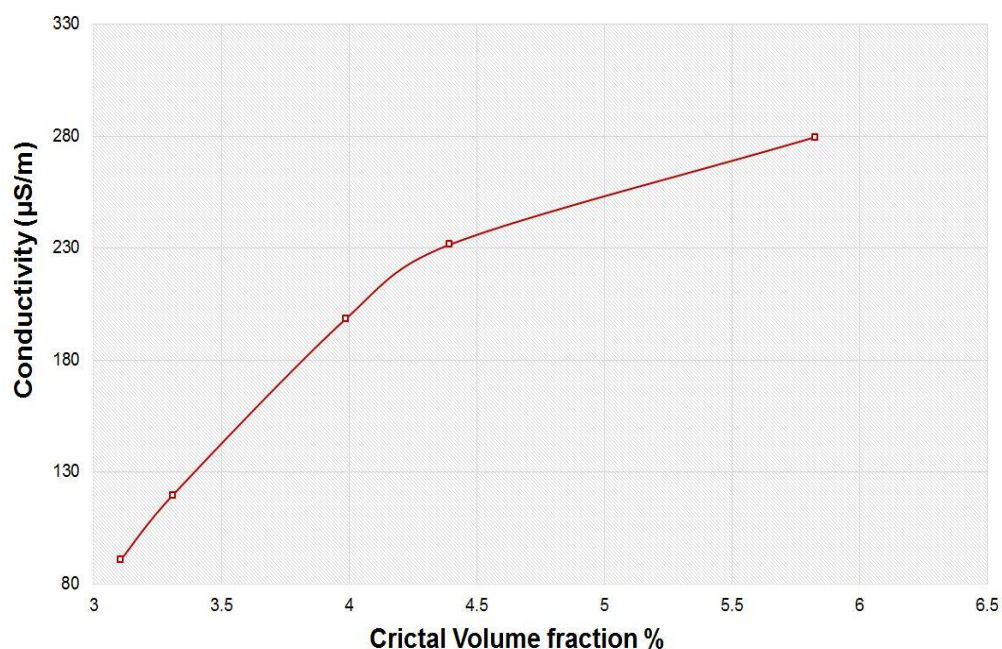


Figure 7.3 Optimisation of the critical volume fraction of the graphite powder to develop the electrodes of the sensor patch.

The electrodes were shaped in an interdigitated manner with three pairs of electrode fingers. The total surface area (A) of the sensor was around 900 mm² with a length and width of 18 mm and 2 mm of each electrode finger respectively. The interdigital distance (d) between two consecutive electrode fingers was 1.5 mm. The dimensions of the surface area are critical in the chosen application as the effective change in the structure of the sensor patches would reflect the amount of strain induced on them. The number of electrodes fingers on the sensing surface have been repeated to have an increased net electric field [8]. The dimensions of the length and width of the electrodes were made significant enough to encounter the strain when attached to different parts of the body. The advantages of these sensor patches in terms of biomedical aspects lies in the biocompatibility of the raw materials used to process the sensors [641, 644]. Some of the

advantages of having small sizes of the sensor patches are their easy reproducibility, low cost of production, low input power requirement and improved sensitivity and accuracy.

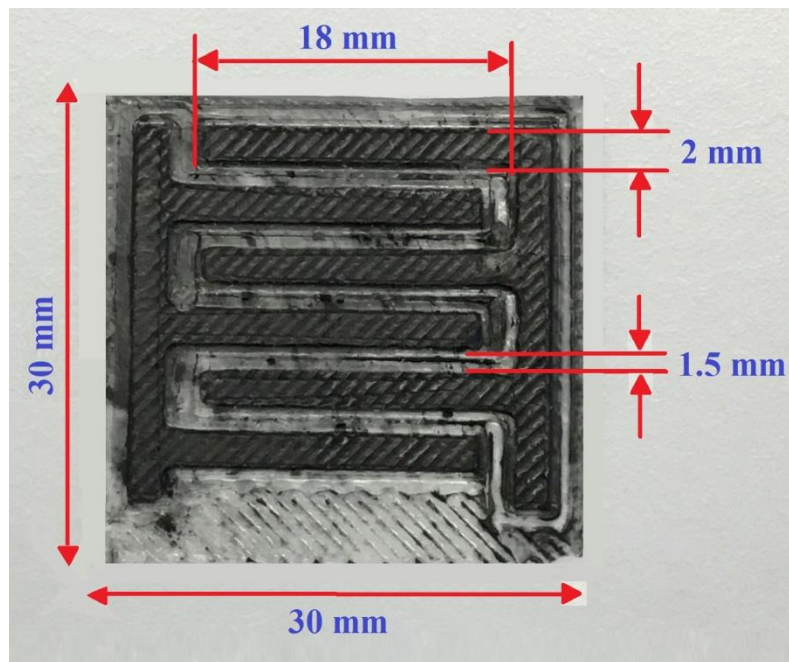


Figure 7.4 Front view of the developed sensor patch. Three pairs of electrode fingers were present, each with a length and width of 18 mm and 2 mm respectively. The total surface area of the sensor patch was 900 mm².

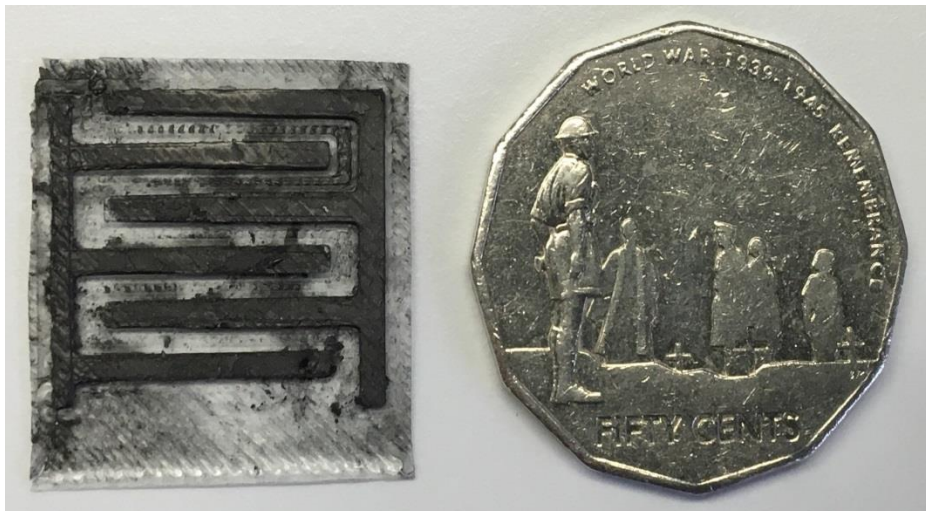


Figure 7.5 Comparison between the sizes of the developed sensor with a 50 cent Australian coin.

The nature of the electrodes of these sensor patches led to an easy operating principle during experimentation. The developed sensor patches were again thoroughly cleaned with 2-isopropanol before using them for characterisation purposes. Figure 7.5 shows a

comparison between the sizes of the developed patch with that of 50 cents of Australian coin to illustrate the small size of the sensor patch. Figure 7.6(a) shows the top-view and cross-sectional views Scanning Electron Microscope (SEM) images of the developed sensor patch taken with a Phenom XL. The PDMS layer came off smoothly and clean on the top of the graphite electrodes (figure 4(A)). A top-view of the electrodes, made of representing the graphite and PDMS mixture, is shown in Figure 4(B). The cross-sectional view of the electrodes is shown in figure 4(C), which was formed by peeling from the 3D-printed mould after the curing process of PDMS.

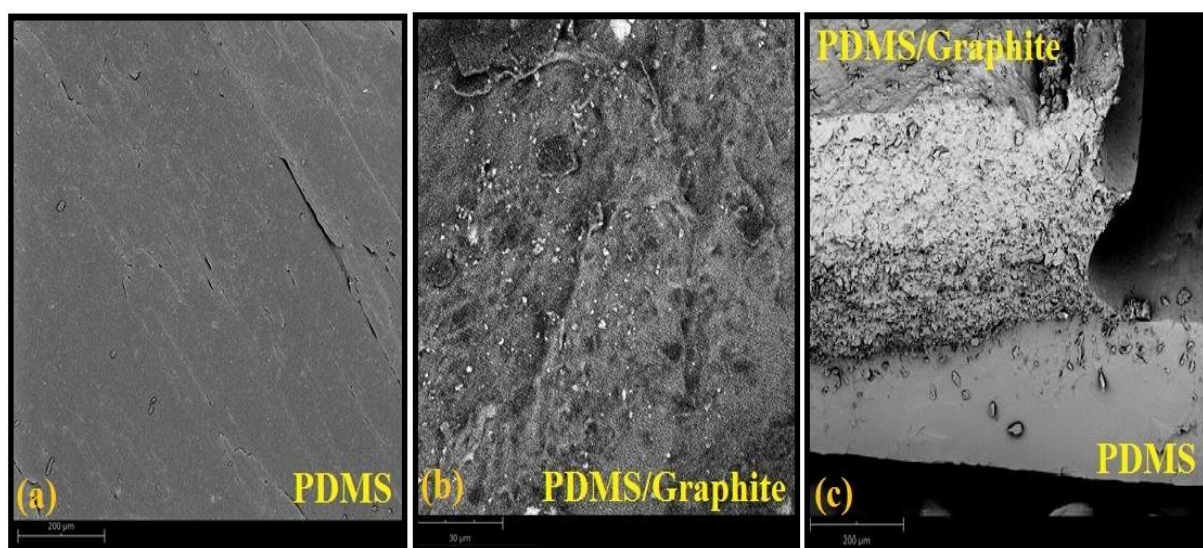


Figure 7.6 SEM images of the developed graphite-PDMS sensor depicting the top-view of (A) PDMS, (B) graphite-PDMS mixture and (C) cross-sectional view of the electrodes.

7.3 Frequency Response and Stress-Strain Measurements

The analysis of the response of the sensor patches was done based on their strain-induced nature. The illustration of the flexibility of the sensor patches is shown in Figure 7.7. Figures 7.8(a) and 7.8(b) show microscopic images taken with a DYNASCOPE microscope and a TOUPCAMTM (UCMOS03100KPA) camera to depict the reference spot and its horizontal movement over the sensor patch respectively. The flexibility of the sensor patches was also analysed by determining the change in the reference spot on the sensor patch between the no-strain and full-strain conditions. The strain was applied horizontally over the sensor patch by fixing one side of the patch with a clamp. The change

in capacitance values with respect to frequency were analysed for four different bending radii (1.5 mm, 3 mm, 4.5 mm, and 6 mm).



Figure 7.7 Image of the developed sensor patch depicting its flexibility.

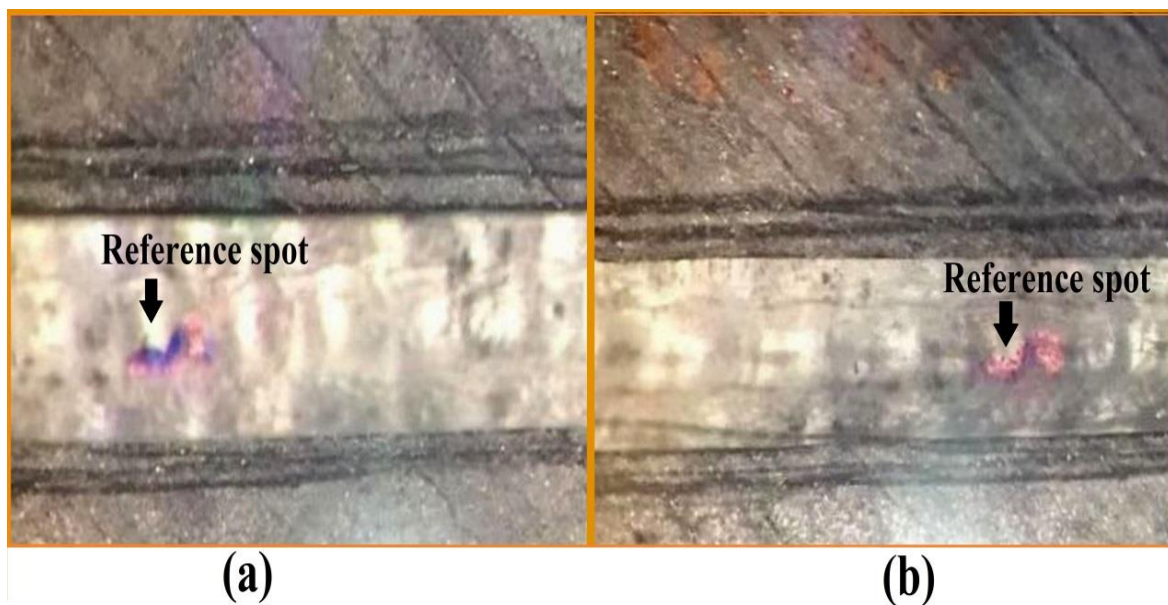


Figure 7.8 Change in the reference spot in the sensor patch to depict their flexibility from (a) no- strain to (b) full-strain condition.

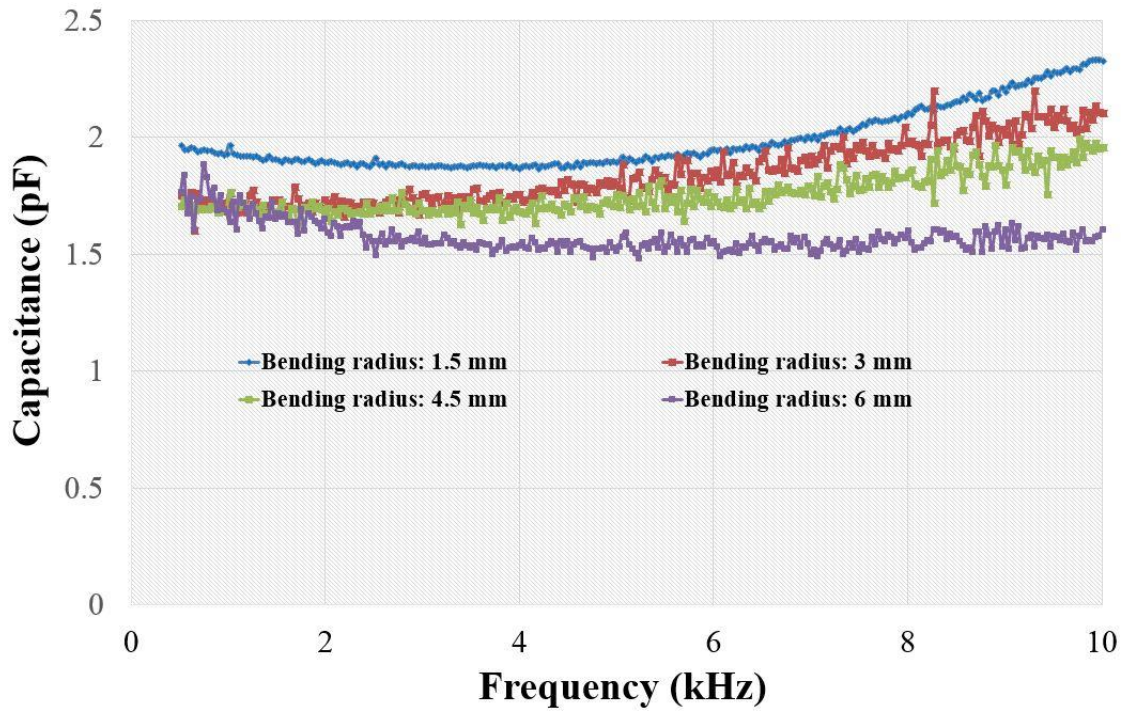


Figure 7.9 Response of the sensor for the frequency sweep done between 1 Hz to 10 kHz at four different bending radii (1.5 mm, 3 mm, 4.5 mm, 6 mm) to determine the operating frequency.

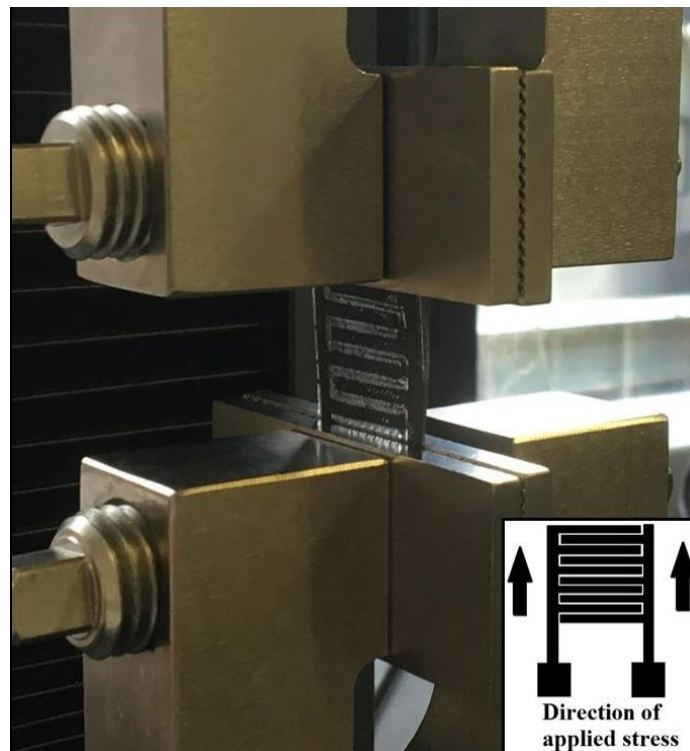


Figure 7.10 Analysis of the stress-strain measurement. The direction of the applied stress shown is in the inset of the figure.

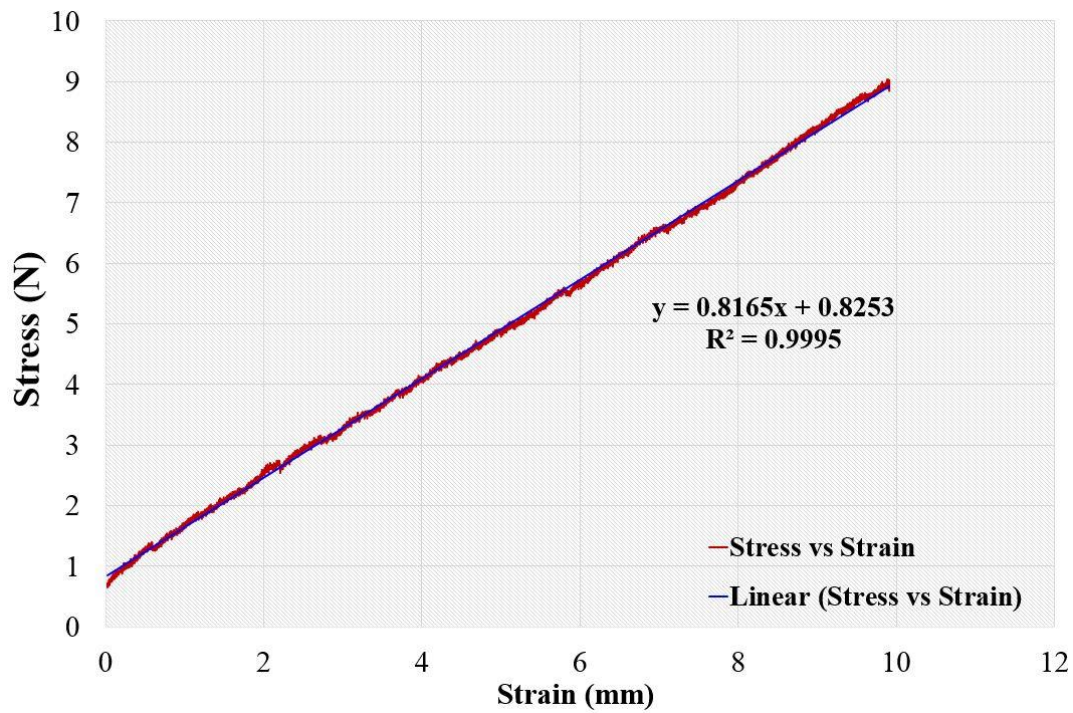


Figure 7.11 Response of the sensor patch in the proportional limit for the stress-strain measurement.

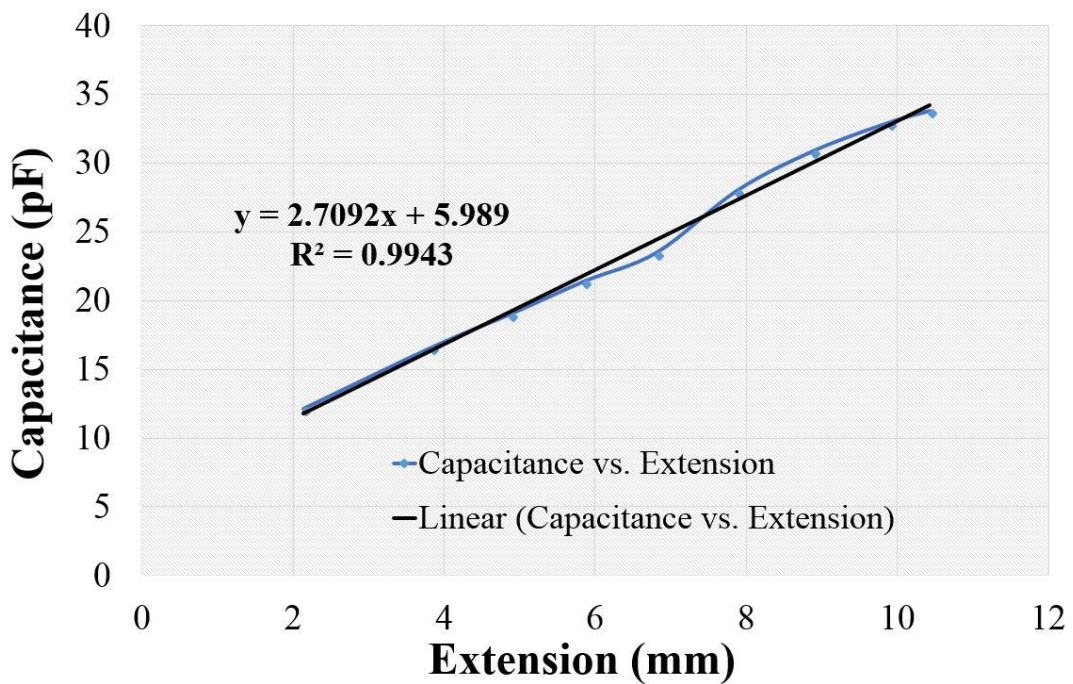


Figure 7.12 Response of the sensor patch for the change in capacitance occurring due to the applied strain.

These values were chosen to cover the range of the different radii of curvature from the slightly bent situation to the highly bended situation. A frequency sweep was done from 1

Hz to 10 kHz at different bending radii of the sensor patches to determine the operating frequency as shown in Figure 7.9. Stress-strain measurement was then performed to determine the tensile strength in terms of Young's modulus (E) and the response of the sensor to the resultant strain in terms of electrical conductivity. Tensile stress was applied in a perpendicular direction to the electrode fingers of the sensor patches as shown in the inset of Figure 7.10. Figure 7.11 shows the stress-strain response of the sensor patches. The load was applied on the sensor patch by fixing one of the two clamps while moving the other one. The response is within the elastic limit of the load-extension curve and the extension follows linearly the applied load with a high regression coefficient. The Young's Modulus (E) of the sensor patches at an extension of 6 mm was 675 kPa, obtained from the calculated values of stress (135 kPa) and strain (0.2). It is seen that the sensor patches were capable of responding linearly with a high coefficient of determination (R^2). The change in response with respect to the strain caused on the patches due to the applied stress is shown in Figure 7.12. The response of the patches changed because of the extension caused in the horizontal direction of the sensor patches causing a change in the effective area (A') and effective interdigital distance (d') of the sensor patches. The sensor patches were extended from the normal position to a maximum of 10.2 mm before the breaking point.

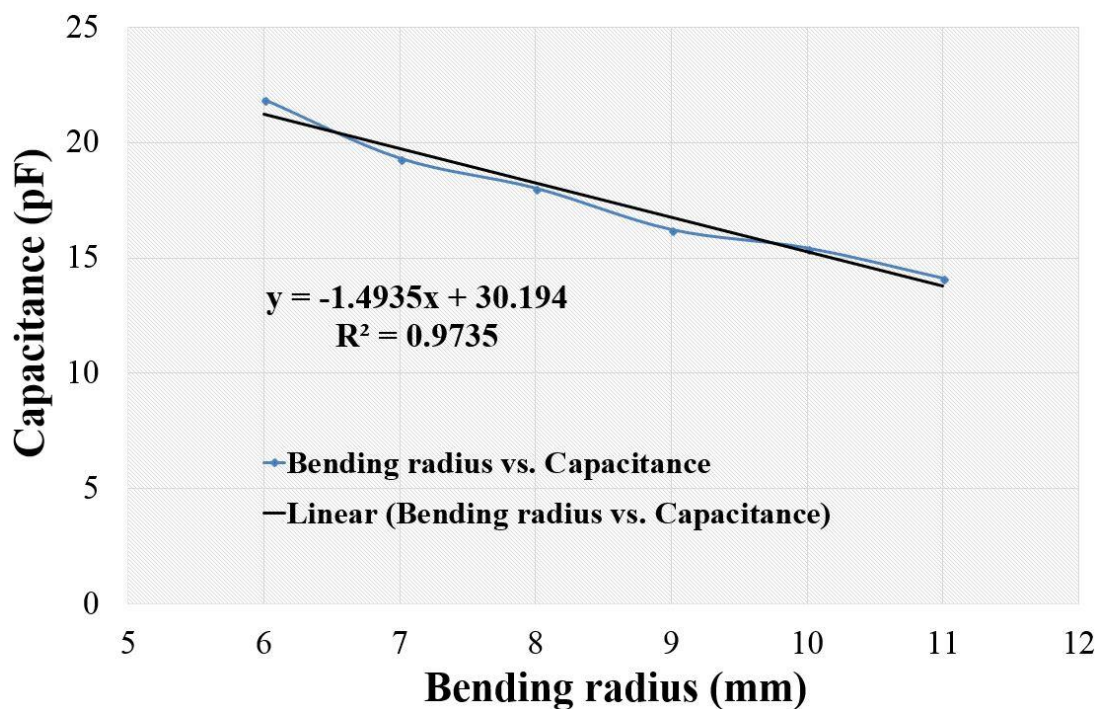


Figure 7.13 Capacitance of the sensor for a bending radius from 11 mm to 6 mm.

The bending response of the sensor patches was tested by bending them by hand so that the electrodes were under compressive load. Figure 7.13 shows the different capacitance values for bending radii of curvature ranging 6 mm to 11 mm. The capacitance decreased with increasing radius. As the condition of the sensor patch changed between the normal and flexed state, the dimensions of the sensor patch oscillated between the normal and compressed. Figure 7.14 shows the change in the capacitance for the normal and bending states of the sensor patch undergoing 10 cycles. The sensor was bent to a small curvature and brought back to its normal. When the sensor patch changed from normal to bent state, the capacitance value decreased from an average value of 35 pF to a value of 2 pF.

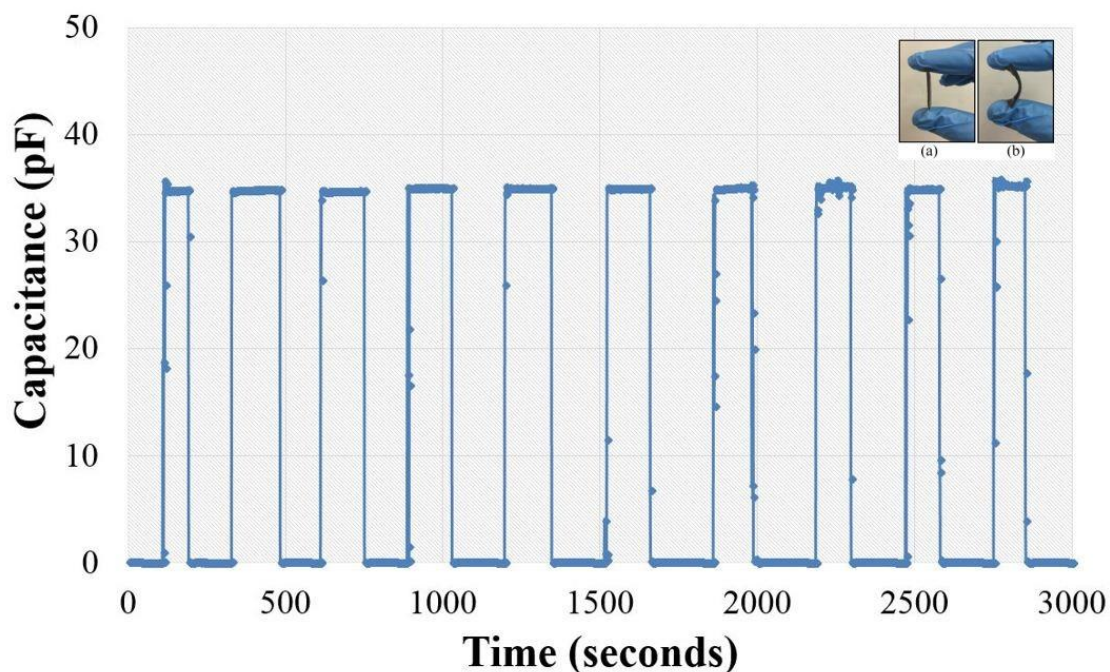


Figure 7.14 Response of the sensor for the experiments bending the sensor patch in a cyclic manner. The bent state of the sensor patch caused a decrease in its conductivity value. The inset of the figure shows the (a) normal and (b) bent states.

This happens due to the increase in the radii of curvature as a result of bending the patch, which decreases the capacitance value, as evident from Figure 7.13. This is advantageous in terms of the application of the sensor patches where they could be used to monitor the movement of a person [16], or tactile sensing of prosthetic limbs [645] based on the strain-sensitive nature of the electrodes. However, the range in the conductivity values for every bending cycle is not the same. This is due the re-orientation of the

conductive fillers in the PDMS with every cycle. The relative resistance was calculated based on the ratio between the changes in resistance with strain to the resistance in its normal condition. Figure 7.15 shows the performance of the sensor patches in terms of the relative resistance to the applied strain. The changes in values were analysed with a fitted polynomial curve with a power of 2. The response of the sensor patches adheres to that of the graphite-based strain sensors [127] which is also evident from the experimental curve being very close to the fitted curve.

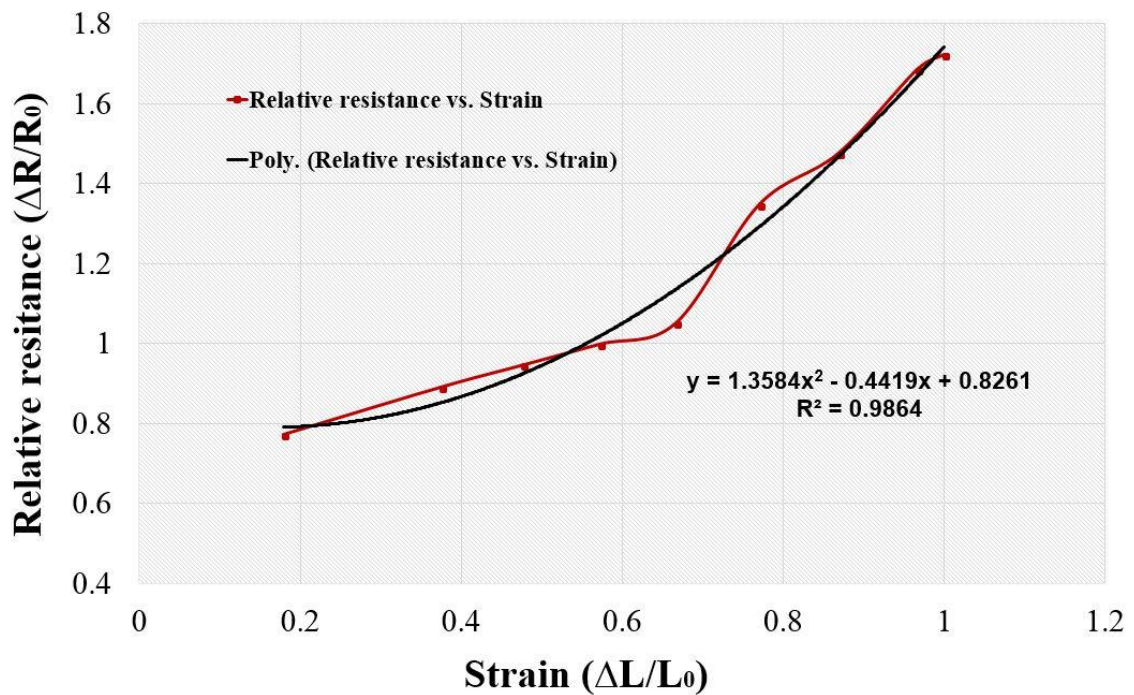


Figure 7.15 Response of the sensor patch in terms of relative resistance with strain.

7.4 Strain Sensing

The utilisation of flexible sensors has held a pivotal role in the field of biomedical applications [646] for quite some time. Sensors developed with different materials have been characterised and implemented for various biomedical applications. There are some commercial pressure bending sensors that could be used as strain and pressure sensors as shown in Table 7.1 that are available commercially in the market. These types of sensors do provide a varied application in the field of biomedical applications, the fabrication cost, size of the sensors and the complexity in the nature of the sensors increase their overall prices. Strain sensing has been one of the popular choices of application where flexible

electronics have been largely employed [433, 647, 648] to analyse the tension caused as a result of the applied stress. Table 7.2 gives a comparative study between the performances of the proposed sensor with other research works done on similar sensors but developed with different methods. The comparisons are made in terms of fabrication technique, size, materials used to fabricate them and their potential applications.

Table 7.1 Comparative study between the flexible sensors commercially available in the market.

Sl. No.	Sensor	Size (mm)	Price (\$)	Application
1	Flexiforce A201	50.8 x 9.7	69.00	Tactile sensors, human symbiotic robots
2	SEN-11207	56.8 x 25.4	47.00	Strain gauges
3	RB-Phi-121	25*11	45.00	Pressure sensors, touch user interface
4	Flexiforce A201-25	58.4 x 17.8	37.35	Touch pads, alarm systems
5	Flexiforce A101	15.6 x 7.6	34.00	Bed monitoring and force sensitive systems

There has been a wide range of biomedical applications of strain sensing which includes the monitoring of breathing [151, 287], blood flow [649], knee movement [112], heart rate [650] etc. Although mercury-based strain gauges have been utilised for strain-sensing purposes for decades, the range of strain and the involvement of mercury for biomedical applications have been their existing limits [154]. Addressing these drawbacks, researchers have been exploiting different conductive materials like CNTs [151, 651, 652], graphene [230, 242, 284], etc. to develop strain sensors with better efficiency in terms of conductivity, gauge factor and potential applications. Even though some of these sensors have been able to provide high sensitivity, their technical complications [154], high fabrication cost [282], and the requirement of expertise to operate them has limited their widespread uses. It is thus the state of the art to develop low-cost, efficient strain sensors capable of rectifying the above-mentioned limitations. This section showcases the fabrication and implementation of 3-D printed mould-based strain sensors which have been used to analyse physiological bending movements.

Table 7.2 Comparative study between the strain sensors developed with different fabrication techniques.

Sl. No.	Fabrication technique	Size (mm)	Materials used	Application	Reference
1	Chemical vapour deposition	60 x 60	Graphene-PDMS	Facial expression, human motions	[229]
2	Thermoplastic processing technology	20 x 20	Carbon black- Thermoplastic elastomer	Body postures and body movements	[653]
3	Screen printing	2 x 2	Silver nanowires- PDMS	Thumb and knee movement	[35]
4	Encapsulation and moulding	150 x 1.8	Copper-PDMS	Implantable medical device	[644]
5	Encapsulation	110 x 80	RF transmitter- PDMS	Body movements	[654]
6	Dip-coating	40 x 40	Silver nanowires- PDMS	Pressure sensing	[655]
7	Sputtering	75 x 50	Copper-PDMS- Kapton	Body movements	[656]
8	Laser cutting	85 x 40	Carbon black- PDMS	Body sensing	[657]
9	Chemical vapour deposition	50 x 10	Carbon Nanotubes-glass fibre	Health monitoring	[658]
10	3-D printing	30 x 30	Graphite-PDMS	Body movements	Our work

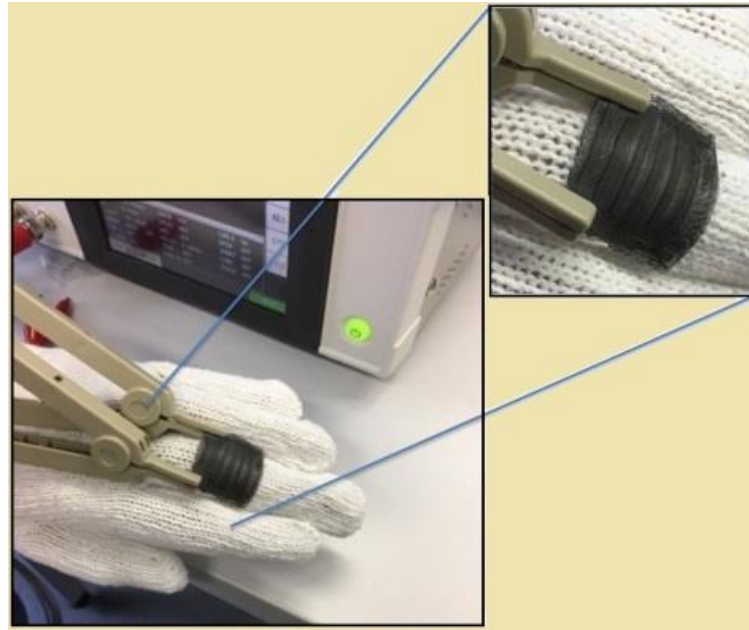
7.4.1 Experimental Setup

The sensor patches were attached on different parts of the body like a finger, knee, elbow and neck. The positions of the sensor patches were fixed such in a way that the bending of the joints induced strain on the patches. The metacarpophalangeal, olecranon and patella were the joints for the finger, elbow and knee which caused a force on the

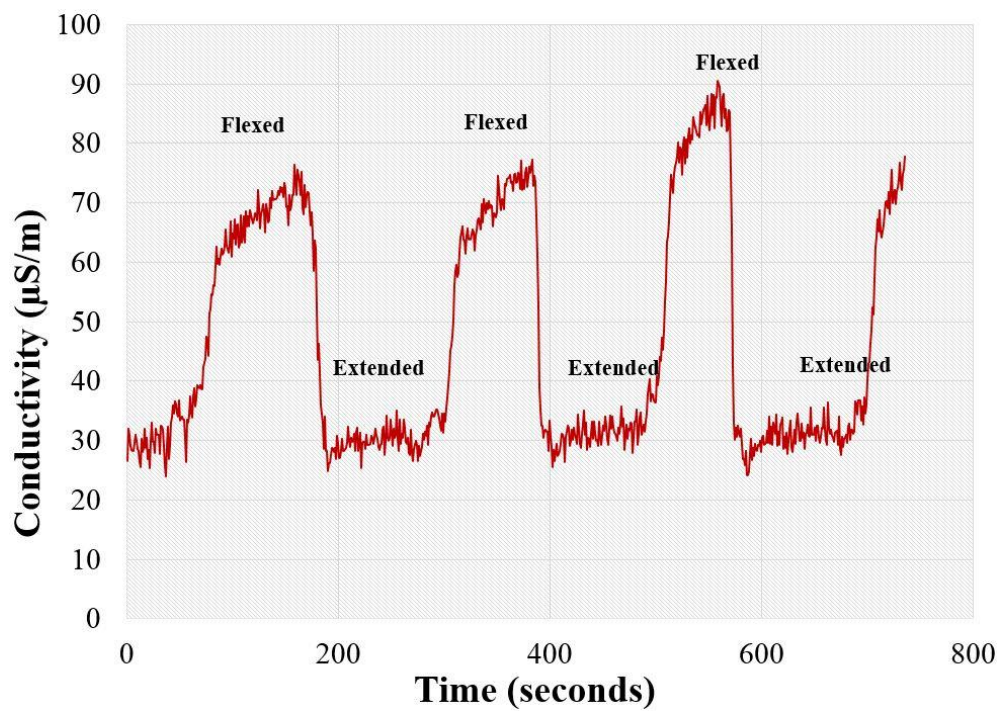
sensing area of the patches. The sensor patch was placed on the upper part of the cervical spine to record the movement of the neck. The movements of the body parts were done in an oscillatory motion to ensure repeatability of the response of the sensor patches and validate their functionality for strain-sensing purposes. The direction of movement for these joints was done in a vertical manner to induce strain perpendicular to the electrode fingers. These four joints were chosen for the strain sensing purposes as they were responsible to exert the highest force in those respective body parts. The force caused by these joints changed the resultant electric field between the electrodes causing a change in the output of the sensor patch. The analysis was done via an impedance analyser using an automatic data acquisition algorithm.

7.4.2 Results and Discussion

A HIOKI IM 3536 High Precision Tester was connected to the bonding pads of the sensor patch with Kelvin probes to record the movement of the sensor patches. The tester was connected to a computer via an USB cable to store the data in Microsoft Office Suite. An alternating voltage of 1 V RMS with the frequency fixed as 5 kHz was provided as the input from the tester. An average of three readings with duration of 5 seconds between each sweep was taken to ensure repeatability of the response of the sensor patches. Figures 7.16 – 7.19 show the attachment of the sensor patch on different parts of the body and their respective responses. Figures 7.16 (a) and 7.16 (b) show the placement of the sensor on the middle finger of a glove and its response respectively. The middle finger was chosen for monitoring purposes due to its highest degree of movement compared to the other fingers. The sensor patch was fixed to the glove with a super glue to ensure its proper attachment.

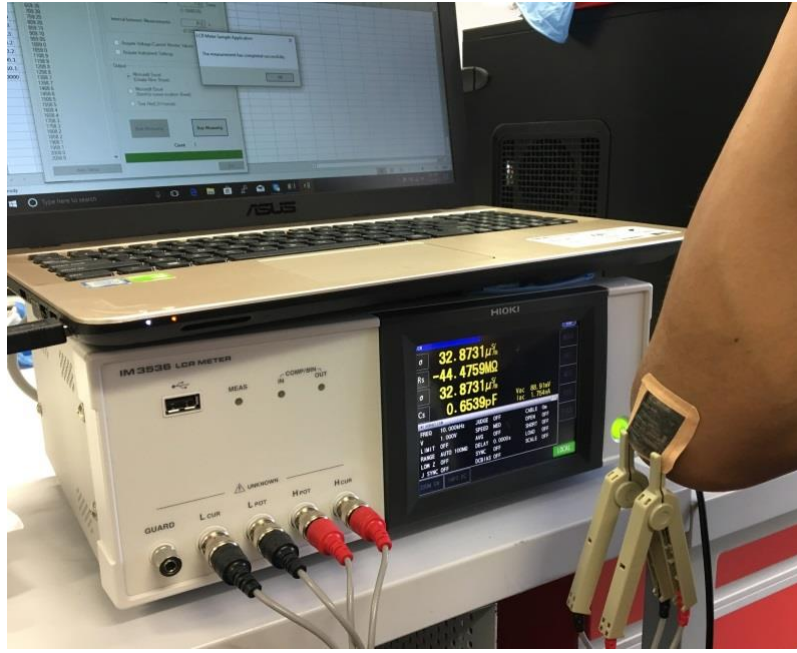


(a)

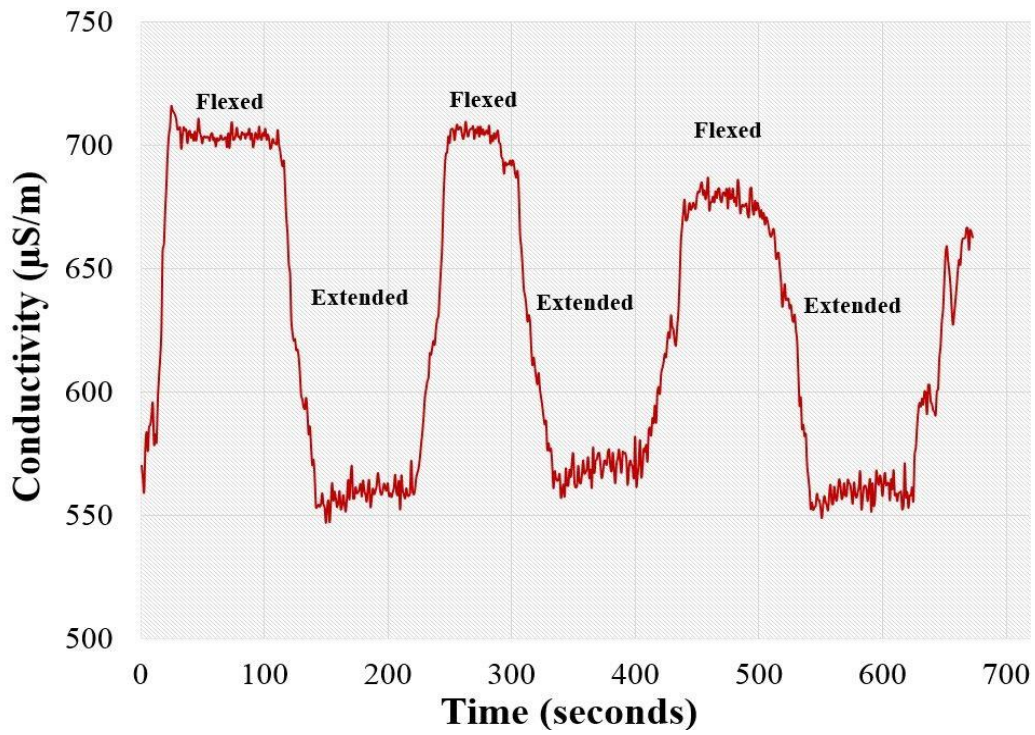


(b)

Figure 7.16 Attachment of the sensor patch on the (a) middle finger of the hand with the assistance of a bandage to determine its (b) movement based on the strain induced on the sensing area of the patches. The two states, flexed and extended, refer to the bent and relaxed condition of the arm respectively.



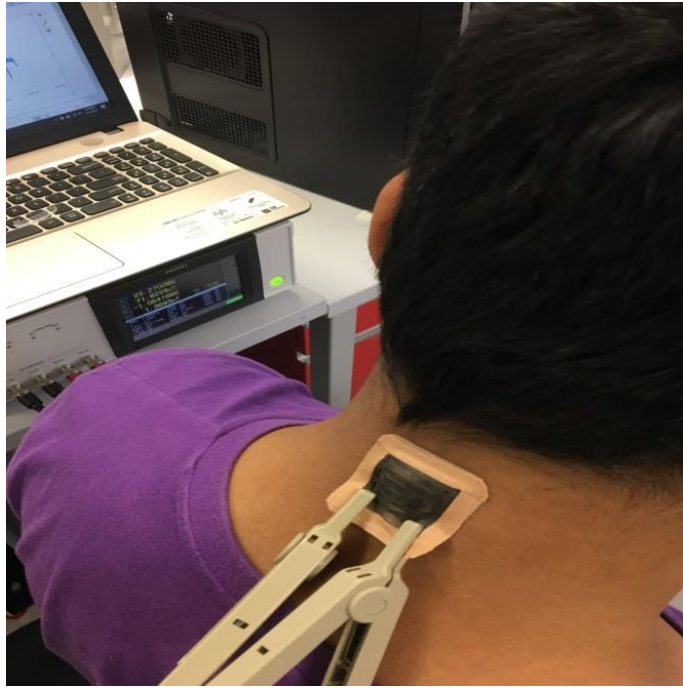
(a)



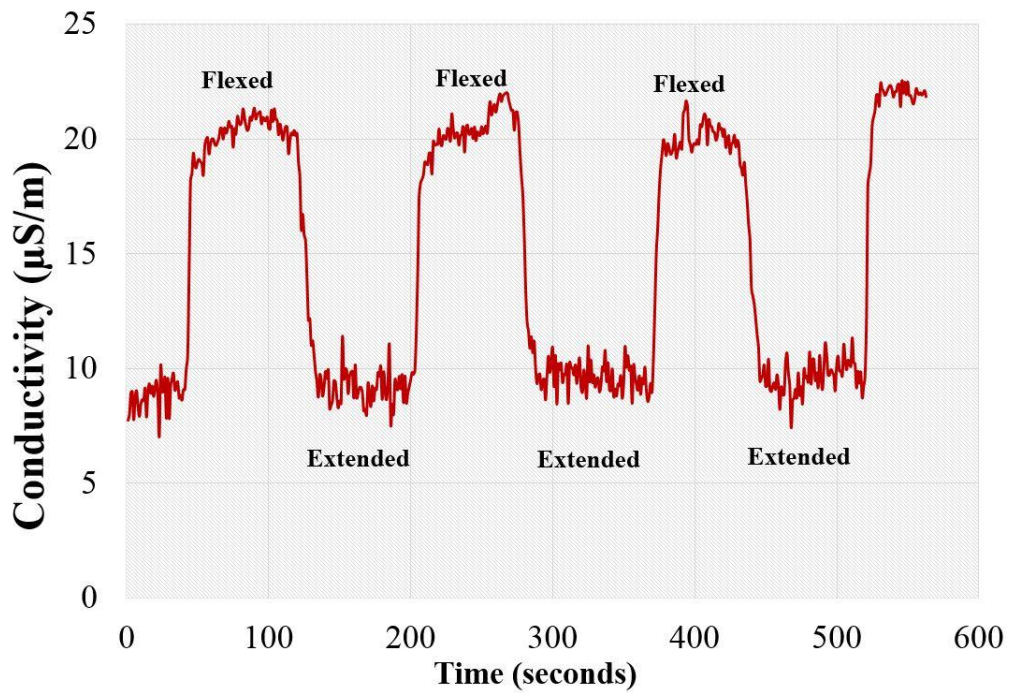
(b)

Figure 7.17 Attachment of the sensor patch on the (a) elbow of the arm with the assistance of a bandage to record its (b) movement based on the strain induced on the sensing area of the patches. The two states, flexed and extended, refer to the bent and relaxed condition of the arm respectively.

The two states shown in the response graph, flexed and extended, refers to the bent and relaxed condition of the finger. Figures 7.17 (a) and 7.17 (b) show the attachment of the patch on the elbow of the arm. The attachment of the sensor patch on the elbow was done by fixing the sensor to a bandage and attaching the latter on the body. The use of the bandage to fix the sensor patch was done to keep in perspective of the different applications of the strain sensors for the detection of human-motion [151], physiological parameters [556], etc. The sensor patch was also able to respond to the induced strain caused by the movement of the elbow and the finger. However, there is a certain difference in the range of the conductivity values between the two responses. The possible reason for this difference could be the higher degree of movement of the elbow with respect to the finger. The sensor patch was also attached to the neck as shown in Figure 7.18 (a) to record its movement. The idea to monitor the movement of the neck is to target people suffering neck injuries or paraplegic patients who have problems tweaking facial muscles [659]. It is seen from Figure 7.18 (b) that the patch was capable to detect the oscillatory motion of the neck. The movement of the leg was monitored as seen from Figures 7.19 (a) and 7.19 (b) by fixing the bandage-assisted sensor patch on the patella of the left leg. The monitoring of the movement of the leg is useful for people having osteoporotic fractures. However, it is seen that the range in the conductivity values during flexed states is not the same for all the cycles. There could be two possible reasons for this behaviour. Firstly, the degree of attachment of the bandage assisted sensor patch on the joints might not be the same for any two flexed cycles. The oscillatory motion might have caused a change in the orientation of the bandage from its preceding position. This occurrence will be minimised during the situation when the monitoring would be done by fixing the sensor patch connected to an embedded system. Secondly, the physio-chemical composition of the graphite powder in the nanocomposite formed electrodes changes every time during the flexed cycle. This changes the resultant response of the sensor patch. Even though, this change might be a concern regarding repeatability of the response, the results would vary within a certain range as a result of the optimisation of the amount of graphite powder in the resultant nanocomposite.



(a)

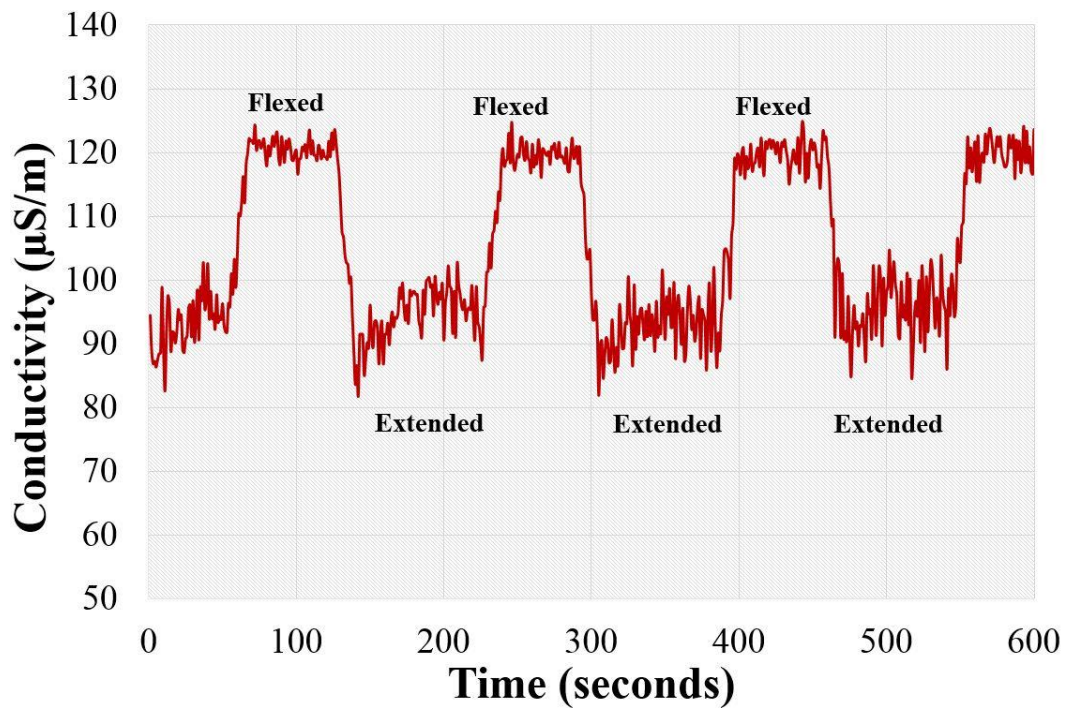


(b)

Figure 7.18 Attachment of the sensor patch on the (c) neck with the assistance of a bandage to record its (b) movements based on the strain induced on the sensing area of the patches. The two states, flexed and extended, refer to the bent and relaxed condition of the arm respectively.



(a)



(b)

Figure 7.19 Attachment of the sensor patch on the (a) knee to record its movements based on the strain induced on the sensing area of the patches. (b) The two states, flexed and extended, refer to the bent and relaxed condition of the arm respectively.

7.4.3 Conclusion

The sensor patches were used for biomedical applications where they were attached to the joints of the fingers and limbs to determine their movement. The advantages of using these types of sensors are their excellent mechanical and electrical properties assisting this type of application. The sensor patches were highly sensitive in nature responding to small strains from that of a finger to large strains from that of the limbs on them. There is however one issue faced during the experiments which need to be rectified for further tuning the sensor patches. All the experiments were performed with wired connections which are not suitable for real-time applications. Wireless communication like active Radio-frequency Identification (RFID) tags can be introduced on the substrate of the sensor patches so that the patches could transmit the signal to the reader at fixed intervals. Instead of attaching the sensor patches with tapes, they can also be cuffed for ubiquitous monitoring purposes. The above-mentioned points, along with experiments on some other above-mentioned applications, will be addressed and reported on in future work.

7.5 Force Sensing

The sensor patches were also used for low - force sensing, measuring between 3.5 mN to 17.5 mN. Low-force sensing holds a key role in different applications like biomedical measurements, microfluidics, tactile sensing, etc. [660] applied low force sensing specially in the field of tactile sensing, They have been used for robotic and upper limb prostheses [661], touch screens was made using it [662] and soft tactile sensors was achieved using it [663]. Although various materials have been used in these research works, there have been certain limitations like high cost, detectable range of operation, complexity in the design and rigidity that are associated with them. For example, even though microfluidic multilayer sensor can measure forces up to 2.5 N [660], their disadvantages lies in the material cost and complexity of the structure. Although, the research from [664] on capacitive polymer tactile sensors are available, the detectable range in this case is too high (20 mN), specially for haptic robotic applications. Our work provides a conjunctive approach on the cost of fabrication, operating principle and detectable range. Our sensors can also detect forces at around 3.5 mN, which could lead to the utilisation of these sensors as wearables for rehabilitation purposes after the patient suffers from stroke, muscle

spasms, etc. In such cases the sensors would enable monitoring of even slight movements of a body part to determine the patient's recovery.

7.5.1 Experimental Setup

The experimental characterisation of the sensor patches was carried out by using an impedance analyser (HIOKI IM 3536 High tester). Kelvin probes were used to connect the patches from one end while they were attached to the clamps or bent during the characterisation procedure. For the experiments, the sensor patches were firmly fixed at the opposite end of the Kelvin probe to determine the changes because of the applied load.

7.5.2 Results and Discussion

The sensor patches were then tested with five different forces, ranging from 3.5 mN to 17.5 mN. The patches were firmly fixed to avoid any movements during experimentation. Different weights of the same shape were placed on the patches in the same location to ensure minimal effects of their area on the results. An average of five experimental readings was taken for each weight.

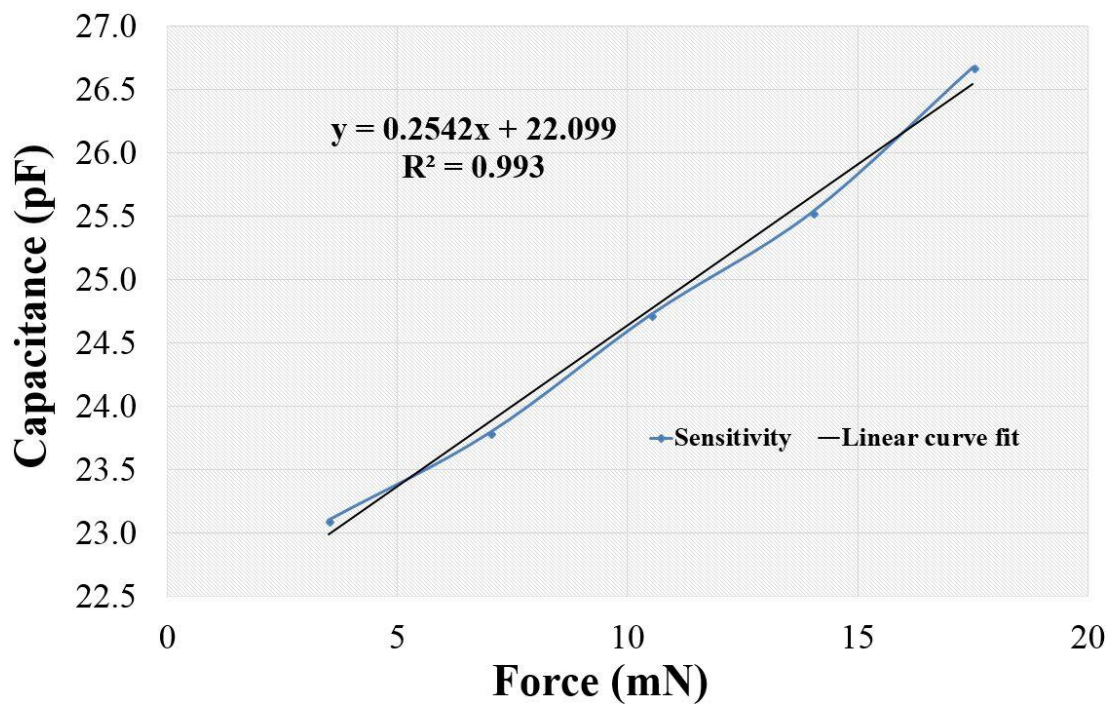


Figure 7.20 Response of the sensor patch for a particular frequency (5 kHz) depicting the different capacitance values for the different experimental weights.

The experiments were done at a frequency value of 5 kHz to determine the change in capacitance as a function of the loading force. As shown in Figure 7.20, the capacitance with respect to force is almost linear with a force sensitivity of $0.2542 \text{ pF} \cdot \text{mN}^{-1}$ in a range from 3.5 mN to 17.5 mN.

7.5.3 Conclusion

Followed by the biomedical applications, the fabricated Graphite/PDMS sensor patches were also employed for low-force sensing applications. The sensors showed a force sensitivity of $0.2542 \text{ pF} \cdot \text{mN}^{-1}$ in a range from 3.5 mN to 17.5 mN. The results show the potential for these sensor patches to be used as cheap and highly efficient force sensors, which can be used to develop low-cost, easy-to-fabricate force-sensing systems for ubiquitous monitoring applications.

7.6 Chapter Summary

The design, characterisation and implementation of the novel Graphite/PDMS sensor patches are showcased in this chapter. The novelty in this approach lies in the development of simplified sensor patches using casting technique on 3-D printed moulds. The casting of graphite and PDMS was done on the top of the moulds to develop the electrode and substrate parts of the patches, respectively. The advantages of these patches lie in its low-cost fabrication, simple operating principle and high performance for the designed applications. Another major advantage is the reliability of the sensors fabrication using this technique in terms of repeatability in the response during characterisation and experimentation. Since, the 3-D printed moulds were used as the template to cast graphite and PDMS on them; it was possible to develop a large number of sensor prototypes with identical dimensions and performances. Once the designs of the dimensions of sensor prototype were done, the fabrication of all the 3-D printed moulds took very less time (around 30 mins including the pre-heating). After the optimisation of the amount of graphite powder, identical performance of the electrode with respect to electrical conductivity was achieved. The repetition of the casting of the PDMS, followed by the adjustment of its height was also being able to be done identically. The differences between the performances of the sensor prototypes in terms of characterisation and experimentation

were negligible. The response of the sensor patches for their characterisation and experimentation were evaluated in terms of the change in electrical conductivity and capacitance with the applied strain. The developed sensor patches were flexible in nature, responding to the stress-strain experiments and oscillatory bending cycles. The use of 3-D printing technique ensured the low-cost of the processed material to develop the moulds, low fabrication time and high repeatability with respect to the structure and dimensions of the developed sensor patches. The amalgamated properties of PDMS and graphite ensured the flexibility of the sensor patches and high electrical conductivity of the electrodes. Other than these applications, these sensor patches can be employed for other biomedical uses like monitoring of blood pressure and oxygen saturation [649], temperature sensor [665], in determining the bone strength and mechanical properties of bones [666, 667], soft robotics [148, 430], piezo-resistive uses [652] and virtual reality and entertainment purposes [155].

8

Conclusion, Challenges and Future Work

Publication pertaining to this chapter:

- **Anindya Nag**, S. C. Mukhopadhyay, and J. Kosel, “Wearable Flexible Sensors: A Review”, **IEEE Sensors Journal**, vol. 17, no. 13, pp. 3949-3960, **July 2017**.

8.1 Conclusion

The work done in my doctoral tenure involves the development of different flexible sensors via printing technology and utilising them in different applications. Four different types of sensor prototypes were fabricated, characterised and employed for industrial (taste, salinity, nitrate sensing), domestic (monitoring of physiological movements and respiration) and scientific (tactile sensing) applications.

The CNT-PDMS sensor patches were nanocomposite-based sensors where the electrodes of the sensor patches were carved out of the top NC layer. The nanocomposite layer was developed by mixing MWCNTs and PDMS at an optimised ratio with a trade-off between the conductivity and flexibility of the resultant sensor patches. The sensor patches were then characterised in terms of their frequency response and stress-strain behaviour. The sensor patches were then employed for monitoring physiological movements and respiration, and for tactile sensing.

The Al-PET sensor patches were developed from a single material using metallised polymer films. The electrodes were carved from the Al side of the thin films with an optimised width of the electrode lines. This was followed by the characterisation of the sensor patches, determining their response towards changes in frequency and stress. The sensor patches were then utilised for tactile measurements to measure the pressure on the patches on different portions of an arm.

The graphene-PI sensor patches were developed from laser induction of commercial polymer films. An optimisation was done with the laser parameters to achieve proper laser induction. The sp^3 hybridised carbon atoms of the polymer films were photo-thermally converted to sp^2 hybridised carbon atoms of the induced graphene. The sensor patches were then characterised with CNLS software to determine their equivalent circuitry while utilizing them for different industrial applications like salinity, taste and nitrate sensing.

The graphite-PDMS sensor patches were developed from casting of graphite and PDMS on 3-D printed moulds. The depth of the trenches developed on the 3-D printed moulds was optimised with a trade-off between the conductivity and critical volume fraction of the graphite powder present in the cast PDMS matrix. The sensor patches were then characterised for their frequency response and stress-strain behaviour, followed by their implementation in monitoring of strain-induced body movements and force sensing.

8.2 Challenges of the existing work

Even though a lot of work has been done with printed flexible sensors, there are still some issues that need to be dealt with. Researchers are trying 24/7 to develop sensors with better performance, for sensitivity and sustainability, than the existing ones, and easier fabrication and implementation, for ubiquitous monitoring. The existing technologies still have some loopholes and bottlenecks that need to be addressed to utilise them in a better way in future. None of the printing technologies has been able to print flexible sensors with a resolution of nanometres scale. The nanowires used for developing electrodes of flexible sensors via nanocomposites, thus compromising their electrical and mechanical characteristics while mixing them with a polymer matrix. The formation of nanocomposites is another issue that needs to be further optimised to negate the decrease in electrical conductivity and alignment of the nano-fillers in the polymer matrix. The spreading of the lines, shadow effects during the offset printing, and hydrophobic problems in contact printing, are some other drawbacks that need to be resolved. The sensor prototypes developed with printing technology need to be scaled down while keeping a consistency in their sensitivity. The utilisation of the sensor prototypes for different applications, especially as wearable sensors, needs to be improved to reduce the overall cost of equipment. Sensors possessing multi-functional principles should be developed to serve in a much more dynamic way. For example, sensors having electrochemical, strain and electrical sensing techniques can be developed with multi-layered structures.

The massive amount of data generated by the wearable sensing system makes it difficult to handle and store them. Also, it becomes a tedious job for the system to determine out the significant data from the massive database for future analysis. Due to the enormous amount of monitored data, there needs to be a proper security system to curb any mishandling and misuse of the received data. Time-varying traffic is another issue raised during data transmission from different sensor nodes in a real-time topological system. This causes a delay in data reception in the monitoring unit, thus decreasing the efficiency of the system. Also, some of the significant data might get lost due to the high traffic generated by AAL applications. The data transmission for a central coordinator system in Wireless Sensor Networks (WSNs) should be handled properly to minimise traffic and the loss of data. The connectivity and interoperability of the embedded system should be significant, to minimise the power and data loss. From a patient's point of view, the person should not

face any kind of discomfort wearing the sensors for monitoring purposes. There should not be any breach of privacy for the patient from the monitoring. The embedded system attached to the sensor should not loosely attach to the body or clothes worn by the person, as this could alter the data depending on movements and the surrounding environment. There is also a risk of thermal effects of the attached sensors from the tissues of the patient. A lot of factors decide these thermal effects [468]. The number of sensors used in the embedded system should be kept as small as possible. The location of the sensor is also important. The positioning of the sensor on the arm will have more thermal effects than its positioning on the chest. The operating frequency of the sensor and network protocol should be as low as possible. Power consumption by WFSs is another significant issue that needs to be addressed. Sensors like SHIMMER, Telos with low power consumption should be considered for monitoring purposes to reduce the overall power consumed by the sensing systems. The continuous supply of power to the system is another challenge that needs to be addressed in future systems. The system should be designed for on-node processing and reduce the effects of motion artefact and distributed interference.

8.3 Future work

There is a considerable amount of work that can be done with a continuation of the current work. The sensor prototypes can be employed for some other applications in addition to the ones shown in the preceding chapters. For example, the sensor prototypes can be employed as temperature and humidity sensors in conjunction with other applications. For example, the response of the graphene-PI sensor patches towards different temperature and humidity values are shown in Figures 8.1 and 8.2. The change in phase angle (Φ) with respect to frequency was symmetric for temperature values ranging from 30 °C to 50 °C. Even though the frequency sweep was done between 1 Hz and 10 kHz, the operating frequency is between 100 Hz and 5 kHz, where the differences in the phase angles can be clearly seen. The operating frequency range for the humidity values, from 60% RH to 80% RH, was lower than that for the temperature values. Only a frequency ranging between 600 Hz and 930 Hz out of the entire frequency sweep was capable of differentiating the experimental humidity values. It can be understood from these figures that the developed sensor prototypes can be employed for other applications, just making it justifiable to call them multiple-functional sensors.

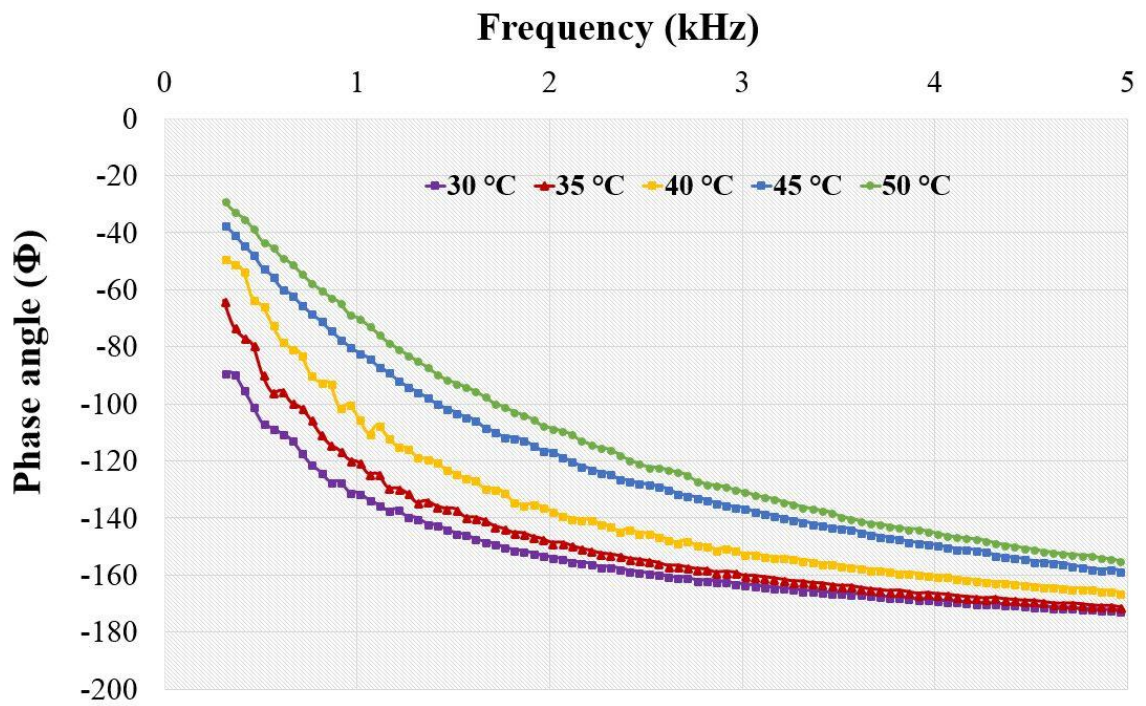


Figure 8.1 Response of the graphene – PI sensor patches towards different temperatures values ranging from 30 °C to 50 °C.

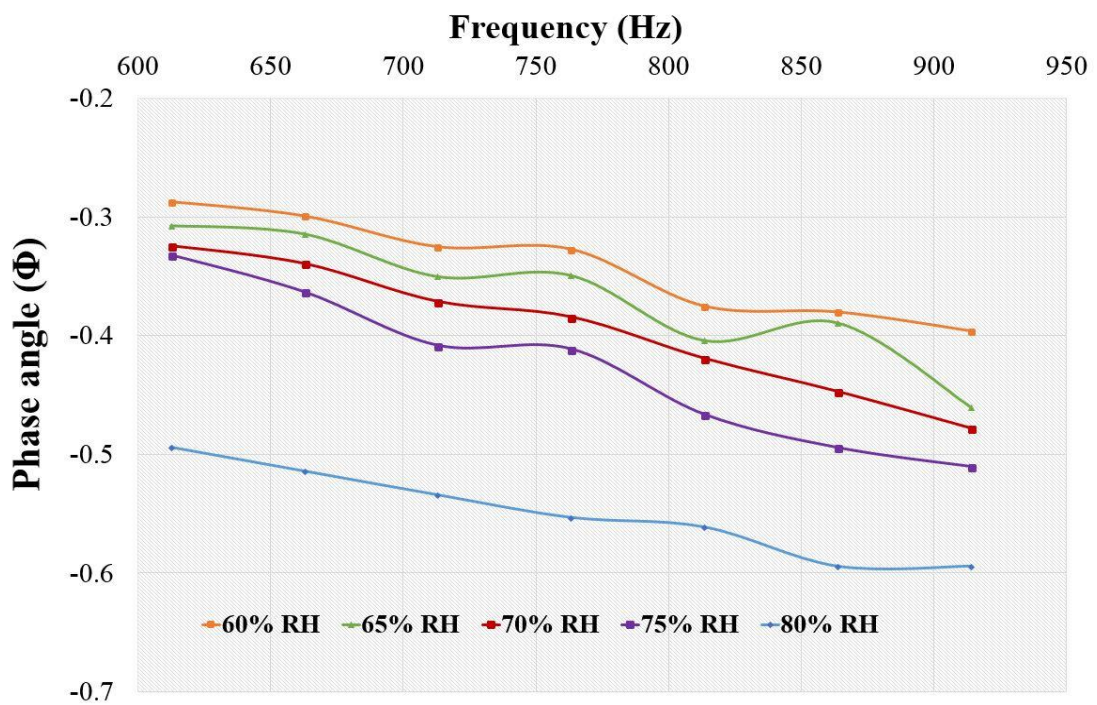


Figure 8.2 Response of the graphene – PI sensor patches towards different humidity values ranging from 60% RH to 80% RH.

There are some other suggestions that can be employed in the work portrayed here to achieve better results. Firstly, the developed sensor prototypes can be improved to fabricate new prototypes which are better than the existing ones in terms of size, robustness, sensitivity, reproducibility, and dynamicity. Printing technology holds a key role in future in the fabrication of new and better sensor prototypes that can be used for multi-function applications. Secondly, the materials that were used to develop the sensor prototypes during my doctoral tenure can be modified in terms of functionalisation to make advanced prototypes. For example, since the selectivity of a material holds a pivotal key in sensing applications, porous materials like graphene that are used to develop the electrodes, can be made selective to a target molecule in different applications. The selectivity of the electrodes can be done with different techniques like molecular imprinted polymer (MIP), non-imprinted polymer (NIP), ion-imprinted polymer (IIP), etc. The selectivity of the materials can also be induced in a way to ensure the reusability of the sensors. The modification of the processed materials can also be done in terms of functionalisation of the substrate and electrode materials to possess increased attributes as sensors. Thirdly, as with the developed sensor prototypes were related to printing technology, sensors developed with direct printing of nanocomposites can be done on flexible substrates to achieve optimised electrical and mechanical properties compared to the manual mixing of nano-fillers to the polymer matrix to form the nanocomposites. The direct printing of nanocomposites on the flexible substrates can be done with techniques like ink-jet printing and screen printing, where the droplets that are dribbled on the substrate are made into nanocomposites which will serve as electrodes for flexible sensors. Sensors with multi-structured layers can be formed with different polymers and conductive materials to give a compact, yet multi-function sensor prototype. The polymer materials along with the electrodes can be stacked on top of one another to operate in a conjugated manner.

There is a prominent future for flexible electronics in wearable systems based on its market values [469]. The market value of printed and flexible electronics is estimated to be over 75 billion USD by 2025 [470]. The estimated figures for the use of flexible sensing systems for the next 10-15 years have been mentioned along with the challenges that the flexible-sensing-system producing companies need to address. There is a substantial opportunity to use these flexible systems for monitoring health parameters. The estimated cost of WFSs by 2020 is more than 3 billion USD [471], and over 40 billion USD with more than 240 million annual unit shipments by 2025 [472]. The challenge for the companies is to design the systems to reduce in the overall fabrication cost. One way to

achieve this is to use cheap, safe and biocompatible materials for the designs. FlexEnable, a UK-based company, has predicted a rise in organic electronics among WFSs [473]. With growing interest of consumers, the companies should design systems which will serve the people, not only to meet the application purposes, but also at low cost; the systems should be made cost-effective so that they can address the wider community in the society. The scope of research work on this topic is increasing every day with the growth in its market value. The growth in MEMS along with Nanoelectromechanical (NEMS) technology is expected to reduce the cost of fabrication of the flexible sensing systems, leading to a wider range of applications in the near future. The utilisation of the existing manufacturing techniques along with upcoming ones will assist in developing new sensing systems and should help people to have a better quality of life in the near future.

References

- [1] S. Soloman, *Sensors handbook*: McGraw-Hill, Inc., 2009.
- [2] P. A. Oberg, *et al.*, *Sensors Applications, Sensors in Medicine and Health Care* vol. 3: John Wiley & Sons, 2006.
- [3] H. Muro, "History and recent progress of MEMS physical sensors," in *Advances in Science and Technology*, 2013, pp. 1-8.
- [4] J. Wang, "Glucose biosensors: 40 years of advances and challenges," *Electroanalysis*, vol. 13, p. 983, 2001.
- [5] H. Meixner, *et al.*, *Sensors, Micro-and Nanosensor Technology: Trends in Sensor Markets* vol. 8: John Wiley & Sons, 2008.
- [6] A. Nag, *et al.*, "Novel Sensing Approach for LPG Leakage Detection: Part I—Operating Mechanism and Preliminary Results," *IEEE Sensors Journal*, vol. 16, pp. 996-1003, 2016.
- [7] A. Nag, *et al.*, "Novel Sensing Approach for LPG Leakage Detection—Part II: Effects of Particle Size, Composition, and Coating Layer Thickness," *IEEE Sensors Journal*, vol. 16, pp. 1088-1094, 2016.
- [8] A. I. Zia, *et al.*, "Development of Electrochemical Impedance Spectroscopy based sensing system for DEHP detection," in *Sensing Technology (ICST), 2011 Fifth International Conference on*, 2011, pp. 666-674.
- [9] A. Mainwaring, *et al.*, "Wireless sensor networks for habitat monitoring," in *Proceedings of the 1st ACM international workshop on Wireless sensor networks and applications*, 2002, pp. 88-97.
- [10] R. Szewczyk, *et al.*, "Habitat monitoring with sensor networks," *Communications of the ACM*, vol. 47, pp. 34-40, 2004.
- [11] C. Otto, *et al.*, "System architecture of a wireless body area sensor network for ubiquitous health monitoring," *Journal of mobile multimedia*, vol. 1, pp. 307-326, 2006.
- [12] M. Segev-Bar and H. Haick, "Flexible sensors based on nanoparticles," *ACS nano*, vol. 7, pp. 8366-8378, 2013.
- [13] S. M. Sze, *Semiconductor sensors* vol. 55: Wiley New York, 1994.
- [14] A. I. Zia, *et al.*, "Introducing molecular selectivity in rapid impedimetric sensing of phthalates," in *Instrumentation and Measurement Technology Conference (I2MTC) Proceedings, 2014 IEEE International*, 2014, pp. 838-843.
- [15] A. Nag and S. C. Mukhopadhyay, "Smart Home: Recognition of activities of elderly for 24/7; Coverage issues," in *Proceedings of the 2014 International Conference on Sensing Technology, Liverpool, UK*, 2014, pp. 480-489.
- [16] A. Nag, *et al.*, "Flexible carbon nanotube nanocomposite sensor for multiple physiological parameter monitoring," *Sensors and Actuators A: Physical*, vol. 251, pp. 148-155, 2016.
- [17] M. S. A. Rahman, *et al.*, "Detection of bacterial endotoxin in food: New planar interdigital sensors based approach," *Journal of Food Engineering*, vol. 114, pp. 346-360, 2013.
- [18] M. S. A. Rahman, *et al.*, *Novel sensors for food inspection: Modelling, fabrication and experimentation*: Springer, 2014.
- [19] N. Suryadevara, *et al.*, "Sensor data fusion to determine wellness of an elderly in intelligent home monitoring environment," in *Instrumentation and Measurement Technology Conference (I2MTC), 2012 IEEE International*, 2012, pp. 947-952.
- [20] M. A. M. Yunus and S. C. Mukhopadhyay, "Development of planar electromagnetic sensors for measurement and monitoring of environmental parameters," *Measurement Science and Technology*, vol. 22, p. 025107, 2011.
- [21] S. C. Mukhopadhyay and C. P. Gooneratne, "A novel planar-type biosensor for noninvasive meat inspection," *Sensors Journal, IEEE*, vol. 7, pp. 1340-1346, 2007.
- [22] A. I. Zia, *et al.*, "Technique for rapid detection of phthalates in water and beverages," *Journal of Food Engineering*, vol. 116, pp. 515-523, 2013.
- [23] Y. Unno, *et al.*, "Development of n-on-p silicon sensors for very high radiation environments," *Nuclear Instruments and Methods in Physics Research Section A: Accelerators, Spectrometers, Detectors and Associated Equipment*, vol. 636, pp. S24-S30, 2011.
- [24] S. Patel, *et al.*, "A review of wearable sensors and systems with application in rehabilitation," *Journal of neuroengineering and rehabilitation*, vol. 9, p. 1, 2012.
- [25] A. Revzin, *et al.*, "Fabrication of poly (ethylene glycol) hydrogel microstructures using photolithography," *Langmuir*, vol. 17, pp. 5440-5447, 2001.
- [26] W.-Y. Chang, *et al.*, "A large area flexible array sensors using screen printing technology," *Journal of display technology*, vol. 5, pp. 178-183, 2009.

- [27] J. T. Muth, *et al.*, "Embedded 3D printing of strain sensors within highly stretchable elastomers," *Advanced Materials*, vol. 26, pp. 6307-6312, 2014.
- [28] C.-T. Wang, *et al.*, "A flexible proximity sensor fully fabricated by inkjet printing," *Sensors*, vol. 10, pp. 5054-5062, 2010.
- [29] M. Schuettler, *et al.*, "Fabrication of implantable microelectrode arrays by laser cutting of silicone rubber and platinum foil The work presented here was carried out at The University of Newcastle, Australia," *Journal of neural engineering*, vol. 2, p. S121, 2005.
- [30] B.-H. Jo, *et al.*, "Three-dimensional micro-channel fabrication in polydimethylsiloxane (PDMS) elastomer," *Journal of microelectromechanical systems*, vol. 9, pp. 76-81, 2000.
- [31] S. C. Mannsfeld, *et al.*, "Highly sensitive flexible pressure sensors with microstructured rubber dielectric layers," *Nature Materials*, vol. 9, pp. 859-864, 2010.
- [32] J. Cai, *et al.*, "Flexible thick-film electrochemical sensors: Impact of mechanical bending and stress on the electrochemical behavior," *Sensors and Actuators B: Chemical*, vol. 137, pp. 379-385, 2009.
- [33] J. Engel, *et al.*, "Development of polyimide flexible tactile sensor skin," *Journal of Micromechanics and Microengineering*, vol. 13, p. 359, 2003.
- [34] K. S. Karimov, *et al.*, "Novel pressure and displacement sensors based on carbon nanotubes," *中国物理 B: 英文版*, pp. 560-563, 2015.
- [35] S. Yao and Y. Zhu, "Wearable multifunctional sensors using printed stretchable conductors made of silver nanowires," *Nanoscale*, vol. 6, pp. 2345-2352, 2014.
- [36] H.-S. Kim, *et al.*, "Intense pulsed light sintering of copper nanoink for printed electronics," *Applied Physics A*, vol. 97, pp. 791-798, 2009.
- [37] S. Gong, *et al.*, "A wearable and highly sensitive pressure sensor with ultrathin gold nanowires," *Nature communications*, vol. 5, 2014.
- [38] A. Alfadhel, *et al.*, "A Magnetoresistive Tactile Sensor for Harsh Environment Applications," *Sensors*, vol. 16, p. 650, 2016.
- [39] Z. Yin, *et al.*, "Inkjet printing for flexible electronics: Materials, processes and equipments," *Chinese Science Bulletin*, vol. 55, pp. 3383-3407, 2010.
- [40] E. B. Secor, *et al.*, "Gravure printing of graphene for large-area flexible electronics," *Advanced Materials*, vol. 26, pp. 4533-4538, 2014.
- [41] S. Khan, *et al.*, "Technologies for printing sensors and electronics over large flexible substrates: a review," *IEEE Sensors Journal*, vol. 15, pp. 3164-3185, 2015.
- [42] D. Tobjörk and R. Österbacka, "Paper electronics," *Advanced Materials*, vol. 23, pp. 1935-1961, 2011.
- [43] M. A. Leenen, *et al.*, "Printable electronics: flexibility for the future," *physica status solidi (a)*, vol. 206, pp. 588-597, 2009.
- [44] V. Subramanian, *et al.*, "Printed electronics for low-cost electronic systems: Technology status and application development," in *Solid-State Device Research Conference, 2008. ESSDERC 2008. 38th European*, 2008, pp. 17-24.
- [45] R. S. Dahiya and S. Gennaro, "Bendable ultra-thin chips on flexible foils," *Sensors Journal, IEEE*, vol. 13, pp. 4030-4037, 2013.
- [46] K. Nomura, *et al.*, "Thin-film transistor fabricated in single-crystalline transparent oxide semiconductor," *Science*, vol. 300, pp. 1269-1272, 2003.
- [47] L. Zhang, *et al.*, "High performance ZnO-thin-film transistor with Ta 2 O 5 dielectrics fabricated at room temperature," *Applied Physics Letters*, vol. 95, p. 072112, 2009.
- [48] R. F. Pease and S. Y. Chou, "Lithography and other patterning techniques for future electronics," *Proceedings of the IEEE*, vol. 96, pp. 248-270, 2008.
- [49] K. H. Choi, *et al.*, "Electrohydrodynamic spray deposition of ZnO nanoparticles," *Japanese journal of applied physics*, vol. 49, p. 05EC08, 2010.
- [50] Y. Li, *et al.*, "Facile synthesis of silver nanoparticles useful for fabrication of high-conductivity elements for printed electronics," *Journal of the American Chemical Society*, vol. 127, pp. 3266-3267, 2005.
- [51] N. A. Luechinger, *et al.*, "Graphene-stabilized copper nanoparticles as an air-stable substitute for silver and gold in low-cost ink-jet printable electronics," *Nanotechnology*, vol. 19, p. 445201, 2008.
- [52] Y. Lee, *et al.*, "Large-scale synthesis of copper nanoparticles by chemically controlled reduction for applications of inkjet-printed electronics," *Nanotechnology*, vol. 19, p. 415604, 2008.
- [53] Y. Zhou, *et al.*, "A universal method to produce low-work function electrodes for organic electronics," *Science*, vol. 336, pp. 327-332, 2012.

- [54] G. B. Blanchet, *et al.*, "Large area, high resolution, dry printing of conducting polymers for organic electronics," *Applied Physics Letters*, vol. 82, pp. 463-465, 2003.
- [55] A. Kamyshny and S. Magdassi, "Conductive nanomaterials for printed electronics," *Small*, vol. 10, pp. 3515-3535, 2014.
- [56] A. Sawhney, *et al.*, "Piezoresistive sensors on textiles by inkjet printing and electroless plating," *MRS Online Proceedings Library Archive*, vol. 920, 2006.
- [57] K. Crowley, *et al.*, "Fabrication of an ammonia gas sensor using inkjet-printed polyaniline nanoparticles," *Talanta*, vol. 77, pp. 710-717, 2008.
- [58] B. Li, *et al.*, "Inkjet printed chemical sensor array based on polythiophene conductive polymers," *Sensors and Actuators B: Chemical*, vol. 123, pp. 651-660, 2007.
- [59] C. Sriprachubwong, *et al.*, "Inkjet-printed graphene-PEDOT: PSS modified screen printed carbon electrode for biochemical sensing," *Journal of Materials Chemistry*, vol. 22, pp. 5478-5485, 2012.
- [60] R. S. Dahiya, *et al.*, "Fabrication of single crystal silicon micro-/nanostructures and transferring them to flexible substrates," *Microelectronic Engineering*, vol. 98, pp. 502-507, 2012.
- [61] E. Fortunato, *et al.*, "High-performance flexible hybrid field-effect transistors based on cellulose fiber paper," *IEEE Electron Device Letters*, vol. 29, pp. 988-990, 2008.
- [62] S. B. Sinnott and R. Andrews, "Carbon nanotubes: synthesis, properties, and applications," *Critical Reviews in Solid State and Materials Sciences*, vol. 26, pp. 145-249, 2001.
- [63] T. W. Odom, *et al.*, "Single-Walled Carbon Nanotubes," *Annals of the New York Academy of Sciences*, vol. 960, pp. 203-215, 2002.
- [64] C. E. Carraher Jr, *Carraher's polymer chemistry*: CRC Press, 2016.
- [65] Y. Ando and S. Iijima, "Preparation of carbon nanotubes by arc-discharge evaporation," *JAPANESE JOURNAL OF APPLIED PHYSICS PART 2 LETTERS*, vol. 32, pp. L107-L107, 1993.
- [66] J. Hutchison, *et al.*, "Double-walled carbon nanotubes fabricated by a hydrogen arc discharge method," *Carbon*, vol. 39, pp. 761-770, 2001.
- [67] W.-W. Liu, *et al.*, "Synthesis and characterization of graphene and carbon nanotubes: A review on the past and recent developments," *Journal of Industrial and Engineering Chemistry*, vol. 20, pp. 1171-1185, 2014.
- [68] S.-P. Chai, *et al.*, "The effect of reduction temperature on Co-Mo/Al₂O₃ catalysts for carbon nanotubes formation," *Applied Catalysis A: General*, vol. 326, pp. 173-179, 2007.
- [69] Y. Ando, *et al.*, "Mass production of multiwalled carbon nanotubes by hydrogen arc discharge," *Journal of Crystal Growth*, vol. 237, pp. 1926-1930, 2002.
- [70] C. Journet, *et al.*, "Large-scale production of single-walled carbon nanotubes by the electric-arc technique," *Nature*, vol. 388, pp. 756-758, 1997.
- [71] T. Guo, *et al.*, "Catalytic growth of single-walled nanotubes by laser vaporization," *Chemical physics letters*, vol. 243, pp. 49-54, 1995.
- [72] S. Lebedkin, *et al.*, "Single-wall carbon nanotubes with diameters approaching 6 nm obtained by laser vaporization," *Carbon*, vol. 40, pp. 417-423, 2002.
- [73] S. Lebedkin, *et al.*, "Near-infrared photoluminescence of single-walled carbon nanotubes prepared by the laser vaporization method," *The Journal of Physical Chemistry B*, vol. 107, pp. 1949-1956, 2003.
- [74] E. Flahaut, *et al.*, "Catalytic CVD synthesis of double and triple-walled carbon nanotubes by the control of the catalyst preparation," *Carbon*, vol. 43, pp. 375-383, 2005.
- [75] Y. Li, *et al.*, "Preparation of monodispersed Fe-Mo nanoparticles as the catalyst for CVD synthesis of carbon nanotubes," *Chemistry of Materials*, vol. 13, pp. 1008-1014, 2001.
- [76] L. C. QIN, "CVD synthesis of carbon nanotubes," *Journal of Materials Science Letters*, vol. 16, pp. 457-459, 1997.
- [77] R. J. Chen, *et al.*, "Noncovalent sidewall functionalization of single-walled carbon nanotubes for protein immobilization," *Journal of the American Chemical Society*, vol. 123, pp. 3838-3839, 2001.
- [78] S. Maruyama, *et al.*, "Low-temperature synthesis of high-purity single-walled carbon nanotubes from alcohol," *Chemical physics letters*, vol. 360, pp. 229-234, 2002.
- [79] C. Li and T.-W. Chou, "Elastic moduli of multi-walled carbon nanotubes and the effect of van der Waals forces," *Composites Science and Technology*, vol. 63, pp. 1517-1524, 2003.
- [80] R. Andrews, *et al.*, "Continuous production of aligned carbon nanotubes: a step closer to commercial realization," *Chemical physics letters*, vol. 303, pp. 467-474, 1999.
- [81] Y. Zhang, *et al.*, "Electric-field-directed growth of aligned single-walled carbon nanotubes," *Applied Physics Letters*, vol. 79, pp. 3155-3157, 2001.

- [82] H. Wang, "Dispersing carbon nanotubes using surfactants," *Current Opinion in Colloid & Interface Science*, vol. 14, pp. 364-371, 2009.
- [83] T. Saito, *et al.*, "Chemical treatment and modification of multi-walled carbon nanotubes," *Physica B: Condensed Matter*, vol. 323, pp. 280-283, 2002.
- [84] G. Y. Li, *et al.*, "Mechanical behavior and microstructure of cement composites incorporating surface-treated multi-walled carbon nanotubes," *Carbon*, vol. 43, pp. 1239-1245, 2005.
- [85] H. Kuzmany, *et al.*, "Functionalization of carbon nanotubes," *Synthetic Metals*, vol. 141, pp. 113-122, 2004.
- [86] M. M. Barsan, *et al.*, "Electrochemical sensors and biosensors based on redox polymer/carbon nanotube modified electrodes: a review," *Analytica chimica acta*, vol. 881, pp. 1-23, 2015.
- [87] A. Ahammad, *et al.*, "Electrochemical sensors based on carbon nanotubes," *Sensors*, vol. 9, pp. 2289-2319, 2009.
- [88] Z.-H. Jin, *et al.*, "Conductive Polymer Coated Carbon Nanotubes to Construct Stretchable and Transparent Electrochemical Sensors," *Analytical chemistry*, 2016.
- [89] A. P. Periasamy, *et al.*, "Amperometric glucose sensor based on glucose oxidase immobilized on gelatin-multiwalled carbon nanotube modified glassy carbon electrode," *Bioelectrochemistry*, vol. 80, pp. 114-120, 2011.
- [90] M. Kaempgen and S. Roth, "Transparent and flexible carbon nanotube/polyaniline pH sensors," *Journal of Electroanalytical Chemistry*, vol. 586, pp. 72-76, 2006.
- [91] D. Lee and T. Cui, "Low-cost, transparent, and flexible single-walled carbon nanotube nanocomposite based ion-sensitive field-effect transistors for pH/glucose sensing," *Biosensors and Bioelectronics*, vol. 25, pp. 2259-2264, 2010.
- [92] J.-D. Qiu, *et al.*, "Amperometric sensor based on ferrocene-modified multiwalled carbon nanotube nanocomposites as electron mediator for the determination of glucose," *Analytical biochemistry*, vol. 385, pp. 264-269, 2009.
- [93] S. H. Lim, *et al.*, "A glucose biosensor based on electrodeposition of palladium nanoparticles and glucose oxidase onto Nafion-solubilized carbon nanotube electrode," *Biosensors and Bioelectronics*, vol. 20, pp. 2341-2346, 2005.
- [94] K.-Y. Hwa and B. Subramani, "Synthesis of zinc oxide nanoparticles on graphene-carbon nanotube hybrid for glucose biosensor applications," *Biosensors and Bioelectronics*, vol. 62, pp. 127-133, 2014.
- [95] X.-H. Pham, *et al.*, "Electrochemical characterization of a single-walled carbon nanotube electrode for detection of glucose," *Analytica chimica acta*, vol. 671, pp. 36-40, 2010.
- [96] Y.-S. Chien, *et al.*, "A novel pH sensor of extended-gate field-effect transistors with laser-irradiated carbon-nanotube network," *IEEE Electron Device Letters*, vol. 33, pp. 1622-1624, 2012.
- [97] A. Münzer, *et al.*, "Random CNT network and regioregular poly (3-hexylthiophen) FETs for pH sensing applications: A comparison," *Biochimica et Biophysica Acta (BBA)-General Subjects*, vol. 1830, pp. 4353-4358, 2013.
- [98] D. Jung, *et al.*, "pH-sensing characteristics of multi-walled carbon nanotube sheet," *Materials Letters*, vol. 116, pp. 57-60, 2014.
- [99] J. Zhou, *et al.*, "Ultrasensitive, Stretchable Strain Sensors Based on Fragmented Carbon Nanotube Papers," *ACS applied materials & interfaces*, vol. 9, pp. 4835-4842, 2017.
- [100] J. Hwang, *et al.*, "Poly (3-hexylthiophene) wrapped carbon nanotube/poly (dimethylsiloxane) composites for use in finger-sensing piezoresistive pressure sensors," *Carbon*, vol. 49, pp. 106-110, 2011.
- [101] N.-K. Chang, *et al.*, "Fabrication of single-walled carbon nanotube flexible strain sensors with high sensitivity," *Applied Physics Letters*, vol. 92, p. 063501, 2008.
- [102] M. Vatani, *et al.*, "Force and slip detection with direct-write compliant tactile sensors using multi-walled carbon nanotube/polymer composites," *Sensors and Actuators A: Physical*, vol. 195, pp. 90-97, 2013.
- [103] X. Yu, *et al.*, "Carbon nanotube-based transparent thin film acoustic actuators and sensors," *Sensors and Actuators A: Physical*, vol. 132, pp. 626-631, 2006.
- [104] D. J. Lipomi, *et al.*, "Skin-like pressure and strain sensors based on transparent elastic films of carbon nanotubes," *Nature nanotechnology*, vol. 6, pp. 788-792, 2011.
- [105] C. Li, *et al.*, "Flexible CNT-array double helices Strain Sensor with high stretchability for Motion Capture," *Scientific reports*, vol. 5, p. 15554, 2015.
- [106] J. Zhou, *et al.*, "Deformable and wearable carbon nanotube microwire-based sensors for ultrasensitive monitoring of strain, pressure and torsion," *Nanoscale*, vol. 9, pp. 604-612, 2017.

- [107] A. Sanli, *et al.*, "Piezoresistive performance characterization of strain sensitive multi-walled carbon nanotube-epoxy nanocomposites," *Sensors and Actuators A: Physical*, vol. 254, pp. 61-68, 2017.
- [108] S. Zhao, *et al.*, "Strain-driven and ultrasensitive resistive sensor/switch based on conductive alginate/nitrogen-doped carbon-nanotube-supported Ag hybrid aerogels with pyramid design," *ACS applied materials & interfaces*, vol. 6, pp. 22823-22829, 2014.
- [109] E. Roh, *et al.*, "Stretchable, transparent, ultrasensitive, and patchable strain sensor for human-machine interfaces comprising a nanohybrid of carbon nanotubes and conductive elastomers," *ACS nano*, vol. 9, pp. 6252-6261, 2015.
- [110] M. Amjadi and I. Park, "Carbon nanotubes-ecoflex nanocomposite for strain sensing with ultra-high stretchability," in *Micro Electro Mechanical Systems (MEMS), 2015 28th IEEE International Conference on*, 2015, pp. 744-747.
- [111] H. Nakamoto, *et al.*, "Stretchable strain sensor based on areal change of carbon nanotube electrode," *IEEE Sensors Journal*, vol. 15, pp. 2212-2218, 2015.
- [112] M. Amjadi, *et al.*, "Ultra-stretchable and skin-mountable strain sensors using carbon nanotubes-Ecoflex nanocomposites," *Nanotechnology*, vol. 26, p. 375501, 2015.
- [113] S. Zhang, *et al.*, "Highly stretchable, sensitive, and flexible strain sensors based on silver nanoparticles/carbon nanotubes composites," *Journal of alloys and compounds*, vol. 652, pp. 48-54, 2015.
- [114] H. Souri, *et al.*, "Electrical properties and piezoresistive evaluation of polyurethane-based composites with carbon nano-materials," *Composites Science and Technology*, vol. 121, pp. 41-48, 2015.
- [115] Y. Ding, *et al.*, "A highly stretchable strain sensor based on electrospun carbon nanofibers for human motion monitoring," *RSC Advances*, vol. 6, pp. 79114-79120, 2016.
- [116] Y. Wang, *et al.*, "Highly stretchable and sensitive piezoresistive carbon nanotube/elastomeric triisocyanate-crosslinked polytetrahydrofuran nanocomposites," *Journal of Materials Chemistry C*, vol. 4, pp. 460-467, 2016.
- [117] S. Zhao, *et al.*, "Percolation threshold-inspired design of hierarchical multiscale hybrid architectures based on carbon nanotubes and silver nanoparticles for stretchable and printable electronics," *Journal of Materials Chemistry C*, vol. 4, pp. 6666-6674, 2016.
- [118] M. Lim, *et al.*, "Comparative study of piezoresistance effect of semiconducting carbon nanotube-Polydimethylsiloxane nanocomposite strain sensor," in *Nanotechnology (IEEE-NANO), 2016 IEEE 16th International Conference on*, 2016, pp. 755-758.
- [119] S. J. Park, *et al.*, "Highly Flexible Wrinkled Carbon Nanotube Thin Film Strain Sensor to Monitor Human Movement," *Advanced Materials Technologies*, vol. 1, 2016.
- [120] M. Park, *et al.*, "Strain-dependent electrical resistance of multi-walled carbon nanotube/polymer composite films," *Nanotechnology*, vol. 19, p. 055705, 2008.
- [121] K. J. Loh, *et al.*, "Multifunctional layer-by-layer carbon nanotube-polyelectrolyte thin films for strain and corrosion sensing," *Smart Materials and Structures*, vol. 16, p. 429, 2007.
- [122] O. Kanoun, *et al.*, "Flexible carbon nanotube films for high performance strain sensors," *Sensors*, vol. 14, pp. 10042-10071, 2014.
- [123] F. Michelis, *et al.*, "Wireless flexible strain sensor based on carbon nanotube piezoresistive networks for embedded measurement of strain in concrete," in *EWSHM-7th European Workshop on Structural Health Monitoring*, 2014.
- [124] C. Yan, *et al.*, "Highly stretchable piezoresistive graphene-nanocellulose nanopaper for strain sensors," *Advanced Materials*, vol. 26, pp. 2022-2027, 2014.
- [125] H. Dai, *et al.*, "Processing and characterization of a novel distributed strain sensor using carbon nanotube-based nonwoven composites," *Sensors*, vol. 15, pp. 17728-17747, 2015.
- [126] G. R. Choi, *et al.*, "Strain Sensing Characteristics of Rubbery Carbon Nanotube Composite for Flexible Sensors," *Journal of nanoscience and nanotechnology*, vol. 16, pp. 1607-1611, 2016.
- [127] S. Tadakaluru, *et al.*, "Stretchable and flexible high-strain sensors made using carbon nanotubes and graphite films on natural rubber," *Sensors*, vol. 14, pp. 868-876, 2014.
- [128] Q. Cao, *et al.*, "Medium-scale carbon nanotube thin-film integrated circuits on flexible plastic substrates," *Nature*, vol. 454, pp. 495-500, 2008.
- [129] D. Jariwala, *et al.*, "Carbon nanomaterials for electronics, optoelectronics, photovoltaics, and sensing," *Chemical Society Reviews*, vol. 42, pp. 2824-2860, 2013.
- [130] Y. Yin and D. Talapin, "The chemistry of functional nanomaterials," *Chemical Society Reviews*, vol. 42, pp. 2484-2487, 2013.

- [131] H. N. Arnold and M. C. Hersam, "Optoelectronic Applications of Monodisperse Carbon Nanomaterials," in *The Wonder of Nanotechnology: Quantum Optoelectronic Devices and Applications*, ed: SPIE, 2013.
- [132] P. H. Lau, *et al.*, "Fully printed, high performance carbon nanotube thin-film transistors on flexible substrates," *Nano Letters*, vol. 13, pp. 3864-3869, 2013.
- [133] A. K. Geim and K. S. Novoselov, "The rise of graphene," *Nature Materials*, vol. 6, pp. 183-191, 2007.
- [134] P. R. Wallace, "The band theory of graphite," *Physical Review*, vol. 71, p. 622, 1947.
- [135] K. Novoselov, *et al.*, "Two-dimensional atomic crystals," *Proceedings of the National Academy of Sciences of the United States of America*, vol. 102, pp. 10451-10453, 2005.
- [136] F. V. Ferreira, *et al.*, "Functionalization of Graphene and Applications," in *Functionalizing Graphene and Carbon Nanotubes*, ed: Springer, 2016, pp. 1-29.
- [137] K. S. Novoselov, *et al.*, "A roadmap for graphene," *Nature*, vol. 490, pp. 192-200, 2012.
- [138] X. Wang, *et al.*, "N-Doped Graphene-SnO₂ Sandwich Paper for High-Performance Lithium-Ion Batteries," *Advanced Functional Materials*, vol. 22, pp. 2682-2690, 2012.
- [139] M. Liu, *et al.*, "Graphene-supported nanoelectrocatalysts for fuel cells: synthesis, properties, and applications," *Chemical reviews*, vol. 114, pp. 5117-5160, 2014.
- [140] Y. Zhao, *et al.*, "Review on the graphene based optical fiber chemical and biological sensors," *Sensors and Actuators B: Chemical*, vol. 231, pp. 324-340, 2016.
- [141] A. Capasso, *et al.*, "Ink-jet printing of graphene for flexible electronics: an environmentally-friendly approach," *Solid State Communications*, vol. 224, pp. 53-63, 2015.
- [142] B. F. Machado and P. Serp, "Graphene-based materials for catalysis," *Catalysis Science & Technology*, vol. 2, pp. 54-75, 2012.
- [143] T. Kuila, *et al.*, "Chemical functionalization of graphene and its applications," *Progress in Materials Science*, vol. 57, pp. 1061-1105, 2012.
- [144] *Graphene sensors: introduction and market status*. Available: <https://www.graphene-info.com/graphene-sensors>. Last accessed on 31st October, 2018.
- [145] M. Pumera, "Graphene in biosensing," *Materials Today*, vol. 14, pp. 308-315, 2011.
- [146] X. Li, *et al.*, "Stretchable and highly sensitive graphene-on-polymer strain sensors," *Scientific reports*, vol. 2, p. 870, 2012.
- [147] Q. Liu, *et al.*, "High-quality graphene ribbons prepared from graphene oxide hydrogels and their application for strain sensors," *ACS nano*, vol. 9, pp. 12320-12326, 2015.
- [148] Y. R. Jeong, *et al.*, "Highly stretchable and sensitive strain sensors using fragmented graphene foam," *Advanced Functional Materials*, vol. 25, pp. 4228-4236, 2015.
- [149] J. Zhao, *et al.*, "Ultra-sensitive strain sensors based on piezoresistive nanographene films," *Applied Physics Letters*, vol. 101, p. 063112, 2012.
- [150] A. H. Pourasl, *et al.*, "Analytical modeling of glucose biosensors based on carbon nanotubes," *Nanoscale research letters*, vol. 9, p. 33, 2014.
- [151] T. Yamada, *et al.*, "A stretchable carbon nanotube strain sensor for human-motion detection," *Nature nanotechnology*, vol. 6, pp. 296-301, 2011.
- [152] D. J. Cohen, *et al.*, "A highly elastic, capacitive strain gauge based on percolating nanotube networks," *Nano Letters*, vol. 12, pp. 1821-1825, 2012.
- [153] U.-H. Shin, *et al.*, "Highly stretchable conductors and piezocapacitive strain gauges based on simple contact-transfer patterning of carbon nanotube forests," *Carbon*, vol. 80, pp. 396-404, 2014.
- [154] L. Cai, *et al.*, "Super-stretchable, transparent carbon nanotube-based capacitive strain sensors for human motion detection," *Scientific reports*, vol. 3, p. 3048, 2013.
- [155] M. Amjadi, *et al.*, "Highly stretchable and sensitive strain sensor based on silver nanowire-elastomer nanocomposite," *ACS nano*, vol. 8, pp. 5154-5163, 2014.
- [156] B.-U. Hwang, *et al.*, "Transparent stretchable self-powered patchable sensor platform with ultrasensitive recognition of human activities," *ACS nano*, vol. 9, pp. 8801-8810, 2015.
- [157] F. Xu and Y. Zhu, "Highly conductive and stretchable silver nanowire conductors," *Advanced Materials*, vol. 24, pp. 5117-5122, 2012.
- [158] W. Hu, *et al.*, "Elastomeric transparent capacitive sensors based on an interpenetrating composite of silver nanowires and polyurethane," *Applied Physics Letters*, vol. 102, p. 38, 2013.
- [159] K. Takei, *et al.*, "Highly sensitive electronic whiskers based on patterned carbon nanotube and silver nanoparticle composite films," *Proceedings of the National Academy of Sciences*, vol. 111, pp. 1703-1707, 2014.

- [160] S. Alwarappan, *et al.*, "Enzyme-doped graphene nanosheets for enhanced glucose biosensing," *The Journal of Physical Chemistry C*, vol. 114, pp. 12920-12924, 2010.
- [161] P. Wu, *et al.*, "Direct electrochemistry of glucose oxidase assembled on graphene and application to glucose detection," *Electrochimica Acta*, vol. 55, pp. 8606-8614, 2010.
- [162] K. Wang, *et al.*, "Enhanced direct electrochemistry of glucose oxidase and biosensing for glucose via synergy effect of graphene and CdS nanocrystals," *Biosensors and Bioelectronics*, vol. 26, pp. 2252-2257, 2011.
- [163] H. Razmi and R. Mohammad-Rezaei, "Graphene quantum dots as a new substrate for immobilization and direct electrochemistry of glucose oxidase: application to sensitive glucose determination," *Biosensors and Bioelectronics*, vol. 41, pp. 498-504, 2013.
- [164] Q. Zeng, *et al.*, "Palladium nanoparticle/chitosan-grafted graphene nanocomposites for construction of a glucose biosensor," *Biosensors and Bioelectronics*, vol. 26, pp. 3456-3463, 2011.
- [165] L. Viry, *et al.*, "Carbon nanotube fiber microelectrodes: Design, characterization, and optimization," *Journal of nanoscience and nanotechnology*, vol. 7, pp. 3373-3377, 2007.
- [166] Y. Shao, *et al.*, "Graphene based electrochemical sensors and biosensors: a review," *Electroanalysis*, vol. 22, pp. 1027-1036, 2010.
- [167] P. R. Solanki, *et al.*, "Multi-walled carbon nanotubes/sol-gel-derived silica/chitosan nanobiocomposite for total cholesterol sensor," *Sensors and Actuators B: Chemical*, vol. 137, pp. 727-735, 2009.
- [168] P. Gou, *et al.*, "Carbon nanotube chemiresistor for wireless pH sensing," *Scientific reports*, vol. 4, 2014.
- [169] L.-C. Jiang and W.-D. Zhang, "A highly sensitive nonenzymatic glucose sensor based on CuO nanoparticles-modified carbon nanotube electrode," *Biosensors and Bioelectronics*, vol. 25, pp. 1402-1407, 2010.
- [170] E. Kurowska, *et al.*, "Silver nanowire array sensor for sensitive and rapid detection of H₂O₂," *Electrochimica Acta*, vol. 104, pp. 439-447, 2013.
- [171] L.-M. Lu, *et al.*, "A nano-Ni based ultrasensitive nonenzymatic electrochemical sensor for glucose: enhancing sensitivity through a nanowire array strategy," *Biosensors and Bioelectronics*, vol. 25, pp. 218-223, 2009.
- [172] M.-J. Song, *et al.*, "Amperometric hydrogen peroxide biosensor based on a modified gold electrode with silver nanowires," *Journal of applied electrochemistry*, vol. 40, pp. 2099-2105, 2010.
- [173] J. Yin, *et al.*, "A hydrogen peroxide electrochemical sensor based on silver nanoparticles decorated silicon nanowire arrays," *Electrochimica Acta*, vol. 56, pp. 3884-3889, 2011.
- [174] Y. Zhu, *et al.*, "Application of ion-sensitive field effect transistors for measuring glial cell K⁺ transport," in *SENSORS, 2016 IEEE*, 2016, pp. 1-3.
- [175] D. Kireev, *et al.*, "Graphene Field-Effect Transistors for In Vitro and Ex Vivo Recordings," *IEEE Transactions on Nanotechnology*, vol. 16, pp. 140-147, 2017.
- [176] M. Marchena, *et al.*, "Direct growth of 2D and 3D graphene nano-structures over large glass substrates by tuning a sacrificial Cu-template layer," *2D Materials*, 2017.
- [177] M. Lavin-Lopez, *et al.*, "Improving the growth of monolayer CVD-graphene over polycrystalline iron sheets," *New Journal of Chemistry*, vol. 41, pp. 5066-5074, 2017.
- [178] N. Woehrl, *et al.*, "Plasma-enhanced chemical vapor deposition of graphene on copper substrates," *AIP Advances*, vol. 4, p. 047128, 2014.
- [179] M. Li, *et al.*, "Controllable Synthesis of Graphene by Plasma-Enhanced Chemical Vapor Deposition and Its Related Applications," *Advanced Science*, vol. 3, 2016.
- [180] J. Kim, *et al.*, "Low-temperature synthesis of large-area graphene-based transparent conductive films using surface wave plasma chemical vapor deposition," *Applied Physics Letters*, vol. 98, p. 091502, 2011.
- [181] Y. Kim, *et al.*, "Low-temperature synthesis of graphene on nickel foil by microwave plasma chemical vapor deposition," *Applied Physics Letters*, vol. 98, p. 263106, 2011.
- [182] S. Lee, *et al.*, "Wafer scale homogeneous bilayer graphene films by chemical vapor deposition," *Nano Letters*, vol. 10, pp. 4702-4707, 2010.
- [183] H. J. Park, *et al.*, "Growth and properties of few-layer graphene prepared by chemical vapor deposition," *Carbon*, vol. 48, pp. 1088-1094, 2010.
- [184] M. Losurdo, *et al.*, "Graphene CVD growth on copper and nickel: role of hydrogen in kinetics and structure," *Physical Chemistry Chemical Physics*, vol. 13, pp. 20836-20843, 2011.
- [185] C. e. N. e. R. Rao, *et al.*, "Graphene: the new two-dimensional nanomaterial," *Angewandte Chemie International Edition*, vol. 48, pp. 7752-7777, 2009.

- [186] K. S. Novoselov, *et al.*, "Electric field effect in atomically thin carbon films," *Science*, vol. 306, pp. 666-669, 2004.
- [187] V. Huc, *et al.*, "Large and flat graphene flakes produced by epoxy bonding and reverse exfoliation of highly oriented pyrolytic graphite," *Nanotechnology*, vol. 19, p. 455601, 2008.
- [188] X. Li, *et al.*, "Highly conducting graphene sheets and Langmuir–Blodgett films," *Nature nanotechnology*, vol. 3, pp. 538-542, 2008.
- [189] J. Chen, *et al.*, "An improved Hummers method for eco-friendly synthesis of graphene oxide," *Carbon*, vol. 64, pp. 225-229, 2013.
- [190] N. Zaaba, *et al.*, "Synthesis of Graphene Oxide using Modified Hummers Method: Solvent Influence," *Procedia Engineering*, vol. 184, pp. 469-477, 2017.
- [191] Z.-S. Wu, *et al.*, "Synthesis of high-quality graphene with a pre-determined number of layers," *Carbon*, vol. 47, pp. 493-499, 2009.
- [192] W. Chen and L. Yan, "Preparation of graphene by a low-temperature thermal reduction at atmosphere pressure," *Nanoscale*, vol. 2, pp. 559-563, 2010.
- [193] A. K. Geim, "Nobel Lecture: Random walk to graphene," *Reviews of modern physics*, vol. 83, p. 851, 2011.
- [194] R. Mas-Balleste, *et al.*, "2D materials: to graphene and beyond," *Nanoscale*, vol. 3, pp. 20-30, 2011.
- [195] *Power of graphene activity*. Available: <http://www.discovere.org/sites/default/files/Power%20of%20Graphene%20activity.pdf>. Last accessed on 31st October, 2018.
- [196] M. Yi and Z. Shen, "A review on mechanical exfoliation for the scalable production of graphene," *Journal of Materials Chemistry A*, vol. 3, pp. 11700-11715, 2015.
- [197] G. Ruan, *et al.*, "Growth of graphene from food, insects, and waste," *ACS nano*, vol. 5, pp. 7601-7607, 2011.
- [198] I. Roy, *et al.*, "Synthesis and characterization of graphene from waste dry cell battery for electronic applications," *RSC Advances*, vol. 6, pp. 10557-10564, 2016.
- [199] T. Somanathan, *et al.*, "Graphene oxide synthesis from agro waste," *Nanomaterials*, vol. 5, pp. 826-834, 2015.
- [200] W. Chen, *et al.*, "Chemical reduction of graphene oxide to graphene by sulfur-containing compounds," *The Journal of Physical Chemistry C*, vol. 114, pp. 19885-19890, 2010.
- [201] H.-K. Seo, *et al.*, "Value-added synthesis of graphene: recycling industrial carbon waste into electrodes for high-performance electronic devices," *Scientific reports*, vol. 5, p. 16710, 2015.
- [202] Y.-J. Kim, *et al.*, "Engineering electrical properties of graphene: chemical approaches," *2D Materials*, vol. 2, p. 042001, 2015.
- [203] Y. You, *et al.*, "Hierarchically micro/mesoporous activated graphene with a large surface area for high sulfur loading in Li–S batteries," *Journal of Materials Chemistry A*, vol. 3, pp. 4799-4802, 2015.
- [204] F. Bonaccorso, *et al.*, "Graphene photonics and optoelectronics," *Nature photonics*, vol. 4, pp. 611-622, 2010.
- [205] J.-N. Fuchs and M. O. Goerbig, "Introduction to the physical properties of graphene," *Lecture notes*, 2008.
- [206] A. C. Neto, *et al.*, "The electronic properties of graphene," *Reviews of modern physics*, vol. 81, p. 109, 2009.
- [207] F. Sattari, "Calculation of current density for graphene superlattice in a constant electric field," *Journal of Theoretical and Applied Physics*, vol. 9, p. 81, 2015.
- [208] K. I. Bolotin, *et al.*, "Ultrahigh electron mobility in suspended graphene," *Solid State Communications*, vol. 146, pp. 351-355, 2008.
- [209] Z. Xu and C. Gao, "Graphene fiber: a new trend in carbon fibers," *Materials Today*, vol. 18, pp. 480-492, 2015.
- [210] E. Pop, *et al.*, "Thermal properties of graphene: Fundamentals and applications," *MRS bulletin*, vol. 37, pp. 1273-1281, 2012.
- [211] C.-W. Huang, *et al.*, "Observing the evolution of graphene layers at high current density," *Nano Research*, vol. 9, pp. 3663-3670, 2016.
- [212] A. Sakhaee-Pour, "Elastic properties of single-layered graphene sheet," *Solid State Communications*, vol. 149, pp. 91-95, 2009.
- [213] L. Donaldson, "Porous 3D graphene that is stronger than steel," ed: Elsevier, 2017.
- [214] *Use of graphene in planes*. Available: <http://www.graphene.manchester.ac.uk/discover/video-gallery/what-is-graphene/graphene-planes/>. Last accessed on 31st October, 2018.

- [215] M. Biron, *Thermoplastics and thermoplastic composites*: William Andrew, 2012.
- [216] K. Zhou, *et al.*, "The influence of graphene based smoke suppression agents on reduced fire hazards of polystyrene composites," *Composites Part A: Applied Science and Manufacturing*, vol. 80, pp. 217-227, 2016.
- [217] H. I. Rasool, *et al.*, "Atomic-scale characterization of graphene grown on copper (100) single crystals," *Journal of the American Chemical Society*, vol. 133, pp. 12536-12543, 2011.
- [218] L. Jiang, *et al.*, "Preparation and characterization of graphene/poly (vinyl alcohol) nanocomposites," *Journal of applied polymer science*, vol. 118, pp. 275-279, 2010.
- [219] Y. Xu, *et al.*, "Flexible graphene films via the filtration of water-soluble noncovalent functionalized graphene sheets," *Journal of the American Chemical Society*, vol. 130, pp. 5856-5857, 2008.
- [220] S. Chaiyakun, *et al.*, "Preparation and characterization of graphene oxide nanosheets," *Procedia Engineering*, vol. 32, pp. 759-764, 2012.
- [221] J. Song, *et al.*, "Preparation and characterization of graphene oxide," *Journal of Nanomaterials*, vol. 2014, 2014.
- [222] F. Yavari and N. Koratkar, "Graphene-based chemical sensors," *The journal of physical chemistry letters*, vol. 3, pp. 1746-1753, 2012.
- [223] C. Wang, *et al.*, "A novel hydrazine electrochemical sensor based on the high specific surface area graphene," *Microchimica Acta*, vol. 169, pp. 1-6, 2010.
- [224] Z. Wang, *et al.*, "An ionic liquid-modified graphene based molecular imprinting electrochemical sensor for sensitive detection of bovine hemoglobin," *Biosensors and Bioelectronics*, vol. 61, pp. 391-396, 2014.
- [225] K. Wang, *et al.*, "Ultrasensitive photoelectrochemical sensing of nicotinamide adenine dinucleotide based on graphene-TiO₂ nanohybrids under visible irradiation," *Analytica chimica acta*, vol. 745, pp. 131-136, 2012.
- [226] C.-L. Sun, *et al.*, "The simultaneous electrochemical detection of ascorbic acid, dopamine, and uric acid using graphene/size-selected Pt nanocomposites," *Biosensors and Bioelectronics*, vol. 26, pp. 3450-3455, 2011.
- [227] Z.-H. Sheng, *et al.*, "Electrochemical sensor based on nitrogen doped graphene: simultaneous determination of ascorbic acid, dopamine and uric acid," *Biosensors and Bioelectronics*, vol. 34, pp. 125-131, 2012.
- [228] S. Kona, *Carbon nanomaterial based vapor sensors*: University of Louisville, 2012.
- [229] Y. Wang, *et al.*, "Wearable and highly sensitive graphene strain sensors for human motion monitoring," *Advanced Functional Materials*, vol. 24, pp. 4666-4670, 2014.
- [230] Z. Jing, *et al.*, "Review of graphene-based strain sensors," *Chinese Physics B*, vol. 22, p. 057701, 2013.
- [231] Y. Tang, *et al.*, "Highly Stretchable and Ultrasensitive Strain Sensor Based on Reduced Graphene Oxide Microtubes–Elastomer Composite," *ACS applied materials & interfaces*, vol. 7, pp. 27432-27439, 2015.
- [232] T. Gan and S. Hu, "Electrochemical sensors based on graphene materials," *Microchimica Acta*, vol. 175, p. 1, 2011.
- [233] M. Liu, *et al.*, "A graphene-based broadband optical modulator," *Nature*, vol. 474, p. 64, 2011.
- [234] P. Avouris and F. Xia, "Graphene applications in electronics and photonics," *MRS bulletin*, vol. 37, pp. 1225-1234, 2012.
- [235] T. Mueller, *et al.*, "Graphene photodetectors for high-speed optical communications," *Nature photonics*, vol. 4, pp. 297-301, 2010.
- [236] A. Martinez and Z. Sun, "Nanotube and graphene saturable absorbers for fibre lasers," *Nature photonics*, vol. 7, pp. 842-845, 2013.
- [237] S. Wu, *et al.*, "Graphene-based electrochemical sensors," *Small*, vol. 9, pp. 1160-1172, 2013.
- [238] W. Wang, *et al.*, "Bio-inspired mechanics of highly sensitive stretchable graphene strain sensors," *Applied Physics Letters*, vol. 106, p. 171903, 2015.
- [239] J. Shi, *et al.*, "Graphene reinforced carbon nanotube networks for wearable strain sensors," *Advanced Functional Materials*, vol. 26, pp. 2078-2084, 2016.
- [240] R. Xu, *et al.*, "Facile fabrication of three-dimensional graphene foam/poly (dimethylsiloxane) composites and their potential application as strain sensor," *ACS applied materials & interfaces*, vol. 6, pp. 13455-13460, 2014.
- [241] A. P. A. Raju, *et al.*, "Wide-Area Strain Sensors based upon Graphene-Polymer Composite Coatings Probed by Raman Spectroscopy," *Advanced Functional Materials*, vol. 24, pp. 2865-2874, 2014.

- [242] Y. Wang, *et al.*, "Super-elastic graphene ripples for flexible strain sensors," *ACS nano*, vol. 5, pp. 3645-3650, 2011.
- [243] S. Pradhan and T. Murmu, "Small scale effect on the buckling of single-layered graphene sheets under biaxial compression via nonlocal continuum mechanics," *Computational materials science*, vol. 47, pp. 268-274, 2009.
- [244] S. Romyantsev, *et al.*, "Selective gas sensing with a single pristine graphene transistor," *Nano Letters*, vol. 12, pp. 2294-2298, 2012.
- [245] B. J. Kim, *et al.*, "Coplanar-gate transparent graphene transistors and inverters on plastic," *ACS nano*, vol. 6, pp. 8646-8651, 2012.
- [246] M. Chakrabarti, *et al.*, "Progress in the electrochemical modification of graphene-based materials and their applications," *Electrochimica Acta*, vol. 107, pp. 425-440, 2013.
- [247] A. T. Lawal, "Synthesis and utilisation of graphene for fabrication of electrochemical sensors," *Talanta*, vol. 131, pp. 424-443, 2015.
- [248] C. Shan, *et al.*, "Direct electrochemistry of glucose oxidase and biosensing for glucose based on graphene," *Analytical chemistry*, vol. 81, pp. 2378-2382, 2009.
- [249] X. Kang, *et al.*, "Glucose oxidase-graphene-chitosan modified electrode for direct electrochemistry and glucose sensing," *Biosensors and Bioelectronics*, vol. 25, pp. 901-905, 2009.
- [250] R. S. Dey and C. R. Raj, "Development of an amperometric cholesterol biosensor based on graphene-Pt nanoparticle hybrid material," *The Journal of Physical Chemistry C*, vol. 114, pp. 21427-21433, 2010.
- [251] Y. He, *et al.*, "Magnetite-graphene for the direct electrochemistry of hemoglobin and its biosensing application," *Electrochimica Acta*, vol. 56, pp. 2471-2476, 2011.
- [252] J.-F. Wu, *et al.*, "Graphene-based modified electrode for the direct electron transfer of cytochrome c and biosensing," *Electrochemistry Communications*, vol. 12, pp. 175-177, 2010.
- [253] R. S. Dey and C. R. Raj, "Redox-functionalized graphene oxide architecture for the development of amperometric biosensing platform," *ACS applied materials & interfaces*, vol. 5, pp. 4791-4798, 2013.
- [254] H. Xu, *et al.*, "Graphene-based nanoprobe and a prototype optical biosensing platform," *Biosensors and Bioelectronics*, vol. 50, pp. 251-255, 2013.
- [255] W. Lv, *et al.*, "DNA-dispersed graphene/NiO hybrid materials for highly sensitive non-enzymatic glucose sensor," *Electrochimica Acta*, vol. 73, pp. 129-135, 2012.
- [256] B. Yuan, *et al.*, "Graphene oxide/nickel oxide modified glassy carbon electrode for supercapacitor and nonenzymatic glucose sensor," *Electrochimica Acta*, vol. 88, pp. 708-712, 2013.
- [257] B. Unnikrishnan, *et al.*, "A simple electrochemical approach to fabricate a glucose biosensor based on graphene-glucose oxidase biocomposite," *Biosensors and Bioelectronics*, vol. 39, pp. 70-75, 2013.
- [258] J. Luo, *et al.*, "A novel non-enzymatic glucose sensor based on Cu nanoparticle modified graphene sheets electrode," *Analytica chimica acta*, vol. 709, pp. 47-53, 2012.
- [259] M. Liu, *et al.*, "Graphene wrapped Cu₂O nanocubes: non-enzymatic electrochemical sensors for the detection of glucose and hydrogen peroxide with enhanced stability," *Biosensors and Bioelectronics*, vol. 45, pp. 206-212, 2013.
- [260] Y. Zhang, *et al.*, "Nonenzymatic glucose sensor based on graphene oxide and electrospun NiO nanofibers," *Sensors and Actuators B: Chemical*, vol. 171, pp. 580-587, 2012.
- [261] Z. Li, *et al.*, "Direct electrochemistry of cholesterol oxidase immobilized on chitosan-graphene and cholesterol sensing," *Sensors and Actuators B: Chemical*, vol. 208, pp. 505-511, 2015.
- [262] M. Zhang, *et al.*, "Cerium oxide-graphene as the matrix for cholesterol sensor," *Analytical biochemistry*, vol. 436, pp. 69-74, 2013.
- [263] O. Akhavan, *et al.*, "Wrapping bacteria by graphene nanosheets for isolation from environment, reactivation by sonication, and inactivation by near-infrared irradiation," *The Journal of Physical Chemistry B*, vol. 115, pp. 6279-6288, 2011.
- [264] D. Du, *et al.*, "Sensitive immunosensor for cancer biomarker based on dual signal amplification strategy of graphene sheets and multienzyme functionalized carbon nanospheres," *Analytical chemistry*, vol. 82, pp. 2989-2995, 2010.
- [265] T.-Y. Chen, *et al.*, "Label-free detection of DNA hybridization using transistors based on CVD grown graphene," *Biosensors and Bioelectronics*, vol. 41, pp. 103-109, 2013.
- [266] Y. Bo, *et al.*, "A novel electrochemical DNA biosensor based on graphene and polyaniline nanowires," *Electrochimica Acta*, vol. 56, pp. 2676-2681, 2011.

- [267] Y. Hu, *et al.*, "Label-free electrochemical impedance sensing of DNA hybridization based on functionalized graphene sheets," *Chemical Communications*, vol. 47, pp. 1743-1745, 2011.
- [268] H. Dong, *et al.*, "Triplex signal amplification for electrochemical DNA biosensing by coupling probe-gold nanoparticles-graphene modified electrode with enzyme functionalized carbon sphere as tracer," *Biosensors and Bioelectronics*, vol. 33, pp. 228-232, 2012.
- [269] M. Zhou, *et al.*, "Electrochemical sensing and biosensing platform based on chemically reduced graphene oxide," *Analytical chemistry*, vol. 81, pp. 5603-5613, 2009.
- [270] F. Gao, *et al.*, "Highly sensitive and selective detection of dopamine in the presence of ascorbic acid at graphene oxide modified electrode," *Sensors and Actuators B: Chemical*, vol. 186, pp. 380-387, 2013.
- [271] S.-J. Li, *et al.*, "Electrochemical detection of dopamine using water-soluble sulfonated graphene," *Electrochimica Acta*, vol. 102, pp. 58-65, 2013.
- [272] L. Yang, *et al.*, "Simultaneous determination of dopamine, ascorbic acid and uric acid at electrochemically reduced graphene oxide modified electrode," *Sensors and Actuators B: Chemical*, vol. 193, pp. 166-172, 2014.
- [273] K. Matsumoto, *et al.*, "Recent advances in functional graphene biosensors," *Journal of Physics D: Applied Physics*, vol. 47, p. 094005, 2014.
- [274] D. Khatayevich, *et al.*, "Selective Detection of Target Proteins by Peptide-Enabled Graphene Biosensor," *Small*, vol. 10, pp. 1505-1513, 2014.
- [275] Y. Ohno, *et al.*, "Label-free biosensors based on aptamer-modified graphene field-effect transistors," *Journal of the American Chemical Society*, vol. 132, pp. 18012-18013, 2010.
- [276] S. Palanisamy, *et al.*, "A novel nonenzymatic hydrogen peroxide sensor based on reduced graphene oxide/ZnO composite modified electrode," *Sensors and Actuators B: Chemical*, vol. 166, pp. 372-377, 2012.
- [277] Y. Ye, *et al.*, "Enhanced nonenzymatic hydrogen peroxide sensing with reduced graphene oxide/ferroferric oxide nanocomposites," *Talanta*, vol. 89, pp. 417-421, 2012.
- [278] J. Ju and W. Chen, "In situ growth of surfactant-free gold nanoparticles on nitrogen-doped graphene quantum dots for electrochemical detection of hydrogen peroxide in biological environments," *Analytical chemistry*, vol. 87, pp. 1903-1910, 2015.
- [279] L. A. Mercante, *et al.*, "One-pot preparation of PEDOT: PSS-reduced graphene decorated with Au nanoparticles for enzymatic electrochemical sensing of H₂O₂," *Applied surface science*, vol. 407, pp. 162-170, 2017.
- [280] C. S. Boland, *et al.*, "Sensitive, high-strain, high-rate bodily motion sensors based on graphene-rubber composites," *ACS nano*, vol. 8, pp. 8819-8830, 2014.
- [281] M. Hempel, *et al.*, "A novel class of strain gauges based on layered percolative films of 2D materials," *Nano Letters*, vol. 12, pp. 5714-5718, 2012.
- [282] S.-H. Bae, *et al.*, "Graphene-based transparent strain sensor," *Carbon*, vol. 51, pp. 236-242, 2013.
- [283] H. Tian, *et al.*, "Scalable fabrication of high-performance and flexible graphene strain sensors," *Nanoscale*, vol. 6, pp. 699-705, 2014.
- [284] Y. Qin, *et al.*, "Lightweight, superelastic, and mechanically flexible graphene/polyimide nanocomposite foam for strain sensor application," *ACS nano*, vol. 9, pp. 8933-8941, 2015.
- [285] Y. Xu, *et al.*, "In-plane and tunneling pressure sensors based on graphene/hexagonal boron nitride heterostructures," *Applied Physics Letters*, vol. 99, p. 133109, 2011.
- [286] T. Q. Trung and N. E. Lee, "Flexible and Stretchable Physical Sensor Integrated Platforms for Wearable Human-Activity Monitoring and Personal Healthcare," *Advanced Materials*, 2016.
- [287] S. Ryu, *et al.*, "Extremely elastic wearable carbon nanotube fiber strain sensor for monitoring of human motion," *ACS nano*, vol. 9, pp. 5929-5936, 2015.
- [288] J. Viventi, *et al.*, "A conformal, bio-interfaced class of silicon electronics for mapping cardiac electrophysiology," *Science translational medicine*, vol. 2, pp. 24ra22-24ra22, 2010.
- [289] Y. Wang, *et al.*, "Ultra-sensitive graphene strain sensor for sound signal acquisition and recognition," *Nano Research*, vol. 8, pp. 1627-1636, 2015.
- [290] X. Li, *et al.*, "Multifunctional graphene woven fabrics," *Scientific reports*, vol. 2, 2012.
- [291] T. Cohen-Karni, *et al.*, "Graphene and nanowire transistors for cellular interfaces and electrical recording," *Nano Letters*, vol. 10, pp. 1098-1102, 2010.
- [292] Y. Banadaki, *et al.*, "A graphene field effect transistor for high temperature sensing applications," in *Proc. SPIE*, 2014, p. 90600F.
- [293] J. Li, *et al.*, "Photosensitive graphene transistors," *Advanced Materials*, vol. 26, pp. 5239-5273, 2014.

- [294] H. Wang, *et al.*, "Graphene electronics for RF applications," *IEEE Microwave Magazine*, vol. 13, pp. 114-125, 2012.
- [295] L. Vicarelli, *et al.*, "Graphene field-effect transistors as room-temperature terahertz detectors," *Nature Materials*, vol. 11, pp. 865-871, 2012.
- [296] M. Amirmazlaghani, *et al.*, "Graphene-si schottky IR detector," *IEEE Journal of Quantum electronics*, vol. 49, pp. 589-594, 2013.
- [297] F. Koppens, *et al.*, "Photodetectors based on graphene, other two-dimensional materials and hybrid systems," *Nature nanotechnology*, vol. 9, pp. 780-793, 2014.
- [298] J. Cheng, *et al.*, "Flexible solution-gated graphene field effect transistor for electrophysiological recording," *Journal of microelectromechanical systems*, vol. 23, pp. 1311-1317, 2014.
- [299] S. Park, *et al.*, "Extremely high-frequency flexible graphene thin-film transistors," *IEEE Electron Device Letters*, vol. 37, pp. 512-515, 2016.
- [300] L. Xiang, *et al.*, "Inkjet-printed flexible biosensor based on graphene field effect transistor," *IEEE Sensors Journal*, vol. 16, pp. 8359-8364, 2016.
- [301] W. Wei, *et al.*, "Graphene field effect transistors on flexible substrate: Stable process and high RF performance," in *Microwave Integrated Circuits Conference (EuMIC), 2016 11th European*, 2016, pp. 165-168.
- [302] N. Petrone, *et al.*, "Graphene field-effect transistors for radio-frequency flexible electronics," *IEEE Journal of the Electron Devices Society*, vol. 3, pp. 44-48, 2015.
- [303] H. Wang, *et al.*, "Mn3O4-graphene hybrid as a high-capacity anode material for lithium ion batteries," *Journal of the American Chemical Society*, vol. 132, pp. 13978-13980, 2010.
- [304] G. Zhou, *et al.*, "Graphene-wrapped Fe3O4 anode material with improved reversible capacity and cyclic stability for lithium ion batteries," *Chemistry of Materials*, vol. 22, pp. 5306-5313, 2010.
- [305] L.-H. Hu, *et al.*, "Graphene-modified LiFePO4 cathode for lithium ion battery beyond theoretical capacity," *Nature communications*, vol. 4, p. 1687, 2013.
- [306] Z.-S. Wu, *et al.*, "Doped graphene sheets as anode materials with superhigh rate and large capacity for lithium ion batteries," *ACS nano*, vol. 5, pp. 5463-5471, 2011.
- [307] A. L. M. Reddy, *et al.*, "Synthesis of nitrogen-doped graphene films for lithium battery application," *ACS nano*, vol. 4, pp. 6337-6342, 2010.
- [308] M. Liu, *et al.*, "Double-layer graphene optical modulator," *Nano Letters*, vol. 12, pp. 1482-1485, 2012.
- [309] A. Grigorenko, *et al.*, "Graphene plasmonics," *Nature photonics*, vol. 6, pp. 749-758, 2012.
- [310] *Graphene photodetector enhanced by fractal golden 'snowflake'*. Available: <https://phys.org/news/2017-01-graphene-photodetector-fractal-golden-snowflake.html>
- [311] F. Xia, *et al.*, "Ultrafast graphene photodetector," *Nature nanotechnology*, vol. 4, pp. 839-843, 2009.
- [312] A. Pospischil, *et al.*, "CMOS-compatible graphene photodetector covering all optical communication bands," *Nature photonics*, vol. 7, pp. 892-896, 2013.
- [313] H. Jang, *et al.*, "Graphene-Based Flexible and Stretchable Electronics," *Advanced Materials*, vol. 28, pp. 4184-4202, 2016.
- [314] C.-C. Lu, *et al.*, "High mobility flexible graphene field-effect transistors with self-healing gate dielectrics," *ACS nano*, vol. 6, pp. 4469-4474, 2012.
- [315] S.-K. Lee, *et al.*, "Stretchable graphene transistors with printed dielectrics and gate electrodes," *Nano Letters*, vol. 11, pp. 4642-4646, 2011.
- [316] S.-K. Lee, *et al.*, "All graphene-based thin film transistors on flexible plastic substrates," *Nano Letters*, vol. 12, pp. 3472-3476, 2012.
- [317] J. Meng, *et al.*, "Vertically Architected Stack of Multiple Graphene Field-Effect Transistors for Flexible Electronics," *Small*, vol. 11, pp. 1660-1664, 2015.
- [318] C. R. Dean, *et al.*, "Boron nitride substrates for high-quality graphene electronics," *Nature nanotechnology*, vol. 5, pp. 722-726, 2010.
- [319] B. Zhan, *et al.*, "Graphene Field-Effect Transistor and Its Application for Electronic Sensing," *Small*, vol. 10, pp. 4042-4065, 2014.
- [320] R. R. Nair, *et al.*, "Fine structure constant defines visual transparency of graphene," *Science*, vol. 320, pp. 1308-1308, 2008.
- [321] F. Wang, *et al.*, "Gate-variable optical transitions in graphene," *Science*, vol. 320, pp. 206-209, 2008.
- [322] G. Konstantatos, *et al.*, "Hybrid graphene-quantum dot phototransistors with ultrahigh gain," *Nature nanotechnology*, vol. 7, pp. 363-368, 2012.
- [323] T. Q. Trung, *et al.*, "High Thermal Responsiveness of a Reduced Graphene Oxide Field-Effect Transistor," *Advanced Materials*, vol. 24, pp. 5254-5260, 2012.

- [324] T. Q. Trung, *et al.*, "A flexible reduced graphene oxide field-effect transistor for ultrasensitive strain sensing," *Advanced Functional Materials*, vol. 24, pp. 117-124, 2014.
- [325] A. Inaba, *et al.*, "A graphene FET gas sensor gated by ionic liquid," in *Micro Electro Mechanical Systems (MEMS), 2013 IEEE 26th International Conference on*, 2013, pp. 969-972.
- [326] C.-H. Kim, *et al.*, "Effect of Temperature and Humidity on NO_2 and NH_3 Gas Sensitivity of Bottom-Gate Graphene FETs Prepared by ICP-CVD," *IEEE Electron Device Letters*, vol. 33, pp. 1084-1086, 2012.
- [327] M. Gautam and A. H. Jayatissa, "Graphene based field effect transistor for the detection of ammonia," *Journal of Applied Physics*, vol. 112, p. 064304, 2012.
- [328] Z. Zhang, *et al.*, "Hydrogen gas sensor based on metal oxide nanoparticles decorated graphene transistor," *Nanoscale*, vol. 7, pp. 10078-10084, 2015.
- [329] B. Mailly-Giacchetti, *et al.*, "pH sensing properties of graphene solution-gated field-effect transistors," *Journal of Applied Physics*, vol. 114, p. 084505, 2013.
- [330] P. K. Ang, *et al.*, "Solution-gated epitaxial graphene as pH sensor," *Journal of the American Chemical Society*, vol. 130, pp. 14392-14393, 2008.
- [331] Y. Ohno, *et al.*, "Electrolyte-gated graphene field-effect transistors for detecting pH and protein adsorption," *Nano Letters*, vol. 9, pp. 3318-3322, 2009.
- [332] I.-Y. Sohn, *et al.*, "pH sensing characteristics and biosensing application of solution-gated reduced graphene oxide field-effect transistors," *Biosensors and Bioelectronics*, vol. 45, pp. 70-76, 2013.
- [333] N. Lei, *et al.*, "Simple graphene chemiresistors as pH sensors: fabrication and characterization," *Measurement Science and Technology*, vol. 22, p. 107002, 2011.
- [334] Y. Wen, *et al.*, "The Electrical Detection of Lead Ions Using Gold-Nanoparticle-and DNAzyme-Functionalized Graphene Device," *Advanced healthcare materials*, vol. 2, pp. 271-274, 2013.
- [335] W. Fu, *et al.*, "High mobility graphene ion-sensitive field-effect transistors by noncovalent functionalization," *Nanoscale*, vol. 5, pp. 12104-12110, 2013.
- [336] K. Maehashi, *et al.*, "Selective ion sensors based on ionophore-modified graphene field-effect transistors," *Sensors and Actuators B: Chemical*, vol. 187, pp. 45-49, 2013.
- [337] T. Zhang, *et al.*, "Self-assembled 1-octadecanethiol monolayers on graphene for mercury detection," *Nano Letters*, vol. 10, pp. 4738-4741, 2010.
- [338] H. G. Sudibya, *et al.*, "Electrical detection of metal ions using field-effect transistors based on micropatterned reduced graphene oxide films," *ACS nano*, vol. 5, pp. 1990-1994, 2011.
- [339] O. Akhavan and E. Ghaderi, "Toxicity of graphene and graphene oxide nanowalls against bacteria," *ACS nano*, vol. 4, pp. 5731-5736, 2010.
- [340] S. Prolongo, *et al.*, "Advantages and disadvantages of the addition of graphene nanoplatelets to epoxy resins," *European Polymer Journal*, vol. 61, pp. 206-214, 2014.
- [341] D. G. Papageorgiou, *et al.*, "Graphene/elastomer nanocomposites," *Carbon*, vol. 95, pp. 460-484, 2015.
- [342] L.-C. Tang, *et al.*, "The effect of graphene dispersion on the mechanical properties of graphene/epoxy composites," *Carbon*, vol. 60, pp. 16-27, 2013.
- [343] D. Haag and H. Kung, "Metal Free Graphene Based Catalysts: A Review," *Topics in Catalysis*, vol. 57, 2014.
- [344] M. S. Mannoor, *et al.*, "Graphene-based wireless bacteria detection on tooth enamel," *Nature communications*, vol. 3, p. 763, 2012.
- [345] W. HyungáCheong, *et al.*, "Wearable, wireless gas sensors using highly stretchable and transparent structures of nanowires and graphene," *Nanoscale*, vol. 8, pp. 10591-10597, 2016.
- [346] S. J. Koester, "High quality factor graphene varactors for wireless sensing applications," *Applied Physics Letters*, vol. 99, p. 163105, 2011.
- [347] D. A. Deen, *et al.*, "Graphene-based quantum capacitance wireless vapor sensors," *IEEE Sensors Journal*, vol. 14, pp. 1459-1466, 2014.
- [348] T. Le, *et al.*, "Inkjet-printed graphene-based wireless gas sensor modules," in *Electronic Components and Technology Conference (ECTC), 2012 IEEE 62nd*, 2012, pp. 1003-1008.
- [349] J. S. Lee, *et al.*, "Wireless hydrogen smart sensor based on Pt/graphene-immobilized radio-frequency identification tag," *ACS nano*, vol. 9, pp. 7783-7790, 2015.
- [350] Z. S. Wu, *et al.*, "Ultrathin Printable Graphene Supercapacitors with AC Line-Filtering Performance," *Advanced Materials*, vol. 27, pp. 3669-3675, 2015.
- [351] D. A. Brownson and C. E. Banks, "Fabricating graphene supercapacitors: highlighting the impact of surfactants and moieties," *Chemical Communications*, vol. 48, pp. 1425-1427, 2012.

- [352] E. O. Polat and C. Kocabas, "Broadband optical modulators based on graphene supercapacitors," *Nano Letters*, vol. 13, pp. 5851-5857, 2013.
- [353] J. J. Yoo, *et al.*, "Ultrathin planar graphene supercapacitors," *Nano Letters*, vol. 11, pp. 1423-1427, 2011.
- [354] M. Pumera, "Electrochemistry of graphene: new horizons for sensing and energy storage," *The Chemical Record*, vol. 9, pp. 211-223, 2009.
- [355] M. Pumera, *et al.*, "Graphene for electrochemical sensing and biosensing," *TrAC Trends in Analytical Chemistry*, vol. 29, pp. 954-965, 2010.
- [356] D. A. Brownson and C. E. Banks, "Graphene electrochemistry: an overview of potential applications," *Analyst*, vol. 135, pp. 2768-2778, 2010.
- [357] Y. Liu, *et al.*, "Direct observation of high photoresponsivity in pure graphene photodetectors," *Nanoscale research letters*, vol. 12, p. 93, 2017.
- [358] *Advantages and Disadvantages of Graphene.* Available: <https://samaterials.wordpress.com/2014/03/27/advantages-and-disadvantages-of-graphene/>
- [359] S.-M. Lee, *et al.*, "Graphene as a flexible electronic material: mechanical limitations by defect formation and efforts to overcome," *Materials Today*, vol. 18, pp. 336-344, 2015.
- [360] S. Karoui, *et al.*, "Nickel-assisted healing of defective graphene," *ACS nano*, vol. 4, pp. 6114-6120, 2010.
- [361] D. R. Dreyer, *et al.*, "The chemistry of graphene oxide," *Chemical Society Reviews*, vol. 39, pp. 228-240, 2010.
- [362] Y. Wu, *et al.*, "High-frequency, scaled graphene transistors on diamond-like carbon," *Nature*, vol. 472, pp. 74-78, 2011.
- [363] H. C. Schniepp, *et al.*, "Functionalized single graphene sheets derived from splitting graphite oxide," *The Journal of Physical Chemistry B*, vol. 110, pp. 8535-8539, 2006.
- [364] *Graphene Market Trends.* Available: http://www.strategyr.com/MarketResearch/Graphene_Market_Trends.asp. Last accessed on 31st October, 2018.
- [365] *Graphene Market Overview.* Available: <https://www.alliedmarketresearch.com/graphene-market>. Last accessed on 31st October, 2018.
- [366] *Graphene Market Reports.* Available: <https://www.graphene-info.com/tags/market-reports>. Last accessed on 31st October, 2018.
- [367] C. Liao, *et al.*, "Flexible organic electronics in biology: materials and devices," *Advanced Materials*, vol. 27, pp. 7493-7527, 2015.
- [368] J. van den Brand, *et al.*, "Flexible and stretchable electronics for wearable health devices," *Solid-State Electronics*, vol. 113, pp. 116-120, 2015.
- [369] C.-Y. Chen, *et al.*, "Flexible PDMS electrode for one-point wearable wireless bio-potential acquisition," *Sensors and Actuators A: Physical*, vol. 203, pp. 20-28, 2013.
- [370] J.-H. Moon, *et al.*, "Wearable polyimide-PDMS electrodes for intrabody communication," *Journal of Micromechanics and Microengineering*, vol. 20, p. 025032, 2010.
- [371] T. Someya and T. Sekitani, "Bionic skins using flexible organic devices," in *2014 IEEE 27th International Conference on Micro Electro Mechanical Systems (MEMS)*, 2014, pp. 68-71.
- [372] T. Fujita, *et al.*, "Flexible sensor for human monitoring system by using P (VDF/TrFE) thin film," in *2012 Fifth International Conference on Emerging Trends in Engineering and Technology*, 2012, pp. 75-79.
- [373] D. Ha, *et al.*, "Polymer-based miniature flexible capacitive pressure sensor for intraocular pressure (IOP) monitoring inside a mouse eye," *Biomedical microdevices*, vol. 14, pp. 207-215, 2012.
- [374] A. P. Tjahyono, *et al.*, "A five-fingered hand exoskeleton driven by pneumatic artificial muscles with novel polypyrrole sensors," *Industrial Robot: An International Journal*, vol. 40, pp. 251-260, 2013.
- [375] Y. Zang, *et al.*, "Advances of flexible pressure sensors toward artificial intelligence and health care applications," *Materials Horizons*, vol. 2, pp. 140-156, 2015.
- [376] K. K. Sadasivuni, *et al.*, "Transparent and flexible cellulose nanocrystal/reduced graphene oxide film for proximity sensing," *Small*, vol. 11, pp. 994-1002, 2015.
- [377] B. S. Shim, *et al.*, "Smart electronic yarns and wearable fabrics for human biomonitoring made by carbon nanotube coating with polyelectrolytes," *Nano Letters*, vol. 8, pp. 4151-4157, 2008.
- [378] K. Jost, *et al.*, "Knitted and screen printed carbon-fiber supercapacitors for applications in wearable electronics," *Energy & Environmental Science*, vol. 6, pp. 2698-2705, 2013.

- [379] J. Wang, *et al.*, "A highly sensitive and flexible pressure sensor with electrodes and elastomeric interlayer containing silver nanowires," *Nanoscale*, vol. 7, pp. 2926-2932, 2015.
- [380] Y. Hasegawa, *et al.*, "Fabrication of a wearable fabric tactile sensor produced by artificial hollow fiber," *Journal of Micromechanics and Microengineering*, vol. 18, p. 085014, 2008.
- [381] S. L. P. Tang, "Recent developments in flexible wearable electronics for monitoring applications," *Transactions of the Institute of Measurement and Control*, vol. 29, pp. 283-300, 2007.
- [382] D. Vilela, *et al.*, "Flexible sensors for biomedical technology," *Lab on a Chip*, vol. 16, pp. 402-408, 2016.
- [383] G. A. Zelada-Guillén, *et al.*, "Label-free detection of Staphylococcus aureus in skin using real-time potentiometric biosensors based on carbon nanotubes and aptamers," *Biosensors and Bioelectronics*, vol. 31, pp. 226-232, 2012.
- [384] K. Saetia, *et al.*, "Spray-Layer-by-Layer Carbon Nanotube/Electrospun Fiber Electrodes for Flexible Chemiresistive Sensor Applications," *Advanced Functional Materials*, vol. 24, pp. 492-502, 2014.
- [385] D. P. Rose, *et al.*, "Adhesive RFID sensor patch for monitoring of sweat electrolytes," *IEEE Transactions on Biomedical Engineering*, vol. 62, pp. 1457-1465, 2015.
- [386] C. Liao, *et al.*, "Flexible organic electrochemical transistors for highly selective enzyme biosensors and used for saliva testing," *Advanced Materials*, vol. 27, pp. 676-681, 2015.
- [387] I. Graz, *et al.*, "Flexible ferroelectric field-effect transistor for large-area sensor skins and microphones," *Applied Physics Letters*, vol. 89, p. 073501, 2006.
- [388] M. Melzer, *et al.*, "Wearable magnetic field sensors for flexible electronics," *Advanced Materials*, vol. 27, pp. 1274-1280, 2015.
- [389] P. Lorwongtragool, *et al.*, "A novel wearable electronic nose for healthcare based on flexible printed chemical sensor array," *Sensors*, vol. 14, pp. 19700-19712, 2014.
- [390] K.-I. Jang, *et al.*, "Soft network composite materials with deterministic and bio-inspired designs," *Nature communications*, vol. 6, 2015.
- [391] J. C. Yeo and C. T. Lim, "Emerging flexible and wearable physical sensing platforms for healthcare and biomedical applications," *Microsystems & Nanoengineering*, vol. 2, p. 16043, 2016.
- [392] L. Francioso, *et al.*, "Flexible thermoelectric generator for wearable biometric sensors," in *Sensors, 2010 IEEE*, 2010, pp. 747-750.
- [393] E. Y. Song and K. B. Lee, "IEEE 1451.5 standard-based wireless sensor networks," in *Advances in Wireless Sensors and Sensor Networks*, ed: Springer, 2010, pp. 243-271.
- [394] J. Haartsen, "Bluetooth-The universal radio interface for ad hoc, wireless connectivity," *Ericsson review*, vol. 3, pp. 110-117, 1998.
- [395] R. Ohmura, *et al.*, "B-pack: a bluetooth-based wearable sensing device for nursing activity recognition," in *2006 1st International Symposium on Wireless Pervasive Computing*, 2006, p. 6 pp.
- [396] M. Strauss, *et al.*, "The handwave bluetooth skin conductance sensor," in *International Conference on Affective Computing and Intelligent Interaction*, 2005, pp. 699-706.
- [397] A. Burns, *et al.*, "SHIMMER™—A wireless sensor platform for noninvasive biomedical research," *IEEE Sensors Journal*, vol. 10, pp. 1527-1534, 2010.
- [398] M. Johnson, *et al.*, "A comparative review of wireless sensor network mote technologies," in *Sensors, 2009 IEEE*, 2009, pp. 1439-1442.
- [399] J. Polastre, *et al.*, "Telos: enabling ultra-low power wireless research," in *IPSN 2005. Fourth International Symposium on Information Processing in Sensor Networks, 2005.*, 2005, pp. 364-369.
- [400] C. Zhou, *et al.*, "Flexible structured high-frequency film bulk acoustic resonator for flexible wireless electronics," *Journal of Micromechanics and Microengineering*, vol. 25, p. 055003, 2015.
- [401] C. Park, *et al.*, "An ultra-wearable, wireless, low power ECG monitoring system," in *2006 IEEE Biomedical Circuits and Systems Conference*, 2006, pp. 241-244.
- [402] Y. Hao and R. Foster, "Wireless body sensor networks for health-monitoring applications," *Physiological measurement*, vol. 29, p. R27, 2008.
- [403] V. Jones, *et al.*, "Remote monitoring for healthcare and for safety in extreme environments," in *M-Health*, ed: Springer, 2006, pp. 561-573.
- [404] U. Maurer, *et al.*, "eWatch: a wearable sensor and notification platform," in *International Workshop on Wearable and Implantable Body Sensor Networks (BSN'06)*, 2006, pp. 4 pp.-145.
- [405] A. C. W. Wong, *et al.*, "A 1 V wireless transceiver for an ultra-low-power SoC for biotelemetry applications," *IEEE Journal of Solid-State Circuits*, vol. 43, pp. 1511-1521, 2008.
- [406] E. Jovanov and A. Milenkovic, "Body area networks for ubiquitous healthcare applications: opportunities and challenges," *Journal of medical systems*, vol. 35, pp. 1245-1254, 2011.

- [407] P. S. Hall and Y. Hao, "Antennas and propagation for body-centric wireless networks," *Norwood, MA*, 2006.
- [408] K. Malzahn, *et al.*, "Wearable electrochemical sensors for in situ analysis in marine environments," *Analyst*, vol. 136, pp. 2912-2917, 2011.
- [409] X. Pu, *et al.*, "A Self-Charging Power Unit by Integration of a Textile Triboelectric Nanogenerator and a Flexible Lithium-Ion Battery for Wearable Electronics," *Advanced Materials*, vol. 27, pp. 2472-2478, 2015.
- [410] X. Xiao, *et al.*, "Fiber-based all-solid-state flexible supercapacitors for self-powered systems," *ACS nano*, vol. 6, pp. 9200-9206, 2012.
- [411] F.-R. Fan, *et al.*, "Transparent triboelectric nanogenerators and self-powered pressure sensors based on micropatterned plastic films," *Nano Letters*, vol. 12, pp. 3109-3114, 2012.
- [412] M. Ha, *et al.*, "Triboelectric generators and sensors for self-powered wearable electronics," *ACS nano*, vol. 9, pp. 3421-3427, 2015.
- [413] W. Zeng, *et al.*, "Fiber-based wearable electronics: a review of materials, fabrication, devices, and applications," *Advanced Materials*, vol. 26, pp. 5310-5336, 2014.
- [414] W. Tao, *et al.*, "Gait analysis using wearable sensors," *Sensors*, vol. 12, pp. 2255-2283, 2012.
- [415] Y. Jiang, *et al.*, "A PVDF-based flexible cardiorespiratory sensor with independently optimized sensitivity to heartbeat and respiration," *Procedia Engineering*, vol. 5, pp. 1466-1469, 2010.
- [416] J. A. Patterson, *et al.*, "A flexible, low noise reflective PPG sensor platform for ear-worn heart rate monitoring," in *2009 Sixth International Workshop on Wearable and Implantable Body Sensor Networks*, 2009, pp. 286-291.
- [417] S. Choi and Z. Jiang, "A novel wearable sensor device with conductive fabric and PVDF film for monitoring cardiorespiratory signals," *Sensors and Actuators A: Physical*, vol. 128, pp. 317-326, 2006.
- [418] S. Iguchi, *et al.*, "A flexible and wearable biosensor for tear glucose measurement," *Biomedical microdevices*, vol. 9, pp. 603-609, 2007.
- [419] H. Kudo, *et al.*, "A flexible and wearable glucose sensor based on functional polymers with Soft-MEMS techniques," *Biosensors and Bioelectronics*, vol. 22, pp. 558-562, 2006.
- [420] Y. H. Kwak, *et al.*, "Flexible glucose sensor using CVD-grown graphene-based field effect transistor," *Biosensors and Bioelectronics*, vol. 37, pp. 82-87, 2012.
- [421] X. Wang, *et al.*, "Silk-molded flexible, ultrasensitive, and highly stable electronic skin for monitoring human physiological signals," *Advanced Materials*, vol. 26, pp. 1336-1342, 2014.
- [422] R. B. Katragadda and Y. Xu, "A novel intelligent textile technology based on silicon flexible skins," *Sensors and Actuators A: Physical*, vol. 143, pp. 169-174, 2008.
- [423] S. Bauer, "Flexible electronics: Sophisticated skin," *Nature Materials*, vol. 12, pp. 871-872, 2013.
- [424] D. Son, *et al.*, "Multifunctional wearable devices for diagnosis and therapy of movement disorders," *Nature nanotechnology*, vol. 9, pp. 397-404, 2014.
- [425] S. Choi, *et al.*, "Stretchable heater using ligand-exchanged silver nanowire nanocomposite for wearable articular thermotherapy," *ACS nano*, vol. 9, pp. 6626-6633, 2015.
- [426] I. R. Mineev, *et al.*, "Electronic dura mater for long-term multimodal neural interfaces," *Science*, vol. 347, pp. 159-163, 2015.
- [427] J. Di, *et al.*, "Stretch-triggered drug delivery from wearable elastomer films containing therapeutic depots," *ACS nano*, vol. 9, pp. 9407-9415, 2015.
- [428] J. S. Petrofsky, *et al.*, "Effect of heat and cold on tendon flexibility and force to flex the human knee," *Medical science monitor*, vol. 19, pp. 661-667, 2013.
- [429] J. M. Mayer, *et al.*, "Continuous low-level heat wrap therapy for the prevention and early phase treatment of delayed-onset muscle soreness of the low back: a randomized controlled trial," *Archives of physical medicine and rehabilitation*, vol. 87, pp. 1310-1317, 2006.
- [430] D. Kang, *et al.*, "Ultrasensitive mechanical crack-based sensor inspired by the spider sensory system," *Nature*, vol. 516, pp. 222-226, 2014.
- [431] K.-I. Jang, *et al.*, "Rugged and breathable forms of stretchable electronics with adherent composite substrates for transcutaneous monitoring," *Nature communications*, vol. 5, 2014.
- [432] F.-Y. Chang, *et al.*, "Flexible strain sensors fabricated with carbon nano-tube and carbon nano-fiber composite thin films," *Thin solid films*, vol. 518, pp. 7343-7347, 2010.
- [433] X. Xiao, *et al.*, "High-Strain Sensors Based on ZnO Nanowire/Polystyrene Hybridized Flexible Films," *Advanced Materials*, vol. 23, pp. 5440-5444, 2011.

- [434] J. J. Park, *et al.*, "Highly stretchable and wearable graphene strain sensors with controllable sensitivity for human motion monitoring," *ACS applied materials & interfaces*, vol. 7, pp. 6317-6324, 2015.
- [435] C. Pang, *et al.*, "A flexible and highly sensitive strain-gauge sensor using reversible interlocking of nanofibres," *Nature Materials*, vol. 11, pp. 795-801, 2012.
- [436] G. Schwartz, *et al.*, "Flexible polymer transistors with high pressure sensitivity for application in electronic skin and health monitoring," *Nature communications*, vol. 4, p. 1859, 2013.
- [437] G. Matzeu, *et al.*, "Advances in wearable chemical sensor design for monitoring biological fluids," *Sensors and Actuators B: Chemical*, vol. 211, pp. 403-418, 2015.
- [438] A. J. Bandodkar, *et al.*, "Tattoo-Based Wearable Electrochemical Devices: A Review," *Electroanalysis*, vol. 27, pp. 562-572, 2015.
- [439] E. Bakker, *et al.*, "Selectivity of potentiometric ion sensors," *Analytical chemistry*, vol. 72, pp. 1127-1133, 2000.
- [440] W. Jia, *et al.*, "Electrochemical tattoo biosensors for real-time noninvasive lactate monitoring in human perspiration," *Analytical chemistry*, vol. 85, pp. 6553-6560, 2013.
- [441] S. Berchmans, *et al.*, "An epidermal alkaline rechargeable Ag-Zn printable tattoo battery for wearable electronics," *Journal of Materials Chemistry A*, vol. 2, pp. 15788-15795, 2014.
- [442] A. J. Bandodkar, *et al.*, "Tattoo-based potentiometric ion-selective sensors for epidermal pH monitoring," *Analyst*, vol. 138, pp. 123-128, 2013.
- [443] A. J. Bandodkar, *et al.*, "Epidermal tattoo potentiometric sodium sensors with wireless signal transduction for continuous non-invasive sweat monitoring," *Biosensors and Bioelectronics*, vol. 54, pp. 603-609, 2014.
- [444] T. Guinovart, *et al.*, "A potentiometric tattoo sensor for monitoring ammonium in sweat," *Analyst*, vol. 138, pp. 7031-7038, 2013.
- [445] S. Coyle, *et al.*, "Fibers and fabrics for chemical and biological sensing," *Research Journal of Textile and Apparel*, vol. 14, pp. 63-72, 2010.
- [446] Y. Tian, *et al.*, "A new cross-linkable oxygen sensor covalently bonded into poly (2-hydroxyethyl methacrylate)-co-polyacrylamide thin film for dissolved oxygen sensing," *Chemistry of Materials*, vol. 22, pp. 2069-2078, 2010.
- [447] H. Kudo, *et al.*, "A flexible transcutaneous oxygen sensor using polymer membranes," *Biomedical microdevices*, vol. 9, pp. 1-6, 2007.
- [448] D. Satake, *et al.*, "A sensor for blood cell counter using MEMS technology," *Sensors and Actuators B: Chemical*, vol. 83, pp. 77-81, 2002.
- [449] A. Lisiewski, *et al.*, "Fly-ear inspired micro-sensor for sound source localization in two dimensions," *The Journal of the Acoustical Society of America*, vol. 129, pp. EL166-EL171, 2011.
- [450] S. C. Ko, *et al.*, "Micromachined air-gap structure MEMS acoustic sensor using reproducible high-speed lateral etching and CMP process," *Journal of Micromechanics and Microengineering*, vol. 16, p. 2071, 2006.
- [451] A. Dittmar, *et al.*, "A non invasive wearable sensor for the measurement of brain temperature," in *Engineering in Medicine and Biology Society, 2006. EMBS'06. 28th Annual International Conference of the IEEE*, 2006, pp. 900-902.
- [452] I. Korhonen, *et al.*, "Health monitoring in the home of the future," *IEEE Engineering in medicine and biology magazine*, vol. 22, pp. 66-73, 2003.
- [453] F. Axisa, *et al.*, "Flexible technologies and smart clothing for citizen medicine, home healthcare, and disease prevention," *IEEE Transactions on Information Technology in Biomedicine*, vol. 9, pp. 325-336, 2005.
- [454] C.-T. Huang, *et al.*, "A wearable yarn-based piezo-resistive sensor," *Sensors and Actuators A: Physical*, vol. 141, pp. 396-403, 2008.
- [455] M. Pacelli, *et al.*, "Textile piezoresistive sensors for biomechanical variables monitoring," in *Engineering in Medicine and Biology Society, 2006. EMBS'06. 28th Annual International Conference of the IEEE*, 2006, pp. 5358-5361.
- [456] M. Rothmaier, *et al.*, "Textile pressure sensor made of flexible plastic optical fibers," *Sensors*, vol. 8, pp. 4318-4329, 2008.
- [457] J. Zhong, *et al.*, "Fiber-based generator for wearable electronics and mobile medication," *ACS nano*, vol. 8, pp. 6273-6280, 2014.
- [458] Z. Li and Z. L. Wang, "Air/Liquid-Pressure and Heartbeat-Driven Flexible Fiber Nanogenerators as a Micro/Nano-Power Source or Diagnostic Sensor," *Advanced Materials*, vol. 23, pp. 84-89, 2011.

- [459] H. Kim, *et al.*, "A wearable fabric computer by planar-fashionable circuit board technique," in *2009 Sixth International Workshop on Wearable and Implantable Body Sensor Networks*, 2009, pp. 282-285.
- [460] J. Yoo, *et al.*, "A wearable ECG acquisition system with compact planar-fashionable circuit board-based shirt," *IEEE Transactions on Information Technology in Biomedicine*, vol. 13, pp. 897-902, 2009.
- [461] W.-Y. Chang, *et al.*, "Characterization and fabrication of wireless flexible physiological monitor sensor," *Sensors and Actuators A: Physical*, vol. 143, pp. 196-203, 2008.
- [462] H. Kim, *et al.*, "A 1.12 mW continuous healthcare monitor chip integrated on a planar fashionable circuit board," in *2008 IEEE International Solid-State Circuits Conference-Digest of Technical Papers*, 2008, pp. 150-603.
- [463] J. Yoo, *et al.*, "A 5.2 mw self-configured wearable body sensor network controller and a 12 w wirelessly powered sensor for a continuous health monitoring system," *Solid-State Circuits, IEEE Journal of*, vol. 45, pp. 178-188, 2010.
- [464] A. Colombo, *et al.*, "Flexible indoor localization and tracking based on a wearable platform and sensor data fusion," *IEEE Transactions on Instrumentation and Measurement*, vol. 63, pp. 864-876, 2014.
- [465] M. Sibinski, *et al.*, "Flexible temperature sensors on fibers," *Sensors*, vol. 10, pp. 7934-7946, 2010.
- [466] W. Gao, *et al.*, "Fully integrated wearable sensor arrays for multiplexed in situ perspiration analysis," *Nature*, vol. 529, pp. 509-514, 2016.
- [467] K. Takei, *et al.*, "Toward Flexible and Wearable Human-Interactive Health-Monitoring Devices," *Advanced healthcare materials*, vol. 4, pp. 487-500, 2015.
- [468] P. Bagade, *et al.*, "Evidence-based development approach for safe, sustainable and secure mobile medical app," in *Wearable Electronics Sensors*, ed: Springer, 2015, pp. 135-174.
- [469] *Flexible Smart Sensors and the Future of Health*. Available: <https://www.engadget.com/2015/09/21/flexible-smart-sensors-and-the-future-of-health/>. Last accessed on 31st October, 2018.
- [470] *The State of Flexible and Printed Electronics*. Available: http://www.printedelectronicsnow.com/issues/2015-03-01/view_features/the-state-of-flexible-and-printed-electronics. Last accessed on 31st October, 2018.
- [471] *2016-2026: Market Forecasts*. Available: <http://www.idtechex.com/research/reports/wearable-sensors-2016-2026-market-forecasts-technologies-players-000470.asp>. Last accessed on 31st October, 2018.
- [472] *The Wearable Technology Ecosystem: 2016 - 2030 - Opportunities, Challenges, Strategies, Industry Verticals And Forecasts*. Available: http://www.openpr.com/news/348933/The-Wearable-Technology-Ecosystem-2016-2030-Opportunities-Challenges-Strategies-Industry-Verticals-And-Forecasts.html?_hstc=197865264.638cea001f4f55aadbd731e528921f0a.1482980112036.1482980112036.1482980112036.1&_hssc=197865264.1.1482980112037&_hsfp=1381054282. Last accessed on 31st October, 2018.
- [473] *Organic Electronics Will Play a Key Role in Increasing the Utility of Wearables*. Available: <https://www.wearable-technologies.com/2016/03/organic-electronics-will-play-a-key-role-in-increasing-the-utility-of-wearables/>. Last accessed on 31st October, 2018.
- [474] T.-T. Ngo, *et al.*, "Design and Realization of a Planar Interdigital Microsensor for Biological Medium Characterization," in *Next Generation Sensors and Systems*, ed: Springer, 2016, pp. 23-54.
- [475] R. Matsuzaki and A. Todoroki, "Wireless flexible capacitive sensor based on ultra-flexible epoxy resin for strain measurement of automobile tires," *Sensors and Actuators A: Physical*, vol. 140, pp. 32-42, 2007.
- [476] M. R. R. Khan and S.-W. Kang, "Highly sensitive multi-channel IDC sensor array for low concentration taste detection," *Sensors*, vol. 15, pp. 13201-13221, 2015.
- [477] A. I. Zia, *et al.*, "Rapid and molecular selective electrochemical sensing of phthalates in aqueous solution," *Biosensors and Bioelectronics*, vol. 67, pp. 342-349, 2015.
- [478] M. E. E. Alahi, *et al.*, "A temperature-compensated graphene sensor for nitrate monitoring in real-time application," *Sensors and Actuators A: Physical*, vol. 269, pp. 79-90, 2018.
- [479] N. Afsarimanesh, *et al.*, "Molecularly Imprinted Polymer-Based Electrochemical Biosensor for Bone Loss Detection," *IEEE Transactions on Biomedical Engineering*, 2017.
- [480] N. Afsarimanesh, *et al.*, "Sensors and Instrumentation towards early detection of osteoporosis," in *Instrumentation and Measurement Technology Conference Proceedings (I2MTC), 2016 IEEE International*, 2016, pp. 1-6.

- [481] L. Cai, *et al.*, "Super-stretchable, transparent carbon nanotube-based capacitive strain sensors for human motion detection," *Scientific reports*, vol. 3, 2013.
- [482] A. Nag, *et al.*, "Strain induced graphite/PDMS sensors for biomedical applications," *Sensors and Actuators A*, vol. 271, pp. 257-269, 2018.
- [483] A. Lasia, "Electrochemical impedance spectroscopy and its applications," in *Modern aspects of electrochemistry*, ed: Springer, 2002, pp. 143-248.
- [484] T. Pajkossy and R. Jurczakowski, "Electrochemical impedance spectroscopy in interfacial studies," *Current Opinion in Electrochemistry*, vol. 1, pp. 53-58, 2017.
- [485] D. Armani, *et al.*, "Re-configurable fluid circuits by PDMS elastomer micromachining," in *Micro Electro Mechanical Systems, 1999. MEMS'99. Twelfth IEEE International Conference on*, 1999, pp. 222-227.
- [486] T. Fujii, "PDMS-based microfluidic devices for biomedical applications," *Microelectronic Engineering*, vol. 61, pp. 907-914, 2002.
- [487] B.-H. Jo, *et al.*, "Three-dimensional micro-channel fabrication in polydimethylsiloxane (PDMS) elastomer," *Microelectromechanical Systems, Journal of*, vol. 9, pp. 76-81, 2000.
- [488] M. C. Gower, "Excimer laser microfabrication and micromachining," in *First International Symposium on Laser Precision Microfabrication (LPM2000)*, 2000, pp. 124-131.
- [489] D. Snakenborg, *et al.*, "Microstructure fabrication with a CO₂ laser system," *Journal of Micromechanics and microengineering*, vol. 14, p. 182, 2004.
- [490] C. X. F. Lam, *et al.*, "Scaffold development using 3D printing with a starch-based polymer," *Materials Science and Engineering: C*, vol. 20, pp. 49-56, 2002.
- [491] N. Herzer, *et al.*, "Fabrication of patterned silane based self-assembled monolayers by photolithography and surface reactions on silicon-oxide substrates," *Chemical Communications*, vol. 46, pp. 5634-5652, 2010.
- [492] B.-J. De Gans, *et al.*, "Inkjet printing of polymers: state of the art and future developments," *Advanced materials*, vol. 16, pp. 203-213, 2004.
- [493] S. Frankland, *et al.*, "The stress-strain behavior of polymer-nanotube composites from molecular dynamics simulation," *Composites Science and Technology*, vol. 63, pp. 1655-1661, 2003.
- [494] B. Najafi, *et al.*, "Ambulatory system for human motion analysis using a kinematic sensor: monitoring of daily physical activity in the elderly," *Biomedical Engineering, IEEE Transactions on*, vol. 50, pp. 711-723, 2003.
- [495] K. Altun and B. Barshan, "Human activity recognition using inertial/magnetic sensor units," in *Human behavior understanding*, ed: Springer, 2010, pp. 38-51.
- [496] K. Malhi, *et al.*, "A Zigbee-based wearable physiological parameters monitoring system," *Sensors Journal, IEEE*, vol. 12, pp. 423-430, 2012.
- [497] S. D. T. Kelly, *et al.*, "Towards the implementation of IoT for environmental condition monitoring in homes," *Sensors Journal, IEEE*, vol. 13, pp. 3846-3853, 2013.
- [498] N. K. Suryadevara and S. C. Mukhopadhyay, "Wireless sensor network based home monitoring system for wellness determination of elderly," *Sensors Journal, IEEE*, vol. 12, pp. 1965-1972, 2012.
- [499] A. Arena, *et al.*, "Flexible ethanol sensors on glossy paper substrates operating at room temperature," *Sensors and Actuators B: Chemical*, vol. 145, pp. 488-494, 2010.
- [500] C. Ashruf, "Thin flexible pressure sensors," *Sensor Review*, vol. 22, pp. 322-327, 2002.
- [501] D. Briand, *et al.*, "Why going towards plastic and flexible sensors?," *Procedia engineering*, vol. 25, pp. 8-15, 2011.
- [502] C. Charton, *et al.*, "Development of high barrier films on flexible polymer substrates," *Thin Solid Films*, vol. 502, pp. 99-103, 2006.
- [503] T. L. Hayes, *et al.*, "Unobtrusive assessment of walking speed in the home using inexpensive PIR sensors," in *Engineering in Medicine and Biology Society, 2009. EMBC 2009. Annual International Conference of the IEEE*, 2009, pp. 7248-7251.
- [504] H. Pfützner, *et al.*, "Magnetostrictive bilayers for multi-functional sensor families," *Sensors and Actuators A: Physical*, vol. 129, pp. 154-158, 2006.
- [505] L. Mehnen, *et al.*, "Magnetostrictive bilayer sensors—a survey," *Journal of alloys and compounds*, vol. 369, pp. 202-204, 2004.
- [506] E. Kaniusas, *et al.*, "Method for continuous nondisturbing monitoring of blood pressure by magnetoelastic skin curvature sensor and ECG," *Sensors Journal, IEEE*, vol. 6, pp. 819-828, 2006.
- [507] V. M. Crabtree, *et al.*, "Periodic limb movement disorder of sleep in children," *Journal of Sleep Research*, vol. 12, pp. 73-81, 2003.

- [508] K. Aminian and B. Najafi, "Capturing human motion using body-fixed sensors: outdoor measurement and clinical applications," *Computer Animation and Virtual Worlds*, vol. 15, pp. 79-94, 2004.
- [509] K. D. Nguyen, *et al.*, "A wearable sensing system for tracking and monitoring of functional arm movement," *Mechatronics, IEEE/ASME Transactions on*, vol. 16, pp. 213-220, 2011.
- [510] C.-C. Yang and Y.-L. Hsu, "A review of accelerometry-based wearable motion detectors for physical activity monitoring," *Sensors*, vol. 10, pp. 7772-7788, 2010.
- [511] E. S. Sazonov, *et al.*, "Monitoring of posture allocations and activities by a shoe-based wearable sensor," *Biomedical Engineering, IEEE Transactions on*, vol. 58, pp. 983-990, 2011.
- [512] J. Bell, *et al.*, "Early detection of sit-to-stand transitions in a lower limb orthosis," in *Engineering in Medicine and Biology Society (EMBC), 2015 37th Annual International Conference of the IEEE*, 2015, pp. 5028-5031.
- [513] P. A. Leonard, *et al.*, "A fully automated algorithm for the determination of respiratory rate from the photoplethysmogram," *Journal of Clinical Monitoring and Computing*, vol. 20, pp. 33-36, 2006.
- [514] L. Nilsson, *et al.*, "Monitoring of respiratory rate in postoperative care using a new photoplethysmographic technique," *Journal of Clinical Monitoring and Computing*, vol. 16, pp. 309-315, 2000.
- [515] T. Reinvo, *et al.*, "Measurement of respiratory rate with high-resolution accelerometer and EMFit pressure sensor," in *Sensors Applications Symposium, 2006. Proceedings of the 2006 IEEE*, 2006, pp. 192-195.
- [516] S. Jung, *et al.*, "Point-of-care temperature and respiration monitoring sensors for smart fabric applications," *Smart Materials and Structures*, vol. 15, p. 1872, 2006.
- [517] C. R. Merritt, *et al.*, "Textile-based capacitive sensors for respiration monitoring," *IEEE Sensors journal*, vol. 9, pp. 71-78, 2009.
- [518] M. Warkentin, *et al.*, "New and fast method to quantify respiration rates of bacterial and plankton communities in freshwater ecosystems by using optical oxygen sensor spots," *Applied and environmental microbiology*, vol. 73, pp. 6722-6729, 2007.
- [519] N. Bu, *et al.*, "Monitoring of respiration and heartbeat during sleep using a flexible piezoelectric film sensor and empirical mode decomposition," in *2007 29th Annual International Conference of the IEEE Engineering in Medicine and Biology Society*, 2007, pp. 1362-1366.
- [520] Y.-Y. Chiu, *et al.*, "Development of a piezoelectric polyvinylidene fluoride (PVDF) polymer-based sensor patch for simultaneous heartbeat and respiration monitoring," *Sensors and Actuators A: Physical*, vol. 189, pp. 328-334, 2013.
- [521] C. H. Lau, *et al.*, "The effect of functionalization on structure and electrical conductivity of multi-walled carbon nanotubes," *Journal of Nanoparticle Research*, vol. 10, pp. 77-88, 2008.
- [522] P. Erik Scheme MSc and P. Kevin Englehart PhD, "Electromyogram pattern recognition for control of powered upper-limb prostheses: State of the art and challenges for clinical use," *Journal of rehabilitation research and development*, vol. 48, p. 643, 2011.
- [523] A. Muzumdar, *Powered Upper Limb Prostheses: Control, Implementation and Clinical Application; 11 Tables*: Springer Science & Business Media, 2004.
- [524] A. Fougner, *et al.*, "Control of upper limb prostheses: terminology and proportional myoelectric control—a review," *Neural Systems and Rehabilitation Engineering, IEEE Transactions on*, vol. 20, pp. 663-677, 2012.
- [525] G. Fortino, *et al.*, "Enabling effective programming and flexible management of efficient body sensor network applications," *Human-Machine Systems, IEEE Transactions on*, vol. 43, pp. 115-133, 2013.
- [526] K. Odame and D. Du, "Towards a smart sensor interface for wearable cough monitoring."
- [527] M. C. Carrozza, *et al.*, "The CyberHand: on the design of a cybernetic prosthetic hand intended to be interfaced to the peripheral nervous system," in *Intelligent Robots and Systems, 2003.(IROS 2003). Proceedings. 2003 IEEE/RSJ International Conference on*, 2003, pp. 2642-2647.
- [528] J. J. Boland, "Flexible electronics: Within touch of artificial skin," *Nature materials*, vol. 9, pp. 790-792, 2010.
- [529] J. Dargahi, "A piezoelectric tactile sensor with three sensing elements for robotic, endoscopic and prosthetic applications," *Sensors and Actuators A: Physical*, vol. 80, pp. 23-30, 2000.
- [530] G. Cannata, *et al.*, "An embedded artificial skin for humanoid robots," in *Multisensor Fusion and Integration for Intelligent Systems, 2008. MFI 2008. IEEE International Conference on*, 2008, pp. 434-438.

- [531] A. Trampuz, *et al.*, "Advances in the laboratory diagnosis of prosthetic joint infection," *Reviews in Medical Microbiology*, vol. 14, pp. 1-14, 2003.
- [532] W. Zimmerli, "Prosthetic-joint-associated infections," *Best Practice & Research Clinical Rheumatology*, vol. 20, pp. 1045-1063, 2006.
- [533] (2013). *Touch-Sensitive Prosthetic Limbs Take Step Forward in Monkey Study*. Available: <http://www.livescience.com/40405-touch-sensitive-prosthetic-limbs-monkey-study.html>. Last accessed on 31st October, 2018.
- [534] J. Singh, *et al.*, "Flexible and mechanical strain resistant large area SERS active substrates," *Nanoscale*, vol. 4, pp. 3410-3414, 2012.
- [535] C. Lee, *et al.*, "Graphene-based flexible NO₂ chemical sensors," *Thin solid films*, vol. 520, pp. 5459-5462, 2012.
- [536] M. Akiyama, *et al.*, "Flexible piezoelectric pressure sensors using oriented aluminum nitride thin films prepared on polyethylene terephthalate films," *Journal of Applied Physics*, vol. 100, p. 114318, 2006.
- [537] X. Wang, *et al.*, "Dynamic pressure mapping of personalized handwriting by a flexible sensor matrix based on the mechanoluminescence process," *Advanced Materials*, vol. 27, pp. 2324-2331, 2015.
- [538] *Laser cutting and engraving of PET*. Available: <https://www.eurolaser.com/materials/pet-petg/>. Last accessed on 31st October, 2018.
- [539] *Cutting PET with CO₂ laser*. Available: <http://www.gccworld.com/showcase.php?act=view&no=138>. Last accessed on 31st October, 2018.
- [540] A. De La Escosura-Muñiz, *et al.*, "Nanoparticles-based nanochannels assembled on a plastic flexible substrate for label-free immunosensing," *Nano Research*, vol. 8, pp. 1180-1188, 2015.
- [541] *Aluminium - Advantages and Properties of Aluminium*. Available: <http://www.azom.com/article.aspx?ArticleID=1446>. Last accessed on 31st October, 2018.
- [542] M. Radovanovic and M. Madic, "Experimental investigations of CO₂ laser cut quality: a review," *Revista de Tehnologii Neconventionale*, vol. 15, p. 35, 2011.
- [543] A. Sundaramurthy, *et al.*, "Toward nanometer-scale optical photolithography: utilizing the near-field of bowtie optical nanoantennas," *Nano letters*, vol. 6, pp. 355-360, 2006.
- [544] S. Ito, *et al.*, "Fabrication of screen-printing pastes from TiO₂ powders for dye-sensitised solar cells," *Progress in photovoltaics: research and applications*, vol. 15, pp. 603-612, 2007.
- [545] T. Lippert, "Laser application of polymers," in *Polymers and Light*, ed: Springer, 2004, pp. 51-246.
- [546] F. R. Wagner, "Scanning excimer laser ablation of poly (ethylene terephthalate)(pet) and its application to rapid prototyping of channels for microfluidics," 2000.
- [547] J. Capek, *et al.*, "Tactile sensor," ed: Google Patents, 1988.
- [548] M. R. Cutkosky, *et al.*, "Force and tactile sensors," in *Springer Handbook of Robotics*, ed: Springer, 2008, pp. 455-476.
- [549] J. Dargahi and S. Najarian, "Advances in tactile sensors design/manufacturing and its impact on robotics applications-a review," *Industrial Robot: An International Journal*, vol. 32, pp. 268-281, 2005.
- [550] Y.-J. Yang, *et al.*, "An integrated flexible temperature and tactile sensing array using PI-copper films," *Sensors and Actuators A: Physical*, vol. 143, pp. 143-153, 2008.
- [551] J. Engel, *et al.*, "Polymer micromachined multimodal tactile sensors," *Sensors and Actuators A: physical*, vol. 117, pp. 50-61, 2005.
- [552] K. Takei, *et al.*, "Nanowire active-matrix circuitry for low-voltage macroscale artificial skin," *Nature Materials*, vol. 9, p. 821, 2010.
- [553] M. Ramuz, *et al.*, "Transparent, optical, pressure-sensitive artificial skin for large-area stretchable electronics," *Advanced Materials*, vol. 24, pp. 3223-3227, 2012.
- [554] M. Ying, *et al.*, "Silicon nanomembranes for fingertip electronics," *Nanotechnology*, vol. 23, p. 344004, 2012.
- [555] C. Li, *et al.*, "Flexible dome and bump shape piezoelectric tactile sensors using PVDF-TrFE copolymer," *Microelectromechanical Systems, Journal of*, vol. 17, pp. 334-341, 2008.
- [556] W. H. Yeo, *et al.*, "Multifunctional epidermal electronics printed directly onto the skin," *Advanced Materials*, vol. 25, pp. 2773-2778, 2013.
- [557] R. S. Dahiya, *et al.*, "Tactile sensing—from humans to humanoids," *Robotics, IEEE Transactions on*, vol. 26, pp. 1-20, 2010.
- [558] R. S. Dahiya, *et al.*, "Towards tactile sensing system on chip for robotic applications," *Sensors Journal, IEEE*, vol. 11, pp. 3216-3226, 2011.

- [559] Y. Jeong, *et al.*, "Psychological tactile sensor structure based on piezoelectric nanowire cell arrays," *RSC Advances*, vol. 5, pp. 40363-40368, 2015.
- [560] M. Shimojo, *et al.*, "A tactile sensor sheet using pressure conductive rubber with electrical-wires stitched method," *Sensors Journal, IEEE*, vol. 4, pp. 589-596, 2004.
- [561] H. Kawasaki, *et al.*, "Dexterous anthropomorphic robot hand with distributed tactile sensor: Gifu hand II," *Mechatronics, IEEE/ASME Transactions On*, vol. 7, pp. 296-303, 2002.
- [562] P. Saccomandi, *et al.*, "Microfabricated tactile sensors for biomedical applications: a review," *Biosensors*, vol. 4, pp. 422-448, 2014.
- [563] J. Park, *et al.*, "Fingertip skin-inspired microstructured ferroelectric skins discriminate static/dynamic pressure and temperature stimuli," *Science advances*, vol. 1, p. e1500661, 2015.
- [564] J. Lin, *et al.*, "Laser-induced porous graphene films from commercial polymers," *Nature communications*, vol. 5, 2014.
- [565] *Graphene paints a corrosion-free future.* Available: <http://www.manchester.ac.uk/discover/news/graphene-paints-a-corrosion-free-future>. Last accessed on 31st October, 2018.
- [566] *EIS Spectrum Analyzer.* Available: <http://www.abc.chemistry.bsu.by/vi/analyser/>. Last accessed on 31st October, 2018.
- [567] *Natural environment.* Available: <http://www.environment.nsw.gov.au/salinity/basics/naturalenvironment.htm>. Last accessed on 31st October, 2018.
- [568] *Changes in Marine Salinity Levels.* Available: http://pisaster.genetics.uga.edu/groups/evolution3000/wiki/cb536/Changes_in_Marine_Salinity_Levels.html. Last accessed on 31st October, 2018.
- [569] C. Wu, *et al.*, "Salinity sensor based on polyimide-coated photonic crystal fiber," *Optics express*, vol. 19, pp. 20003-20008, 2011.
- [570] S. Robinson and R. Nakkeeran, "Photonic crystal based sensor for sensing the salinity of seawater," in *Advances in Engineering, Science and Management (ICAESM), 2012 International Conference on*, 2012, pp. 495-499.
- [571] S. Wang, *et al.*, "Modeling optical microfiber loops for seawater sensing," *Applied optics*, vol. 51, pp. 3017-3023, 2012.
- [572] H. A. Rahman, *et al.*, "Fiber-optic salinity sensor using fiber-optic displacement measurement with flat and concave mirror," *IEEE Journal of selected topics in quantum electronics*, vol. 18, pp. 1529-1533, 2012.
- [573] "Murray-Darling Basin Authority annual report 2015-16."
- [574] C. Huber, *et al.*, "Optical sensor for seawater salinity," *Fresenius' journal of analytical chemistry*, vol. 368, pp. 196-202, 2000.
- [575] N. Reul, *et al.*, "Sea surface salinity observations from space with the SMOS satellite: A new means to monitor the marine branch of the water cycle," *Surveys in Geophysics*, vol. 35, pp. 681-722, 2014.
- [576] L. Men, *et al.*, "A multiplexed fiber Bragg grating sensor for simultaneous salinity and temperature measurement," *Journal of Applied Physics*, vol. 103, p. 053107, 2008.
- [577] D. Gadani, *et al.*, "Effect of salinity on the dielectric properties of water," 2012.
- [578] D. M. Le Vine, *et al.*, "Aquarius and remote sensing of sea surface salinity from space," *Proceedings of the IEEE*, vol. 98, pp. 688-703, 2010.
- [579] H. Rahman, *et al.*, "Tapered plastic multimode fiber sensor for salinity detection," *Sensors and Actuators A: Physical*, vol. 171, pp. 219-222, 2011.
- [580] E. Scudiero, *et al.*, "Simultaneous monitoring of soil water content and salinity with a low-cost capacitance-resistance probe," *Sensors*, vol. 12, pp. 17588-17607, 2012.
- [581] J. Jonsson, *et al.*, "Towards chip-based salinity measurements for small submersibles and biologgers," *International Journal of Oceanography*, vol. 2013, 2013.
- [582] S. Bhat, "Salinity (conductivity) sensor based on parallel plate capacitors," 2005.
- [583] D. Malarde, *et al.*, "High-resolution and compact refractometer for salinity measurements," *Measurement Science and Technology*, vol. 20, p. 015204, 2008.
- [584] P. Grosso, *et al.*, "Practical versus absolute salinity measurements: New advances in high performance seawater salinity sensors," *Deep Sea Research Part I: Oceanographic Research Papers*, vol. 57, pp. 151-156, 2010.
- [585] A. V. Mamishev, *et al.*, "Interdigital sensors and transducers," *Proceedings of the IEEE*, vol. 92, pp. 808-845, 2004.

- [586] M. S. A. Rahman, *et al.*, "Experimental Investigation: Impedance Characterization," in *Novel Sensors for Food Inspection: Modelling, Fabrication and Experimentation*, ed: Springer, 2014, pp. 37-71.
- [587] D. Ha, *et al.*, "Recent achievements in electronic tongue and bioelectronic tongue as taste sensors," *Sensors and Actuators B: Chemical*, vol. 207, pp. 1136-1146, 2015.
- [588] *Taste disorders*. Available: <https://www.nidcd.nih.gov/health/taste-disorders>. Last accessed on 31st October, 2018.
- [589] *Taste disorder 'prevalent in children'*. Available: <http://www.sbs.com.au/news/article/2011/04/26/taste-disorder-prevalent-children>. Last accessed on 31st October, 2018.
- [590] Q. Chen, *et al.*, "Determination of caffeine content and main catechins contents in green tea (*Camellia sinensis* L.) using taste sensor technique and multivariate calibration," *Journal of Food Composition and Analysis*, vol. 23, pp. 353-358, 2010.
- [591] A. Riul, *et al.*, "An artificial taste sensor based on conducting polymers," *Biosensors and Bioelectronics*, vol. 18, pp. 1365-1369, 2003.
- [592] Y. Tahara and K. Toko, "Electronic tongues—a review," *IEEE Sensors Journal*, vol. 13, pp. 3001-3011, 2013.
- [593] C. Krantz-Rülcker, *et al.*, "Electronic tongues for environmental monitoring based on sensor arrays and pattern recognition: a review," *Analytica chimica acta*, vol. 426, pp. 217-226, 2001.
- [594] Z. Haddi, *et al.*, "Instrumental assessment of red meat origins and their storage time using electronic sensing systems," *Analytical Methods*, vol. 7, pp. 5193-5203, 2015.
- [595] K. Toko, *et al.*, "Taste sensor: Electronic tongue with global selectivity," *Essentials of Machine Olfaction and Taste*, pp. 87-174, 2016.
- [596] S. Etoh, *et al.*, "Taste sensor chip for portable taste sensor system," *Sens. Mater*, vol. 20, pp. 151-160, 2008.
- [597] E. A. Baldwin, *et al.*, "Electronic noses and tongues: Applications for the food and pharmaceutical industries," *Sensors*, vol. 11, pp. 4744-4766, 2011.
- [598] P. Ciosek and W. Wróblewski, "Potentiometric electronic tongues for foodstuff and biosample recognition—An overview," *Sensors*, vol. 11, pp. 4688-4701, 2011.
- [599] A. L. Huang, *et al.*, "The cells and logic for mammalian sour taste detection," *Nature*, vol. 442, p. 934, 2006.
- [600] E. S. Medeiros, *et al.*, "A taste sensor array based on polyaniline nanofibers for orange juice quality assessment," *Sensor Letters*, vol. 7, pp. 24-30, 2009.
- [601] G. Q. Zhao, *et al.*, "The receptors for mammalian sweet and umami taste," *Cell*, vol. 115, pp. 255-266, 2003.
- [602] *The Five Senses of Sensors - Taste* Available: <https://www.digikey.com/en/articles/techzone/2011/jul/the-five-senses-of-sensors---taste>. Last accessed on 31st October, 2018.
- [603] *Concentration of chemicals in food samples*. Available: http://www.testmeters.com.au/files/2014/12/Sodium_and_Salt_Content_in_Food_Samples.pdf. Last accessed on 31st October, 2018.
- [604] *Electrical Conductivity of Aqueous Solutions*. Available: <http://www.colby.edu/chemistry/CH141/CH141L/CH141Lab4Fall2009.pdf>. Last accessed on 31st October, 2018.
- [605] M. J. Kim, *et al.*, "Electrochemical behavior of citric acid and its influence on Cu electrodeposition for damascene metallization," *Journal of The Electrochemical Society*, vol. 162, pp. D354-D359, 2015.
- [606] J. Juansah and W. Yulianti, "Studies on Electrical Behavior of Glucose Using Impedance Spectroscopy," in *IOP Conference Series: Earth and Environmental Science*, 2016, p. 012039.
- [607] F. Zhao, *et al.*, "An Electrochemical Sensor for L-Tryptophan Using a Molecularly Imprinted Polymer Film Produced by Copolymerization of o-Phenylenediamine and Hydroquinone," *Analytical Letters*, vol. 47, pp. 1712-1725, 2014.
- [608] *Properties of the Phosphate Group*. Available: <http://www.tud.ttu.edu/im/Tonu.Reintamm/shabarova/4.4.html>. Last accessed on 31st October, 2018.
- [609] D. Robinson, *et al.*, "A review of advances in dielectric and electrical conductivity measurement in soils using time domain reflectometry," *Vadose Zone Journal*, vol. 2, pp. 444-475, 2003.
- [610] M. Malicki and R. Walczak, "Evaluating soil salinity status from bulk electrical conductivity and permittivity," *European Journal of Soil Science*, vol. 50, pp. 505-514, 1999.

- [611] N. Bhattacharyya and R. Bandhopadhyay, "Electronic nose and electronic tongue," in *Nondestructive Evaluation of Food Quality*, ed: Springer, 2010, pp. 73-100.
- [612] A. Wild and K. Cameron, "Nitrate leaching through soils and environmental considerations with special reference to recent work in the United Kingdom," in *Soil nitrogen as fertilizer or pollutant*, ed, 1980.
- [613] R. Hester, *et al.*, "Fertilizers and nitrate leaching," in *Agricultural chemicals and the environment*, ed, 1996, pp. 1-26.
- [614] K. Cameron, *et al.*, "Nitrogen losses from the soil/plant system: a review," *Annals of Applied Biology*, vol. 162, pp. 145-173, 2013.
- [615] R. Monaghan, *et al.*, "Nutrient management in New Zealand pastures—recent developments and future issues," *New Zealand journal of agricultural research*, vol. 50, pp. 181-201, 2007.
- [616] L. M. Holland and G. J. Doole, "Implications of fairness for the design of nitrate leaching policy for heterogeneous New Zealand dairy farms," *Agricultural water management*, vol. 132, pp. 79-88, 2014.
- [617] R. Davies-Colley and B. Wilcock, "Water quality and chemistry in running waters," *Freshwaters of New Zealand. Christchurch: New Zealand Hydrological Society and New Zealand Limnological Society*, 2004.
- [618] J. D. Brender, *et al.*, "Dietary nitrites and nitrates, nitrosatable drugs, and neural tube defects," *Epidemiology*, vol. 15, pp. 330-336, 2004.
- [619] W. L. Daniel, *et al.*, "Colorimetric nitrite and nitrate detection with gold nanoparticle probes and kinetic end points," *Journal of the American Chemical Society*, vol. 131, pp. 6362-6363, 2009.
- [620] F. R. Greer and M. Shannon, "Infant methemoglobinemia: the role of dietary nitrate in food and water," *Pediatrics*, vol. 116, pp. 784-786, 2005.
- [621] P. J. Squillace, *et al.*, "VOCs, pesticides, nitrate, and their mixtures in groundwater used for drinking water in the United States," *Environmental Science & Technology*, vol. 36, pp. 1923-1930, 2002.
- [622] W. H. Organization. (2017, 27/02/2017). *Water-related diseases*. Available: http://www.who.int/water_sanitation_health/diseases-risks/diseases/methaemoglobin/en/. Last accessed on 31st October, 2018.
- [623] B. Narayana and K. Sunil, "A spectrophotometric method for the determination of nitrite and nitrate," *Eurasian Journal of Analytical Chemistry*, vol. 4, pp. 204-214, 2009.
- [624] K. M. Miranda, *et al.*, "A rapid, simple spectrophotometric method for simultaneous detection of nitrate and nitrite," *Nitric oxide*, vol. 5, pp. 62-71, 2001.
- [625] A. Dudwadkar, *et al.*, "Application of ion chromatography for the determination of nitrate in process streams of thermal denitration plant," *Separation Science and Technology*, vol. 48, pp. 2425-2430, 2013.
- [626] B. A. Pellerin, *et al.*, "Optical techniques for the determination of nitrate in environmental waters: Guidelines for instrument selection, operation, deployment, maintenance, quality assurance, and data reporting," *Quality Assurance, and Data Reporting. In: Techniques and Methods*, pp. 1-D5, 2013.
- [627] A. A. Ensafi and M. Amini, "Highly selective optical nitrite sensor for food analysis based on Lauth's violet-triacetyl cellulose membrane film," *Food Chemistry*, vol. 132, pp. 1600-1606, 2012.
- [628] X. Wang, *et al.*, "Mechanism and experiment of planar electrode sensors in water pollutant measurement," *IEEE Transactions on Instrumentation and Measurement*, vol. 64, pp. 516-523, 2015.
- [629] B. Schazmann and D. Diamond, "Improved nitrate sensing using ion selective electrodes based on urea-calixarene ionophores," *New Journal of Chemistry*, vol. 31, pp. 587-592, 2007.
- [630] X.-H. Pham, *et al.*, "Electrochemical detection of nitrite using urchin-like palladium nanostructures on carbon nanotube thin film electrodes," *Sensors and Actuators B: Chemical*, vol. 193, pp. 815-822, 2014.
- [631] A. Devices. (04/09/2017). *AD5933: Impedance Analyzer*. Available: <http://www.analog.com/media/en/technical-documentation/data-sheets/AD5933.pdf>. Last accessed on 31st October, 2018.
- [632] Arduino. (2017, 4/09/2017). *Arduino Uno WiFi*. Available: <https://store.arduino.cc/usa/arduino-uno-wifi>. Last accessed on 31st October, 2018.
- [633] Thingspeak. (2017, 26/08/2017). *Thingspeak*. Available: <https://thingspeak.com/>. Last accessed on 31st October, 2018.
- [634] A. Website. (2017, 26/08/2017). *Ciao*. Available: <https://www.arduino.cc/en/Reference/Ciao>. Last accessed on 31st October, 2018.

- [635] (4/09/2017). *Circuit maker*. Available: <https://circuitmaker.com/>. Last accessed on 30th July, 2018.
- [636] D. Cochlin. (2014, 28/08/2017). *Graphene paints a corrosion-free future*. Available: <http://www.manchester.ac.uk/discover/news/graphene-paints-a-corrosion-free-future/>. Last accessed on 30th July, 2018.
- [637] A. K. Geim, "Graphene: Status and Prospects," *Science*, vol. 324, pp. 1530-1534, 2009.
- [638] A. Nag, *et al.*, "Urinary incontinence monitoring system using laser-induced graphene sensors," in *SENSORS, 2017 IEEE*, 2017, pp. 1-3.
- [639] *Advantages of thermoplastics*. Available: <https://www.online-sciences.com/industries/thermoplastics-properties-types-uses-advantages-and-disadvantages/>. Last accessed on 30th July, 2018.
- [640] M. Nour, *et al.*, "Nanocomposite carbon-PDMS membranes for gas separation," *Sensors and Actuators B: Chemical*, vol. 161, pp. 982-988, 2012.
- [641] T. Chang-bin, *et al.*, "Electro-spark alloying using graphite electrode on titanium alloy surface for biomedical applications," *Applied surface science*, vol. 257, pp. 6364-6371, 2011.
- [642] B. Tymrak, *et al.*, "Mechanical properties of components fabricated with open-source 3-D printers under realistic environmental conditions," *Materials & Design*, vol. 58, pp. 242-246, 2014.
- [643] S. Malekie and F. Ziaie, "Study on a novel dosimeter based on polyethylene-carbon nanotube composite," *Nuclear Instruments and Methods in Physics Research Section A: Accelerators, Spectrometers, Detectors and Associated Equipment*, vol. 791, pp. 1-5, 2015.
- [644] S. H. Kim, *et al.*, "Flexible, stretchable and implantable PDMS encapsulated cable for implantable medical device," *Biomedical Engineering Letters*, vol. 1, pp. 199-203, 2011.
- [645] A. Nag, *et al.*, "Transparent biocompatible sensor patches for touch sensitive prosthetic limbs," in *Sensing Technology (ICST), 2016 10th International Conference on*, 2016, pp. 1-6.
- [646] A. Chen and S. Chatterjee, "Nanomaterials based electrochemical sensors for biomedical applications," *Chemical Society Reviews*, vol. 42, pp. 5425-5438, 2013.
- [647] S. Stassi, *et al.*, "Flexible tactile sensing based on piezoresistive composites: A review," *Sensors*, vol. 14, pp. 5296-5332, 2014.
- [648] B. Hu, *et al.*, "External-Strain Induced Insulating Phase Transition in VO₂ Nanobeam and Its Application as Flexible Strain Sensor," *Advanced Materials*, vol. 22, pp. 5134-5139, 2010.
- [649] P. Binger, *et al.*, "Highly flexible capacitive strain gauge for continuous long-term blood pressure monitoring," *Biomedical microdevices*, vol. 14, pp. 573-581, 2012.
- [650] S. Park, *et al.*, "Stretchable Energy-Harvesting Tactile Electronic Skin Capable of Differentiating Multiple Mechanical Stimuli Modes," *Advanced Materials*, vol. 26, pp. 7324-7332, 2014.
- [651] G. Yin, *et al.*, "A carbon nanotube/polymer strain sensor with linear and anti-symmetric piezoresistivity," *Journal of composite materials*, vol. 45, pp. 1315-1323, 2011.
- [652] H. Zhao, *et al.*, "Carbon nanotube yarn strain sensors," *Nanotechnology*, vol. 21, p. 305502, 2010.
- [653] C. Mattmann, *et al.*, "Sensor for measuring strain in textile," *Sensors*, vol. 8, pp. 3719-3732, 2008.
- [654] S. Cheng and Z. Wu, "A Microfluidic, Reversibly Stretchable, Large-Area Wireless Strain Sensor," *Advanced Functional Materials*, vol. 21, pp. 2282-2290, 2011.
- [655] J. Ge, *et al.*, "A Stretchable Electronic Fabric Artificial Skin with Pressure-, Lateral Strain-, and Flexion-Sensitive Properties," *Advanced Materials*, vol. 28, pp. 722-728, 2016.
- [656] P. K. Yang, *et al.*, "A Flexible, Stretchable and Shape-Adaptive Approach for Versatile Energy Conversion and Self-Powered Biomedical Monitoring," *Advanced Materials*, vol. 27, pp. 3817-3824, 2015.
- [657] M. Weigel, *et al.*, "Iskin: flexible, stretchable and visually customizable on-body touch sensors for mobile computing," in *Proceedings of the 33rd Annual ACM Conference on Human Factors in Computing Systems*, 2015, pp. 2991-3000.
- [658] J. Sebastian, *et al.*, "Health monitoring of structural composites with embedded carbon nanotube coated glass fiber sensors," *Carbon*, vol. 66, pp. 191-200, 2014.
- [659] O. O. Rakibet, *et al.*, "Epidermal passive RFID strain sensor for assisted technologies," *IEEE Antennas and Wireless Propagation Letters*, vol. 13, pp. 814-817, 2014.
- [660] R. D. P. Wong, *et al.*, "Flexible microfluidic normal force sensor skin for tactile feedback," *Sensors and Actuators A: Physical*, vol. 179, pp. 62-69, 2012.
- [661] M. I. Tiwana, *et al.*, "Characterization of a capacitive tactile shear sensor for application in robotic and upper limb prostheses," *Sensors and Actuators A: Physical*, vol. 165, pp. 164-172, 2011.
- [662] H.-K. Kim, *et al.*, "Capacitive tactile sensor array for touch screen application," *Sensors and Actuators A: Physical*, vol. 165, pp. 2-7, 2011.

- [663] L. Viry, *et al.*, "Flexible three-axial force sensor for soft and highly sensitive artificial touch," *Advanced Materials*, vol. 26, pp. 2659-2664, 2014.
- [664] H.-K. Lee, *et al.*, "Real-time measurement of the three-axis contact force distribution using a flexible capacitive polymer tactile sensor," *Journal of Micromechanics and Microengineering*, vol. 21, p. 035010, 2011.
- [665] W.-P. Shih, *et al.*, "Flexible temperature sensor array based on a graphite-polydimethylsiloxane composite," *Sensors*, vol. 10, pp. 3597-3610, 2010.
- [666] S. Bhalla and S. Bajaj, "Bone characterization using piezotransducers as biomedical sensors," *Strain*, vol. 44, pp. 475-478, 2008.
- [667] P. Dharap, *et al.*, "Nanotube film based on single-wall carbon nanotubes for strain sensing," *Nanotechnology*, vol. 15, p. 379, 2004.